

Zakrys, Linas (2012) Mechanistic and functional analysis of Slit-Robo proteins. PhD thesis

<http://theses.gla.ac.uk/3672/>

Copyright and moral rights for this thesis are retained by the author

A copy can be downloaded for personal non-commercial research or study, without prior permission or charge

This thesis cannot be reproduced or quoted extensively from without first obtaining permission in writing from the Author

The content must not be changed in any way or sold commercially in any format or medium without the formal permission of the Author

When referring to this work, full bibliographic details including the author, title, awarding institution and date of the thesis must be given.

Mechanistic and functional analysis of Slit-Robo proteins

Linus Zakrys

Submitted in fulfilment of the requirements for the Degree of
Doctor of Philosophy

Institute of Molecular Cell and Systems Biology
College of Medical Veterinary and Life Sciences
University of Glasgow
September 2012

Abstract

Slits are large secreted proteins which mediate their functions by binding to single pass transmembrane receptors called Robo. This signalling axis was first identified as a pivotal guidance mechanism in the development of the nervous system. A repulsive activity of Slit proteins controls the projection and movement of Robo expressing neurons in *Drosophila* and vertebrates. Slit and Robo expression is not limited to the nervous system or development only, they were found to be expressed in many different tissues both in embryo and adult organism. Correspondingly, the Slit-Robo signalling axis now is implicated in many other biological and pathological processes such as angiogenesis, cancer and tissue remodelling. This study sought to investigate two different aspects of the Slit-Robo signalling system: Robo1 transmembrane signalling mechanism and possible Slit-Robo roles within the immune system.

Robos and other type I transmembrane receptors are unable to transmit signal across the membrane within a single molecule because a single transmembrane α -helix restricts propagation of conformational changes between extracellular and intracellular parts of the protein. Therefore, the type I receptors usually act as homo- or heterooligomers, formation or dissociation of which is controlled by ligand binding. Based on indirect evidence a similar transmembrane signalling mechanism was suggested for Robo receptors. It was hypothesized that Slit binding induces changes in oligomeric state of Robo which in turn initiates downstream signalling events. In order to test this hypothesis and determine details of the transmembrane signalling mechanism, the oligomeric state of Robo1 receptor was assessed in live cells using two different fluorescence resonance energy transfer (FRET) based methods. A strong FRET signal was observed between differently tagged Robo1 proteins, indicating that the receptor forms oligomers in the resting state. However, contrary to the initial hypothesis, the addition of Slit2 protein did not have an observable effect on the FRET signal and thus on receptor oligomeric state. Moreover, Robo1 proteins were found to form higher density domains within the cell membrane. This property could be abolished by removing the intracellular part of the protein indicating constant Robo1 association with intracellular structures. These data show that the Robo1 transmembrane signalling mechanism might be more complicated than initially expected and likely involves structural changes within the Robo1 oligomer or Robo1 complexes with other proteins.

The Slit-Robo signalling axis was linked to the immune system when it was demonstrated that Slit2 is able to inhibit chemotactic leukocyte migration and reduce inflammatory responses in mice. However, the precise role of these proteins remained unknown. In order to gain further insight into possible Slit-Robo functions within the immune system promoter analysis was performed with the aim to identify transcription factors responsible for the control of these proteins. Among many putative transcription factors discovered, Foxn1 was the most prominent as its binding site was identified both in Slit2 and Slit3 promoters. Development and functions of thymus, a primary lymphoid organ responsible for T cell development, is regulated by Foxn1 and since thymic activity includes active and abundant leukocyte movement into, out-of and within the organ, a hypothesis was suggested that Slits contribute to regulation of these processes. Quantitative Slit2-Slit3 expression studies and assessment of embryonic thymus cellular composition in Slit2 knockout mouse were employed to test this hypothesis. Quantitative PCR revealed that both Slit2 and Slit3 are downregulated four-fold in thymic epithelial cells starting embryonic stage E13, however no differences in cellular composition of embryonic thymi were detected between wild type and Slit2 knockout animals using flow cytometry. Possible Slit2 and Slit3 redundancy might be the reason for the lack of observable effects, unfortunately a Slit3 knockout model was unavailable for these studies. Interestingly, flow cytometry also revealed that in addition to thymic epithelial cells, Slit2 is expressed by pericyte type cells surrounding the thymic vasculature. It seems that Slit proteins have intricate and regulated expression patterns within the thymus, however their precise role remains an open question.

In summary, data collected during this study illuminates two different aspects of the Slit-Robo signalling system. Both of them, despite Slits being secreted proteins, hint at short-range, possibly even juxtacrine, ligand – receptor interactions. Given Robo receptor evolutionary connections to cell adhesion molecules and Slit affinity to heparan sulphate it is not a completely unexpected finding.

Table of contents

Abstract	2
Table of contents	4
List of figures	7
List of tables	9
Acknowledgements	10
Author's declaration	11
List of abbreviations	12
1 Introduction	14
1.1 General Introduction	14
1.2 Slits - guidance cues	14
1.3 Robos – receptors for Slit	17
1.4 Slit-Robo signalling	23
1.4.1 Robo transmembrane signalling mechanism	23
1.4.2 Robo downstream signalling	26
1.5 Slit-Robo biological functions	33
1.5.1 Development and wiring of nervous system	33
1.5.2 Muscular and cardiac system development	36
1.5.3 Kidney development	38
1.5.4 Lung development	39
1.5.5 Other developmental functions	39
1.5.6 Angiogenesis	40
1.5.7 Cancer	46
1.5.8 Leukocytes and immune response	49
1.6 Final thoughts about Slit-Robo proteins	52
1.7 Receptor oligomerisation-methods and techniques	53
1.7.1 Co-immunoprecipitation	53
1.7.2 Resonance energy transfer	54
1.7.3 Fluorescence recovery after photobleaching	58
1.7.4 Bimolecular fluorescence complementation	59
1.8 Aims of the project	59
2 Materials and methods	60
2.1 Materials	60

2.1.1	Reagents, enzymes, medium components and kits	60
2.1.2	Buffers and microbiological culture	60
2.1.3	Oligonucleotides	61
2.1.4	Bacteria strains	61
2.2	Methods	63
2.2.1	RNA extraction	63
2.2.2	cDNA synthesis.....	64
2.2.3	Genomic DNA extraction	65
2.2.4	Construction of custom polylinker.....	65
2.2.5	PCR	65
2.2.6	Plasmid DNA extraction and purification.....	66
2.2.7	Digestion of DNA with restriction enzymes.....	66
2.2.8	DNA dephosphorylation	66
2.2.9	DNA ligation.....	67
2.2.10	DNA gel electrophoresis.....	67
2.2.11	DNA purification from gel.....	67
2.2.12	Preparation of competent bacterial cells	67
2.2.13	Bacterial transformation.....	68
2.2.14	Cell maintenance.....	68
2.2.15	Transient cell transfection.....	69
2.2.16	Stable cell line generation	69
2.2.17	Immunocytochemistry	69
2.2.18	Recombinant Slit2 purification	70
2.2.19	Protein crosslinking.....	70
2.2.20	Preparation of cell lysates	70
2.2.21	Co-immunoprecipitation	71
2.2.22	Sodium dodecyl sulphate polyacrylamide gel electrophoresis	71
2.2.23	Western blotting.....	71
2.2.24	Transwell migration assays.....	72
2.2.25	FRET imaging.....	72
2.2.26	Time resolved FRET	73
2.2.27	Protein arrays	74
2.2.28	QPCR	74
2.2.29	RAC1 assay.....	75
2.2.30	Robo1 antibody purification	75

2.2.31	Animals	75
2.2.32	Primary cell isolation	75
2.2.33	FACS and cell sorting	76
2.2.34	<i>In silico</i> promoter analysis	77
3	Study of Robo1 transmembrane signalling mechanism.....	78
3.1	Introduction	78
3.2	Gene cloning and construct validation	78
3.2.1	Slit2 and Robo1 cloning and construct design.....	78
3.2.2	Purification and characterisation of Slit2.....	80
3.2.3	Expression and characterisation of Robo1 constructs.....	81
3.2.4	Signalling activity of Robo1 constructs	84
3.3	Robo1 oligomeric state assessment with FRET imaging.....	87
3.4	Robo1 oligomeric state assessment with time-resolved FRET	89
3.5	Robo1 oligomeric state assessment with co-immunoprecipitation	92
3.6	Robo1 oligomerisation determinants.....	94
3.7	Discussion	95
4	Study of Slit-Robo role in the immune system	129
4.1	Introduction	129
4.2	Slit-Robo expression profiling	130
4.2.1	Slit-Robo expression in mouse organs and tissues	130
4.2.2	Slit-Robo expression in cell lines.....	131
4.2.3	Slit-Robo expression in <i>ex vivo</i> leukocytes.....	131
4.3	Transcription factor binding site analysis.....	133
4.4	Slit function in thymus	136
4.4.1	Slit2 and Slit3 expression in TECs	138
4.4.2	Analysis of Slit2 knockout mice	139
4.5	Discussion	143
5	Final discussions	162
	References	166

List of figures

Figure 1.1 Organisation of Slit proteins.....	15
Figure 1.2 Organisation of Robo proteins.....	18
Figure 1.3 Structure of Robo Ig domains and conformations adopted by various IgCAM proteins.....	19
Figure 1.4 Structure of Slit-Robo complex.....	20
Figure 1.5 Putative Robo transmembrane signalling mechanisms	24
Figure 1.6 Robo downstream signalling	27
Figure 1.7 Slit-Robo role in midline crossing and longitudinal tract formation.....	34
Figure 1.8 Heart lumen formation in <i>Drosophila</i>	37
Figure 3.1 Slit2 and Robo1 constructs	102
Figure 3.2 Slit2-(His) ₆ expression and secretion	103
Figure 3.3 Slit2-(His) ₆ purification	104
Figure 3.4 Biological activity of Slit2.....	105
Figure 3.5 Expression of Robo1 constructs	106
Figure 3.6 Cellular distribution of Robo1 constructs in transiently transfected HEK 293T cells	107
Figure 3.7 Characterisation of double stable cell lines expressing Robo1 constructs	108
Figure 3.8 Cellular distribution of Robo1 constructs in HEK 293 Flp-In T-REX cells	109
Figure 3.9 Differential membrane distribution of truncated and full-length Robo1 constructs	110
Figure 3.10 Slit2-Robo1 interactions	111
Figure 3.11 Modulation of Rac1 activity	112
Figure 3.12 Lack of detectable Robo1-srGAP1 interactions	113
Figure 3.13 Slit2-Robo1 interactions fail to modulate ERK 1/2 activity.....	114
Figure 3.14 The molecular basis of FRET imaging experiments	115
Figure 3.15 FRET analysis of Robo1 oligomerisation in transiently transfected HEK 293T cells	116
Figure 3.16 Generation of potentially oligomerisation-deficient Robo1 constructs.....	117
Figure 3.17 FRET analysis of potentially oligomerisation-deficient Robo1 constructs....	118
Figure 3.18 FRET analysis of Robo1 oligomerisation in HEK 293 Flp-In T-REX cells..	119
Figure 3.19 Basis of a TR-FRET experiment	120
Figure 3.20 Expression of SNAP-tagged Robo1 constructs	121
Figure 3.21 SNAP tagged Robo1 construct validation	122
Figure 3.22 TR-FRET measurements	123
Figure 3.23 Co-immunoprecipitation of differently tagged Robo1 constructs.....	124
Figure 3.24 Crosslinking and co-immunoprecipitation of differently tagged Robo1 constructs	125
Figure 3.25 Mapping the sites of Robo1 oligomerisation.....	126
Figure 3.26 Structural conservation of putative Robo1 oligomerisation sites	127
Figure 3.27 Dimerisation interfaces of I-set Ig proteins	128
Figure 4.1 Slit-Robo expression in mouse organs and tissues	147
Figure 4.2 Slit-Robo expression in cell lines	148
Figure 4.3 Robo1 expression assessment by flow cytometry	149

Figure 4.4 Purification of Robo1 (DSHB) antibody	150
Figure 4.5 Verification of Robo1 (DSHB) antibody function	151
Figure 4.6 CpG islands in the putative Slit2 promoter	152
Figure 4.7 Phylogenetic footprinting	153
Figure 4.8 Putative Foxn1 binding site	154
Figure 4.9 Dissection of embryonic thymus	155
Figure 4.10 Slit2 and Slit3 expression in TECs during thymic development.....	156
Figure 4.11 Embryonic thymus analysis in Slit2 knockout mice	157
Figure 4.12 Genotyping of Slit2 knockout mouse embryos	158
Figure 4.13 Comparison of thymocyte composition in wild type and Slit2 knockout embryos	159
Figure 4.14 Comparison of TEC composition in wild type and Slit2 knockout embryos.	160
Figure 4.15 Identification of GFP ⁺ cell population in embryonic thymus.....	161

List of tables

Table 2.1 Oligonucleotides used in this study	62
Table 2.2 List of antibodies used for Western blotting.....	72
Table 2.3 List of antibodies used for flow cytometry	76
Table 4.1 Transcription factors potentially involved in regulation of Slit-Robo expression	134

Acknowledgements

First of all, I would like to thank professors Graeme Milligan and Gerry Graham for the opportunity to freely pursue my scientific ideas and for help and guidance during this pursuit. In terms of personal and professional development I could not have better PhD.

I am deeply grateful to all members of Molecular Pharmacology and Chemokine research groups. Without your selfless help and willingness to share knowledge this project simply would not exist. Additionally, I would like to say a separate "thank you" to Nicola Smith, Eliza Alvarez Curto, Richard Ward, John Pediani and Chantevy Pou for all those scientific and not so discussions and for brilliant moments of "lab madness".

I would like to thank Wellcome Trust 4-year PhD programme directors Prof. Bill Cushley, Prof. Darren G. Monckton and Dr Olwyn Byron for their support and help, especially during my first year in Glasgow.

I would like to acknowledge Prof. Graham Anderson, Dr Amanda White and Natalie Roberts for help with embryonic thymus and TEC purification. A big thank to Dr Helen Baldwin for help with human PBMCs. I am really greatfull to Dr George Baillie and Dr Yuan Sin for help with protein arrays.

Last, but defiantly not the least, I would like to thank my parents.

*Brangūs Tėveliai, visa tai tapo įmanoma tik dėl Jūsų pasiaukojančio darbo ir paramos.
Ačiū Jums už viską.*

Author's declaration

I declare that this thesis and the results presented within are entirely my own work except where otherwise stated. No part of this thesis has been previously submitted for a degree at any university.

Linas Zakrys

List of abbreviations

BM	bone marrow
bp	base pair
BRET	bioluminescence resonance energy transfer
BSA	bovine serum albumin
CAGE	cap analysis gene expression
CAM	cell adhesion molecule
CC	conserved cytoplasmic motif
cDNA	complementary DNA
CER	cerulean fluorescent protein
CIT	citrine fluorescent protein
CMV	cytomegalo virus
CNS	central nervous system
Ct	threshold cycle
cTEC	cortical thymic epithelial cells
DN	double negative
dNTP	deoxynucleotide triphosphate
DP	double positive
E	embryonic day
ECM	extracellular matrix
EDTA	ethylenediaminetetraacetic acid
EGF	epidermal growth factor
ERK	extracellular signal regulated kinase
EST	expressed sequence tags
FACS	fluorescence activated cell sorting
FBS	foetal bovine serum
FLAG	FLAG epitope tag
FLIM	fluorescence-lifetime imaging microscopy
FNIII	fibronectin type III domain
FRET	fluorescence resonance energy transfer
FSC	forward scatter
GAP	GTPase-activating protein
GAPDH	Glyceraldehyde 3-phosphate dehydrogenase
GEF	guanine nucleotide exchange factor
GPCR	G protein-coupled receptor
GST	glutathione S-transferase
HEPES	4-(2-hydroxyethyl)-1-piperazineethanesulfonic acid
HS	heparan sulphate
HSC	haematopoietic stem cells
Ig	immunoglobulin
IgCAMs	immunoglobulin like cell adhesion molecules
LRR	leucine-rich repeat
MOPS	morpholinopropane sulfonic acid
mTEC	medullary thymic epithelial cells

myc	myc epitope tag
PAGE	polyacrylamide gel electrophoresis
PBMC	peripheral blood mononuclear cell
PBS	phosphate buffered saline
PCR	polymerase chain reaction
PI3K	phosphatidylinositol-3-kinase
QPCR	quantitative PCR
RET	resonance energy transfer
RIPA	radioimmune precipitation assay buffer
ROI	region of interest
RTK	receptor tyrosine kinases
RT-PCR	reverse transcriptase polymerase chain reaction
SDS	sodium dodecyl sulphate
SP	single positive
TAE	Tris acetate EDTA
TEC	thymic epithelial cells
TCR	T cell receptor
TM	transmembrane region
TPA	phorbol 12-myristate 13-acetate
TR-FRET	time-resolved fluorescence resonance energy transfer
TRIS	2-Amino-2-hydroxymethyl-propane-1,3-diol
TSS	transcription start sites

1 Introduction

1.1 General Introduction

One of the great evolutionary events in the history of life was rise of multicellular organisms. While carrying obvious advantages, multicellularity creates the need for intercellular communication systems. One can imagine that molecules which initially were utilised only for mechanical cell-to-cell adhesion soon developed additional signalling roles. As organisms became more and more complex, this primordial intercellular signalling network was constantly expanding and accommodating new functions: development, tissue repair and immune responses. So it is hardly surprising that many cell adhesion molecules, initially considered mainly as a "sticky coat" of the cell, turned out to be crucial receptors for intercellular communication, in some cases literally determining life and death of the cell.

There are four main classes of cell adhesion molecules: cadherins, integrins, immunoglobulin like cell adhesion molecules (IgCAMs) and selectins. Among them IgCAMs are the biggest, the most ancient and the most diverse group. Recent advances revealed a new subgroup of IgCAM molecules, the so called Robo receptors. Together with their cognate ligands Slits, Robo proteins form the Slit-Robo signalling axis which possesses unique structural and functional features setting Robos apart from other IgCAM molecules and making them compelling research subjects.

1.2 Slits - guidance cues

The Slit locus was first identified by genetic screens for mutations affecting development in *Drosophila* (Nusslein-Volhard et al, 1984). Further studies showed that it corresponds to the gene coding a large secreted protein crucial for the correct wiring of commissural neurons (Rothberg et al, 1988; Rothberg et al, 1990). Exact Slit functions remained vague until it was shown that Slit is a repulsive guidance cue during development of the nervous system. It was demonstrated that Slit acts as a ligand for the so called Robo receptors and repels neuron growth cones both in *Drosophila* and mammals (Brose et al, 1999; Kidd et al, 1999; Li et al, 1999; Yuan et al, 1999). Currently, it seems that the Slit-Robo signalling axis is preserved in the majority if not all bilateral organisms.

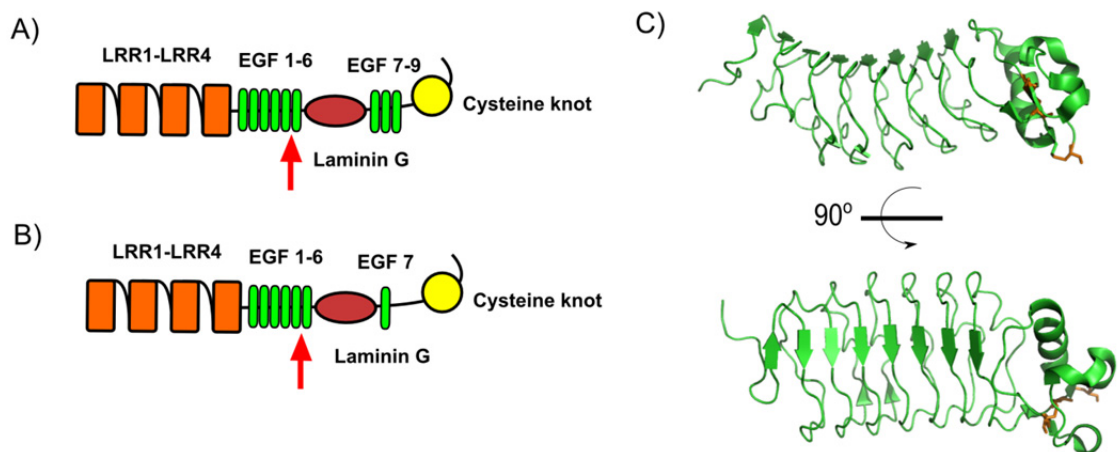


Figure 1.1 Organisation of Slit proteins

Schematic illustration of mammalian (A) and *Drosophila* (B) Slit proteins. Red arrows indicates site of proteolytic cleavage. Structure of human LRR2 domain (C; pdb id: 2V9T) shows typical horseshoe conformation. Cysteine residues forming disulphide bridges and restricting interdomain linker flexibility are marked in yellow.

Drosophila has a single Slit gene while three different Slit orthologs were identified in vertebrates - Slit1, Slit2 and Slit3 (Banfi et al, 1996; Holmes et al, 1998; Itoh et al, 1998; Nakayama et al, 1998). All three share a highly similar sequence and identical domain organisation. The defining feature of Slits is a unique tandem of four leucine-rich repeat (LRR) domains followed by six epidermal growth factor-like (EGF) domains, a laminin G domain, an additional three EGF domains (only one in invertebrates) and a C-terminal cysteine knot domain (Figure 1.1A and B). Because of this complex domain composition, a typical full-length Slit protein consists of 1500 amino acids and has molar mass of approximately 170 kDa.

Little is known about the tertiary or quaternary organisation of Slit proteins. Three-dimensional structures were successfully solved only for separate leucine-rich domains: LRR2, LRR3 and LRR4 (Howitt et al, 2004; Morlot et al, 2007b; Seiradake et al, 2009). Differently from all other LRR type proteins, these domains contain an additional disulphide bridge restricting flexibility of the interdomain linker (Figure 1.1C). This structural hindrance most likely enforces complex and compact structure of the N-terminal LRR tandem (Hohenester et al, 2006). The Slit LRR4 domain forms dimers both in solution and crystals (Howitt et al, 2004; Seiradake et al, 2009). Additionally, C-terminal cysteine knot domains are known as protein modules for dimerisation, so one could expect that full-length Slit proteins form homodimers. However, the LRR1-LRR4 tandem is monomeric in solution, as is full-length Slit1 in native PAGE (Hohenester, 2008; Tanno et al, 2004). The possibility exists that Slit dimerisation depends on heparan sulphate

(Seiradake et al, 2009), but overall, the existence and biological relevance of Slit dimers remains to be determined.

Biochemical experiments with truncated Slit forms show that the LRR2 domain is sufficient for Robo binding and activation *in vitro* (Howitt et al, 2004). This fact naturally begs a question – what functions do the other Slit domains possess? Slit binds heparan sulphate (HS) with high affinity and binding sites are mapped to LRR2, LRR4 and the C-terminal part of the protein (Hussain et al, 2006; Ronca et al, 2001; Seiradake et al, 2009). Some additional information can be inferred from Slit domain composition. Both LRR and EGF domains are usually found among extracellular proteins and receptors. LRR and EGF domains are known to mediate protein-protein interactions (Rothberg & Artavanis-Tsakonas, 1992). The laminin G domain is found in laminin, agrin and other extracellular matrix (ECM) proteins and thus is likely responsible for recognising and binding ECM components (Rothberg & Artavanis-Tsakonas, 1992). The C-terminal cysteine knot is an unusual structural element often shared by proteins that otherwise have very little sequence homology. They appear to be required for protein secretion and/or oligomerisation (Isaacs, 1995). Interestingly, *in vivo*, Slits are subjected to partial but specific proteolysis which separates the Robo binding LRR tandem (140 kDa N-terminal fragment, Slit-N) from laminin G and cysteine knot domains (40-60 kDa C-terminal fragment, Slit-C). The responsible proteases remain unknown, although the mechanism seems to be shared among species as different as *Drosophila* and *Bos taurus* (Brose et al, 1999; Patel et al, 2001; Wang et al, 1999; Whitford et al, 2002). The N-terminal fragment retains biological activity, however, it has far lower affinity for heparan sulphate than the full-length protein or its C-terminal part, and thus is expected to be more diffusible within tissues (Ronca et al, 2001). This led to proposals that the elaborate Slit composition coupled with proteolysis is necessary for diffusion control and gradient formation. Nevertheless, the uncleavable Slit form was able to fully rescue Slit knockout mutations in *Drosophila*, showing that at least in this system, Slit proteolysis is not critical for its functions (Coleman et al, 2010). Other experiments indicate that proteolytic Slitforms might have different biological effects. Both human Slit2 and Slit2-N can repulse axons, however only Slit2-N causes collapse of growth cones (Ba-Charvet et al, 2001). In another study, human Slit1-N failed to repel axons, yet similarly to full-length protein, was able to induce dendritic growth and branching (Whitford et al, 2002). In both cases, the mode of Slit action strongly depended on neuron type and the assay employed and since there were no systematic follow-up studies, the biological significance of Slit proteolysis remains largely unknown.

In addition to ECM binding, the complex Slit structure might be necessary for interaction with other secreted proteins or even with alternative receptors. Brose et al, 1999 reported high affinity interactions between human Slit2 and another neuron guidance molecule netrin, although the functional relevance of this observation remains unknown. Yeast two-hybrid screens revealed that Slit2 also binds a Gremlin/Drm protein (Chen et al, 2004). This protein belongs to the Dan protein family, members of which directly bind and antagonise bone morphogenic proteins (Gazzerro & Canalis, 2006). Interestingly, like Slit, Dan proteins contain a cysteine knot domain, however, the biological relevance of Slit-Gremlin binding remains vague.

The concept that Slits have additional, Robo-independent receptors cannot be discarded completely. The phenotype of the cumulative Slit1/Slit2/Slit3 knockout was considerably different from that of the Robo1/Robo2 knockout implying that Slits have Robo-independent functions (Jaworski et al, 2010). One of the candidates as an alternative Slit receptor could be a protein called Eva-1 (putative mammalian homolog is C21orf63), which was shown to bind Slit and act as its receptor/co-receptor in *C. elegans* (Fujisawa et al, 2007). The extracellular part of Eva-1 contains two carbohydrate binding lectin domains. Bioinformatical analysis predicts many putative glycosylation sites in Slits. In accordance, full-length proteins and some of the separate domains migrate more slowly on SDS-PAGE than would be expected from their molecular mass suggesting some kind of posttranslational modification (Brose et al, 1999; Rothberg et al, 1990). Furthermore, an N-acetylglucosamine residue can be identified in the crystal structure of the LRR3 domain (Morlot et al, 2007a). So it seems that Slits are heavily N-glycosylated and thus could serve as ligands for the lectin-like receptor Eva-1.

Another alternative, Robo-independent Slit signalling mechanism was suggested by Seiradake et al, 2009. They observed that, even though the Slit domain LRR4 does not bind Robo receptors, it affects axon growth in a somewhat similar way as LRR2. This effect was also HS dependent. The authors speculated that Slit was able to signal via LRR4 - syndecan interactions (Seiradake et al, 2009). However, this idea is not compatible with the finding that, while total syndecan knockout is detrimental, removal of the cytoplasmic syndecan domain does not affect Slit signalling in *Drosophila* (Chanana et al, 2009; Schulz et al, 2011).

1.3 Robos – receptors for Slit

Like Slits, Robos were first identified in *Drosophila* by a genetic screen for mutations affecting development of neuronal pathways in CNS (Seeger et al, 1993). One of

the identified mutations caused circular axon misrouting and hence was called roundabout, shortened to robo. Kidd et al, 1998a cloned and characterised the corresponding gene showing that it encodes a cell surface receptor belonging to the immunoglobulin (Ig) superfamily of cell adhesion molecules. Three different Robo genes have been identified in

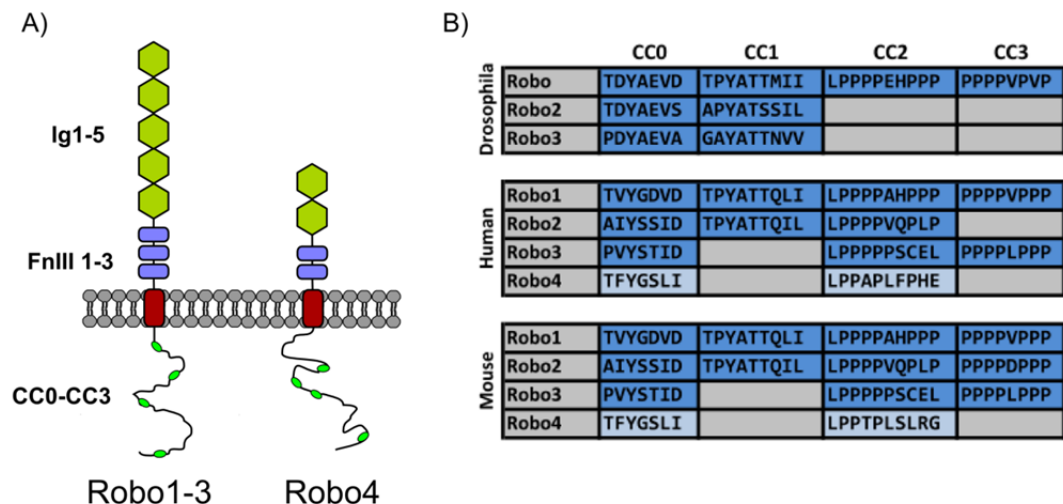


Figure 1.2 Organisation of Robo proteins

Schematic illustration of Robo structure (A) and table listing cytoplasmic fragments in different Robo proteins (B). Robo4 CC sequences are marked in a different colour because their identity is debatable. In Figure A, green colour represents Ig domains, blue - FNIII domains, brown – transmembrane domains, and dark green – conserved cytoplasmic motifs.

Drosophila (Robo, Robo2, Robo3) and four in mammals (Robo1/Dutt1, Robo2, Robo3/Rig1, Robo4/Magic Roundabout) (Huminiacki et al, 2002; Kidd et al, 1998a; Rajagopalan et al, 2000a; Simpson et al, 2000b; Sundaresan et al, 1998; Yuan et al, 1999). It must be stressed however, that those two families were created by independent duplications and invertebrate Robo2 is not an ortholog of mammalian Robo2. Typical Robo is a single pass membrane protein and contains an N-terminal tandem of 5 Ig domains followed by 3 fibronectin type III domains (FnIII), a transmembrane helix and a poorly conserved intracellular part (Figure 1.2A). The exception is Robo4 receptor which has only two Ig and two FNIII domains in the extracellular part of the protein.

Crystal structures are available for the first two Ig domains of human and *Drosophila* Robo1, however, the overall folding of Robo proteins remains unknown (Figure 1.3A) (Fukuhara et al, 2008; Morlot et al, 2007b). Some structural information can be gleaned by analysing other, better described IgCAM family members. Neural cell adhesion molecule (NCAM, 5 Ig domains and 2 FNIII domains) most likely adopts a relatively extended, rod-like form (Kulahin et al, 2011; Soroka et al, 2010). Deleted in colorectal carcinoma (DCC, 4 Ig domains and 6 FNIII domains), L1 (6 Ig domains and 5 FNIII domains) and axonin (6

Ig domains and 4 FNIII domains) form “hooks” where the linker between Ig2 and Ig3 is severely bent and Ig1 and Ig2 adjoin Ig3 and Ig4 respectively (Freigang et al, 2000; Pocock et al, 2008). An even more complicated conformation is observed in DSCAM molecule (10 Ig domains and 6 FnIII domains), which assumes a complex folded shape (Vidi et al, 2011) (Figure 1.3B, D and C respectively). Intriguingly, some structural Robo features hint at the possible overall folding of this receptor. *Drosophila* and human Ig1-Ig2 fragments adopt

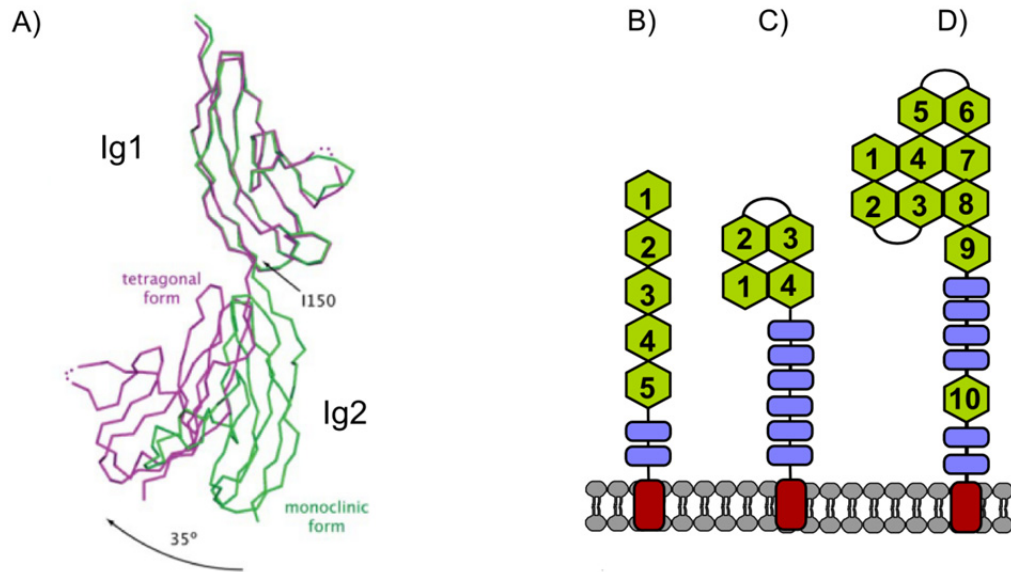


Figure 1.3 Structure of Robo Ig domains and conformations adopted by various IgCAM proteins

Human and *Drosophila* Robo1 Ig1-2 domains can be crystallised in two different conformations indicating that Robo ectodomain might adopt a non-extended structure (A). In agreement, extracellular domains of IgCAM family proteins are known to adopt several different conformations: extended like NCAM (B), “hook” like axonin (C) or complex “S” like structure like DSCAM (D). Cytoplasmic domains are omitted for clarity. Figure A was adapted from Fukuhara et al, 2008.

two different conformations during crystallisation – one is fully extended, while the other is significantly bent via an interdomain linker (Figure 1.3A) (Fukuhara et al, 2008; Morlot et al, 2007b). Moreover, the fragment of linker between Ig2 and Ig3 seen in the human Robo1 structure makes a sharp turn, which might be necessary for Ig2 packing against the Ig3 and IgCAM “hook” formation (Morlot et al, 2007b). Taking all facts into account, Robo proteins are likely to accommodate at least a partially packed, non-extended structure, which in turn might depend on receptor signalling state.

Robo receptors were shown to interact with Slit proteins genetically and biochemically by many independent studies. A partial Slit-Robo complex structure shows the second LRR domain from Slit protein binding to the first Ig domain of Robo (Figure 1.4) (Morlot et al, 2007b). This interaction mode is in a good agreement with biochemical data, which identified the same domains as determinants for Slit-Robo interaction using truncations

and deletions (Howitt et al, 2004; Liu et al, 2004). It is generally believed that structural and functional details of Slit-Robo interactions are the same for all family members, since the Slit-Robo interface consists of well conserved amino acids. This assumption is indirectly confirmed by promiscuous interactions where all Slits bind all Robos (Kd 5-50 nM) with the only exception being Robo4 (Ba-Charvet et al, 2001; Brose et al, 1999; Camurri et al, 2005). Conserved amino acids responsible for Slit binding in Robo1-Robo3 are not preserved in Robo4. While some groups observed Slits directly binding to Robo4

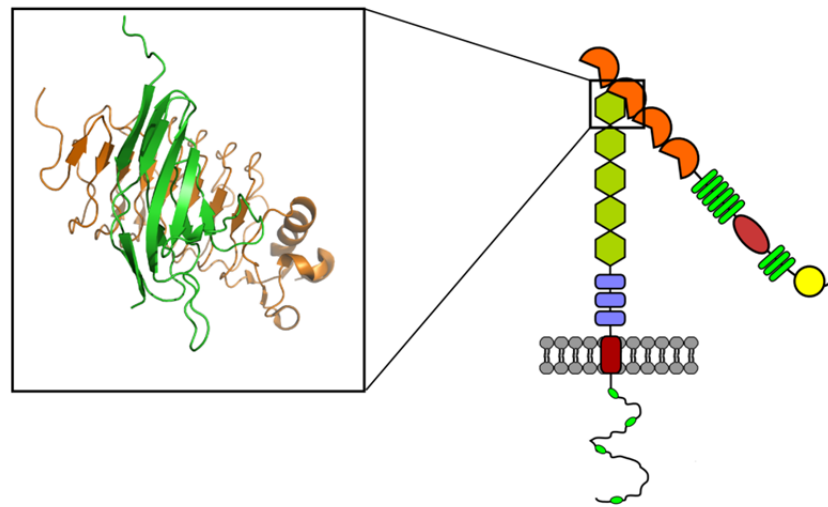


Figure 1.4 Structure of Slit-Robo complex

LRR2 domain from Slit (orange) binds Ig1 domain (green) from Robo forming signalling competent complex.

by co-immunoprecipitation (Park et al, 2003; Zhang et al, 2009), many others failed to replicate these experiments using Biacore assays (Hohenester et al, 2006; Koch et al, 2011; Suchting et al, 2005). Similarly, Sheldon et al, 2009 showed that the soluble extracellular part of Robo1, but not Robo4, was able to quench chemotactic effects of recombinant Slit2. On the other hand, functional and genetic studies demonstrate that Slit2 plays an important role in the vasculature and mammary glands by acting through the Robo4 receptor (Jones et al, 2008; Jones et al, 2009; London et al, 2010; Marlow et al, 2010). Consolidation of these observations led to a hypothesis that a co-receptor is required for Slit mediated Robo4 activation, with Robo1 and syndecans suggested for this role so far (Kaur et al, 2008; Sheldon et al, 2009).

Syndecans, or more precisely their polysaccharide chains, heparan sulphate and chondroitin sulphate, are extremely important in Slit-Robo interactions and signalling. It is well established that biochemical or genetic HS removal diminishes Slit-Robo interactions and disrupts associated biological functions *in vivo* (Hu, 2001; Johnson et al, 2004; Piper et

al, 2006; Ronca et al, 2001; Steigemann et al, 2004). Biochemical and structural data indicate that HS binds to a second LRR domain from Slit and a first Ig domain from Robo i.e. the same domains that mediate Slit-Robo interactions (Fukuhara et al, 2008; Hussain et al, 2006). Fukuhara et al, 2008 suggests that upon association, Slit and Robo form a continuous positively charged surface which in turn binds a HS chain forming a ternary complex. It appears that heparan sulphate has multiple roles in Slit-Robo signalling. First of all, as described above it might be necessary for Slit concentration and presentation. Second, it takes part in stabilising a productive signalling complex. Unexpectedly, recent genetic experiments in *Drosophila* indicate that negative syndecan Slit-Robo interactions are possible as well (Schulz et al, 2011). The authors demonstrated that the syndecan knockout phenotype in tracheal cells is caused by a gain in Slit-Robo2 signalling. How syndecan suppresses its target remains unknown. Syndecan's effects were independent of its cytoplasmic domain and thus unlikely to be mediated by signalling. The authors speculate that syndecans affect Robo levels by interfering with its delivery or retraction from the cell surface (Schulz et al, 2011). Obviously, an even bigger unanswered question is what factors determine syndecan's mode of action and its switching from enhancement to suppression.

In addition to interactions with Slit and heparan sulphate, Robo's ectodomain was recently shown to associate with other membrane proteins. Banerjee et al, 2010 demonstrated that in *Drosophila* the single pass transmembrane protein Neurexin IV displays dose dependent genetic interactions with Slit and Robo proteins. Neurexin IV knockout altered cellular Robo distribution in neurons and caused mild abnormalities in nervous system development somewhat resembling that of the Robo knockout. Biochemical experiments revealed a direct interaction between Robo and Neurexin IV. Slit appears to facilitate complex formation, but generally it was expendable and Robo-Neurexin IV binding was observed without it (Banerjee et al, 2010). The Neurexin IV cytoplasmic domain was also expendable as its ectodomain was sufficient for Robo binding and knockout phenotype rescue (Banerjee et al, 2010). Neurexin IV is a molecular component of *Drosophila* septate junctions (tight junction-like structures in invertebrates) (Baumgartner et al, 1996). Its mammalian homologue, CNTNAP2, functions in cell-cell adhesion, especially in organisation of myelinated fibers (Poliak et al, 1999; Traka et al, 2003). It is tempting to speculate that Neurexin IV is a Robo co-receptor, since weak interaction between Slit and Neurexin IV was observed in *Drosophila* embryos deficient in Robo. However, the possibility that other Robo family members were responsible for this effect cannot be

discarded and this notion of Neurexin IV as co-receptor needs further experimental scrutiny. Similarly, Hernández-Miranda et al, 2011 showed direct interactions between Robo1 and neuropilin1 in mice. The authors noticed that Robo1 deficient mouse neurons are significantly less responsive to semaphorins. Semaphorins are soluble or membrane bound extracellular proteins with very versatile functions, including axon guidance, immune response and bone development (Yazdani & Terman, 2006). Semaphorins are ligands that act through their receptor, plexin, which can also recruit neuropilins as co-receptors (Yazdani & Terman, 2006). Covasphere aggregation assays and co-immunoprecipitation studies revealed that Robo1 directly associates with neuropilin1, but not with plexin or neuropilin2. These interactions were mediated by Robo1 Ig1-Ig2 domains as deletion of this region abolished neuropilin1 binding (Hernández-Miranda et al, 2011). Finally, the extracellular Robo4 domain was suggested to act as a membrane-bound ligand *in trans* for the UNC5B receptor (Koch et al, 2011). The authors, using various biophysical, biochemical and functional tools made a compelling case for this model, however, it is difficult to believe that Robo4 is only a ligand. Robo4 retains the Robo-specific cytoplasmic tail and was demonstrated to be an active receptor in various different cells (Jones et al, 2009; Kaur et al, 2006; Sheldon et al, 2009). It is more likely that Robo4 has different modes of signalling which in turn vary between different cells. Also, Robo4 is the most diverged Robo family member, so it is unlikely that this type of interaction is present in other Robo proteins.

The intracellular part of Robo is of special interest. It is on average a 600-800 amino acids long, poorly conserved polypeptide. It has no identifiable domains, catalytic activity or even secondary structure and thus most likely is an intrinsically unstructured protein. The only defining feature of Robo's intracellular part is several short conserved stretches of amino acids, so-called conserved cytoplasmic motifs (CC). Historically, four of these are described in the literature (CC0-CC3), however close inspection of sequence alignments reveals several additional highly conserved sequence patches (personal observations). The exact composition of the CC motifs varies between different Robo proteins, indicating signalling and functional diversity within the Robo family (Figure 1.2B). Since Robo does not possess catalytic activity, it must exert its signal transduction by binding various adaptors and signalling molecules within the cell (see section 1.4.2). In this situation, a lack of rigid structure might be advantageous, as it allows greater flexibility and more variable binding partners. Binding flexibility and diversity, in fact, is one of the main

functional properties attributed to other intrinsically unstructured proteins (Dunker et al, 2008).

1.4 Slit-Robo signalling

1.4.1 Robo transmembrane signalling mechanism

One of the first questions about Slit-Robo signalling is how the single pass receptor Robo transmits signal across the cellular membrane. Receptors built from multiple transmembrane helices, like G protein-coupled receptors (GPCR) transmit signal by conformational changes where helices are shifted in relation to each other (Milligan & Smith, 2007). Single pass membrane proteins cannot undergo membrane-spanning conformational changes as a single helix is not sufficient to transmit structural changes between intracellular and extracellular domains. Many single pass receptors, like receptor tyrosine kinases (RTK) or Toll-like receptors, thus rely on changes in oligomerisation state to transmit signal across the membrane (Kang & Lee, 2011; Li & Hristova, 2010). A substantial amount of evidence indicates that Robos utilise oligomerisation for their signalling as well.

IgCAMs, as their name implies, tend to have multiple binding abilities. Homomeric protein oligomerisation, heteromeric association with other proteins, cis- as well as trans-interaction with receptors from other cell surfaces are all reported for members of this family. Robos do not make an exception. Covasphere aggregation assays, where fluorescent beads are coated with protein of interest and their aggregation is directly observed with microscope, demonstrated that extracellular parts of human Robo1, Robo2 and Robo3 are homomeric molecules which in addition can form heteromeric complexes (Camurri et al, 2005; Hernández-Miranda et al, 2011; Hivert et al, 2002). Robo1 also interacts with Robo4, as they can be co-precipitated and Robo4 can retain Robo1 in intracellular vesicles of COS-7 cells (Kaur et al, 2008; Sheldon et al, 2009). On the other hand, Biocore assays failed to detect any Robo1-Robo4 ectodomain interactions (Koch et al, 2011; Suchting et al, 2005). Using gel filtration and native PAGE, Yoshikawa et al, 2008 showed that the extracellular Robo4 domain is an oligomer and exists as a dimer or even trimer *in vitro*. Attempts to identify determinants responsible for homophilic Robo interactions were inconclusive, with data indicating that mammalian Robo-Robo binding might be driven by multiple and redundant sites (Liu et al, 2004). In *Drosophila*, multimerisation was observed for Robo2 but not for Robo. Chimeric Robo-Robo2 constructs with swapped Ig domains revealed that oligomerisation is driven by the Robo2 Ig3-Ig5 fragment (Evans & Bashaw, 2010).

Based on parallels with other IgCAM family members, one might expect that Robos are capable of association in trans. Unfortunately, information about this type of interaction is scarce. Several different genetic and functional studies imply Robo interactions with Slit adsorbed on the other cell surface or even formation of a Robo-Slit-Robo sandwich (Kraut & Zinn, 2004; Strickland et al, 2006). Others were able to observe Slit independent Robo functions and argued that this observation might be explained by Robo-Robo interactions in trans (Parsons et al, 2003).

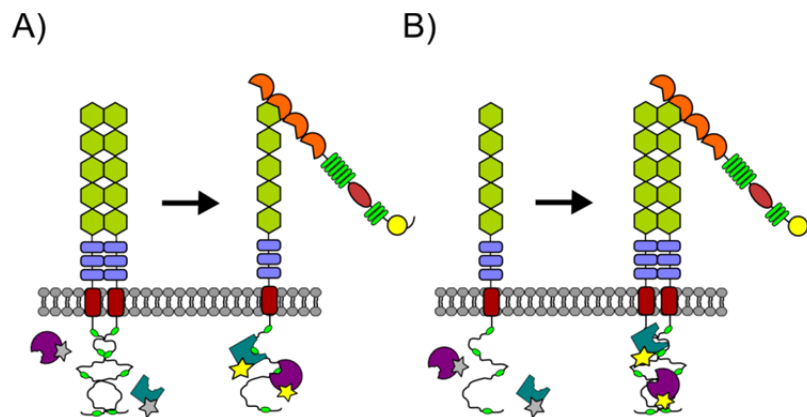


Figure 1.5 Putative Robo transmembrane signaling mechanisms

Robo transmembrane signaling is likely achieved by changes in receptor oligomerisation state. Slit binding may induce oligomer dissociation (A) or monomer association (B) which in turn enables recruitment of signaling molecules within the cell. Dimers are depicted for clarity, but higher order oligomers are possible as well.

Association of Robo cytoplasmic regions was reported as well, although information about it is much more limited. GST pulldown experiments showed that *Drosophila* Robo and Robo2 C-terminal domains can form homo- and heteromers with homophilic interactions being preferred (Simpson et al, 2000b). Kaur et al, 2006 also mentioned oligomerisation of the mammalian Robo4 C-terminal domain which was observed by some third party, however, remained unpublished.

All experimental data strongly indicate that Robo receptors are capable of oligomerisation, so one can argue that Robos transmit signalling across the cellular membrane by changing their oligomerisation state (Hohenester, 2008). Binding of Slit is proposed to cause dissociation or association of Robo molecules, which in turn allows recruitment of downstream signalling molecules by Robo's cytoplasmic tail. A somewhat similar mechanism where a ligand, called netrin, induces receptor oligomerisation has been suggested for another IgCAM family member, DCC (Mille et al, 2009; Stein et al, 2001). Currently it is unclear which oligomerisation state corresponds to activated receptor in the case of Robo and experimental data suggests different conclusions. First of all, it seems

that in many of the cases described above, Robo homophilic interactions were observed in the absence of Slit. These observations directly support a model where inactive Robo exist as an oligomer which dissociates upon Slit binding. On the other hand, Robo constructs lacking their cytoplasmic domain display dominant-negative behaviour (Bashaw & Goodman, 1999; Hammond et al, 2005; Hocking et al, 2010; Jia et al, 2005). Given that this effect is achieved at a functional level and not via secondary effects, such as protein retention or increased degradation, it would mean that a Robo heterodimer consisting of truncated and full-length forms is functionally deficient. This observation is more compatible with a model where Slit induces Robo oligomerisation.

Several independent groups have created and used Robo constructs where either an intracellular or extracellular Robo segment was exchanged with that of the other receptor. Bashaw & Goodman, 1999 created Frazzled (extracellular part) – Robo (intracellular part) and Robo (extracellular part) – Frazzled (intracellular part) hybrids. Frazzled (Fra) is another IgCAM molecule, DCC-like netrin receptor in *Drosophila* which mediates attraction in neurons. The authors successfully achieved reversal of function as Fra-Robo was acting as a repulsive receptor for netrin, while Robo-Fra was acting as an attractive Slit receptor in *Drosophila* embryos. This total exchangeability of intracellular and extracellular parts between Fra and Robo would imply identical transmembrane signalling mechanisms. Frazzled closely resembles DCC both in sequence and domain composition, so one could expect that it follows the activation via oligomerisation mechanism suggested for DCC. This in turn would indicate that Robo's active form is oligomeric. On the other hand, it is worthy noting that Bashaw & Goodman, 1999 used Robo for chimera creation, a receptor which according other papers is not capable of dimerisation (Evans & Bashaw, 2010).

Similarly, Stein & Tessier-Lavigne, 2001 created mammalian Met-Robo1 and trkA-Robo1 chimeras, where Robo's extracellular part was exchanged with extracellular domains of hepatocyte growth factor receptor (Met) or nerve growth factor receptor (trkA). Both Met and trkA are tyrosine kinase receptors responding to hepatocyte growth factor (HGF) or nerve growth factor (NGF) respectively. Neuron growth cones normally do not respond to HGF or NGF, however neurons expressing Met-Robo1 and trkA-Robo1 showed clear repulsive responses to HGF or NGF (Stein & Tessier-Lavigne, 2001). Analogous experiments were also repeated with a trkA-Robo4 chimera in HEK 293 cells. NGF acting via trkA-Robo4, like Slit2 acting via native Robo4, was able to abrogate HEK 293 cell migration towards serum (Park et al, 2003). It is generally accepted that tyrosine kinase

receptors are mediating their signalling by ligand-induced dimerisation or oligomerisation (Li & Hristova, 2010). Since RTK-Robo chimeras were acting in a similar way to full length Robo, one can argue that Robos, like RTK, are undergoing ligand induced oligomerisation.

In summary, while there is little doubt that Robos oligomerise, current experimental data do not clearly favour any of the possible transmembrane signalling models. Ligand-induced Robo dissociation is more supported by direct evidence, as Robo extracellular domains multimerise independently from Slit. On the other hand, many indirect experiments point towards Robo activation by ligand-induced oligomerisation. Clearly, further biochemical and biophysical studies are necessary to resolve this question.

1.4.2 Robo downstream signalling

As mentioned above, Robo receptors do not possess any catalytic activity. From the very beginning it was assumed that Robo signals by recruiting adaptors and other signalling proteins (Figure 1.6). Their unusual, intrinsically unstructured C-terminal domain implies promiscuous and flexible interactions and experimental data more than confirms this picture. Here I will review Robo interacting cytoplasmic proteins and related signalling pathways.

1.4.2.1 Rho family GTPases

Small Rho family GTPases such as RhoA, Rac1 and Cdc42 have emerged as one of the main Slit-Robo signalling effectors. These proteins are key regulators of the actin cytoskeleton and cell movement. Small Rho family GTPases can switch between an active GTP-bound form and an inactive GDP-bound form. The cycling of Rho GTPases between these two states is regulated by guanine nucleotide exchange factors (GEFs) and GTPase-activating proteins (GAPs). GEFs activate GTPases by stimulating release of guanosine diphosphate (GDP) to allow binding of guanosine triphosphate (GTP) while GAPs work to accelerate GTP hydrolysis and thus deactivate GTPases. Twenty different small Rho family GTPases are identified, however GEF and GAP families contain more than 70 members each (Hall, 2005; Heasman & Ridley, 2008). Whilst initially it was believed that each member of small Rho family GTPases' is tailored to a specific function, new data reveal a much more complex picture. It seems that GTPases form spatially and temporally overlapping subcellular pools, where the functional outcome is decided by crosstalk between different Rho GTPases and integration of signals from multiple GEFs and GAPs (Pertz, 2010). This aspect of Rho GTPases is well reflected in Slit-Robo

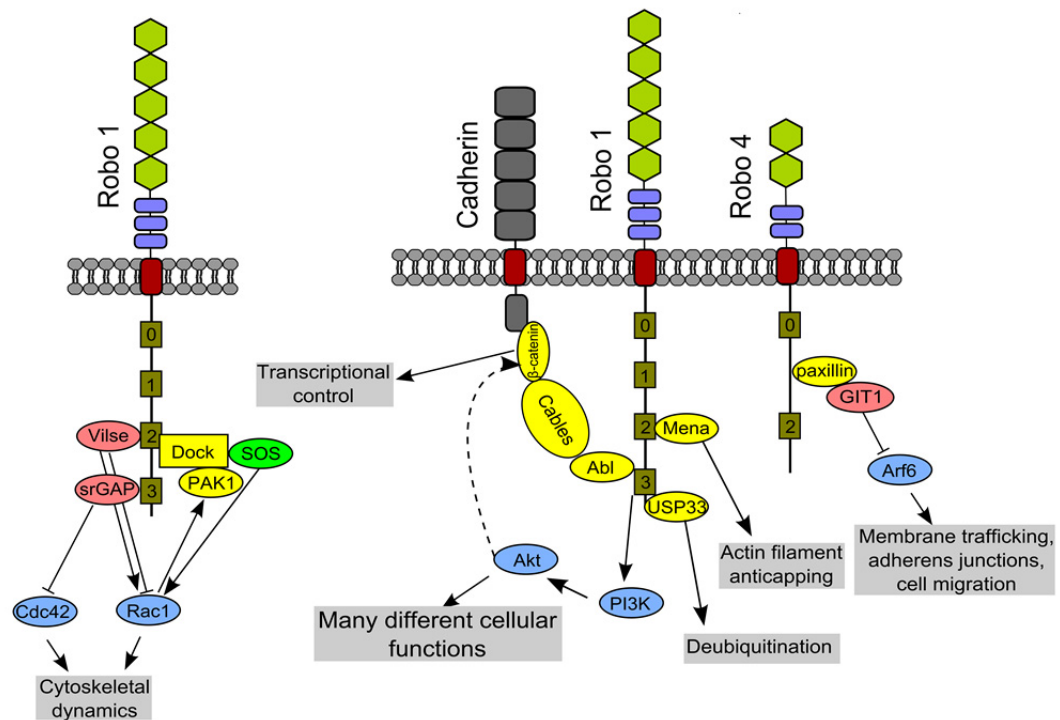


Figure 1.6 Robo downstream signalling

Experimental evidence indicates that Robo receptors control various different aspects of cell functions via Rho family GTPases (see subsection 1.4.2.1), PI3K (see subsection 1.4.2.2), cadherins and β -catenin (see subsection 1.4.2.3), paxillin (see subsection 1.4.2.5) and other molecules described in section 1.4.2

signalling, where Slit acting through the Robo is able to both activate and sequester their activity.

Wong et al, 2001 were first to elucidate a signalling cascade between Robo1 and Rho GTPases. Using Robo1 cytoplasmic domain as bait in a yeast two-hybrid screen they identified a novel family of GAP proteins and called them Slit-Robo GAPs (srGAP). In HEK293 cells, treatment with Slit2 increased srGAP1 binding to Robo1 CC3 motif and caused Cdc42 inactivation. Slit2 also caused activation of Rac1, but this effect was independent from srGAP1 and likely mediated by another pathway (Wong et al, 2001).

Two independent studies revealed another Robo binding GAP protein called Vilse (also known as CrossGAP, CrGAP or ARHGAP39). It binds Robo's CC2 fragment and takes part in regulating Rac1 activity in *Drosophila* (Hu et al, 2005; Lundström et al, 2004). Both studies used genetic tools to elucidate Robo-Vilse signalling details with great success but opposite results. Overexpression of Vilse reduced the severity of the Robo knockout phenotype in *Drosophila* trachea cells, which indicates that Robo acting through Vilse downregulates Rac1 activity (Lundström et al, 2004). On the other hand, overexpression of Vilse in neurons exacerbated the Robo knockout phenotype which

implies that in this particular case, Robo sequesters Vilse to activate Rac1 (Hu et al, 2005). The mechanism behind differential Vilse effects in different cells remains unknown.

GEF proteins are also utilised by the Slit-Robo signalling axis. Incubation with Slit caused recruitment of a GEF protein called Son of sevenless (Sos) to Robo and subsequent Rac1 activation in HEK 293 cells (Yang & Bashaw, 2006). Genetic disturbance of Sos interfered with Robo's functions as an axon guiding molecule, confirming the biological relevance of this signalling pathway in *Drosophila* (Yang & Bashaw, 2006). Sos does not bind Robo directly, instead an adaptor protein Dock (also known as Dreadlock, the mammalian homologue is called Nck) mediates Slit-dependent interactions between them. Deletion of Robo's CC2 or CC3 motif reduced Dock binding, however only the combined removal of CC2 and CC3 was able to abolish binding completely. While interacting with Robo, Dock also recruits the serine/threonine-protein kinase PAK1, which is the main effector of Rac1 and Cdc42 (Fan et al, 2003). One can expect that these interactions are preserved in mammals as well, since it was demonstrated that the mammalian Dock homolog Nck is able to bind Robo1 and Robo2 and is necessary for Slit-Robo functions in rodent neurons (Round & Sun, 2011).

Yeast two-hybrid screening and complementary biochemical experiments showed that Robo4 cytoplasmic domain directly interacts with Wiskott–Aldrich Syndrome Protein (WASP) and its more widely expressed homolog, neural WASP (NWASP) (Sheldon et al, 2009). Additionally, WASP was implicated in Robo4 induced HEK 293 migration (Kaur et al, 2006). WASP is a well known player in actin cytoskeleton regulation. It mediates signalling between Cdc42 and the Arp2/3 complex, which initiates polymerisation and branching of actin filaments. WASP/NWASP is well positioned to serve as a Robo4 effector, but unfortunately, no further structural and functional details are currently available.

Taking all these findings into account, it looks like Robo itself can act as a platform that recruits a whole range of Rho GTPase modulators and downstream effectors, often with opposing functions (Figure 1.6). We are only beginning to unravel this complex knot of interactions and it would be very interesting to see how these promiscuous bindings are regulated and integrated.

1.4.2.2 PI3K and Akt

The phosphoinositide 3-kinase (PI3K) pathway regulates an extraordinarily diverse group of cellular functions: cell proliferation, differentiation, motility, survival and intracellular

trafficking (Vivanco & Sawyers, 2002). This pathway is extremely complex, with many branches and feedback loops and a full description of it is beyond the scope of this text. The core of the pathway consists of PI3K and a serine/threonine protein kinase called Akt. In response to external stimuli, PI3K activates Akt by causing its phosphorylation via secondary messengers. In turn, Akt may phosphorylate many different targets around the cell.

More and more evidence is emerging that the PI3K – Akt pathway is modulated by Slit-Robo signalling. It seems that Robo directly interacts with PI3K as treatment with Slit2 induced Robo1 and p85 (one of the PI3K subunits) co-immunoprecipitation in eosinophils (Ye et al, 2010). Recombinant Slit2 inhibited Akt phosphorylation in breast cancer cells, Jurkat cells (T lymphocyte like cells) and myoepithelial cells (Macias et al, 2011; Prasad et al, 2004; Prasad et al, 2007). Similarly, overexpression of Slit2 caused reduction of Akt phosphorylation in breast cancer cells (Prasad et al, 2008) while knockdown led to increased phosphorylation in lung cancer cells (Tseng et al, 2010). On the other hand, incubation with Slit2 activated PI3K in HUVEC cells and PI3K inhibitors were able to disrupt Slit2 induced attraction and tubulogenesis in HUVEC cells (Wang et al, 2003). Likewise, treatment with Slit2 promoted angiogenesis through mTORC2-dependent activation of Akt, while PI3K and Akt inhibitors significantly impaired pro-angiogenic Slit2 effects in primary vascular endothelial cells (Dunaway et al, 2011). What factors determine these differential interactions between Slit-Robo and PI3K-Akt remain unknown.

1.4.2.3 *Abl, Wnt and Cadherins*

Multiple studies show interactions between Slit-Robo and Wnt signalling pathways. The Wnt pathway is primarily known for its role in development and cancer, but is also involved in normal physiological functions of the adult organism (Logan & Nusse, 2004). In the resting state epithelial cell β -catenin is bound by cadherins at the adherens junctions where it links cadherins to the actin cytoskeleton. Free β -catenin is bound by a multiprotein degradation complex, one component of which is glycogen synthase kinase 3 (GSK3 β). GSK3 β phosphorylates β -catenin and triggers its ubiquitination and degradation thus keeping the concentration of free cytoplasmic β -catenin low. Wnt ligand acting via the Frizzled receptor inactivates the degradation complex and causes accumulation of cytoplasmic β -catenin. β -catenin is eventually translocated to the nucleus where it activates the LEF1/TCF transcription factor and stimulates expression of target genes (Logan & Nusse, 2004).

Slit-Robo signalling appears to modulate the Wnt pathway in several different ways. The cytoplasmic tyrosine kinase Abl was the first identified link between Slit-Robo and Wnt signalling pathways. Abl binds to the CC3 motif and is able to phosphorylate several different tyrosine residues in the human Robo1 cytoplasmic domain (Bashaw et al, 2000). These modifications were directly detected only when Robo-expressing cells were co-transfected with a constitutively active Abl form, however genetic and functional studies indicate that Abl mediated Robo phosphorylation antagonises Robo activity in *Drosophila* and thus likely is biologically relevant (Bashaw et al, 2000). Abl appears to associate with Robo independently of Slit binding (Rhee et al, 2002). However, upon binding Slit, the Robo-Abl complex recruits the scaffold protein Cables, which in turn associates with N-cadherin-bound β -catenin. This results in Abl-mediated phosphorylation of β -catenin and its transportation to the nucleus (Rhee et al, 2007; Rhee et al, 2002). In this way the Slit-Robo signalling axis achieves a twofold effect. First of all, loss of β -catenin should lead to rapid loss of N-cadherin mediated cell adhesion. Indeed, Robo antagonises E-cadherin adhesion during *Drosophila* heart lumen formation (see section 1.5.2) (Santiago-Martínez et al, 2008). Second, Slit induced β -catenin translocation to the nucleus causes transcriptional activation via the classical Wnt pathway and thus might induce long term effects on cellular functions (Rhee et al, 2007).

Interestingly, many independent studies report an alternative intersection of Slit-Robo and Wnt signalling pathways with directly opposing effects to those reported by Rhee et al, 2007. In breast and lung cancer cells Slit2, acting via the PI3K and Akt pathway described above, activated GSK3 β by reducing its phosphorylation. In turn this led to increased β -catenin phosphorylation and destruction, augmented association between β -catenin and E-cadherin and stronger E-cadherin mediated adhesion (Prasad et al, 2008; Tseng et al, 2010). Similarly, another study with primary and immortalised basal myoepithelial cells showed that Slit2 induces β -catenin redistribution from nuclear to cytosol/membrane fractions (Macias et al, 2011). Although not addressing Slit-Robo and Wnt interplay directly, in agreement with these observations, many authors also noted that Slit-Robo signalling stabilises cadherins in the cellular membrane (London et al, 2010; Shiau & Bronner-Fraser, 2009; Stella et al, 2009).

At this point it would seem that positive Slit-Robo signalling effects on cadherin functions are observed more often than negative. Factors determining these different modes of action remain unknown. Since in some cases Slit-Robo proteins had no observable effects on N-cadherin or β -catenin (Yiin et al, 2009), it is tempting to speculate that the presence or

correct localisation of signalling intermediates channels Slit-Robo signalling in one or the other direction.

Additionally, it appears that Robo and cadherins have more intricate, possibly Wnt pathway unrelated interactions. Bauer et al, 2011 showed that in an oral squamous cell carcinoma cell line, overexpression of P-cadherin increased expression and secretion of Slit2, but not other Slit proteins. This indicates transcriptional feedback loops between cadherin and the Slit-Robo signalling axis and adds yet another layer of complexity.

1.4.2.4 Mena

Kidd et al, 1998a noticed that the Robo intracellular sequence contains a potential binding site for a *Drosophila* protein called Enabled (also known as Ena, three homologs are identified in mammals: Mena, VASP and Evl). Consequently, the same group showed that in *Drosophila* Ena genetically and biochemically interacts with Robo. They identified CC2 as the main Ena binding site, however others might exist as well, since a construct lacking CC2 was able to retain some Ena binding capability and repulsive activity (Bashaw et al, 2000). In agreement with these data, Ena co-localisation with Robo was observed during heart lumen formation in *Drosophila* (Santiago-Martínez et al, 2008). Vertebrate Robo4 also directly interacts with Mena (Jones et al, 2009; Park et al, 2003). Other vertebrate Robo family members are thought to bind Mena as well since they all contain the CC2 motif. Mena family proteins usually are concentrated at focal adhesion points, the edge of the lamellipodium and the tips of filopodia of migratory cells. Some unresolved questions remain, but at the molecular level Mena proteins are generally attributed actin anti-capping functions i.e. they enable actin filament extension even in the presence of high local concentration of capping proteins (Bear & Gertler, 2009). At the functional level, Mena has important roles in morphogenesis, axon guidance and cell migration. Therefore, this protein family is perfectly positioned to serve as Robo effectors. Unfortunately, little is known about Mena functions in the context of the Slit-Robo signalling axis. In *Drosophila* and *C. elegans*, Ena binding to Robo was necessary for the repulsive effects of the receptor, however there was no obvious relation between Robo interactions with Slit and Ena recruitment (Bashaw et al, 2000; Yu et al, 2002). There is a possibility that Ena is constantly associated with Robo and that the receptor functions as a heterocomplex. On the other hand, Fan et al, 2003 reported a weak but repeatable correlation between cell treatment with Slit and Robo-Ena association. Either way, signalling pathways employed downstream of Robo-Ena/Mena remain unknown.

1.4.2.5 Arf6

A yeast two-hybrid screen with the Robo4 cytoplasmic domain as bait identified the adaptor protein Hic-5 as a potential Robo4 interacting protein (Jones et al, 2009). Hic-5 is a paralogue of the better described paxillin and since both proteins were immunoprecipitated by the Robo4 cytoplasmic tail, further studies were focused on paxillin. Full length Robo4 was able to immunoprecipitate paxillin only after treatment with Slit2 protein. The Robo4 region responsible for paxillin binding was broadly identified as a stretch of 35 amino acids between CC0 and CC2 (Jones et al, 2009). This region is poorly conserved in other Robo family members, so paxillin binding to other Robo proteins remains unknown, even doubtful. Paxillin is able to recruit GIT1 protein which acts as a GTPase-activating protein for ADP-ribosylation factor 6 (Arf6). This Paxillin-GIT1-Arf6 module is utilised by several different signalling systems and plays a crucial role in membrane traffic, adherens junction turnover and epithelial cell migration (Nishiya et al, 2005). Slit2 treatment reduced Arf6 activity in endothelial cells and these effects were dependent on Robo4-paxillin-GIT1 interactions (Jones et al, 2009). VEGFR and integrin signalling promotes activation of Arf6, therefore the authors suggested a model where Slit2 stimulates recruitment of a paxillin–GIT1 complex to the cytoplasmic tail of the Robo4 receptor, causing local inactivation of Arf6 and intersection of pro-angiogenic VEGFR and integrin signalling (Jones et al, 2009). In agreement with this model, a recent study observed that Slit2 reduced Arf6 activation and had anti-angiogenic effects in mice corneas with virus-induced keratitis (Mulik et al, 2011).

1.4.2.6 USP33

A yeast two-hybrid screen has also demonstrated that the Robo1 cytoplasmic tail recruits ubiquitin specific protease 33 (USP33/VDU1). Further biochemical studies showed that USP33 binds to the Robo1 CC3 fragment and Slit2 has no observable effect on this interaction (Yuasa-Kawada et al, 2009a; Yuasa-Kawada et al, 2009b). USP33 is a deubiquitinating enzyme which protects proteins from proteosomal degradation and regulates receptor trafficking. USP33 together with USP20 removes ubiquitination from the β 2 adrenergic receptor, inhibits its lysosomal trafficking and promotes recycling and resensitization of the receptor (Berthouze et al, 2009; Li et al, 2002). Relatively little is known about endogenous Robo ubiquitination and its biological relevance, as it was only detected after Robo1 and ubiquitin ligase were contranfectured into HEK 293 cells (Yuasa-Kawada et al, 2009b). However, it was demonstrated that USP33 is necessary for Slit-Robo mediated inhibition of breast cancer cell migration and the collapse of neuron growth cones (Yuasa-Kawada et al, 2009a; Yuasa-Kawada et al, 2009b). Microscopy and biotin

labelling experiments showed that Slit2 induced USP33 dependent Robo1 receptor redistribution from vesicles to plasma membrane in the breast cancer cell line MDA231 (Yuasa-Kawada et al, 2009a). Similarly, knockdown of USP33 in neurons reduced Robo1 level in plasma membrane, but only if cells were stimulated with Slit2 (Yuasa-Kawada et al, 2009b). The authors argued that USP33 may protect Robo1 from degradation or facilitate its recycling from endocytic vesicles. Contrary to these observations and speculations, proteosomal inhibitors had no effect on Slit2 induced retinal growth cone collapse (Piper et al, 2006). Further studies and independent confirmation are necessary to establish the role of ubiquitination in Slit-Robo signalling. This topic is of particular importance, since currently little is known Robo1 desensitisation.

1.5 Slit-Robo biological functions

1.5.1 Development and wiring of nervous system

The Slit-Robo signalling axis most likely first emerged as a mechanism to control neuronal migration and guide axon projections in bilateral organisms. Bilateral organisms can be divided into two mirror image halves by a longitudinal axis of symmetry. The same virtual axis in the central nervous system (CNS) is called the midline and it is an important part of its organisation. Axons that cross the midline and link two sides of the nervous systems are called commissural axons. They are crucial for transferring sensory information and organising co-ordinated motor responses. Crossing the midline poses a challenge for neuron growth cones, since initially they must be attracted to the midline and then that attraction switched to repulsion to prevent re-crossing. A series of elegant studies established the mechanism behind midline crossing for *Drosophila* and mice and in both cases Slit-Robo proteins were an essential part of it (Figure 1.7).

Midline glial cells express Slit and netrin proteins. Netrin acts via the DCC receptor to attract commissural growth cones. Meanwhile, premature repulsive effects of Slit are evaded by downregulating cell surface Robo. In *Drosophila*, a protein called comm sorts Robo from the Golgi into endosomes not allowing it to reach the growth cone. After crossing the midline, an unknown mechanism downregulates the expression level of comm, Robo reaches the cell surface and makes axon growth cones sensitive to repellent Slit (Keleman et al, 2002; Kidd et al, 1998b). Midline crossing in vertebrates follows basically the same mechanism, where Robo activity is downregulated before and upregulated after crossing the midline. Vertebrates, however, do not have a known comm protein orthologue and employ a different mechanism to control the temporal and spatial activity of Robo. Chen et al, 2008 demonstrated that two differently spliced Robo3 forms

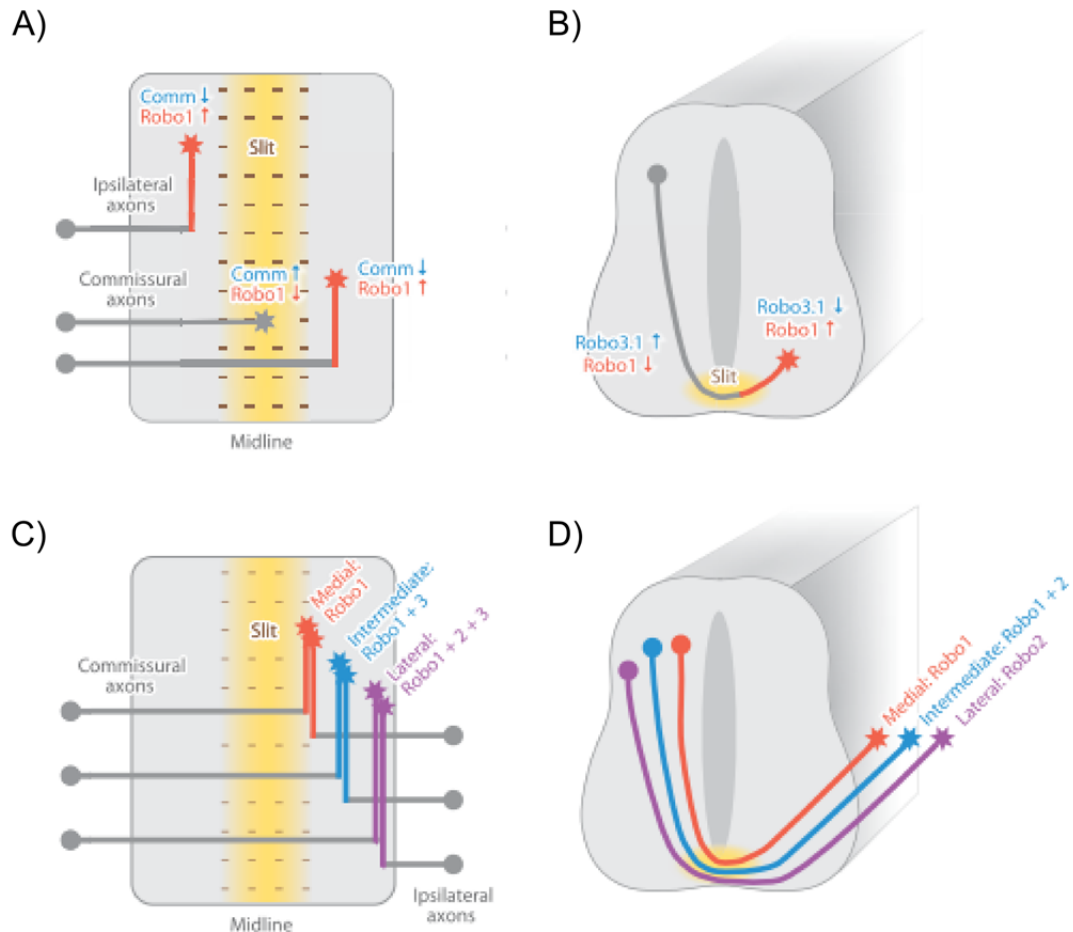


Figure 1.7 Slit-Robo role in midline crossing and longitudinal tract formation

Schematic view of midline crossing by axons and longitudinal tract positioning in *Drosophila* (A and C) and vertebrates (B and D). In *Drosophila*, Slit expressed by midline repels Robo expressing neuron growth cones thus preventing axons crossing into the opposite side. Commissural axons express protein comm which downregulated Robo at the cell surface and thus enables midline crossing. Midline re-crossing in these axons is prevented by downregulation of comm and consequent Robo delivery to the cell surface (A). In mammals midline crossing is regulated by Robo3.1, an alternative Robo3 splicing form. In commissural axons it antagonises Robo1 and thus allows successful crossing of the midline. When growth cone reaches the opposite side, Robo3.1 is downregulated removing Robo1 inhibition and thus preventing midline re-crossing (B). After crossing the midline both mammals and *Drosophila* axons are sorted into different longitudinal tracts which occupy specific positions in relation to the midline: medial, intermediate and lateral (C and D). "Robo code" hypothesis suggests that axons are sorted into these tracts according to expressed Robo type. Alternatively, it was suggested that total cumulative concentration of Robo, but not the type of Robo, determines axon sorting into longitudinal tracts. Figure taken from de Wit et al, 2011.

are expressed in commissural neurons. Robo3.1, which differs from Robo3.2 by a dozen amino acids at the very end of the C-terminal domain, is expressed before crossing the midline. Robo3.1 blocks Robo1 and Robo2 activity thus negating repulsive functions of Slit. When the midline is crossed, neurons switch to Robo3.2 expression, which appears to cooperate with Robo1 and Robo2 in sensing Slit repulsion (Chen et al, 2008; Sabatier et al, 2004). Moreover, in the presence of Slit2, Robo1 binds to the DCC receptor and abolishes netrin-induced attraction, further facilitating repulsion and

preventing midline recrossing by commissural axon growth cones (Stein & Tessier-Lavigne, 2001).

After crossing the midline, commissural axons turn longitudinally and extend in parallel to the midline forming so called longitudinal axon tracts. Within these tracts axons are organised into discrete threads which occupy specific positions in relation to the midline: medial, intermediate and lateral. Experimental evidence strongly indicates that axon sorting into these specific threads is achieved through Slit-Robo signalling (Figure 1.7B and D). In *Drosophila*, longitudinal axons have a striking Robo expression pattern: medial axons express only Robo, intermediate axons express Robo and Robo3 while lateral axons express all three Robos (Rajagopalan et al, 2000b; Simpson et al, 2000a). These observations led to the so called “Robo code” hypothesis according to which Robo homologues have differential Slit binding and/or downstream signalling and thus, by acting in combination are able to sort axons into different longitudinal threads. Genetic gain- and loss-of function studies strongly support this model. Robo3 knockout in *Drosophila* caused axons to shift from intermediate into the medial zone. Similarly, heterologous expression of Robo3 shifted medial axons into more lateral pathways (Rajagopalan et al, 2000b; Simpson et al, 2000a). However, two recent papers cast serious doubt over the “Robo code”. Spitzweck et al, 2010 directly demonstrated the irrelevance of the “Robo code” by generating and analysing a series of “Robo swaps”, where each of the three Robo receptors was expressed from three different robo loci. It turned out that Robo is essential and cannot be substituted by either Robo2 or Robo3 when it comes to preventing midline re-crossing. However, the choice of longitudinal pathway does not depend on Robo subtype, since knocking in either Robo or Robo2 into the Robo3 locus completely rescued the longitudinal phenotype of Robo3 knockout *Drosophila* (Spitzweck et al, 2010). Similarly, Evans & Bashaw, 2010 showed that overexpression of Robo3 or Robo2, in the background of double Robo/Robo2 or Robo/Robo3 knockout respectively, is sufficient to shift axons laterally. These observations also argue against a combinatorial “Robo code”. Overall, these results are more compatible with a model where the longitudinal pathway is specified by the total Robo level, with higher combined receptor expression driving axons further away from the midline.

The majority of our knowledge about the role of Robo in lateral axon positioning comes from *Drosophila* because of their simpler anatomy and the availability of genetic tools. Nevertheless, several studies hint that Robos fulfil a similar role in vertebrates. In Robo1 knockout mouse embryos, the medial axon threads are reduced and the dorsal threads are

thicker, suggesting a lateral shift of the Robo2 expressing axons. Conversely, in Robo2 knockout embryos, the medial threads are thicker, and the dorsal are thinner, indicating a medial shift of Robo1 positive axons (Long et al, 2004). Finally, chick commissural axons that misexpress Robo2 fail to cross the midline and preferentially adopt a longitudinal pathway (Reeber et al, 2008).

In addition to commissural axon guidance during midline crossing, Slit-Robo control general axon targeting within the CNS. They are responsible for proper axon path finding in the visual systems of the *Drosophila*, zebrafish and mice (Fricke et al, 2001; Hutson & Chien, 2002; Pappu et al, 2011; Plump et al, 2002; Tayler et al, 2004). Another part of the CNS with a well described Slit-Robo role is the olfactory system. In *Drosophila*, distinct subtypes of olfactory axons express unique combinations of Robo proteins and thus are targeted to different positions in the olfactory lobes (Jhaveri et al, 2004). In mice, Slit and Robo gradients “sort” axons expressing the same odorant receptor and force them to converge on the same glomerulus (Cho et al, 2007; Cho et al, 2009; Nguyen-Ba-Charvet et al, 2008). At least in *Drosophila*, Slit-Robo also guide neuron wiring outside the CNS. In combination with netrin/Frazzelled they target motoneuron dendrites to their respective muscle field (Brierley et al, 2009; Mauss et al, 2009).

All Slit-Robo functions described so far were related to axon growth cone guidance. However, ample evidence exists that Slit-Robo signalling is able to control migration of neuronal cells. Slit-Robo control cortical interneuron migration as Robo1 knockout mice embryos had substantially higher numbers of migratory interneurons in their cortex (Andrews et al, 2008; Andrews et al, 2006; Andrews et al, 2007). Likewise, olfactory bulb interneuron migration relies on repulsive Slit activity (Hu, 1999). Interestingly, Kaneko et al, 2010 suggests that Slit expressed by migratory neurons helps to clear a path from Robo-expressing glia. This leads to formation of so called “glia tubes” which facilitate migration of young neuron chains (Kaneko et al, 2010).

1.5.2 Muscular and cardiac system development

Slit and Robo proteins are not restricted to the nervous system. They are expressed in a wide variety of tissues and organs suggesting additional roles to those during nervous system development. The first evidence that Slits and Robos have additional functions came from studies in *Drosophila* myoblast migration. The midline source of Slit in fly embryos repels Robo-expressing myoblasts from the midline, but after a while, the same cells change their behaviour and require Robo to extend toward Slit expressing muscle attachment sites (Kidd et al, 1999; Kramer et al, 2001). This switch possibly plays an

essential role in the generation of muscular architecture, however the mechanism behind the switch remains unknown. Subsequently, Halperin-Barlev & Kalcheim, 2011 demonstrated that the Slit-Robo signalling axis takes part in organising the avian muscular system. Vertebrate muscles develop from somites, transient epithelial structures which further develop into dermomyotome and sclerotome. The earliest muscle progenitors, called pioneer myoblasts, arise from somites and engage in complex migration which lays down the pattern for further waves of myoblast migration and muscle development. Pioneer myoblasts express Robo2, whereas the dermomyotome and caudal sclerotome express Slit1. Knocking down either Robo2 or Slit1 with RNAi interfered with pioneer myoblast migration and subsequent muscle fibre formation (Halperin-Barlev & Kalcheim, 2011). Given these remarkable functional similarities between *Drosophila* and birds, one

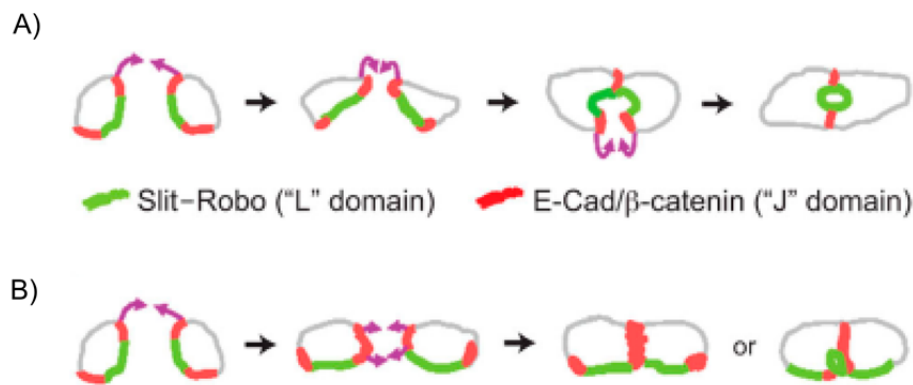


Figure 1.8 Heart lumen formation in *Drosophila*

In wild type *Drosophila* adjacent cardioblasts fuse together via E-cadherin expressing cell surface domains. Slit-Robo proteins prevent full fusion and enable lumen formation (A). If Slit-Robo signalling axis is deficient, no lumen or small ectopic lumen is formed (B). Figure taken from Helenius and Beitel, 2008.

can expect that mammalian muscle development involves similar mechanisms.

The Slit-Robo axis also plays an important role in the development of the heart. In *Drosophila*, the heart is formed by two bilateral groups of heart precursor cells which migrate towards the midline of the embryo and then fuse to form a linear heart tube. Several independent studies, albeit with some contradictory details, revealed that proper migration, alignment, polarisation and fusion of these precursor myoblasts depends on Slit, Robo and Robo2 proteins (MacMullin & Jacobs, 2006; Qian et al, 2005; Santiago-Martínez et al, 2006). At the end of this migratory phase, heart precursor cells acquire a concave shape with Slit-Robo proteins accumulated on the concave surface (Figure 1.8). Adhesive E-cadherin interactions seal opposing myoblast edges, while repulsive Slit-Robo

signalling prevents total cell-cell fusion and prevents the newly formed lumen from complete closure (Santiago-Martínez et al, 2008; Medioni et al, 2008).

The early stages of *Drosophila* heart formation are similar to those of vertebrates and given the strongly conserved Slit-Robo role in neuron guidance, one can expect that chordate heart formation involves Slit-Robo signalling as well. Indeed, in zebrafish, Slit2, Robo1 and Robo4 appear to regulate cardiac development (Fish et al, 2011). The authors demonstrated that vascular endothelial growth factor (VEGF) acting via its cognate receptor VEGFR2 is a main mediator of heart precursor cell migration. Slit and Robos in this system act as cardioblast migration inhibitors, however what functions they actually confer remain unclear. Most interestingly, miRNA-218 regulates Robo1 expression during heart development in zebrafish (also see sections 1.5.6 and 1.5.7 for more miRNA functions in angiogenesis and cancer). Knockdown of miRNA-218 or overexpression of Robo1, and unexpectedly knockdown of Robo1, caused delayed migration and abnormal heart development, showing that precise titration of Robo1 is necessary for correct myoblast migration (Fish et al, 2011).

The role of Slit-Robo in the development of the mammalian cardiac system currently remains vague. Medioni et al, 2010 showed that Slit2, Slit3, Robo1 and Robo2 are expressed in the developing mouse heart, however, Slit or Robo knockout animals generally do not suffer from serious cardiac abnormalities (Andrews et al, 2006; Plump et al, 2002; Xian et al, 2001b). Slit3 knockout mice had enlarged right ventricles, however it is difficult to assess these changes since the animals suffered from diaphragmatic hernia and many organs were dislodged from their natural positions (Liu et al, 2003). The alternative explanation that single knockouts failed to reveal cardiac phenotypes because of Slit or Robo redundancy between different family members is also possible.

1.5.3 Kidney development

Homozygous Slit2 knockout mice die at birth because of multiple developmental defects including abnormal kidneys (Plump et al, 2002). Slit3 knockouts caused kidney and ureter agenesis in some animals, however when these organs did form they appeared normal (Liu et al, 2003). Homozygous Robo2 knockout animals had similar kidney deformations as Slit2 knockouts, indicating that Slit2-Robo2 signalling is necessary for correct organogenesis of the kidney (Grieshammer et al, 2004). Murine kidney originates from a single nephric duct outgrowth called the ureteric bud (UB), formation of which is controlled by glial cell line-derived neurotrophic factor (GDNF). In Slit2 and Robo2 knockout embryos, multiple ectopic UB are formed leading to the development and fusion

of multiple ureters and kidney (Grieshammer et al, 2004). Given the repulsive nature of Slit-Robo signalling, one could expect that Slit2 restricts ectopic ureteric buds by repelling UB-forming cells, however no evidence was found to support this assumption. The authors instead favoured a different model, where Slit2 signals through Robo2 to inhibit GDNF expression. This idea is based on the fact that the Slit2 knockout kidney phenotype can be rescued by reducing GDNF dosage (Grieshammer et al, 2004). The mechanism by which Slit2-Robo2 interact with GDNF remains unknown and additional studies are needed to clarify exactly how UB restriction is achieved.

1.5.4 Lung development

Homozygous mouse embryos with defective Robo1 alleles show delayed lung maturation, reduced lung volume and increased amounts of mesenchymal tissue. The few animals that survived postnatally had abnormal and hyperplastic bronchial epithelium (Xian et al, 2001b). Independently, a microarray based screen also identified Slit3 as one of the factors controlling lung development (Greenberg et al, 2004). Expression profiling revealed that Slit2, Slit3, Robo1 and Robo2 are expressed mainly in the mesenchymal tissue of developing lungs, although epithelial localisation was also observed for Robo1 and Robo2 (Anselmo et al, 2003; Greenberg et al, 2004). Lung mesenchyme undergoes dramatic tissue remodelling during organogenesis which incorporates cell differentiation, apoptosis and migration. Given the already known functions of Slit-Robo in other organs and tissues, it is reasonable to suspect that Slit-Robo plays an important role in organising cellular lung architecture. Unfortunately, at this stage little is known about the mechanism involved.

While *Drosophila* have no real lungs, they employ the so called tracheal system, an elaborate whole body spanning network of air filled tubes, which bring oxygen and remove carbon dioxide. Most fascinatingly, development of the tracheal system in *Drosophila* is guided by Slit-Robo signalling. Slit, Robo and Robo2 are indispensable for correct tracheal branch outgrowth towards their target tissue (Englund et al, 2002). The authors also suggest that in this system Slit can cause both attractive and repulsive responses, where the effects of Slit are determined by different combinations of Robo and Robo2 receptors (Englund et al, 2002).

1.5.5 Other developmental functions

In situ hybridisation with whole-mount mouse embryos revealed striking Slit-Robo expression patterns in developing limbs (Holmes et al, 1998; Vargesson et al, 2001; Yuan et al, 1999). For example, at stages E11.5 and E13.5, Slit2 was strongly expressed in all interdigital spaces (Holmes et al, 1998; Yuan et al, 1999). At stage E13.5 Robo1 is

expressed along the borders of developing digits, however this pattern gradually changes and at E15.5 Robo1 expressing regions form “rings” roughly marking the joints of the digits (Vargesson et al, 2001). Strangely enough, despite these beautiful expression patterns no further work has been done regarding the role of Slit-Robo in limb development. The authors speculated about a possible Slit-Robo role in apoptosis, axon innervations or myoblast migration, but only speculation about myoblast migration has some supporting evidence as Slits and Robos co-localise with the migratory myoblast marker Pax7 (Vargesson et al, 2001).

Expression profiling also hints at a possible Slit-Robo role in the development and functions of the ovary. Slit2, Slit3, Robo1, Robo2 and Robo4 were expressed in fetal sheep ovary, with Robo2 and Robo4 levels changing significantly across different gestation stages (Dickinson et al, 2010). Slit-Robo proteins might also have important functions in adult ovaries during luteolysis (Dickinson et al, 2008). The corpus luteum, also known as the yellow body, is a temporary endocrine structure in mammalian ovaries formed from the follicle after ovulation. It produces progesterone and other hormones which facilitate various processes related to fertilisation and pregnancy. If the oocyte is not fertilised, the corpus luteum stops secreting progesterone and decays in a process called luteolysis. If egg fertilisation and implantation occurs, human chorionic gonadotropin (hCG) is released, saving the corpus luteum from degradation and thereby prolonging its functions. Dickinson et al, 2008 showed that Slit2, Slit3, Robo1 and Robo2 are expressed in the corpus luteum. Moreover, Slit2, Slit3 and Robo3 expression was increased in late stages of luteolysis and significantly reduced after corpus luteum “rescue” *in vivo* with exogenous hCG. Likewise, treatment with hCG significantly inhibited Slit2, Slit3 and Robo2 expression in cultured luteinized granulosa cells (Dickinson et al, 2008). Luteolysis involves a considerable amount of tissue remodelling so the idea that the Slit-Robo signalling axis might play a role is not too far-fetched. This study also suggests that Slit-Robo expression might be regulated by hormones, although so far this has not been observed in any other system. As a side note, although most likely it is evolutionarily unrelated to mammals, proper gonad formation in *Drosophila* also depends on functional Slit-Robo proteins (Weyers et al, 2011).

1.5.6 Angiogenesis

Formation of new blood vessels is achieved by two different processes: vasculogenesis and angiogenesis. Vasculogenesis is *de novo* formation of the vascular system during embryo development. Angiogenesis, on the other hand, is the formation of new blood vessels from

already existing vessels by endothelial cell sprouting. Angiogenesis is crucial for normal functioning of the adult organism, but it also plays a major role in various pathological processes like cancer, diabetic retinopathy or psoriasis (Pandya et al, 2006; Risau, 1997). VEGF is a major regulator of angiogenesis; it promotes endothelial proliferation, migration and formation of capillary tube structure. In addition to VEGF, many other signalling molecules promote or suppress angiogenesis and Slit-Robo proteins, especially Robo4, play a substantial role in the regulation of angiogenesis.

Because of its divergent structure, Robo4 was the last family member to be discovered. Originally identified as a possible endothelial marker by a computational screen, Robo4 expression indeed co-localised with the vasculature and especially with sites of intensive angiogenesis (Huminiecki et al, 2002; Park et al, 2003). Initially described as a very specific endothelial marker (Huminiecki et al, 2002; Okada et al, 2008; Seth et al, 2005), Robo4 is now reported to be additionally expressed by hematopoietic stem cells and vascular smooth muscle cells (Liu et al, 2006; Shibata et al, 2008; Smith-Berdan et al, 2011). In agreement, Robo4 was detected in many endothelial cell lines *in vitro*: human umbilical vein endothelial cells (HUVEC), human dermal microvascular endothelial cells (HDMEC), and mammary microvascular endothelial cells (HMME2). While Robo4 seems to be a ubiquitous marker of endothelial cells, coexpression of Robo1, Robo3, Slit2 and Slit3 was also reported, but levels varied between different tissues (Liu et al, 2006; Small et al, 2010; Zhang et al, 2009).

The role of Robo4 in angiogenesis has attracted intense interest from the scientific community, but despite substantial advances, fundamental details such as the identity of the Robo4 ligand and the actual effects of Robo4 on blood vessel formation remain somewhat obscure. Even relatively simple assays, such as transwell cell migration, are reported to give outright opposite results. Park et al, 2003 and Seth et al, 2005 demonstrated that Slit2 prevents HMVEC or HUVEC migration towards VEGF, meanwhile Wang et al, 2003 and Howitt et al, 2004 successfully used Slit2 protein as an attractant for HUVEC cells. Matters were complicated even more by the fact that HUVEC cells express Robo1. As mentioned above (see section 1.3), the ability of Robo4 to bind Slit2 is debatable, so it is unclear which protein was responsible for these functional Slit2 effects. Two independent studies tried to resolve these discrepancies by selectively knocking down Robo1 and Robo4 expression in HUVEC cells with siRNA (Kaur et al, 2008; Sheldon et al, 2009). In both cases Slit2 showed pro-migratory effects on HUVEC cells, however while Kaur et al, 2008 reported an increase in Slit2 activity after Robo4 was

depleted, under the same conditions Sheldon et al, 2009 observed a reduced HUVEC response to Slit2. Both papers demonstrated Robo1 association with Robo4 by co-immunoprecipitation. Sheldon et al, 2009 additionally showed that overexpression of Robo4 induced excessive filopodia in HUVEC cells, while knockdown of Robo1 abolished this effect. Moreover, Slit2 activity on HUVEC cells was blocked by soluble Robo1, but not by the Robo4 ectodomain, indicating significant crosstalk between Robo1 and Robo4. On the other hand, Kaur et al, 2008 showed that Robo4, but not Robo1, mediates HUVEC attraction to serum, which presumably contains an as yet unknown VEGF-independent ligand. While these studies failed to clarify existing contradictions, they are pointing to possible reasons for them. It appears that even in such a simple system as *in vitro* HUVEC migration, Robo4 effects are highly context dependent and rely heavily on crosstalk with other Robo proteins.

Different *in vivo* models were used to assess Slit-Robo roles in angiogenesis with predictably different outcomes. As many other cancer cells (see section 1.5.7), the human malignant melanoma cell line A375 expresses Slit2 protein. A375 cell-derived solid tumours in xenografted mice developed microvessels to sustain themselves. This ability was diminished by administration of a soluble extracellular Robo1 domain or anti-Robo1 antibody (R5) and enhanced by the presence of Slit2 (Wang et al, 2003). While these results clearly support a positive role of Slit-Robo in angiogenesis, little can be inferred about the exact mechanism since authors have not addressed the possible presence of other Slit-Robo proteins in their model and acknowledged that the anti-Robo1 antibody might cross-react with other Robo proteins. The same group extended their observations, albeit with the same shortcomings, and demonstrated that the R5 antibody, which presumably blocks Slit2-Robo1 interactions, reduced angiogenesis in the chick embryo chorioallantoic membrane. They also showed that the same antibody is able to reduce new vessel formation and growth in DMBA (7,12-Dimethylbenz(a)anthracene)-induced hamster buccal pouch squamous cell carcinoma (Wang et al, 2003). The most convincing evidence that the Slit-Robo signalling axis promotes angiogenesis unexpectedly came from work with Slit3. Zhang et al, 2009 showed that endothelial and smooth muscle cells from lung, brain and kidney, but not from liver and heart, express Slit3. They proceeded to demonstrate that Robo3 stimulated proliferation in HUVEC and lung endothelial cells (LuEC) and promoted their motility and migration. They also showed that in their hands Slit3 binds both Robo1 and Robo4, however only Slit3-Robo4 binding affects HUVEC and LuEC migration. Treatment with Slit3 initiated sprouting of microvessels in an *ex vivo* rat

aortic ring assay and enhanced angiogenesis in chicken chorioallantoic membrane and mouse corneal assays. The authors also revealed vascular abnormalities in the developing diaphragm of homozygous Slit3 knockout animals (Zhang et al, 2009).

Robo4 knockdown in zebrafish led to a temporal and spatial disruption of embryonic vascular development. This knockdown phenotype indicates a possible role of Robo4 as a guidance cue for the developing vasculature, however the underlying mechanism remains elusive (Bedell et al, 2005). Jones et al, 2008 tried to ascertain Robo4 functions in mammals by generating Robo4 knockout mice with a reporter gene inserted within the Robo4 locus. Surprisingly, homozygous Robo4 knockout mice were completely viable and fertile, with no obvious defects in vasculature development or function. The reporter gene showed that Robo4 is expressed in more mature parts of blood vessels and not in pioneering sprouting cells. These observations were incompatible with the “guidance” theory, therefore the authors hypothesized that Robo4 is required to maintain vascular stability. In agreement with this assumption they showed that treatment with recombinant Slit2 inhibits lung endothelial cell migration and tube formation, decreases VEGF induced vascular permeability *in vitro* and *in vivo*, and also reduces pathological angiogenesis in oxygen-induced retinopathy in mice (Jones et al, 2008). All these effects were assumed to be mediated by Slit2-Robo4 interactions, since the effects of recombinant Slit2 were abrogated in Robo4 knockout animals and cells. The authors also suggested that Robo4 promoted vascular stability by antagonising VEGF signalling (Jones et al, 2008). It is also worth mentioning that in direct contradiction to Zhang et al, 2009, Jones et al, 2008 showed that Slit3 had identical effects to those of Slit2 and acted in an anti-angiogenic manner, even though both studies used similar assays. In a follow-up publication, the same group extended their observations and showed that Slit2, acting via Robo4, controlled vascular stability during inflammation (London et al, 2010). One of the effects of inflammation is leakage of blood vessels, which if uncontrolled can lead to tissue oedema and organ damage. The authors demonstrated that treatment with recombinant Slit2 reduces vascular permeability and increases animal survival in pulmonary inflammation, polymicrobial sepsis and influenza infection models (London et al, 2010). These effects were Robo4 dependent as they disappeared in Robo4 knockout animals.

Use of recombinant Slit2 proteins is a potentially problematic approach, as some authors speculated that the source of experimental contradictions might be varying methods of Slit preparation (Marlow et al, 2010). This makes genetic experiments particularly attractive and Marlow et al, 2010 analyzed how various combinations of Slit-Robo knockouts affect

vascularisation of mammary glands in mice. The authors showed that in their experimental system, Slit2 and Slit3 are expressed by mural cells (smooth muscle cells and pericytes surrounding small blood vessels) while Robo4 and Robo1 are present in endothelial cells. Additionally, Robo1 is expressed in surrounding epithelial cells of the gland. Only combined Slit2^{+/-} Slit3^{-/-} (homozygous Slit2 knockout is lethal, hence heterozygous mice were used instead) and Robo1^{-/-} Robo4^{-/-} knockouts affected vascular composition. In both cases vessel density was increased about twofold. Robo1^{-/-} Robo4^{-/-} mice also showed increased autophosphorylation of VEGFR2. All these observations support findings from Jones et al, 2008 and London et al, 2010 and their idea that Robo4 antagonises VEGF signalling and thus acts as an anti-angiogenic and vasculature stabilising factor.

Slit2 and Slit3 are closely related proteins so their redundancy was not unexpected. On the other hand, the necessity to remove both Robo1 and Robo4 before any phenotypic effects were observed is more puzzling. If Robo1 and Robo4 were forming functional heterodimers as proposed by others (Kaur et al, 2008; Sheldon et al, 2009), knockdown of either should have functional consequences. Marlow et al, 2010 proposed a possible explanation of this phenomenon. They showed that Robo1 expressed on surrounding epithelial cells of the gland, acting via an unknown mechanism, suppresses expression of pro-angiogenic signalling molecules VEGF and CXCL12. The authors suggest a model where Slits and Robo4 acts as “brakes” to VEGF. Removing them would not cause a change in phenotype under normal conditions. It takes a secondary pro-angiogenic stimulus, in this case upregulation of VEGF and CXCL12 caused by Robo1 knockout, for a phenotype to manifest itself.

Koch et al, 2011 added another twist to the Robo4 story. Since in their hands Slit2 was not binding Robo4, the authors performed a bio-layer interferometry-based protein-protein interaction screen to identify possible Robo4 ligands. A vascular-specific netrin receptor UNC5B was detected as a Robo4 ectodomain interacting protein and this interaction was further confirmed with surface plasmon resonance (Koch et al, 2011). Both soluble or membrane bound Robo4 ectodomains were able to activate UNC5B downstream signalling pathways, but not the other way around. Activated UNC5B counteracted VEGF signalling by inhibiting VEGF-mediated Src kinase activation. Likewise, blocking Robo4-UNC5B interactions with specific antibodies substantially increased angiogenesis and vascular permeability *in vivo* (Koch et al, 2011). This study largely confirms observations that Robo4 is dispensable for development, but necessary for maintenance of blood vessel

integrity under inflammatory stress. On the other hand, these experiments show that instead of being a receptor, Robo4 is a membrane bound ligand for UNC5B which mediates the vascular effects. Koch et al, 2011 findings raise more questions than answers. It is doubtful that Robo4 is only a cell surface bound ligand, as it retains a cytoplasmic tail and appears to be an active receptor in other experimental systems (Jones et al, 2009; Kaur et al, 2006; Sheldon et al, 2009). Most likely these divergent data illuminate separate parts of a complex signalling system, the full picture of which is yet to be revealed.

As mentioned previously, the introns of Slit2 and Slit3 encode a microRNA molecule called miRNA-218. This feature is well preserved evolutionarily and conserved between animals as different as zebrafish and humans (Fish et al, 2011; Small et al, 2010; Tie et al, 2010). Small et al, 2010 showed that miRNA-218 is able to repress Robo1 and Robo2 expression, as well as some other components of the Slit-Robo signalling axis, like srGAP2 and enzymes necessary for heparan sulphate biosynthesis. Blocking miRNA-218 in the mammalian retina led to increased vascular permeability but decreased density and thickness (Small et al, 2010). Blocking of miRNA-218 also caused greater HUVEC migration in a scratch healing assay, while overexpression reduced it. It is difficult to unambiguously infer a Robo1 role from these experiments. Robo4 does not seem to be targeted by miRNA-218 and the authors speculate that a miRNA-218 feedback loop might be responsible for regulating the Robo1-Robo4 ratio and hence formation of the Robo1-Robo4 heterodimer (Small et al, 2010). In turn this might decide overall the outputs of Slit-Robo signalling in the vasculature.

Dunaway et al, 2011 tried to consolidate published pro- and anti-angiogenic Slit effects and concluded that Slit tends to be angiogenic alone and angiostatic in the presence of VEGF. They suggested that some tertiary factor, induced by VEGF, can modulate endothelial cell responses to Slit. Accordingly, Slit2 alone promoted angiogenesis through activation of Akt in primary vascular endothelial cells and *in vivo* models. However, the presence of a protein called ephrin-A reversed Slit2 activity and converted it into an anti-angiogenic factor (Dunaway et al, 2011). Ephrin-A is a surface bound ligand for the Eph family receptor tyrosine kinases whose expression in endothelial cells is induced by VEGF. Ephs and ephrins, like Slit-Robo, are major players in axon and neuron guidance, cell migration and vascular development. A remarkable feature of the ephrin/Eph signalling axis is its ability to transduce signals in both ways, from ligand to receptor expressing cells and vice versa (Pasquale, 2010). The exact mechanism of crosstalk between Slit-Robo and Ephrin-Eph pathways, as well as its biological relevance remains

unknown. It is tempting to speculate that this interplay between Slit2 and ephrin-A1 is required for temporary separation of pro-angiogenic VEGF stimulus and stabilising Slit-Robo effects. One can suggest, that initial pro-angiogenic VEGF signals bypass Slit-Robo blockade and among other effects switches ephrin-A1 synthesis on. In turn Ephrin-A1 accumulates and switches Slit signalling into angiostatic mode.

Proper functioning of the vasculature depends on a balance between angiogenic stimuli and angiostatic factors, and it seems that Slit-Robo mirrors this duality and metastability when it comes to their role in angiogenesis. It is also worth mentioning that Slit-Robo are not the only neuronal guidance cues employed in regulation of the vasculature. Three other major signalling pathways responsible for nervous system development, semaphorin-neuropilin, ephrin-Eph and netrin-UNC5 play even more important roles than Slit-Robo (Lu et al, 2004; Wilson et al, 2006). As mentioned above, some of them, like neuropilin1, UNC5 and ephrin-A1, are already known to interact with the Slit-Robo signalling pathway. Given the currently observed high variation of experimental results, it might be a good strategy to analyse all these signalling pathways together, since functional relations forged in neuron wiring might be preserved in vasculature regulation.

1.5.7 Cancer

In addition to physiological functions, Slit-Robo seems to play a role in pathological conditions like cancer. Xian et al, 2001b observed that Robo1 gene maps within the third chromosome region often subjected to deletions in lung and breast cancer. Accordingly, heterozygous Robo1 knockout mice are prone to developing lymphomas and carcinomas about 3 times more often than control animals, with invasive lung adenocarcinoma being the predominant pathology (Xian et al, 2001a). It was also demonstrated that breast and kidney tumour cells tend to have a hypermethylated Robo1 promoter which silences its expression (Dallol et al, 2002). Similar epigenetic Slit2 silencing was observed in lung, breast, colorectal and glioma tumours and hepatocellular carcinoma (Dallol et al, 2003a; Dallol et al, 2003b; Jin et al, 2008). Slit1 promoter hypermethylation was detected in glioma cell lines while Slit3 was frequently silenced in breast, lung, colorectal and glioma tumour cell lines and in primary breast tumours and gliomas (Dickinson et al, 2004). Narayan et al, 2006 also showed that all Slits, Robo1 and Robo3 are epigenetically inactivated during the early stages of cervical cancer. In the clinic, downregulation of Robo1 and Robo2 strongly correlated with poorer survival of patients with oral cavity cancer (Ghosh et al, 2008), while low Slit2 expression was associated with poorer clinical outcome in lung and breast cancer (Brantley-Sieders et al, 2011; Tseng et al, 2010). All

these observations would suggest that Slit-Robo act as tumour suppressor genes. On the other hand, many other tumour cell lines and primary tumours do express Slit-Robo proteins (Schmid et al, 2007; Wang et al, 2003). Increased expression of different Slit-Robo proteins was observed in prostate cancer, colorectal cancer and hepatocellular carcinoma (Gröne et al, 2006; Ito et al, 2006; Latil et al, 2003). A clinical study also revealed that elevated expression of Slit and Robo1 proteins in endometrial cancer was associated with higher risk of recurrence (Ma et al, 2010). All these data demonstrate that Slit-Robo proteins are linked to cancer in an intricate and complex way.

Some reports show that Slit-Robo proteins can directly control cancer cell proliferation and apoptosis. Re-expression of Slit2 in colorectal carcinoma and glioma cancer cell lines, which have their innate Slit2 epigenetically silenced, induced growth suppression and apoptosis (Dallol et al, 2003a; Dallol et al, 2003b). *In vitro* cancer cell proliferation was suppressed by recombinant Slit2 in hepatocellular carcinomas, esophageal squamous cell carcinomas and breast cancer cells (Jin et al, 2008; Kim et al, 2008; Marlow et al, 2008; Prasad et al, 2008). Kim et al, 2008 also observed an increased number of apoptotic cells in solid tumours derived from Slit2 transfected HT1080 cells. However, these Slit2 apoptotic effects are far from ubiquitous. There are equally abundant reports of Slit2 having no detectable effect on cancer cell proliferation or apoptosis (Dai et al, 2011; Schmid et al, 2007; Tseng et al, 2010; Werbowetski-Ogilvie et al, 2006; Yiin et al, 2009). Generally, it seems that Slit-Robo play only secondary roles in cancer cell survival. One can argue that in some cases malignant transformation distorts cell signalling systems in such a way that the Slit-Robo signalling axis gains new functions that are harmful to cancer cells and thus is silenced epigenetically.

Angiogenesis is another cancer pathology area where Slit-Robo proteins could play an important role. Tumour survival completely depends on its ability to induce angiogenesis to get accesses to oxygen and nutrients. Robo4 and Robo1 functions in angiogenesis are well documented (see section 1.5.6), but surprisingly, little is known about it in the context of cancer. As mentioned above, one group reported pro-angiogenic Slit2-Robo1 effects in A375 cell derived solid tumours and DMBA-induced hamster buccal pouch squamous cell carcinoma (Wang et al, 2003; Wang et al, 2008). No other studies have addressed this topic. Given the obvious importance of this area it is doubtful that it has been ignored. More likely this informational vacuum was created by the bias of negative results, and indeed, some authors mention in passing that they have failed to observe any Slit effects on the density of tumour blood vessels (Kim et al, 2008).

The most widely accepted model suggests that tumours produce growth factors and signalling molecules to attract blood vessels. However, more recently it was proposed that endothelial cells establish a vascular niche themselves, which actively promotes tumour survival with growth factors and other signalling molecules (Butler et al, 2010). Brantley-Sieders et al, 2011 demonstrated that EphA2 receptor tyrosine kinase knockout increases Slit2 expression in endothelial cells, which in turn suppresses tumour growth *in vitro* and *in vivo*. The authors argue that this is an example of a vascular niche in action, since, EphA2 is often overexpressed in tumour vasculature, presumably causing Slit2 suppression and tumour growth promotion.

Slit-Robo proteins primarily are known as cell motility regulators, so a lot of studies have concentrated on their possible role in metastasis. It is relatively well established that the CXCR4/CXCL12 axis drives breast cancer metastasis to bones, lungs and lymph nodes (Muller et al, 2001). Prasad et al, 2004 used the classical Boyden chamber assay to evaluate possible Slit2 effects on this migration. The lower part of the Boyden chamber was loaded with media containing CXCL12 and Slit2 or respective controls. Cells were pre-treated with Slit2 for 30 minutes and then added to the upper part of chamber. In this setup, Slit2 significantly inhibited cancer cell migration towards CXCL12. Additionally, the same authors showed that treatment with Slit2 reduced cancer cell invasion through Matrigel and adhesion to various substrates (Prasad et al, 2004). Using an identical experimental setup, Schmid et al, 2007 largely confirmed these observations, however they also noticed that Slit2, when placed in the lower chamber only, acted as attractant for the same breast cancer cells. To complicate matters even more, glioma cells were repelled by Slit2. When Slit2 was added to the lower chamber, glioma cell migration into it decreased, while Slit2 addition to the upper chamber facilitated cell movement from it. When the Slit2 gradient was destroyed by adding equal amounts of protein into each chamber, Slit2 lost its effect on glioma cell migration (Mertsch et al, 2008).

In vitro experiments have generally displayed inhibitory Slit2 effects on metastasis. Slit2-transfected fibrosarcoma cells (HT1080), when injected into athymic mice, formed less metastases in comparison to those transfected with vector only (Kim et al, 2008).

Expression of Slit2 also inhibits glioma cell infiltration into the brain parenchyma (Yiin et al, 2009). On the other hand, Tie et al, 2010 reported that in gastric cancer cells Slit2-Robo1 signalling actively triggers metastasis. The authors found that decreased expression of a known Robo1 suppressor, miRNA-218 (see sections 1.5.2 and 1.5.6), is associated with advanced clinical stage, lymph node metastasis and poor prognosis for patients. They

also isolated gastric cancer sublines with different metastatic potential and found that Robo1 was expressed at high levels in invasive cells and at low levels in non-invasive cells, whereas miR-218 had the opposite expression pattern. Re-expression of miRNA-218 or direct knockdown of Robo1 led to reduced invasiveness both *in vitro* and *in vivo* (Tie et al, 2010). It appears that in cancerous cells, like in endothelial cells, Slit-Robo signalling and its effects strongly depend on cellular context, tissue of origin and crosstalk with other signalling pathways.

1.5.8 Leukocytes and immune response

One of the more unexpected Slit-Robo functions was uncovered when Wu et al, 2001 showed that Slit2 is able to inhibit chemotactic leukocyte movement. Directional leukocyte migration is a crucial process in the inflammatory response and it is primarily regulated by positive guidance cues like chemokines. Endogenous negative regulators of chemotaxis are relatively unknown and could potentially serve as broad spectrum anti-inflammatory agents. Nevertheless, Slit-Robo role within the immune system has attracted considerably less interest than other fields. Systematic and consistent analysis of Slit-Robo expression in leukocytes is not published yet. Different studies have reported Robo1 expression on the majority of MHC II type cells (B cells, macrophages, dendritic cells (DC)), as well as monocytes, eosinophils and neutrophils (Geutskens et al, 2010; Guan et al, 2003; Kanellis et al, 2004; Tole et al, 2009; Ye et al, 2010). However, information about the other members of the Slit-Robo family is scarce, possibly reflecting an absence of expression as negative results usually remain unreported. Of those reported, Slit3 expression was induced by treatment with lipopolysaccharide (LPS) in primary macrophages (Tanno et al, 2007), while Robo4 is expressed in hematopoietic stem cells (HSC) but its expression is lost after differentiation (Shibata et al, 2008; Smith-Berdan et al, 2011). So it seems that Robo1 is the main player in the hematopoietic system.

Wu et al, 2001 was the first to demonstrate leukocyte chemotaxis inhibition by Slit2 in transwell migration assays. Since then many other studies were able to replicate similar results using identical assays but different cells and chemokines: peripheral blood mononuclear cell (PBMC) and CXCL12, HL-60 and fMLP (N-formyl Met-Leu-Phe) (Wu et al, 2001); ex-vivo leukocytes and CCL2, CCL5, CX3CL1, fMLP (Kanellis et al, 2004); Jurkat cells, primary monocytes and CXCL12 (Chen et al, 2004; Prasad et al, 2007); primary neutrophils and fMLP, C5a, CXCL-8 (Tole et al, 2009). Interestingly, time-lapse microscopy revealed that Slit2 affects directional cell movement but not random movement or speed (Tole et al, 2009; Yuasa-Kawada et al, 2009a). This indicates that Slit2

effects in leukocytes are solely anti-chemotactic, as it abolishes the sense of direction but not the ability to move.

The ability of Slit2 to stop leukocyte migration was confirmed in multiple *in vivo* models. Recombinant Slit2 reduced hapten-induced Langerhans cell migration in skin explants (Guan et al, 2003). These effects were efficiently blocked by soluble Robo1 extracellular domain confirming that Slit2-Robo1 signalling is mediating inhibition. Treatment with Slit2 also reduced inflammatory responses in a contact hypersensitivity model (Guan et al, 2003). In this experiment, Slit2 was injected into the dorsal side of one ear, which was then painted with the hapten. Five days later, the second ear was painted with the same hapten and inflammation intensity evaluated. Treatment with Slit2 arrested Langerhans cells within the first ear, as was demonstrated by immunohistochemistry, and consequently significantly reduced swelling in the second ear, since less Langerhans cells were able to reach draining lymph nodes and activate T cells (Guan et al, 2003). The authors speculated that Slit2, which is constitutively expressed in the skin, might be necessary for steady state retention of Langerhans cells within the skin. Similar results were observed in a kidney inflammation model, where recombinant Slit2 treatment reduced leukocyte infiltration into the kidneys and considerably improved renal histology and function (Kanellis et al, 2004). The authors also observed that the inflammation induced a downregulation of endogenous Slit2 in the kidneys and was further able to exacerbate inflammation by blocking endogenous Slit2 with antibodies (Kanellis et al, 2004). Likewise, Tole et al, 2009 observed leukocyte recruitment inhibition by recombinant Slit2 administration in peritoneal inflammation.

While the majority of published papers demonstrate negative Slit effects on leukocyte migration, two recent studies unexpectedly revealed Slit as a potentiating agent for chemotaxis. Ye et al, 2010 showed that *in vitro* Slit2 inhibits neutrophil migration but activates chemotactic responses in eosinophils. They also observed an identical effect in lung inflammation models. Within the lungs, Slit2 is expressed by Clara cells, forming a Slit2 gradient along the bronchus-alveoli axis (high to low expression levels). Challenging the lungs with LPS or ovalbumin induced neutrophil and eosinophil infiltration, respectively. In turn, mice overexpressing Slit2 had lower neutrophil, but higher eosinophil infiltration (Ye et al, 2010). The authors show that the response is geared towards one or the other outcome by differential expression of the downstream signalling molecule srGAP1 (see section 1.4.2). Neutrophils express high levels of srGAP1 and thus the Slit-Robo axis is steered towards the inhibitory srGAP1-mediated signalling. Eosinophils have

considerably lower srGAP1 expression, hence the “pro-migratory” PI3K-Akt pathway becomes the primary Slit-Robo effector (Ye et al, 2010).

Even more unexpectedly, Geutskens et al, 2010 showed that Slit1 and Slit3 promote monocyte migration in transwell assays and a peritonitis model. Earlier studies using similar assays showed strong inhibitory Slit2 effects on monocyte migration (Chen et al, 2004; Prasad et al, 2007). One can argue that different Slit proteins might have different functions, and Geutskens et al, 2010 experiments seem to suggest exactly that. However, there are several issues with this model. First of all, the authors have not tested Slit2 themselves, even though Slit2 is commercially available from the same supplier they obtained the other Slit proteins from. Given how variable Slit effects are in other systems, it is crucial to perform these experiments in parallel. Second, the Slit3 concentration used by the authors was 10-100 times higher than those usually used for Slit2 in other publications (Geutskens et al, 2010). Third, Slit proteins have 70% sequence identity, and Robo binding residues are even more highly conserved. Moreover, all three mammalian Slit proteins bind Robo1 with almost identical affinity (Suchting et al, 2005). This does not completely discard the possibility that different Slit proteins might have diverse functions, but makes it unlikely; indeed, this was never directly observed before. Slit-Robo signalling flexibility and its strong dependency on cellular context is widely known (see sections 1.5.6 and 1.5.7) and it is more likely that once again Slits may enhance or reduce the chemotactic movement of leukocytes depending on cell differentiation, relative expression of the Robo1 receptor or other unknown factors.

As mentioned above, Robo4 is specifically expressed in HSCs while bone marrow (BM) stromal cells express Slit2 (Shibata et al, 2008). Additionally, Smith-Berdan et al, 2011 showed that the level of Robo4 was very low in fetal HSCs residing in liver but was upregulated once HSC moved to the bone marrow. HSCs residing within bone marrow retain high Robo4 expression, but lose it upon leaving the BM. Consistent with these findings, Robo4 knockout mice showed disturbed HSC localisation. Robo4-deficient HSCs more readily left the BM and entered the peripheral blood. Poorer BM engraftment and compensatory CXCR4 and CXCL12 upregulation were also observed (Smith-Berdan et al, 2011). Based on these experiments and previous knowledge about HSC homing, the authors suggested a model where CXCR4 and CXCL12 guide cells over a long range towards the BM. Once within the niche, Robo4 helps HSCs to establish and maintain stable engraftment. The exact mechanism by which this is achieved remains unknown. Slit2 is expressed by BM stromal cells, but *in vitro* assays failed to reveal any Slit2 effects

in HSC migration or proliferation (Smith-Berdan et al, 2011). On the other hand, if Slit2 is required for Robo4 mediated cell-cell adhesion, solution based assays would fail to detect it.

1.6 Final thoughts about Slit-Robo proteins

One constantly recurring aspect of Slit-Robo signalling and function is the strong dependency on cellular context. Contradictory findings are often reported even when researchers are using very similar experimental setups. Slit-Robo proteins are a new, quickly expanding research area so in some cases those discrepancies might appear simply because of the novelty of the field. Nevertheless it does not explain such a high prevalence of inconsistencies and thus the importance of context most likely represents actual properties of the Slit-Robo signalling axis.

Robos are somewhat unique receptors in terms of their structural organisation. No other membrane protein was reported to contain a 700 amino acid long unstructured polypeptide as its cytoplasmic domain so far. Our knowledge about intrinsically unstructured proteins implies an exceptional variety of Robo binding partners and this view is largely confirmed by experimental data. Signalling molecules with directly opposite functions, like GAP's and GEF's (see section 1.4.2), are known to be recruited by Robo. So one can argue that Robo context dependency is hardwired in its structure.

An alternative model is that context dependency arises from “deeper” downstream signalling networks. Perfect examples here are small Rho family GTPases, which appear to be the main Robo signalling targets. As mentioned above (see section 1.4.2), Cdc42, Rac1 and RhoA exist as a complex interconnected signalling network, where the functional outcome results from integration of many different modulators. In this case context dependency is not so much a property of the Robos themselves, but of the signalling network lying downstream.

With two recent publications we begin to uncover possible mechanisms behind Robo's dependency on cellular context. As already mentioned above, the presence of Ephrin-A was enough to switch Slit2 effects from pro-angiogenic to anti-angiogenic in endothelial cells (Dunaway et al, 2011). Unfortunately, the precise mechanism of crosstalk remains unknown. The Ephrin/Eph kinase signalling axis can transmit signal in both directions, so it is not even clear which part of it is responsible for crosstalk. Similarly, Slit2 inhibits neutrophil but activates eosinophil chemotaxis (Ye et al, 2010). These differential Slit2 effects were determined by srGAP1 expression level. Neutrophils express high levels of

srGAP1 protein which directly interacts with Robo1 and transmits inhibitory signalling. Eosinophils have considerably lower amounts of srGAP1, hence P3IK binds Robo1 instead of srGAP1 and mediates promigratory effects (Ye et al, 2010). This latter example shows how competition between Robo1 binding partners determines the overall signalling outcome and supports the idea that context dependency is an innate feature of Robo receptors.

1.7 Receptor oligomerisation-methods and techniques

Receptor oligomerisation is driven by protein-protein interactions and thus relies on similar techniques. In some cases it is even possible to reconstruct a oligomeric state of the receptor by expressing and analysing separate receptor domains as soluble proteins. Obviously, the major difference between cytoplasmic proteins and receptors is that the latter are functioning within the phospholipid bilayer, and substantial evidence shows that transmembrane domains and membrane lipids are important elements of receptor-receptor interactions (Hubert et al, 2010). This aspect puts considerable constraints on the design of experiments and most of them are done with solubilised receptors (co-immunoprecipitation) or *in vivo* with intact cells (resonance energy transfer methods, bimolecular fluorescence complementation etc).

1.7.1 Co-immunoprecipitation

Co-immunoprecipitation is probably the simplest and most straightforward approach to detect receptor oligomerisation. In its simplest form, two receptor constructs differentially tagged with epitope tags are co-expressed in a heterologous system. Cells are lysed and one of the proteins is immunoprecipitated with a corresponding antibody. If the second protein interacts with the immunoprecipitated receptor, it will be co-precipitated and SDS-PAGE followed by Western blotting with the second antibody will reveal its presence. Method variation with untagged endogenous proteins from native tissues is also possible. This approach however is often limited by the availability of suitable antibodies and low endogenous expression of native proteins. Use of native proteins also is not suitable for detection of homooligomerisation, as without an additional tag it is impossible to discriminate between directly precipitated and co-precipitated molecules. Although co-immunoprecipitation is a standard technique, it has its own share of problems and shortcomings. A lot of problems arise from the necessity to optimise properties of the lysis buffer. Cell lysis buffer for co-immunoprecipitation must be able to solubilise the proteins in question, yet preserve protein-protein interactions. Sometimes this requires a great deal of empirical optimisation and troubleshooting (variations in detergent composition and

ionic strength are most common), before these opposing buffer properties are combined for a particular protein (Harlow & Lane, 1999). This issue is especially relevant for receptors, since their solubilisation requires the use of more aggressive detergents at relatively higher concentrations, which might destroy weaker protein-protein interactions giving false-negative results. On the other hand, some receptors, especially those with multiple membrane spanning helices, have large hydrophobic surfaces which can lead to nonspecific aggregation, giving false-positive results. To counter these shortcomings various strategies and control experiments must be employed. Weak and transient receptor associations can be "fixed" using chemical crosslinking before cell lysis. A vast selection of crosslinking reagents is available from commercial suppliers with varying chemistry and linker length. Crosslinking reagents with different cell permeability properties also can be selected, allowing specific crosslinking of extracellular parts of the receptor only (Melcher, 2004). Nonspecific aggregation at least in some cases can be ruled out by a control experiment, where differentially tagged receptors are expressed in different cells and those cells are mixed before lysis and co-immunoprecipitation. However, as always, care must be taken when interpreting results, as receptors capable of interaction in *trans* might create the impression of aggregation.

1.7.2 Resonance energy transfer

Biophysical methods based on resonance energy transfer (RET) between two different molecules have already become standard tools for the measurement of receptor oligomerisation. Many different approaches and methodologies have been derived, however the same fundamental principle lays at the heart of each of these techniques. If the emission spectrum of one fluorophore (donor) overlaps with the absorption spectrum of another (acceptor), energy can be transferred from donor to acceptor. This transfer does not depend on the exchange of photons; it primarily occurs via resonation of donor and acceptor dipoles. The German physicist Theodor Förster developed theory describing RET more than fifty years ago, which can be expressed by the following formulae:

$$[1.1] \quad E = \frac{R_0^6}{R_0^6 - r^6}$$

$$[1.2] \quad r = R_0 \left(\frac{1}{E} - 1 \right)^{1/6}$$

$$[1.3] \quad E = 1 - \frac{\tau_{DA}}{\tau_D}$$

$$[1.4] \quad E = 1 - \frac{F_{DA}}{F_D}$$

E here represents energy transfer efficiency, r – distance between fluorophores and R_0 marks the so called Förster distance, which incorporates all other factors affecting RET and

is a constant for a given fluorophore pair. It is noteworthy that the Förster distance includes an orientation factor, since RET depends on the alignment of donor and acceptor dipoles. Energy transfer is most efficient when dipoles are parallel and totally disappears if donor and acceptors dipoles are aligned perpendicularly. Formula [1.1] can be rearranged into [1.2] demonstrating that, by knowing the energy transfer efficiency E it is possible to calculate the distance between fluorophores. Experimentally, E values can be established by measuring either the fluorescence lifetime [1.3] or fluorescence intensity [1.4] of the donor under two different conditions, with the acceptor present (DA) or not (D).

Förster distance can also be defined as the distance between fluorophores which gives 50% RET efficiency. Typical values of R_0 are 20-100 Å. These values are very similar to the diameter of biological macromolecules and hence RET is a convenient tool for measuring distances between two proteins. Additionally, the power of six dependency between RET efficiency and the distance between fluorophores makes distance measurements extremely sensitive. Changes as small as 1-2 Å can be detected under the right conditions. All of these useful properties make RET an extremely popular "molecular ruler" to assess conformational changes and interactions between biomolecules.

1.7.2.1 Fluorescence resonance energy transfer

The classical RET method, called fluorescence resonance energy transfer (FRET), measures RET between two fluorophores. In this situation, RET manifests itself as donor quenching and excitation of acceptor, since energy is transferred from donor to acceptor. Historically, FRET was first used to evaluate protein or DNA interactions and conformational changes in solution (Clegg, 1995; Selvin, 1995; Wu & Brand, 1994). Biological macromolecules were usually labelled with chemical fluorophores and fluorescence intensity or fluorescence lifetime measurements were conducted in a cuvette with a fluorometer. Under this setup it was relatively easy to control the experimental conditions and concentrations of fluorophores, which allowed relatively straightforward quantification of energy transfer efficiency. Unfortunately, this method could not be used to study receptor oligomerisation and the development of new technical approaches was needed where FRET could be measured in intact cells. Although attempts to measure FRET *in vivo* by injecting prelabeled proteins into a cell were made early on, *in vivo* techniques really gained prominence only with development of FRET fluorophore pairs based on green fluorescent protein (GFP) (Carlson & Campbell, 2009).

GFP based FRET pairs facilitate FRET measurements between proteins residing in cells, including membrane receptors, by removing tedious and problematic protein labelling and

injection procedures. Nevertheless, this method has its own shortcomings. Cells are not homogenous and have substantial background fluorescence, thus the actual measurements are usually performed offline from images taken with a fluorescence microscope. Most standard and popular widefield microscopy systems are only able to measure fluorescence intensities but not fluorescence lifetimes. Fluorescence intensity, as opposed to lifetime, directly depends on fluorophore concentration and needs to be accounted for before an actual energy transfer efficiency is calculated. In a standard experiment two samples, one containing donor and acceptor, the other containing only donor at the same concentration as in the first sample, would be measured and energy efficiency calculated according to formula [1.4]. Ironically, it is impossible to know or strictly control natively expressed fluorophore concentrations. Protein expression is subject to biological variation and concentrations will vary from cell to cell and even within cell regions, making it impossible to have two samples with an identical donor concentration. The exception is FRET sensors, where donor and acceptor are connected by the same polypeptide and thus their concentration is always equal.

Several different approaches can help to circumvent this limitation. First of all, in some situations the calculation of energy transfer efficiency is dispensable. If one needs to know only relative changes in FRET, without calculating actual distances, one can use an index devised from fluorescence intensity measures which roughly represent FRET intensity. This approach is also called sensitized emission FRET imaging. Many different indices are suggested by different researchers, each of them having slight advantages under certain experimental circumstances (Gordon et al, 1998; Xia & Liu, 2001; Berney & Danuser, 2003). Generally they are adequate to assess receptor oligomerisation states. A drawback of this approach is that absolute values of a particular index depend on the optical pathway and thus will not be comparable between different microscopes or even different filter sets. To address this problem, the so called constant G was suggested, which can be measured for each device and used to normalise FRET indices (Chen et al, 2006; Gordon et al, 1998).

The second FRET measurement technique is to remove acceptor from the sample by photobleaching. If FRET is present, donor fluorescence is quenched because some of the donor energy is transferred to the acceptor. Photobleaching the acceptor fluorophore releases this quenching and increases the donor fluorescence. In this situation, energy transfer efficiency can be calculated directly by formula [1.4] since we know donor fluorescence intensity with and without acceptor in the same sample. The main

disadvantage of this method is its destructive nature, as the sample can only be used once and thus time-lapse and dynamic measurements are impossible. Additionally, it is not always easy to obtain complete acceptor destruction without affecting the donor and even a small remaining fraction of active acceptor can lead to gross errors in distance calculations (Berney & Danuser, 2003).

The most precise and least ambiguous, but technically most complex and demanding FRET measurement method is fluorescence-lifetime imaging microscopy (FLIM). Energy transfer efficiency can be directly calculated from donor and acceptor lifetimes according to formula [1.3] without the need for concentration corrections. FLIM, however, has its own share of problems. Sophisticated equipment, rarely available within most life science laboratories, is needed to perform these measurements. Data analysis is not trivial, as the fluorescence lifetimes of GFP derivatives are often multiexponential and overlap with many endogenous cell fluorophore lifetimes. Rigorous mathematical analysis and careful interpretation are needed when analysing FLIM data (Chang et al, 2007).

Advances in the chemistry of lanthanide complexes have created another biologically relevant label for FRET measurements. Lanthanide cryptates are chemically stable, biologically inert compounds with uniquely long fluorescence lifetimes. The average fluorescence lifetime of common fluorophores is in the range of nanoseconds, while the fluorescence lifetime of lanthanide cryptates reach micro and even milliseconds. A method called time-resolved FRET (TR-FRET) utilises this difference to separate FRET signal from background fluorescence (Bazin et al, 2002). After the excitation impulse, fluorescence measurements are delayed for 10-60 microseconds, thus excluding background noise and collecting only lanthanide cryptate fluorescence. TR-FRET is a sensitive and precise method which allows employment of relatively simple, high-through equipment like plate readers, thus becoming the method of choice in industrial settings. In TR-FRET, terbium or europium cryptates serve as a FRET donor, while the FRET acceptor is usually phycobilliprotein and its derivatives, although other molecules can also be used. Obviously, it is impossible to encode these labels genetically, so fluorophore-conjugated antibodies are usually employed to label cell surface receptors (Maurel et al, 2004). Donor and acceptor labelled antibodies against common epitope tags are commercially available from several different suppliers. New, irreversible protein labelling techniques like Snap-tag or Clip-tag are commercially adapted to time-resolved FRET as well.

1.7.2.2 Bioluminescence resonance energy transfer

Bioluminescence resonance energy transfer (BRET) is a natural phenomenon observed in bioluminescent jellyfish and sea polyps. A bioluminescent protein, aequorin in the case of *Aequora victoria*, oxidises its substrate coelenterazine and emits blue light. GFP absorbs part of the aequorin energy via resonance energy transfer and emits its own green fluorescence giving jellyfish an overall greenish luminescence. It is interesting to notice that even though GFP has become a standard tool in cellular biology, actual BRET biological functions remain vague (Alieva et al, 2008).

BRET is based on resonance energy transfer so its efficiency is distance-dependent and can be used to monitor protein-protein interactions, including oligomerisation of receptors. Originally, BRET systems used luciferase from the sea pansy *Renilla reniformis* (RLUC) as donor, coelenterazine as substrate for RLUC and enhanced yellow fluorescent protein (eYFP) as acceptor (Xu et al, 1999). Both RLUC and eYFP are relatively small proteins so they can be fused to a protein of interest and BRET measurements performed in intact cells. Since then, several different modified BRET systems were created modifying and improving donor, acceptor or luciferase substrate characteristics (De et al, 2007; De et al, 2009; Pflieger et al, 2006). The main advantage of BRET over FRET is that there is no need for excitation illumination. This removes various issues related to background fluorescence, photobleaching, phototoxicity and acceptor excitation. BRET's shortcomings are lower light output in comparison to that of FRET and the requirement for external addition of the luciferase substrate.

1.7.3 Fluorescence recovery after photobleaching

Fluorescence recovery after photobleaching (FRAP) is a relatively new technique to study receptor oligomerisation in living cells (Dorsch et al, 2009). In this technique, yellow fluorescent protein (YFP) is fused to an extracellular part of one receptor, while the other receptor carries cyan fluorescent protein (CFP) at its intracellular part. The constructs are coexpressed in cells, a small area of the cell membrane is bleached and the time-course of fluorescence recovery is monitored. The speed and extent of fluorescence recovery depends on lateral mobility of tagged proteins. It is possible to reduce this mobility by burdening receptor with bound antibodies. Anti YFP antibody will bind YFP-tagged receptors reducing their mobility and impairing fluorescence recovery of this construct as observed by YFP fluorescence. Anti YFP antibody does not affect recovery of CFP signal, unless there are direct associations between YFP and CFP tagged receptors. If the receptors in question oligomerise, the anti YFP antibody will affect recovery of both YFP and CFP

fluorescence. Quantitative FRAP studies can provide information about complex stability and the level of oligomerisation (Dorsch et al, 2009).

1.7.4 Bimolecular fluorescence complementation

Bimolecular fluorescence complementation (BiFC) is a method based on structural reconstitution of the fluorescent protein. A fluorescent protein is split into two inactive parts and those parts are fused to the proteins of interest. Separately these constructs are not fluorescent, but if they interact, complementary FP fragments are brought into proximity which leads to spontaneous reconstitution of active fluorescent protein. The intensity of the observed fluorescence is therefore directly proportional to extent of protein-protein association and can be evaluated using standard laboratory equipment like a fluorescence microscope or plate reader. A more complicated BiFC setup, using several fluorescent proteins with different spectral characteristics, can be used to detect multiple protein-protein interactions (Vidi et al, 2011). The main shortcoming of BiFC is the irreversible nature of complementation. Once functional FP is formed, interacting proteins usually would not be separated again. This makes dynamic time-lapse experiments almost impossible. BiFC also is prone to false positive results, since weak and transient interactions can be stabilised by complementation itself.

1.8 Aims of the project

The first aim of this project is to investigate Robo1 transmembrane signalling mechanisms. Published data indicates that Robo, like many other single pass membrane receptors, most likely transmits its signal across the membrane by changing its oligomerisation state (Hohenester, 2008). I will use a range of biochemical and biophysical techniques to determine Robo oligomeric status in resting and signalling competent states. Establishing this hopefully will help to elucidate mechanism of Robo1 transmembrane signalling.

The second aim of my study is to elucidate the role of Slit-Robo within the immune system. Robo1 protein is expressed by various leukocytes, Slit-Robo signalling affects inflammation and inflammation affects Slit-Robo expression levels. Experimental evidence indicates a functional connection between the immune system and the Slit-Robo signalling axis, however, the precise role or underlying mechanisms remain unknown. Using multiple approaches I will establish an initial working hypothesis and then I will test it using appropriate methods.

2 Materials and methods

2.1 Materials

2.1.1 Reagents, enzymes, medium components and kits

The majority of chemicals were from Sigma-Aldrich (Poole, Dorset, UK) or Fisher Scientific (Leicester, UK). DNA restriction endonucleases, GoTaq polymerase, calf intestinal alkaline phosphatase (CIAP), Wizard Plus SV Miniprep kit and T4 ligase were from Promega (Southampton, UK). TRIzol, protein markers, NuPage Novex pre-cast 4-12 % Bis-Tris gels, NuPage MOPS SDS running buffer, antibody-Alexa Fluor® 594 conjugates and SuperScript III were purchased from Invitrogen (Paisley, UK). RNeasy kit, QIAfilter Plasmid Maxi Kit, PCR purification kit, DNeasy blood and tissues and QIAquick gel extraction kit were from (Qiagen Crawley, UK). High fidelity Phusion polymerase was from New England Biolabs (MA, USA). Polynucleotide kinase, complete EDTA-free protease inhibitor tablets, collagenase D, DNase I and DNA markers were from Roche (Lewes, UK). Agarose was from Flowgen Biosciences (Nottingham, UK). Secondary horseradish conjugated antibodies were from GE Healthcare Life Sciences (Little Chalfont, UK). Red PCR Master Mix was from Rovalab (Teltow, Germany). X-ray film was from Konica (Hohenbrunn, Germany). ECL reagent and BCA assay was purchased from Pierce (Tattenhall, UK). Rac1/CDC42 activation assay kit was from Millipore. SNAP-Lumi4-Tb cryptate and SNAP-Red were purchased from Cisbio Bioassays (Codolet, France). SYBR Green PCR Master Mix was from Applied Biosystems.

2.1.2 Buffers and microbiological culture

Phosphate Buffered Saline (PBS) (10 x)

137 mM NaCl, 2.7 mM KCl, 1.5 mM KH_2PO_4 , 8 mM Na_2HPO_4 , pH 7.4

Diluted 1 in 10 prior to use and stored at 4°C

Tris Buffered Saline (TBS) (10 x)

20 mM Tris-base, 150 mM NaCl, pH 7.4

Diluted 1 in 10 prior to use and stored at room temperature

Tris-EDTA (TE) Buffer

10 mM Tris, 0.1 mM EDTA, pH 7.4

Radioimmune precipitation assay (RIPA) Buffer (2x)

100 mM HEPES (pH7.4), 300 mM NaCl, 2 % (v/v) Triton X-100, 1 % (w/v) Na deoxycholate, 0.2 % (w/v) SDS . Stored at 4°C. Diluted 1:2 prior to use with:
0.5 M NaF, 0.5 M EDTA, 0.2 M NaH₂PO₄, 10% (v/v) ethylene glycol, complete
EDTA free protease inhibitor tablet

Physiological Saline Solution

130 mM NaCl, 5 mM KCl, 1 mM CaCl₂, 1 mM MgCl₂, 20 mM HEPES, 10 mM D-glucose, pH 7.4

Laemlli Buffer (6x)

200 mM Tris-HCl, 8 % (w/v) SDS, 0.4 % (w/v) bromophenol blue, 40 % (v/v) glycerol,
500 mM DTT. Stored in aliquots at -20°C

TAE Buffer (50 x) pH 8.0

40 mM Tris base, 5 mM EDTA, 5.71 % (v/v) glacial acetic acid
Diluted 1 in 50 prior to use and stored at room temperature

DNA Gel Loading Buffer (5 x)

0.25 % (w/v) bromophenol blue, 40 % sucrose (w/v) in distilled H₂O

LB medium (Luria-Bertani Medium)

1 % (w/v) bactotryptone, 0.5 % (w/v) yeast extract, 1 % NaCl (w/v), pH 7.4. Sterilised by autoclaving at 126°C

SOC medium

2% (w/v) bactotryptone, 0.5% (w/v) yeast extract, 10mM NaCl, 2.5mM KCl, 10 mM MgCl₂, 20mM glucose. Sterilised by autoclaving at 120°C

2.1.3 Oligonucleotides

All oligonucleotides were purchased from Eurofins MWG and are listed in Table 2.1

2.1.4 Bacteria strains

XL1-Blue *E. coli* - endA1 gyrA96(nal^R) thi-1 recA1 relA1 lac glnV44 F' [::Tn10 proAB⁺ lacI^q Δ(lacZ)M15 Amy Cm^R] hsdR17(r_K⁻ m_K⁺)

ER2925 *E. coli* - ara-14 leuB6 fhuA31 lacY1 tsx78 glnV44 galK2 galT22 mcrA dcm-6 hisG4 rfbD1 R(zgb210::Tn10)TetS endA1 rpsL136 dam13::Tn9 xylA-5 mtl-1 thi-1 mcrB1 hsdR2

Table 2.1 Oligonucleotides used in this study

	ID	Sequence	Notes
Slit2 and Robo1 cloning and construct creation	LZ40	CCGAAAGCTCAAGAGAAGTCC	mSlit2 cloning, flanking left
	LZ41	AGCATGAATTAGTCCAACATGG	mSlit2 cloning, flanking right
	LZ44	TGTAGGGTGTATGGTGTGTGG	mRobo1 cloning, flanking left
	LZ45	TAGCATCGTAAGCCTCTCTGG	mRobo1 cloning, flanking right
	LZ103	TAGGATCCTGCCCCGCCCAGTCTCCTGT	BamHI-Slit2
	LZ104	TATGCGGCCGCTTAGGAGGCACATCTCGCGCAGCCGCACTTC	Slit2-STOP-NotI
	LZ105	CACCATGATCGCGGAGCCTGCTCGCTTTTACCTCTTTG	KpnI-SS-EcoRI-myc-EcoRV linker
	LZ106	GATTAATATGTCTCTGTTCAGGCTCCCGTCTTCGTGAGGAAG	KpnI-SS-EcoRI-myc-EcoRV linker
	LZ107	AATTGGAACAAAACTTATTTCTGAAGAAGATCTGGAT	KpnI-SS-EcoRI-myc-EcoRV linker
	LZ108	ATCCAGATCTTCTTCAGAAATAAGTT	KpnI-SS-EcoRI-myc-EcoRV linker
	LZ109	TTTGTTCGAATTCTTCCTGACGAAG	KpnI-SS-EcoRI-myc-EcoRV linker
	LZ110	ACGGGAGCCTGAACAGAGACATATTAATCCAAAGAGGT	KpnI-SS-EcoRI-myc-EcoRV linker
	LZ111	AAAAGCGAGCAGGCTCCGCGATCATGGTGGTAC	KpnI-SS-EcoRI-myc-EcoRV linker
	LZ112	TCGATATCGGCTCCCGTCTTCGTGAGGAAGATT	EcoRV-mRobo1-XbaI
	LZ113	TATCTAGATCAGCTTTTCAGTTTCCTCTAATTC	EcoRV-mRobo1-XbaI
	LZ114	ATGCGGCCGCTAGTTACTGTTGGCGTGAAGGTAAAG	EcoRV-mRobo1-NotI
	LZ115	ATCTCGAGTATCAAAGAGGAGCGAAGCCGTC	XhoI-mRobo1-XbaI
	LZ116	ATTCTAGATCAGCTTTTCAGTTTCCTCTAATTC	XhoI-mRobo1-XbaI
	LZ125	TAGCGGCCGCATGGTGAGCAAGGGCGAGGAG	NotI-FP forward
	LZ126	TTACTCGAGCTTGACAGCTCGTCCATGCCG	FP-XhoI rev
	LZ127	TTACTCGAGTTACTTGTACAGCTCGTCCATGCCG	FP-STOP-XhoI rev
	LZ128	TAGAATTCGACTACAAGGATGACGATGACAAGGATATCAT	EcoRI-FLAG-EcoRV
	LZ129	ATGATATCCTTGTTCATCGTCATCCTTGTAGTCGAATTCTA	EcoRI-FLAG-EcoRV
	LZ150	CTGATATCGAATTTGGGGTTCCAGTTCAAC	5 Ig deletion
	LZ151	CTGATATCTTAGATTCTCACGAAACCCCGTGT	Ig ir FNIII deletion
	LZ152	TAGAATTCATGGACAAAGACTGCGAAATG	Snap-clip -EcoRI fw
	LZ154	TAGATATCATGGACAAAGACTGCGAAATG	Snap-clip -EcoRV rv
Sequencing	LZ8	GAAGCCAGTCTGAGAGCCAGG	mSlit2 sequencing
	LZ9	AAACTTAGGACATTTGCACTCC	mSlit2 sequencing
	LZ10	CTGCACAACTTGAACCTTCTC	mSlit2 sequencing
	LZ11	AAATTCTTCTCACCAGTAACC	mSlit2 sequencing
	LZ12	AAGTAACAACCGAATAAGCAC	mSlit2 sequencing
	LZ13	GGAGGAACTTGTCACTTAAAG	mSlit2 sequencing
	LZ14	AGAGAAGTGTGAGAAATTGG	mSlit2 sequencing
	LZ15	ACCTGTGAATGTGAGGAAGG	mSlit2 sequencing
	LZ16	ACGATGGTCTCTCTAAAACGG	mRobo1 sequencing
	LZ17	ACTATACGAGGAGGAAAACCTC	mRobo1 sequencing
	LZ18	GAAGTTACTGATGTGATTGC	mRobo1 sequencing
	LZ19	GCAAATGCCTATGGAATTAGT	mRobo1 sequencing
	LZ20	CGAAGTATCACATAAACAAGA	mRobo1 sequencing
	LZ21	AGCCAATTATAACAACCAACT	mRobo1 sequencing
	LZ22	CATGTCCGTAGATGAAAGCT	mRobo1 sequencing
	LZ23	AGTGTCAGTTTCATCCGATGG	mRobo1 sequencing

Expression studies in mouse cells	LZ55	GGCAAACATTACACGCTCAA	hSlit1 expression detection forward
	LZ56	CTTCATCTGCGTCTTGGTGA	hSlit1 expression detection reverse
	LZ57	TGGCTATCAGGGAGAAAAGTG	hSlit2 expression detection forward
	LZ58	CCGCTGTCTTCATCTGTGG	hSlit2 expression detection reverse
	LZ59	TGACAAGGACACGGCATC	hSlit3 expression detection forward
	LZ60	ACTGCTGGCTGCTTCTGG	hSlit3 expression detection reverse
	LZ61	AAAGTAGCACGACGGCAAAT	hRobo1 expression detection forward
	LZ62	CCTGGCTGGTGTTCAGTTT	hRobo1 expression detection reverse
	LZ63	TCCTGCTATCTCCTTTGGACA	hRobo2 expression detection forward
	LZ64	AACCTAACGGTGGAAGTGA	hRobo2 expression detection reverse
	LZ65	AAGCCTCTCTGTGACCAGGA	hRobo3 expression detection forward
	LZ66	TGATGACCCCATTTTGCTG	hRobo3 expression detection reverse
	LZ67	CGCAGGGGACTCTCTTCTC	hRobo4 expression detection forward
	LZ68	TTTGGGAAAGGTTCTTGGA	hRobo4 expression detection reverse
	LZ71	ACACCCACTCCTCCACCTTT	hGAPDH
	LZ72	TTCTCTTGTGCTCTTGCTG	hGAPDH
Expression studies in human cells	LZ81	ATGGAGCCAACGCGTAGAC	mSlit1 expression detection forward
	LZ82	AATCCCATTTGCTCTGCTG	mSlit1 expression detection reverse
	LZ83	TCACACTTCAGATTGCCACAG	mSlit2 expression detection forward
	LZ84	CCATCCACAGAGGGGAAAG	mSlit2 expression detection reverse
	LZ85	ACAATGACCCCTTGCGACT	mSlit3 expression detection forward
	LZ86	CCACTGCTGGTTGCTTCTG	mSlit3 expression detection reverse
	LZ87	TCCTACAGCCACCAATCCAC	mRobo1 expression detection forward
	LZ88	CTGAGACAAGGGTCCTGAA	mRobo1 expression detection reverse
	LZ89	GAGCCGTCCAGGTCTTCTAA	mRobo2 expression detection forward
	LZ90	GTCGCTGTTTTATCCCTTG	mRobo2 expression detection reverse
	LZ91	AGTGGGAGAGGAGAGTGGT	mRobo3 expression detection forward
	LZ92	GAGCTGTTGGAACCCCTAGA	mRobo3 expression detection reverse
	LZ93	GCTCCTTCCTCGCTGATAC	mRobo4 expression detection forward
	LZ94	GCCTCCACTCCCACAAAG	mRobo4 expression detection reverse
	LZ77	AAAATGGTGAAGGTCGGTGT	mGAPDH,
	LZ78	GTTAGTGGGGTCTCGCTCCT	mGAPDH
	LZ203	AAGACCTGTGCTTCTGTGACG	Slit2 mouse genotyping
	LZ204	AAGTCTAGTAGAGTCGAGCG	Slit2 mouse genotyping
	LZ205	AAACAGGTTTCTACCGCACG	Slit2 mouse genotyping

2.2 Methods

2.2.1 RNA extraction

Tissue samples were flash-frozen in liquid nitrogen and stored at -80°C until required. On the day of the experiment the samples were submerged into the liquid nitrogen and ground into a fine powder using pestle and mortar. Initial crude RNA purification was performed using a TRIzol reagent (Invitrogen) according to the manufacturer's instructions. The pulverized tissue sample was dissolved in the appropriate volume of TRIzol, mixed with

1/5 volume of chloroform and centrifuged at 12000g for 10 min at -4°C. An aqueous upper phase was transferred to a new tube and RNA was precipitated from the solution by adding equal volume of isopropanol and centrifuging the mixture at 10000g for 15 min at -4°C. The supernatant was discarded and RNA pellet dissolved in RNase free water. The second step of RNA purification was performed using RNeasy kit from Qiagen according to the manufacturer's instructions. RNA from cultured cells was extracted omitting the TRIzol step and using the RNeasy kit directly. Quality and concentration of purified RNA was assessed by agarose gel electrophoresis and spectroscopy. To avoid possible RNA degradation, cDNA was synthesized immediately after RNA purification, when it was necessary, the RNA samples were stored at -80°C until required.

2.2.2 cDNA synthesis

cDNA synthesis was performed using SuperScript III (Invitrogen) or AffinityScript (Stratagen) cDNA synthesis kits according to the manufacturers' instructions. Initially, primers were annealed to mRNA

- 1 µg total RNA
- 500 ng oligo(dT) primers
- RNase free water up to 14.2 µl

The mixture was incubated at 65°C for 5 minutes and then cooled slowly to room temperature.

cDNA for Slit-Robo expression analysis was synthesised as follows:

- 14.2 µl total RNA with primers
- 2 µl 10x RT buffer
- 1 µl AffinityScript reverse transcriptase
- 0.5 µl RNase Block
- 2 µl 100 mM DTT
- 0.8 µl 100 mM dNTP

The mixture was incubated at 42°C for 70 minutes to synthesize cDNA, then at 70°C for 15 minutes to inactivate reverse transcriptase.

cDNA for Slit2 and Robo1 cloning was synthesised according to following protocol:

- 14.2 µl total RNA with primer
- 2 µl 10x RT buffer
- 1 µl SuperScript III reverse transcriptase (another 0.5 µl of enzyme was added after 30 minutes)

- 0.5 µl RNase Block
- 2 µl 100 mM DTT
- 0.8 µl 100 mM dNTP

The mixture was incubated at 55°C for 70 minutes to synthesize cDNA, then at 70°C for 15 minutes to inactivate reverse transcriptase. Reactions without reverse transcriptase were routinely used as negative controls to account for possible genomic DNA contamination.

2.2.3 Genomic DNA extraction

Genomic DNA from mouse tissues was extracted using Qiagen "DNeasy blood and tissues" kits according to the manufacturer's instructions.

2.2.4 Construction of custom polylinker

In order to facilitate Robo1 cloning and tagging a new polylinker containing Robo1 signalling sequence and epitope tags was introduced into pcDNA3. Oligonucleotides LZ105-LZ111 were phosphorylated using polynucleotide kinase (Roche):

- 2 µl 10x phosphorylation buffer
- 4 µl 100 µM oligonucleotide
- 1 µl 100 mM dATP
- 1 µl polynucleotide kinase

The reaction mixture was incubated for 30 minutes at 37°C, phosphorylated oligonucleotides were then pooled, incubated at 100°C for 5 minutes and left to cool to room temperature. The formed double stranded DNA sequence was then ligated into the pre-cut pcDNA3 vector.

2.2.5 PCR

Slit2 and Robo1 genes and various constructs were synthesised using Phusion polymerase (NEB) as follows:

- | | |
|-----------------------------|-----------------------|
| ➤ 5 µl cDNA | 95°C -- 3 min |
| ➤ 10 µl 5x HF buffer | 95°C -- 1 min |
| ➤ 500 nM of each primer | 62°C -- 1 min |
| ➤ 0.5 µl Phusion polymerase | 72°C -- 1.5 min |
| ➤ 5 µl 1 mM dNTP | 25 cycles from step 2 |
| ➤ 1.5 µl DMSO | 72°C -- 10min |
| ➤ water up to 50 µl | |

RT-PCR was performed using Red PCR Master Mix (Rovalab) as follows:

- | | |
|------------------------------|---------------|
| ➤ 5 µl 5x Red PCR Master Mix | 95°C -- 3 min |
|------------------------------|---------------|

- 0.5-2 µl cDNA 95°C -- 1 min
 - 500 nM of each primer 55°C -- 1 min
 - water up to to 50 µl of total volume 72°C -- 1min
- 30 cycles from step 2
72°C -- 5min

Genotyping was performed using GoTaq (Promega):

- 50 ng genomic DNA 95°C -- 5 min
- 10 µl 5x GoTaq buffer 94°C -- 1 min
- 500 nM of each primer 65°C -- 1 min
- 200 nM of each dNTP 72°C -- 1.5 min
- 1.25 U GoTaq polymerase 30 cycles from step 2
- Water up to 20 µl 72°C -- 10min

2.2.6 Plasmid DNA extraction and purification

Mini preparations of plasmid DNA from bacterial cultures were performed using Wizard Plus SV Miniprep kit (Promega). QIAfilter Plasmid Maxi Kit (Qiagen) was used to purify larger amounts of plasmid DNA. All kits were used according to the manufacturer's instructions.

2.2.7 Digestion of DNA with restriction enzymes

To carry out cloning, select minipreps or analyse constructs, DNA samples were digested with restriction enzymes as follows:

- 1 µl of appropriate enzyme (Promega)
- 1 µl 10x corresponding buffer (Promega)
- 0.2 - 1 µg DNA
- water up to 10 µl

The mixture was incubated 1 - 3h at temperature indicated by the enzyme supplier.

2.2.8 DNA dephosphorylation

When it was relevant, vector DNA was treated with calf intestinal alkaline phosphatase (CIAP) to remove 5'-phosphate groups.

- 0.05 U CIAP (Promega)
- 30 µl DNA
- 5 µl 10x CIAP buffer
- water up to 50 µl

The mixture was incubated at 37°C for 30 min. Dephosphorylated DNA was purified using "PCR purification kit" from Qiagen according to the manufacturer's instructions.

2.2.9 DNA ligation

To generate required constructs DNA fragments were ligated using T4 DNA ligase. Vector and insert ratio was varied from 1:3 to 1:6. Typical reaction mixture contained:

- 1 U T4 DNA ligase (Promega)
- 1 µl 10x T4 DNA ligase buffer
- 50-100 ng vector DNA and corresponding amount of insert DNA
- water up to 10 µl

The reaction mixture was incubated for 16 h at 4°C and then directly used for bacteria transformation.

2.2.10 DNA gel electrophoresis

Agarose gel DNA electrophoresis was used to analyse digested DNA, verify created constructs or purify required DNA fragments from digestion mixture. 0.8%-1.6% (w/v) agarose gels were prepared in 1x TAE buffer with SYBR Safe DNA stain (SYBR Safe DNA stain was supplied as 10000x concentrate). Samples containing 0.2 - 0.5 µg of DNA were mixed with 6x loading buffer and loaded onto the gel. A DNA marker was also loaded in order to determine the size of visualized bands. The electrophoresis was run at 125 V voltage until bromophenol dye from loading buffer travelled 2/3 of gel length. The DNA fragments were visualized with UV light using a BioRad Gel Doc 2000 transilluminator.

2.2.11 DNA purification from gel

DNA fragments of interest were cut from gel and purified using QIAquick gel extraction kit (Qiagen) as per manufacturer's instructions

2.2.12 Preparation of competent bacterial cells

XL1-Blue *E. coli* strain was streaked onto a LB plate with 50 µg/ml kanamycin and grown overnight at 37°C. The selected single colony was inoculated into 4 ml LB medium, grown overnight at 37°C and then subcultured into 100 ml of LB medium. Once culture reached OD₆₀₀ of 0.5, 50 ml of cells were chilled on ice for 5 min, centrifuged to remove medium and resuspended in 20 ml of ice-cold solution 1 (30 mM KCl, 10 mM RbCl₂, 10 mM CaCl₂, 50 mM MnCl₂, 15% (w/v) glycerol, pH 5.8). Cells were kept on ice for 5 min, centrifuged again to remove solution 1 and resuspended in 2 ml of ice-cold solution 2 (10 mM RbCl₂, 75 mM CaCl₂, 15% (w/v) glycerol, 10 mM MOPS, pH 6.5). After keeping on ice for an additional 15 minutes cells were aliquoted into Eppendorf tubes 200 µl each and stored at -80°C.

2.2.13 Bacterial transformation

Competent *E. coli* cells were incubated with 1-50 ng of DNA on ice for 30 minutes and heat shocked for 2 min at 42°C. After heatshock cells were chilled on ice for 2 min, inoculated into 500 µl of SOC medium and incubated with shaking at 37°C for 1 hour. Finally cells were plated on LB-agar plates with appropriate antibiotic and grown overnight at 37°C.

2.2.14 Cell maintenance

All cells were maintained in a humidified incubator with 95% air and 5% CO₂ at 37°C.

HEK 293T

Human embryonic kidney cells were grown as a monolayer in Dulbecco's Modified Eagle Medium (DMEM) supplemented with 10% (v/v) newborn calf serum, 2nM L-glutamine, 100 U/ml penicillin and 0.1 mg/ml streptomycin.

Flp-In T-Rex HEK 293

Parental Flp-In T-Rex HEK 293 cells were maintained in DMEM (high glucose) supplemented with 10% (v/v) newborn calf serum, 2nM L-glutamine, 100 U/ml penicillin, 0.1 mg/ml streptomycin and 100 µg/ml zeocin.

Flp-In HEK 293 based cell lines

Cell lines based on Flp-In HEK 293 cells were maintained in DMEM (high glucose) supplemented with 10% (v/v) newborn calf serum, 2 mM L-glutamine, 100 U/ml penicillin, 0.1 mg/ml streptomycin, 10 µg/ml blasticidin and 200 µg/ml hygromycin. Double stable cell lines stably expressing two different proteins were maintained in medium additionally supplemented with 1 mg/ml geneticin.

Other cell lines

THP-1, Raji, CA46, ACVA-1, HUT78, JURKAT, K562, MEG-01 and HMC-1 cells were grown in suspension in RPMI 1640 medium supplemented with 10% (v/v) newborn calf serum, 2 mM L-glutamine, 100 U/ml penicillin and 0.1 mg/ml streptomycin.

3T3 and B16 cells were maintained in DMEM supplemented with 10% (v/v) newborn calf serum, 2nM L-glutamine, 100 U/ml penicillin and 0.1 mg/ml streptomycin.

2.2.15 Transient cell transfection

For Western blot analysis, HEK 293T cells were transfected using polyethylenimine (PEI). Day before the transfection 2×10^6 cells were plated in 10 cm tissue culture dishes. Next day, 5 μ g of DNA was combined with 30 μ g of PEI in 500 μ l of 150 mM NaCl solution, thoroughly mixed and incubated for 10 minutes at room temperature. Cell medium was changed to fresh and the DNA-PEI mixture was added to the cells in a drop-wise manner gently mixing the medium.

HEK 293T cells intended for visualisation by microscopy were transfected using Effectene reagent (Qiagen) according to the manufacturer's instructions.

2.2.16 Stable cell line generation

Flp-In T-Rex HEK 293 cells were transfected with a mixture of pcDNA5/FRT/TO vector (harbouring myc-Robo1-CIT, FLAG-Robo1-CER, myc-Robo1-CIT-Robo1 or FLAG-Robo1-CER-Robo1 construct) and the pOG44 vector in a 1:9 ratio with Effectene reagent (Qiagen). After 48 hours, the medium was changed to medium supplemented with 200 μ g/ml hygromycin to initiate selection of stably transfected cells. Resistant clones were induced with 1 mg/ml doxycycline and screened by immunoblotting and immunocytochemistry.

Double stable cell lines were created by transfecting Flp-In T-Rex HEK 293 cells stably expressing myc-Robo1-CIT or myc-Robo1-CIT-Robo1 construct with a pcDNA3 vector harbouring FLAG-Robo1-CER or FLAG-Robo1-CER-Robo1 construct. After 48 hours, the medium was changed to medium supplemented with 1 mg/ml geneticin to initiate selection of stably transfected cells. Resistant clones were induced with 1 mg/ml doxycycline and screened by immunoblotting and immunocytochemistry.

2.2.17 Immunocytochemistry

Cells were grown on poly-D-lysine coated coverslips in 6-well plates and transfected with appropriate Robo1 constructs using Effectene reagent (Qiagen). Next day, cells were washed once for 5 minutes with room-temperature PBS and incubated with Hoechst dye for 15 minutes (in some cases staining with Hoechst was omitted). Cells then were washed again with PBS 2x 5 minutes and fixed by the addition of 2 ml 3.7 % (w/v) formaldehyde for 10 minutes. Fixed cells were washed three times for 5 minutes with PBS and incubated with 3% (w/v) low fat milk in PBS for 10 minutes. Primary anti-FLAG antibody (F7425, Sigma) was added at dilution 1:400 to the cells and incubated for 1 hour. Cells were

washed 3x 5 minutes with PBS and incubated with secondary anti-rabbit antibody conjugated to Alexa Fluor 594 dye (Invitrogen) in 3% (w/v) low fat milk PBS for another hour. Alternatively, SNAP staining was performed by adding SNAP-Surface 549 (Cisbio Bioassays) dye. After the final incubation cells were washed 3x 5 minutes with PBS and coverslips were mounted onto microscope slides using Immu-mount (Thermo Scientific) mounting medium. Mounted coverslips were stored in the dark at 4°C before being imaged using epifluorescence microscopy.

2.2.18 Recombinant Slit2 purification

HEK 293T cells were transferred into medium containing 1% of FBS and transfected with the pcDNA3 vector harbouring Slit2-(His)₆ construct. Supernatant was collected 48 hours later, its pH was adjusted to 7.5 and NaCl was added to final concentration of 500 mM. Slit2-(His)₆ protein from this solution was purified using AKTApurify plus chromatography system with 1 ml HisTrap HP column using a default pre-programmed procedure for His-tagged proteins. Binding buffer composition was 20 mM Na₃PO₄, 500 mM NaCl, 20 mM imidazole, pH 7.4. Elution buffer composition: 20 mM Na₃PO₄, 500 mM NaCl, 500 mM imidazole, pH 7.4

2.2.19 Protein crosslinking

HEK 293T cells transiently co-expressing differently tagged truncated and full-length Robo1 constructs were treated with 100 ng/ml of Slit2 (R&D Systems) or PBS as a negative control for 15 minutes. Cell medium was removed and cells were washed with PBS. DTSP crosslinking reagent (Sigma, D3669), which was stored as 200 mM solution in DMSO, was added into tissue culture dishes with cells in PBS in a dropwise manner to a final concentration of 2 mM. Cells were incubated at room temperature under gentle agitation for 30 min and the crosslinking was stopped and remaining DTSP reagent was neutralised by adding 1 M Tris·HCl (pH 7.4) solution to a final concentration of 50 mM. Cells were incubated for an additional 5 minutes and lysed as described below.

2.2.20 Preparation of cell lysates

Adherent cells were lysed as follows. Medium was removed and cells were washed 3 times with PBS. An appropriate volume of 1x RIPA buffer was added to the cells still attached to the surface of a tissue culture dish, cells were scraped from the flask using a disposable cell scraper and transferred to a centrifuge tube. Cells growing in suspension were centrifuged

at 300g for 5 minutes, medium was removed and the pellet was washed 3 times with PBS. Finally, the pellet was suspended in appropriate volume of 1x RIPA buffer.

The lysates were passed 4x through a 21-gauge needle, rotated for 30 min at 4°C on a rotating wheel and then centrifuged at 14000 g for 10 minutes to remove cell debris. The supernatant was carefully transferred into fresh tubes and the protein concentrations of the samples were determined using BCA assay (Pierce). Samples were used immediately for co-immunoprecipitation or SDS-PAGE or stored at -20°C until required.

2.2.21 Co-immunoprecipitation

The protein concentration of the cell lysates was equalised to 1 µg/µl using 1x RIPA. 30 µl of anti-FLAG antibody conjugated agarose beads (Sigma, A2220) was added to 700 µl of equalised cell lysate and incubated overnight at 4°C on a rotating wheel. In parallel, 100 µl of equalised cell lysate was reserved as a control sample. Next day, the samples were centrifuged at 8000 g for 3 minute at 4°C, the supernatant removed and the beads washed three times in 1x RIPA buffer. Finally, the beads and the control samples were resuspended in 50µl Laemmli buffer and analysed using SDS-PAGE and Western blotting.

2.2.22 Sodium dodecyl sulphate polyacrylamide gel electrophoresis

Protein samples were resolved using sodium dodecyl sulphate polyacrylamide gel electrophoresis (SDS-PAGE). Samples and molecular weight markers were loaded onto pre-cast NuPage Novex bis-tris gels with 4-12 % acrylamide concentration (Invitrogen). NuPage MOPS SDS buffer was used for electrophoresis at 200 V using the XCell Surelock mini-cell gel tank until the dye front reached the foot of the gel.

2.2.23 Western blotting

Following separation of samples by SDS-PAGE proteins were electrophoretically transferred onto nitrocellulose using the XCell II blot module. Proteins were transferred at 30V for 2 hours in transfer buffer (0.2M glycine, 25mM Tris and 20% (v/v) methanol). To block non-specific binding sites, the nitrocellulose was incubated in 5% (w/v) low fat milk, 0.1% (v/v) Tween 20 TBS at room temperature on a shaker for two hours. The membrane was incubated with primary antibody overnight at 4°C in 5% (w/v) low fat milk, 0.1% (v/v) Tween 20 TBS containing the required antibody. After overnight incubation, the membrane was washed 4 times in 0.1% (v/v) Tween 20 TBS over a 20 minute period. Membrane was then incubated with the horseradish peroxidase linked secondary antibody in 5% (w/v) low fat milk, 0.1% (v/v) Tween 20 TBS at room temperature for 20 minutes.

Again, the membrane was washed 4 times in 0.1% (v/v) Tween 20 TBS over a 20 minute period. Finally, the nitrocellulose was incubated for 5 minutes with ECL solution, exposed to blue Kodak film and film developed.

Table 2.2 List of antibodies used for Western blotting

Antigen	Supplier	Dilution	Secondary antibody	Dilution
c-myc (#2272)	Cell Signaling	1:2000	anti- rabbit	1:5000
FLAG (F7425)	Sigma	1:5000	anti-rabbit	1:5000
HIS ₆ (sc-803)	Santa Cruz	1:500	anti-rabbit	1:5000
Robo1 (AF1749)	R&D Systems	1:1000	anti-goat	1:10000
Robo1	DSHB	1:500 or neat hyb. supernatant	anti-mouse	1:5000
ERK1/2 (#4695)	Cell Signaling	1:1000	anti-rabbit	1:5000
phospho ERK1/2 (#9216)	Cell Signaling	1:1000	anti-mouse	1:5000
Slit2 (G19)	Santa Cruz	1:1000	anti-goat	1:10000
srGAP (ab57504)	Abcam	1:500	anti-mouse	1:5000

2.2.24 Transwell migration assays

Transwell migration assays were performed using Corning 12 mm polycarbonate membrane inserts with 3.0 μ m pores. Lower chambers were filled with 600 μ l of migration medium (RPMI, 20mM HEPES, 1% BSA) containing relevant reagents or equal volume of PBS as a negative control. THP-1 cells or human PBMC were suspended in migration medium at a density of 2×10^6 cells per ml, treated with relevant reagents if necessary and 100 μ l of this suspension was placed into upper chamber. The transwell kit was incubated for 3 hours at 37°C in humidified incubator. At the end of incubation the inserts were removed and cells present in lower chamber were counted using MacsQuant flow cytometer.

2.2.25 FRET imaging

Cells were grown on poly-D -lysine-treated glass coverslips and induced with doxycycline or transiently transfected using Effectene (Qiagen) to express the appropriate Cerulean and Citrine-tagged Robo1 constructs. Robo1 construct expressing cells were placed into a microscope chamber containing physiological HEPES-buffered saline solution (130 mM NaCl, 5 mM KCl, 1 mM CaCl₂, 1 mM MgCl₂, 20 mM HEPES, and 10 mM D-glucose, pH 7.4) and imaged using an inverted Nikon TE2000-E microscope (Nikon Instruments). Excitation light was generated from a mercury lamp with monochromator set to 430 and 500 nm for the sequential excitation of Cerulean and Citrine-tagged constructs

respectively. Excitation light was reflected through the objective lens using a cyan/yellow fluorescent protein dual band dichroic filter (Semrock; Rochester, NY, catalog no. FF440/520-Di01). Donor, acceptor and FRET channel images were acquired using the same exposure time (150 or 300 ms) and were detected using either a high speed emission filter wheel (Prior Scientific Instruments, Cambridge, UK) coupled to a 12-bit mode Cool Snap-HQ digital camera or a Quadview 2 (QV2) image splitting device attached to a Cool Snap-HQ2 camera operated in 14-bit mode. Using the emission filter wheel configuration donor, acceptor and FRET signals were sequentially detected using 542/27 and 472/30 nm emitters supplied by Semrock. Detection of equivalent signals using the QV2 image splitter was achieved using the following Chroma (Chroma, Brattleboro, VT), ET series dichroic and emitters: ET t505LPXR dichroic, ET535/30m, ET 470/30m. Hardware was controlled and data collected using Metamorph software (version 7.6.3 Molecular Devices, Sunnydale, CA). Saved donor, acceptor and FRET channel images were background-subtracted, and RFRET index was calculated as follows:

$$RFRET = \frac{I_F}{(I_A - I_D B_{DA})B_{AF} + (I_D - I_A B_{AD})B_{DF}}$$

B_{DA} and B_{AD} represent the proportion of donor or acceptor bleed through into the acceptor and donor channel, respectively. B_{AF} and B_{DF} represent the amount of acceptor and donor contamination in the raw FRET signal channel. All bleed through coefficients were calculated from control cells expressing Cerulean or Citrine alone. I_D , I_B and I_F represent the average fluorescence intensity of region of interest (ROI) for donor, acceptor and FRET channels respectively. Dozens of ROIs were measured in three randomly selected view fields for each sample. Final results are presented as a mean of 6 individual transfection or inductions.

2.2.26 Time resolved FRET

HEK 293T cells were transiently transfected with the myc-SNAP-Robo1-CIT or myc-SNAP-Robo1-CIT-Robo1 constructs, incubated for 24 hours and then transferred into a 96 well plate at a density of 50 000 cells per well. Next day the growth medium was replaced with 100 µl labelling medium (Cisbio Bioassays) containing appropriate concentrations of SNAP-Lumi4-Tb and SNAP-Red labels (Cisbio Bioassays). Plates were incubated for 1 h at 37 °C, 5% CO₂ in a humidified atmosphere and washed four times with labelling medium. Finally, plates were either read directly after this or Slit2 (R&D Systems) was

added to a final concentration of 100 ng/ml and the plate monitored over time course of 45 minutes. Emission signals from the SNAP-Lumi4-Tb cryptate (620 nm), the FRET signal resulting from the acceptor SNAP-Red (665 nm) and fluorescence intensity of Citrine fluorescent protein (530 nm) were recorded using a PheraStar FS (BMG Labtech) plate reader.

2.2.27 Protein arrays

Peptide libraries based on rat Robo1 sequence (NCBI Reference Sequence: NP_071524.1) were synthesized on cellulose membranes using Fmoc (9-fluorenylmethyloxycarbonyl) chemistry with the AutoSpot Robot ASS 222 (Intavis Bioanalytical Instruments). The interactions of spotted peptides with Robo1-Fc chimera (Robo1 extracellular domain fused to human Fc fragment, R&D Systems) were determined by overlaying the cellulose membranes with 50 µg/ml of Robo1-Fc protein in 1% (w/v) milk powder solution in 0.1% (v/v) Tween 20 TBS buffer. Bound Robo1-Fc protein was detected with anti-human Ig antibody coupled with horseradish peroxidase as in Western blotting.

2.2.28 QPCR

QPCR analysis was performed using SYBR Green chemistry and Applied Biosystems 7900HT QPCR machine. Copy number of gene of interest was determined from standard curves generated by amplifying serial dilutions of standard templates (PCR fragments of gene of interest with known concentration). In parallel with samples and standards, non-template reactions were used to control for non-specific amplification. Primers for detection and standard synthesis were designed using Primer3Plus software (<http://www.bioinformatics.nl/cgi-bin/primer3plus/primer3plus.cgi>) and are listed in Table 1. The detection primers when possible were designed to span intron-exon boundaries to prevent amplification of genomic DNA. Each sample or standard was undertaken in triplicate (three PCR replicates for each biological replicate). A typical QPCR reaction mixture contained:

- 10 µl 2x Power SYBR Green mix (Applied Biosystems)
- 50 pmol of each primer
- 2 µl of cDNA
- water up to 20 µl of total volume

Thermal cycle conditions were as follows: 1 cycle at 95°C for 10 min, 40 cycles 95°C for 15s, 60°C for 1 min.

2.2.29 RAC1 assay

Rac1 activity was measured using Rac1/CDC42 activation assay kit according to the manufacturer's instructions (Millipore). Briefly, cells were lysed and active GTP bound Rac1 was precipitated from the lysate with agarose beads coated with GST fusion-protein corresponding to the p21-binding domain of human PAK1. Samples were run on SDS-PAGE and Western blot analysis was used to evaluate amount of activated Rac1.

2.2.30 Robo1 antibody purification

Hybridomas producing Robo1 antibody were acquired from The Developmental Studies Hybridoma Bank (University of Iowa) and grown in Iscove's DMEM medium supplemented with 10% (v/v) heat inactivated FBS and 0.5 mg/ml gentamicin. Spent hybridoma medium was collected and its composition adjusted to match that of binding buffer by adding $(\text{NH}_4)_2\text{SO}_4$ to a final concentration of 0.8 M and adjusting pH to 7.5. The mixture then was subjected to purification using AKTApurify plus chromatography system and 1 ml HiTrap IgM HP column. A default pre-programmed procedure for IgM purification was employed with following buffer compositions: binding buffer - 20 mM Na_3PO_4 , 0.8 M $(\text{NH}_4)_2\text{SO}_4$, pH 7.5; elution buffer #1 - 20 mM Na_3PO_4 , pH 7.5; elution buffer #2 - 20 mM Na_3PO_4 , 30% (v/v) isopropanol, pH 7.5

2.2.31 Animals

Slit2 knockout animals of CD-1/129Sv outbred genetic background were generated by Plump and colleagues (Plump et al, 2002). Cryo-preserved spermatozoa of these animals were obtained from Mutant Mouse Regional Resource Centers (MMRRC, University of California, Davis) and animals were rederived by MRC Harwell (Harwell Science and Innovation Campus, Oxfordshire, UK) using CD-1 mice as oocyte donor. Rederived animals were transferred to the Central Research Facility, University of Glasgow and bred and maintained there during course of the experiments. All mice were genotyped using tail tip biopsies and PCR. C57BL/6 mice were bred and maintained in the same facility under similar conditions. All procedures were carried out in accordance with United Kingdom Home Office regulations under the auspices of appropriate Project and Personal Licences.

2.2.32 Primary cell isolation

Embryonic thymic cell suspensions were prepared as follows. C57BL/6 or Slit2 +/- timed pregnant mice were sacrificed by CO_2 inhalation. Embryos were immediately dissected, decapitated and kept in RPMI medium supplemented with 10% (v/v) FBS, 2mM L-glutamine, 100 U/ml penicillin and 0.1 mg/ml streptomycin (further referred as complete

RPMI) until embryonic thymi were dissected. Individual Slit2 knockout embryonic thymi, or pooled C57BL/6 embryonic thymi, were incubated at 37°C for 60 minutes in 700 µl or 2 mL respectively of 0.125% (w/v) Collagenase D and 0.1% (w/v) of DNase I (both from Roche) in RPMI-1640, with regular agitation. Finally, samples were mashed through 50µm cell strainer, centrifuged at 350g for 5 minutes and resuspended in cold FACS buffer (PBS with 5 mM EDTA and 2% FCS).

Human PBMCs were kind gift of Dr H. Baldwin and were prepared from heparinised human blood using Ficoll.

2.2.33 FACS and cell sorting

Cells were suspended in 100 µl of FACS buffer and Fc block (Miltenyi Biotec, UK) was added to the cells at a dilution of 1:20 and incubated for 10 minutes on ice to block non-specific antibody binding. Then fluorescently-labelled antibodies or isotype controls were added to the same buffer and cells incubated on ice for additional 15 minutes. Samples were washed twice with 1 ml chilled FACS buffer, cells pelleted by centrifugation at 350g at 4°C and resuspended in 100 µl of FACS buffer. When appropriate, cells were stained with secondary avidin-APC conjugate (BD Biosciences). After final wash step cells were resuspended in 100 µl of FACS buffer with 4 µl of viability dye Via-Probe (BD Biosciences) added. Samples were analysed using the MACSQuant (Miltenyi Biotec, UK) flow cytometer. Acquisition parameters were established using unstained and single-stained cells. Results were analysed and visualised using FlowJo software (Treestar Inc. USA). All antibodies were used at final concentrations between 1-5 µg/ml.

TEC sorting was performed by Dr A. White at School of Immunity and Infection MRC Centre for Immune Regulation, University of Birmingham. Embryonic thymi were disintegrated into single cell suspensions as described in section 2.2.32 Cells were stained with CD45 and EpCAM antibodies and CD45⁻ EpCAM⁺ cells were collected using MoFlo XDP (Beckman Coulter) cell sorter.

Table 2.3 List of antibodies used for flow cytometry

Antigen	Clone	Supplier
Ly51-PE	BP-1	BD Bioscience
CD8-PE	53-6.7	Miltenyi Biotec
CD45-Vioblue	30F11.1	Miltenyi Biotec

CD4-APC	GK1.5	Miltenyi Biotec
EpCAM-APC	G8.8	Abcam
MHCII-APC/Cy7	M5/114.15.2	BioLegend
Robo1-biotin	BAF1749	R&D Systems

2.2.34 *In silico* promoter analysis

Sequences for mammalian Slit and Robo promoter analysis were retrieved from NCBI Entrez Genome database (<http://www.ncbi.nlm.nih.gov/sites/genome>). Five thousand base pairs (5000 bp) of upstream sequence from the start codon ATG were retrieved for each gene of interest for the following mammalian species: *Homo sapiens*, *Bos Taurus*, *Canis lupus familiaris*, *Mus musculus*, *Macaca mulatta*, *Rattus norvegicus*, *Equus caballus*. Retrieved sequences were analysed for inter-species conserved TATA boxes and other core promoter elements using MatInspector (Cartharius et al, 2005; <http://www.genomatix.de/>). CpG islands were identified using CpG Island Searcher (Takai & Jones, 2003; <http://www.uscnorris.com/cpgislands2/cpg.aspx>). Transcription factor binding sites (TFBS) were identified using DiaAlign software (Cartharius et al, 2005; <http://www.genomatix.de/>). Information about transcription start sites was obtained from Cap-Analysis of Gene Expression (CAGE) database (<http://fantom31p.gsc.riken.jp/cage/mm5/>).

3 Study of Robo1 transmembrane signalling mechanism

3.1 Introduction

Robo proteins, like all single pass transmembrane receptors, have a limitation – a single receptor molecule is not sufficient to transmit signal across the cellular membrane. Receptors containing a single transmembrane helix therefore react to ligand binding by conformational changes within stable multimeric complex (e.g. integrins), changes in oligomeric state (e.g. receptor kinases) or intricate clustering (e.g. T cell receptor). Based on existing experimental evidence and parallels with other IgCAM molecules Hohenester hypothesised that Robo receptors transmit signal across the membrane by changing their oligomeric state (Hohenester, 2008). This suggestion, however, is founded on circumstantial evidence and direct proof is still lacking. Moreover, the precise transmembrane signalling mechanism also remains to be established, as both ligand induced oligomerisation and dissociation are possible.

The main goal of the studies described in this chapter was to test the hypothesis that transmembrane Robo signalling involves changes in protein oligomerisation and to establish the directionality of those changes. In order to achieve this, FRET based methods and co-immunoprecipitation were used to gauge mouse Robo1 oligomeric state in live cells before and after treatment with its cognate ligand Slit2. Slit2 and Robo1 were selected as experimental models for this project because these particular proteins are the most widely expressed and the best characterised members of the Slit and Robo families (see sections 1.2 and 1.3). Additionally, Robo1 seems to be a prototypic family member as other Robos most likely originated from it by duplications followed by divergent evolution.

3.2 Gene cloning and construct validation

3.2.1 Slit2 and Robo1 cloning and construct design

FRET measurements and co-immunoprecipitation require heterologous expression of proteins tagged with the corresponding fluorophores and epitope tags. Moreover, purified Slit2 protein was necessary for the planned experiments as a ligand, thus the first task was cloning of Slit2 and Robo1 proteins.

Both Slit2 and Robo1 are relatively large transcripts (~4.5 kb each) so special steps were taken to ensure successful cloning. First of all, mouse brains were used as a source of RNA, since brain expresses Slit and Robo proteins at higher levels than other tissues. Second, a RT-PCR reaction was modified to enhance synthesis of long cDNA molecules

(see section 2.2.2). Last, a cloning PCR reaction was also tailored to facilitate synthesis of long fragments (see section 2.2.5). Synthesized PCR fragments encoding full length Slit2 and Robo1 cDNA were cloned into a pCR4-TOPO vector using a commercial TOPO TA cloning kit (Invitrogen) and fully sequenced to validate them. Sequence comparison against a RefSeq database (National Center for Biotechnology Information (NCBI)) revealed that the cloned cDNA is identical to mouse Slit2 (RefSeq NM178804) and Robo1 (RefSeq NM019413) respectively.

Design of a Slit2 construct was relatively straightforward. The original pCR4-TOPO-Slit2 plasmid was used as a template for PCR with modified primers synthesising a KpnI-SS-Slit2-(His)₆-NotI DNA fragment. The Slit2 construct was left with its native signal sequence (SS) to ensure protein secretion. The PCR fragment was digested with appropriate restriction enzymes and ligated into a pcDNA3 vector, putting the construct under control of a CMV promoter and enabling its expression in eukaryotic cells (Figure 3.1A).

Design of Robo1 constructs was more complicated. First of all, the Robo1 constructs had to be tagged with fluorescent proteins meeting FRET pair requirements. GFP spectral variants Cerulean (CER, donor) and Citrine (CIT, acceptor) were selected for this purpose because of their superior characteristics (Rizzo et al, 2004). A standard practise for this type of experiments is to fuse the fluorescent proteins in-frame to the C-terminal end of the protein of interest. However, this was not an option for the Robo1 constructs, since a large, presumably unstructured cytoplasmic domain might obscure FRET measurements simply because of its size and unpredictable structure. In order to circumvent this problem two different proteins were engineered: a truncated Robo1 construct, where the cytoplasmic Robo1 domain was exchanged for the fluorescent protein, and a full-length Robo1 construct, where the fluorescent protein was inserted in the middle of Robo1, thirty amino acids below the transmembrane domain (Figure 3.1B and C). Robo1 was also N-terminally tagged with myc and FLAG epitope tags to facilitate protein detection and enable co-immunoprecipitation experiments. Since Robo1 has a cleavable N-terminal signal sequence, the epitope tags must be inserted after it. To accommodate all these requirements, a special subcloning strategy was devised for Robo1. First of all, an artificial DNA sequence was assembled from separate oligonucleotides and cloned into pcDNA3 plasmid creating a custom polylinker containing a Kozak sequence, a Robo1 signal sequence, an epitope tag and sites for restriction enzymes (Figure 3.1D). Then, different Robo1 fragments and fluorescent proteins were inserted step by step via restriction sites

creating truncated and full-length constructs with appropriate modifications. In total four Robo1 constructs were created: SS-myc-Robo1-CIT, SS-FLAG-Robo1-CER, SS-myc-Robo1-CIT-Robo1, SS-FLAG-Robo1-CER-Robo1 (Figure 3.1B and C). All constructs were validated by sequencing.

3.2.2 Purification and characterisation of Slit2

Expression of Slit2-(His)₆ protein first of all was verified using Western blot. HEK 293T cells were transiently transfected with pcDNA3-Slit2-(His)₆ plasmid or mock DNA and lysed 48 hours later. Additionally, a sample of spent cell growth medium was collected to assess Slit2-(His)₆ secretion. All samples were analysed by Western blotting with anti-His antibodies. A specific band, approximately 180-190 kDa in size, was detected both in the lysate and growth medium of transfected cells, but not in the lysate of cells transfected with an unrelated construct or naive HEK 293T cells (Figure 3.2). Theoretically, Slit2-(His)₆ should migrate as a protein with molar mass of 175 kDa, however Slit2 is usually heavily glycosylated so an increase in apparent molecular mass is not surprising and in fact was reported by others (see section 1.2). Slit2 is also known to be cleaved into two fragments migrating with apparent molar mass of 140 kDa and 40-60 kDa respectively, however no obvious cleavage products were observed in this experiment (Figure 3.2).

In order to use Slit2 as a ligand one needs to purify it. Slit2 is a secreted protein, so an obvious strategy was to purify Slit2-(His)₆ from cultivated cell medium. The standard HEK 293T medium contains 10% of fetal bovine serum (FBS) which unnecessarily burdens protein purification. To facilitate Slit2-(His)₆ purification, HEK 293T cells were grown as usual but were transferred into medium with a low concentration of serum (1%) before transfection with the Slit2-(His)₆ construct. The cultivated cell medium was collected 48 hours after transfection and Slit2-(His)₆ was purified from it using Ni²⁺ chelating chromatography (Figure 3.3A). Collected fractions were tested using SDS-PAGE and immunoblotting with anti-His and anti-Slit2 antibodies, demonstrating the correct identity and molar mass of the purified protein (Figure 3.3B and C). Interestingly, staining with the anti-His antibody revealed an approximately 60 kDa band which could correspond to the C-terminal cleavage product, since it would contain the His tag and would be purified together with the full-length construct. It is likely that the cleavage products were not observed in the previous experiments because of low concentration as they became detectable only after Ni²⁺ chelating chromatography enriched them. Relevant Slit2-(His)₆ fractions, as determined by SDS-PAGE and immunoblotting, were pooled together and further concentrated using Amicon spin concentrators. This step was also used to exchange

a high salt buffer, carried over from chromatography, into phosphate buffered saline (PBS). Concentrated Slit2-(His)₆ protein was stored at -4°C.

Published data show that Slit2 is able to inhibit leukocyte movement towards chemokines and since it is the simplest Slit2 activity readout available, a leukocyte transwell migration assay (also known as Boyden chamber assay) was chosen to monitor Slit2-(His)₆ activity. In order to test in house prepared Slit2-(His)₆, monocyte-like THP-1 cells were incubated with 90 ng/ml of Slit2-(His)₆ for 15 minutes and then placed into the upper part of a Boyden chamber. Meanwhile, the lower part of the chamber was filled with migration medium containing 100 ng/ml of the chemokine CCL2 and the whole chamber was incubated for 3 hours allowing cells to migrate. At the end of the experiment migrated cells in the lower well were counted using flow cytometry. Negative and positive controls lacking Slit2-(His)₆ or without chemokine treatment were performed in parallel. As expected, treatment with Slit2-(His)₆ significantly reduced THP-1 migration towards CCL2 demonstrating biological activity of the purified protein (Figure 3.4A).

In-house Slit2 preparation was labour intensive and expensive. Therefore once commercial analogues became available they were used instead of locally prepared Slit2-(His)₆. As with in house prepared ligand, biological activity of commercial mouse Slit2 (R&D Systems) was tested using the leukocyte migration assay. Human peripheral blood mononuclear cells (PBMC) were incubated with 100 ng/ml of Slit2 (R&D Systems) for 15 minutes and then placed into the upper part of the Boyden chamber. The lower part was filled with medium containing 10 ng/ml of the chemokine CXCL12, cells were allowed to migrate for three hours and then counted using flow cytometry. In parallel, control experiments were conducted by omitting Slit2 or CXCL12. As expected, CXCL12 induced substantial cell migration which was inhibited by Slit2 treatment (Figure 3.4B). Slit2 pre-incubation with a soluble Robo1-Fc chimera (R&D Systems) abolished the inhibitory Slit2 properties, further demonstrating that inhibition of chemotaxis is dependent on Slit2 (Figure 3.4B).

3.2.3 Expression and characterisation of Robo1 constructs

The HEK 293T cell line is a standard expression vehicle for various proteins because of its high transfection efficiency, rapid growth and relatively easy maintenance. Although originally thought to be human kidney epithelial cells, HEK 293T cells have a transcription profile more similar to that of neuronal cells (Shaw et al, 2002) and thus should contain all signalling machinery necessary for Robo1 function. Moreover, this cell line was already successfully used to express Robo proteins in other studies (Hu et al, 2001; Yang et al,

2006). All this made HEK 293T cells an ideal cell model both for general expression and for more detailed FRET measurements.

First of all, expression and identity of each Robo1 construct was checked using Western blot. HEK 293T cells were transiently transfected with corresponding constructs, incubated for 24 hours and then lysed. Samples of cell lysates were resolved by SDS-PAGE and immunoblotted with anti-myc or anti-FLAG antibodies. Both antibodies were able to specifically detect their corresponding constructs (Figure 3.5). The molar mass of all constructs, as inferred from migration within the gel, was significantly higher than theoretical. Truncated and full-length Robo1 proteins migrated with an apparent mass of 180 kDa and 220 kDa respectively, although theoretically their mass is 130 kDa and 206 kDa. Similar alternations in mobility were reported previously and attributed to N-glycosylation (Howitt et al, 2004), therefore this experiment confirmed efficient expression and correct identity of tested Robo1 constructs.

Cellular distribution and co-localisation of Robo1 constructs within live HEK 293T cells was characterised using fluorescence microscopy. HEK 293T cells were transiently transfected with each Robo1 construct and 24 hours later inspected with an inverted epifluorescence microscope, directly visualising the incorporated Citrine or Cerulean fluorescent proteins. An expression pattern consistent with cell surface localisation was observed for each tested construct (Figure 3.6). Additionally, cells were co-transfected with two differently tagged Robo1 constructs and co-localisation of Citrine and Cerulean fluorescence was examined using Metamorph software. Fluorescence intensity values of corresponding pixels from the Citrine and Cerulean images were used as the X and Y coordinates in a scatter plot. This plot shows correlation between Citrine and Cerulean fluorescence intensity which can be quantified by calculating Pearson's correlation coefficient. Both truncated and full-length Robo1 constructs showed a strong co-localisation between differently tagged Robo1 proteins with Pearson's correlation coefficient values of 0.98 and 0.96 respectively, which indicates highly similar cellular distribution of the constructs (Figure 3.6).

Transient transfection of eukaryotic cells is prone to gross protein overexpression and high variability and as a result is not an ideal protein expression method for FRET experiments. While initial pilot studies can be performed with transiently transfected cells, a cell line stably expressing proteins of interest is a preferable experimental system. Consequently, HEK 293 cell lines stably expressing Robo1 constructs were generated to complement

experiments based on transient expression. Initially using the commercial Flp-In T-REX system (Invitrogen), four separate “single” HEK 293 stable cell lines were created expressing myc-Robo1-CIT, FLAG-Robo1-CER, myc-Robo1-CIT-Robo1 or FLAG-Robo1-CER-Robo1 constructs from a locus controlled by a tetracycline promoter. Then, a second construct, FLAG-Robo1-CER or FLAG-Robo1-CER-Robo1 was incorporated randomly into the genome of cells able to express myc-Robo1-CIT or myc-Robo1-CIT-Robo1. The outcome of these procedures was two double stable cell lines, co-expressing either truncated or full-length proteins. In each case, one construct was expressed constantly (FLAG-Robo1-CER or FLAG-Robo1-CER-Robo1), while the other was tetracycline inducible (myc-Robo1-CIT or myc-Robo1-CIT-Robo1) (Figure 3.7A and B).

The double stable cell lines initially were tested for Robo1 expression using Western blotting. Cells were incubated with increasing amounts of doxycycline (DOX, a tetracycline analogue) for 24 hours, lysed, samples of lysate resolved using SDS-PAGE and then immunoblotted with anti-myc and anti-FLAG antibodies. As expected, the FLAG tagged constructs were constantly expressed, while expression of the myc tag construct was induced by 2 ng/ml and 8 ng/ml of doxycycline for truncated and full length constructs respectively (Figure 3.7C and D). It is noteworthy that a non-specific band (~170 kDa) observed in all Western blots where HEK 293 lysates are analysed using anti-FLAG antibody is missing in Figure 3.7C. This is not a gel cropping artefact and image faithfully represents the original data. The non-specific band generally has lower intensity and in this particular case most likely completely disappeared because of some chemiluminescence artefact. These conclusions are supported by the fact that the non-specific band can be observed in an identical experiment with the same cell line but different doxycycline concentrations (Figure 3.7 E).

In order to verify Robo1 protein cellular distribution, the double stable HEK 293 Flp-In T-REX cell lines were incubated with 10 ng/ml of doxycycline for 24 hours and inspected with an inverted epifluorescence microscope. Direct visualisation of Citrine and Cerulean fluorescent proteins revealed constant expression of the Cerulean tagged constructs, doxycycline dependent induction of the Citrine labelled Robo1 and cell surface delivery of all proteins of interest (Figure 3.8). Co-localisation of differentially tagged constructs was high, although lower than that observed in transiently transfected cells. Closer inspection of merged images revealed that constitutively expressed Robo1 constructs (red pseudocolour) tended to have higher presence within intracellular vesicles than inducible

(green pseudocolour) Robo1 genes (Figure 3.8). This result is not surprising, since a constitutively expressed protein has higher concentration and may have higher presence in various transport/recycling/degradation pathways than recently induced protein.

Close inspection of images also revealed differential distribution of truncated and full-length Robo1 constructs within the membrane. Truncated Robo1 constructs were distributed across the membrane more or less evenly, while full-length Robo1 was concentrated into patch-like structures, usually within cell-cell contacts (Figure 3.8A and B). This phenomenon was further inspected at higher resolution using confocal microscopy. “Single” stable HEK 293 Flp-In T-REX cells were incubated with 10 ng/ml of doxycycline for 24 hours to induce expression of myc-Robo1-CIT or myc-Robo1-CIT-Robo1 constructs. Cells then were fixed and Citrine fluorescence imaged with the confocal microscope (Figure 3.9). Results clearly showed differential truncated and full-length Robo1 construct distribution within the membrane and thus confirmed previous observations with live cells. All three stable cell lines expressing full-length Robo1 constructs (myc-Robo1-CIT-Robo1, FLAG-Robo1-CER-Robo1 and both of them together) showed this particular distribution. Although less obvious because of higher variability, this phenomenon was also noticeable in transiently transfected HEK 293T cells. The presence of the patch-like structures was not related to protein expression level, since their formation had no detectable correlation with doxycycline concentration or incubation times. Taking all this into account, the most likely explanation for these observations is that full-length Robo1 uses its C-terminal part to anchor to unknown subcellular structures and therefore accumulates at certain points within the cellular membrane.

3.2.4 Signalling activity of Robo1 constructs

Western blotting and microscopy demonstrates that all Robo1 constructs are of the expected molecular mass and have clear membrane localisation. These facts already strongly indicate that proteins are natively folded and have no gross deficiencies.

Nevertheless, the Robo1 constructs were further tested for their ability to bind Slit2. HEK 293T cells were transiently transfected with a FLAG-Robo1-CER-Robo1 construct and 24 hours later cells were incubated with 100 ng/ml of Slit2 (R&D Systems) for 15 minutes in their growth medium. Cells were then lysed and the FLAG-Robo1-CER-Robo1 protein was immunoprecipitated from the lysate using anti-FLAG antibody-coated agarose beads. Commercial Slit2 (R&D Systems) contains a His₁₀ tag and hence an anti-His antibody was used to detect co-precipitated Slit2. Western blotting revealed that immunoprecipitation of

FLAG-Robo1-CER-Robo1 specifically co-precipitated Slit2 as no pull-down was observed with mock transfected cells (Figure 3.10). This experiment shows that the Robo1 construct interacts with Slit2 present in the cell medium.

Robo1 produces its signalling activities via a C-terminal domain so truncated Robo1 constructs that lack the cytoplasmic tail are expected to be signalling deficient. On the other hand, full-length Robo1 should be able to signal as native Robo1 does. Robo1 does not possess enzymatic activity and it signals by recruiting various adaptor molecules. Previous studies have indicated that the main downstream signalling pathways for Robo1 involve the small Rho family GTPases Cdc42 and Rac1, whose activity is often used as a proxy for Robo1 activation (Wong et al, 2001; Yang & Bashaw, 2006). Consequently, signalling capabilities of the myc-Robo1-CIT-Robo1 construct were also assessed via its ability to modulate activity of endogenous Rac1.

HEK 293 Flp-In T-REX cells were incubated with 10 ng/ml of doxycycline for 24 hours to induce expression of the myc-Robo1-CIT-Robo1 construct. Then cells were treated for 5 minutes with 100 ng/ml of Slit2 (R&D Systems) or 100 nM of TPA (12-O-tetradecanoylphorbol-13-acetate) as a positive control for Rac1 activation. According to some reports Slit2 is able to inhibit Rac1 activation (Lundström et al, 2004), therefore Slit2 ability to reduce Rac1 activation by TPA was also tested by treating cells with both of them. Initially cells were incubated with Slit2 for 5 minutes, then with TPA for an additional 5 minute period. Cells were then lysed and Rac1 activity was assessed using a Cdc42/Rac1 activity measurement kit (Millipore) as per manufacturer's instructions. General assay quality was poor as high background obscured the already low specific signal (Figure 3.11A). Although any effect was not statistically significant, TPA treatment consistently increased band intensity in all relevant samples. Treatment with Slit2, however, had no clear effects on basal or TPA-induced Rac1 activity (Figure 3.11B). Efforts to optimise this assay were not successful and these studies remain inconclusive. The Slit2-Robo1 signalling axis in this particular experimental system either does not activate Rac1 or the assay used is not sensitive enough to detect the effect.

Several groups have reported that upon activation Robo1 directly binds srGAP1 protein (see section 1.4.2). This recruitment could also potentially serve as a proxy for Robo1 activation. To test this possibility expression of the FLAG-Robo1-CER-Robo1 construct was induced in HEK 293 Flp-In T-REX cells by treatment with 10 ng/ml of doxycycline for 24 hours. Cells then were treated with 100 ng/ml of Slit2 (R&D Systems) for 15

minutes, lysed and the Robo1 construct precipitated from the lysate using anti-FLAG antibody-coated agarose beads. Co-precipitation of endogenous srGAP1 was probed using an anti-srGAP1 antibody, however no specific Slit2-induced srGAP1 co-precipitation was detected (Figure 3.12).

Pipper and colleagues identified ERK1/2 phosphorylation and activation as one of the events downstream of Robo1 signalling, thus ERK1/2 phosphorylation could potentially serve as an assay for Robo1 activation (Pipper et al, 2006). In order to test this possibility, expression of myc-Robo1-CIT-Robo1 construct was induced by incubating serum-starved HEK 293 Flp-In T-REX cells with 50 ng/ml of doxycycline for 24 hours. Cells then were treated with 100 ng/ml Slit2 (R&D Systems) for 5 and 15 minutes respectively or with 10% FBS for 1 minute as a positive control. Cells were lysed and a fraction of phosphorylated, active ERK1/2 was determined using Western blotting with antibodies specific for phosphorylated or total ERK1/2. As expected, treatment with 10% FBS caused an increase in phosphorylation of ERK1/2, however treatment with Slit2 had no detectable effects on ERK1/2 activation (Figure 3.13A).

Alternatively, Prasad and colleagues showed that Slit2 is able to inhibit ERK1/2 activation, therefore a Robo1 signalling assay based on ERK1/2 inhibition was also tested (Prasad et al, 2004). Expression of myc-Robo1-CIT-Robo1 was induced in serum-starved HEK 293 Flp-In T-REX cells by incubating them with 50 ng/ml of doxycycline for 24 hours. Cells were pre-incubated with 100 ng/ml of Slit2 (R&D Systems) for 15 minutes and then ERK1/2 was activated by adding 10% FBS for 1 or 5 minutes. As expected, treatment with FBS increased ERK1/2 phosphorylation, however Slit2 had no observable inhibitory effects on the extent of ERK1/2 activation (Figure 3.13B).

Two different reasons might provide a basis for a failure to unambiguously observe full-length Robo1 signalling activity. First of all, it is possible that the assays used were not adequate to detect Robo1 activity. Assessment of Robo1 signalling has always been problematic. Assays based on downstream signalling molecules and physiological effects are ambiguous and often have produced contradicting results even for highly similar experimental protocols (see section 1.4.2 and 1.6). Therefore, it is possible that an absence of detectable Robo1 signalling activity was caused by a failure to employ a correct assay or correct assay conditions. On the other hand, one cannot discard the possibility that the full-length Robo1 constructs, produced for these studies are in some manner deficient. Insertion of a fluorescent protein might have affected the ability of Robo1 to bind adaptor molecules

within the cell. Fusion of a fluorescent protein usually can be relatively safely guided by knowledge of the secondary or domain structure of the "host" protein. In the case of Robo1, its cytoplasmic part is most likely an intrinsically disordered protein, so naturally all attempts to predict its secondary structure or domain organisation *in silico* were fruitless. In this situation an insertion site for the fluorescent proteins was selected randomly, close to the cell membrane to minimise possible variations in FRET distance. Known functional fragments (CC0-CC3) remained undisturbed, however, since our knowledge about intrinsically unstructured proteins and their binding mechanisms is vague at best, it is possible that an insertion of a rigid structured domain affects functions of the Robo1 cytoplasmic tail. On the other hand, full-length Robo1 is anchored to supramolecular structures within the cell, which indicates that the cytoplasm tail of Robo1 retains at least some functionality. Moreover, the Robo1 constructs show other signs of a "healthy" protein: they were transported to the cell surface and capable of binding Slit2. Therefore, it is reasonable to assume that at least the extracellular part of the protein is natively folded and functional.

3.3 Robo1 oligomeric state assessment with FRET imaging

One of the ways to assess Robo1 oligomeric state and its dependency upon the ligand in live cells is FRET imaging, based on sensitised emission of the acceptor. The basis of such studies is quite straightforward. Let us assume that Robo1 in the resting state exists as a dimer. This association would bring fluorescent proteins into close proximity allowing energy transfer between the fluorophores (Figure 3.14A). If Slit2 causes the Robo1 dimer to dissociate, incubation of live cells with the ligand would increase average distances between the receptors and their incorporated fluorescent protein thus reducing FRET signal (Figure 3.14B). The same principles are valid for an opposite mechanism, i.e. ligand induced association. Here initially one would observe a low FRET signal which would be increased by the addition of the ligand.

Although transient transfection has considerable shortcomings, when it comes to FRET imaging, the relatively straightforward nature of these experiments makes transiently transfected cells a good starting model for FRET analysis. HEK 293T cells growing on glass coverslips were transiently transfected with Robo1 constructs. The following day a coverslip fragment with cells was transferred into a microscope chamber and donor and acceptor fluorescence was imaged as described in section 2.2.25 (Figure 3.15). In order to assess Slit2 effects on FRET, cells were incubated with 90 ng/ml of Slit2 (in house produced) for 30 minutes before collecting the images. FRET signal was quantified from

the acquired images and expressed as a RFRET index as described in section 2.2.25. The RFRET index for untreated cells expressing truncated Robo1 constructs was 1.81 ± 0.02 while treated cells showed a RFRET signal of 1.82 ± 0.04 (Figure 3.15, B). Identical experiment with full-length Robo1 constructs yielded the RFRET signal of 1.44 ± 0.03 and 1.46 ± 0.02 respectively (Figure 3.15C). These values indicate that both truncated and full-length Robo1 receptors form oligomers in live cells, since RFRET index values above 1 reflect energy transfer. However, in both cases Slit2 failed to induce observable differences in the RFRET index, which shows absence of changes in distances between Robo1 constructs, effectively implying that the oligomeric state of Robo1 is not affected by Slit2.

Diffusion of membrane proteins is restricted to two-dimensional space and hence random molecular collisions along with non-specific protein-protein interactions are much more prevalent and therefore need to be accounted for (Vogel et al, 2006). Experiments with other proteins and general experience within the group shows that RFRET index values of 1.81 and 1.44 measured for Robo1 constructs are relatively high and most likely well above random “collisional” FRET level. Nevertheless, this assumption was tested experimentally by generating a set of potentially non-oligomerising Robo1 constructs.

As mentioned before, exact determinants responsible for Robo1 oligomerisation remain unknown, however, it appears that the extracellular part of the protein is sufficient to drive these interactions. Therefore, a Robo1 construct lacking the cytoplasmic tail was further truncated, deleting either all five Ig domains (SS-FLAG-Robo1(Δ Ig)-CER) or Ig and FnIII domains all together (SS-FLAG-Robo1(Δ Ig Δ FnIII)-CER) (Figure 3.16A). These newly generated constructs were checked for expression and correct cell surface delivery using immunocytochemistry (Figure 3.16B and C). Verified constructs were co-transfected with the SS-myc-Robo1-CIT construct and FRET was measured as described above.

Additionally, potential FRET was measured between SS-myc-Robo1-CIT and the Robo1-unrelated human muscarinic acetylcholine receptor M3 tagged with Cerulean. N-terminal deletions reduced FRET signal to levels similar to that of the presumed nonspecific interactions between Robo1 and the acetylcholine receptor (Figure 3.17). This experiment demonstrates that in this particular system “collisional” non-specific FRET signal corresponds to 1.2-1.3 and is well below FRET values observed for oligomerisation competent Robo1 constructs.

As mentioned above, transient transfection is not the best experimental system for assessing protein-protein interactions and therefore stable cell lines were created in parallel

with transient expression experiments (see section 3.2.3). HEK 293 Flp-In T-REX cells were grown on glass coverslips and expression of Robo1 constructs was induced by incubating cells with 50 ng/ml of doxycycline for 24 hours. A fragment of the coverslip was transferred into the microscope chamber and donor and acceptor fluorescence was imaged as described in section 2.2.25 (Figure 3.18A). In order to assess Slit2 effects on FRET, cells were incubated with 100 ng/ml of Slit2 (R&D Systems) for 30 minutes before collecting further images. Once again, a strong FRET signal was observed between the differentially tagged Robo1 constructs, however Slit2 had no detectable effects on the values of a RFRET index (Figure 3.18B and C).

Taken together the FRET imaging experiments strongly suggest that Robo1 exists as an oligomer *in vivo*, but contrary to the original hypothesis Slit2 had no observable effects on the oligomeric state of the receptor. Interestingly, full-length Robo1 constructs generally showed lower RFRET index values than C-terminally truncated proteins. Since full-length Robo1 seems to be anchored to other proteins within the cell, it is possible that these interactions affect distance between fluorophores or their orientation. Alternatively, one can never dismiss the possibility of unknown experimental artefacts related to FRET imaging itself, therefore results from FRET imaging were complemented with alternative methods.

3.4 Robo1 oligomeric state assessment with time-resolved FRET

Time resolved FRET (TR-FRET) is another method suitable for assessing protein-protein interactions in live cells. Although based on the same fundamental principles, TR-FRET differs from the FRET imaging methodologically: TR-FRET measurements are performed with cell populations and different fluorophores and equipment is employed. Therefore the TR-FRET experiment is a good alternative approach to verify original observations based on the FRET imaging.

In order to perform a TR-FRET experiment a protein of interest needs to be labelled with specific fluorophores which cannot be encoded genetically. Hence, a SNAP tag was added to already existing Robo1 constructs. This tag, based on a modified O6-alkylguanine-DNA alkyltransferase reacts with benzylguanine derivatives, leading to irreversible covalent labelling of the protein with a synthetic probe (Figure 3.19A). A EcoRV-SNAP-EcoRV fragment was synthesised using PCR and appropriate synthetic oligonucleotides, digested with EcoRV and ligated in to a pcDNA5 vector harbouring truncated or full-length Robo1 constructs. This way the SNAP tag was added to the extracellular domain of Robo1

between a myc epitope tag and the Robo1 sequence creating myc-SNAP-Robo1-CIT and myc-SNAP-Robo1-CIT-Robo1 constructs respectively (Figure 3.19B).

One of the advantages of the SNAP labelling system is that a single construct is sufficient for TR-FRET experiments as it can be labelled with both donor and acceptor by applying a mixture of them during a cell labelling step. Two different SNAP substrates, benzylguanine conjugated either with Lumi4-Tb (donor, Tb cryptate) or RED (acceptor, a proprietary fluorophore from Cisbio Bioassays), were used for these experiments. The rationale of TR-FRET experiments is very similar to that of FRET imaging. If Robo1 oligomerises, this association would bring fluorophores into close proximity allowing energy transfer between them and high TR-FRET signal (Figure 3.19C). Similarly, an oligomer dissociation caused by Slit2 would increase the average distance between fluorophores causing a reduction in TR-FRET signal (Figure 3.19D). An opposite mechanism, ligand-induced association, is also possible.

Newly created SNAP-tagged Robo1 constructs first of all were verified for correct expression and cell surface delivery. HEK 293T cells were transfected with myc-SNAP-Robo1-CIT, myc-SNAP-Robo1-CIT-Robo1 or appropriate vehicle controls, incubated for 24 hours and then lysed. Samples of cell lysates were resolved by SDS-PAGE and immunoblotted with anti-SNAP and anti-myc antibodies. Both antibodies were able to specifically detect their corresponding constructs (Figure 3.20). Additionally, for immunocytochemistry experiment HEK 293T cells were transiently transfected with myc-SNAP-Robo1-CIT, myc-SNAP-Robo1-CIT-Robo1 or a truncated Robo1 construct without a SNAP tag. Next day cells were fixed and stained with Hoechst and SNAP-Surface 549, a cell impermeant, fluorescent SNAP substrate. Observed staining patterns of the SNAP specific dye and its co-localisation with the fluorescence from the Citrine fluorescent protein indicated successful expression and cell surface delivery of the constructs (Figure 3.21).

SNAP substrates conjugated with donor or acceptor have different SNAP binding rates, therefore one needs to establish an optimal donor/acceptor concentration ratio used for cell labelling. In order to achieve this, HEK 293T cells were transfected with myc-SNAP-Robo1-CIT, myc-SNAP-Robo1-CIT-Robo1 or corresponding negative control plasmids, maintained for 24 hours and then transferred into a 96 well plate. Next day cells were labelled with a mixture of both substrates where donor concentration was kept constant at 50 nM and acceptor concentration varied between 15 nM and 2 μ M. Samples were excited

at 340 nm and a raw TR-FRET signal measured at 665 nm using a PHERAstar FS plate reader (BMG Labtech). As expected, the strength of the TR-FRET signal was dependent upon the acceptor (RED) concentration and followed a bell-shaped distribution, as an excess of either donor or acceptor is expected to result in formation of non productive donor-donor or acceptor-acceptor labelled pairs (Figure 3.22A). The optimal donor/acceptor ratio, yielding the maximal raw TR-FRET signal, was determined to be 2.3 (Lumi4-Tb/ RED) both for the truncated and full length Robo1 construct. The bell-shaped curve observed during acceptor titration is consistent with basal oligomerisation of both Robo1 constructs as this kind of dependency should not exist without Robo1-Robo1 association. Absolute raw TR-FRET values also show Robo1 oligomerisation as they are comparable to those observed for other oligomeric proteins within the group. Differences in the TR-FRET signal strength observed between the truncated and full-length constructs are most likely caused by differential protein expression levels. A raw TR-FRET signal measured at 665 nm is not normalised for protein expression levels and thus a smaller truncated Robo1 construct, expressed at higher levels, yields a higher TR-FRET signal.

In order to assess effects of Slit2 on TR-FRET, HEK 293T cells were transfected with myc-SNAP-Robo1-CIT or myc-SNAP-Robo1-CIT-Robo1 constructs, incubated for 24 hours and then transferred into a 96 well plate. Next day cells were labelled with an optimal mixture of donor and acceptor SNAP substrates (50 nM Lumi4-Tb, 115 nM RED). Cells then were washed to remove unconjugated fluorophores and Slit2 (R&D Systems) was added into the wells to a final concentration of 100 ng/ml. Alternatively, an equal volume of vehicle was added as a negative control. The resulting TR-FRET signal was monitored over the subsequent 45 minute period.

The addition of the ligand might affect the general optical properties of the sample in the plate well, so in these situations TR-FRET is usually expressed as a ratio between acceptor fluorescence and donor fluorescence (I_{665}/I_{620}) to normalise all externally induced changes (Figure 3.22C). The observed TR-FRET signal in this time course experiment decreased over the time because of acceptor quenching. This phenomenon was observed with other proteins and does not interfere with monitoring of ligand-induced changes (Xu et al, 2011). Nevertheless, in the case of Robo1 constructs, samples treated with Slit2 behaved almost identically to those treated with PBS (Figure 3.22C).

Relatively high differences in a TR-FRET signal were observed for the truncated and full-length Robo1 constructs. In the case of raw TR-FRET, the observed tenfold difference at

least partially can be explained by discrepancy in protein levels. Citrine fluorescence data collected from the same samples as TR-FRET shows that the truncated protein was three times more abundant than the full-length Robo1 construct (Figure 3.22B).

Correspondingly, when the TR-FRET signal is expressed as a I_{665}/I_{620} ratio it becomes normalised for protein concentration and the differences in TR-FRET intensity is reduced approximately three fold. The remaining mismatch is more difficult to explain.

Interestingly enough, this trend, that the truncated construct yields higher energy transfer efficiency than the full-length receptor was observed during FRET imaging experiments as well. One can only speculate that it might be caused by additional protein-protein interactions that full-length Robo1 is capable of.

Overall, TR-FRET measurements yielded similar results and conclusions as FRET imaging. In agreement with the original hypothesis, experimental evidence indicates *in vivo* oligomerisation of both truncated and full-length Robo1 constructs. On the other hand, Slit2 had no detectable effect on the TR-FRET signal, which indicates that the oligomeric state of Robo1 is most likely not affected by binding of the ligand.

3.5 Robo1 oligomeric state assessment with co-immunoprecipitation

In parallel with biophysical studies Robo1 oligomerisation and Slit2 effects on it were assessed using co-immunoprecipitation. All Robo1 constructs were originally designed with different epitope tags (FLAG and myc respectively) and therefore no additional modifications were necessary. HEK293T cells were transiently co-transfected with differently tagged truncated or full-length constructs (myc-Robo1-CIT and FLAG-Robo1-CER; myc-Robo1-CIT-Robo1 and FLAG-Robo1-CER-Robo1), incubated for 24 hours and treated with 100 ng/ml of Slit2 (R&D Systems) or vehicle in cell medium for 15 minutes. After treatment the cells were washed with ice cold PBS and lysed using RIPA (Radioimmunoprecipitation assay buffer). The FLAG-tagged Robo1 constructs were immunoprecipitated from the lysate using anti-FLAG antibody conjugated agarose beads and co-precipitation of the myc-tagged Robo1 constructs was examined using an anti-myc antibody and Western blotting. Limited co-immunoprecipitation was observed for the truncated Robo1 construct and none for the full-length (Figure 3.23).

Given the FRET imaging and TR-FRET results a substantial level of Robo1-Robo1 co-precipitation might have been expected and failure to observe it seemingly contradicts the previous data. However, all energy transfer experiments were performed with intact cells, while the immunoprecipitation experiments were performed under relatively harsh conditions. A RIPA buffer used for cell lysis and receptor solubilisation might be too

denaturing to preserve Robo1 oligomerisation. However, efforts to optimise the cell lysis buffer were fruitless as using a milder detergent and buffer compositions caused non-specific interactions and decreased the fraction of solubilised Robo1 protein.

One possible strategy to circumvent a problem with complex stability is chemical crosslinking. Bifunctional chemical reagents can covalently bridge two interacting proteins linking them together and preserving the complex during cell lysis. In other words, crosslinking can be used to “freeze” an oligomeric state of the receptor, including any changes in it induced by a ligand (Figure 3.24A). A modern crosslinking reagent, like DTSP (3,3'-dithiodipropionic acid di(N-succinimidyl ester)), contains an inner disulphide bridge which is reduced during denaturing SDS-PAGE, therefore crosslinking does not affect protein migration within the gel. An extent of oligomerisation is inferred from Western blot band intensity of co-precipitated proteins.

HEK 293T cells transiently co-expressing differently tagged truncated and full-length Robo1 constructs (myc-Robo1-CIT and FLAG-Robo1-CER; myc-Robo1-CIT-Robo1 and FLAG-Robo1-CER-Robo1) were treated with 100 ng/ml of Slit2 (R&D Systems) or PBS as negative control for 15 minutes. Cell medium was then changed to PBS and cells were crosslinked by incubating them with 2 mM DTSP for 30 minutes. Finally, the cells were lysed using RIPA buffer, FLAG-tagged Robo1 proteins were pulled down from the lysates using anti-FLAG antibody-conjugated beads and co-precipitation of myc tagged Robo1 constructs was analysed using Western blot (Figure 3.24B). Chemical crosslinking slightly increased the co-precipitation efficiency of truncated Robo1 constructs, although, as in the biophysical studies, Slit2 had no obvious effects on Robo1 oligomeric state.

Much more unexpected results of crosslinking were observed when using full-length Robo1 constructs. These were effectively removed from the soluble fraction of cell lysates (Figure 3.24B). A mouse Robo1 cytoplasmic tail contains 31 lysine, residues DTSP reacts with, and being presumably an intrinsically unstructured protein constitutes a good target for the crosslinker. As mentioned before, the full-length Robo1 constructs showed a distinct distribution within the cell membrane, which potentially indicates their association with intracellular structures. It is possible that these structures together with Robo1 were crosslinked by DTSP into insoluble aggregates which were removed from the soluble fraction during centrifugation of cell lysates. The remaining levels of the full-length Robo1 protein were so low that it would have been difficult to detect co-precipitation even if it was present. In order to test this possibility, a FLAG tagged construct representing soluble

Robo1 cytoplasmic domain (FLAG-cRobo1) was transiently expressed in HEK 293T cells. Twenty-four hours after transfection, cell medium was changed to PBS and cells were crosslinked by incubating them with 0, 0.5, 1, or 2 mM of DTSP for 30 minutes. Finally cells were lysed, samples of lysate resolved using SDS-PAGE and then immunoblotted with anti-FLAG antibody (Figure 3.24C). Even incubation with 0.5 mM of DTSP effectively removed the FLAG-cRobo1 construct out of soluble lysate fraction supporting the suggestion that the crosslinking precipitates the full-length Robo1 construct out of lysate.

In summary, efforts to assess Robo1 oligomeric state with co-immunoprecipitation were not really successful. Weak co-precipitation of truncated Robo1 constructs, even though increased by crosslinking, remained barely above detection limits. Under these conditions Slit2 effects on Robo1 oligomerisation would be difficult to detect even if they were present. Co-precipitation of full-length Robo1 was not observed at all. Attempts to stabilise the full-length Robo1 oligomer by chemical crosslinking completely removed it from solution, which in agreement with previous observations suggests that its cytoplasmic tail most likely is bound to as yet unidentified subcellular structures. It is also worthy of note that co-immunoprecipitation, similarly to FRET imaging and TR-FRET experiments, shows that the truncated Robo1 constructs potentially form oligomers more readily than the full-length receptors.

3.6 Robo1 oligomerisation determinants

Earlier attempts to locate determinants responsible for Robo1 oligomerisation using serial domain deletions were inconclusive, indicating that receptor association might be driven by multiple and redundant sites (Liu et al, 2004). However, this approach is relatively blunt and error prone as results can be obscured by collaterally introduced protein folding problems. A protein-protein interaction analysis based on peptide arrays is less biased and has higher resolving power because putative contacts can be mapped within relatively short stretches of amino acids. Therefore the issue of Robo1 oligomerisation determinants was examined using peptide spot arrays. A library of overlapping, 25 amino acid long peptides was designed based on the sequence of the rat Robo1 extracellular domain and spotted on to cellulose membrane, thus creating a protein array where each spot represents a short stretch of the primary rat Robo1 sequence. The rat orthologue was chosen for this particular experiment because commercially available rat Robo1 and a human Fc fragment chimera (Robo1-Fc, R&D Systems) was an ideal reagent to visualise Robo1-Robo1

interactions. First of all, to demonstrate detection specificity, a control overlay was performed by incubating the membrane with a 5% milk powder solution in TBS buffer over night and blotting it with an anti-Fc antibody. As no non-specific signal was detected (Figure 3.25A and B), the same membrane was washed and then incubated with 50 µg/ml of rat Robo1-Fc chimera (R&D Systems) in 5% milk powder solution over night. Next day the membrane was washed to remove non-specifically bound Robo1-Fc and blotted with the anti-Fc antibody to visualise polypeptides on the array that had interacted with Robo1 (Figure 3.25 A and B). Three independent experiments were performed and Robo1 binding polypeptides identified in at least two of them are listed in Figure 3.25C. Mapping of these sequences on to the extracellular Robo1 domain revealed that putative oligomerisation sites are distributed across many different domains. Potential Robo1-Robo1 binding sites were identified in Ig2, Ig3, Ig5, FnIII1, FnIII2 domains as well as within Ig4-Ig5, Ig5-FnIII1 and FnIII1-FnIII2 interdomain linkers, supporting the notion of multiple and possibly redundant Robo1 oligomerisation determinants (Figure 3.25D). Inspection of such identified sequences revealed an interesting pattern. It appears that sites located in Ig2, Ig3 and Ig5 domains cover similar sequences and correspond to roughly the same structural element – a flexible, surface-exposed loop between two beta-sheets (Figure 3.26A and B). It is also worth noting that this particular loop is considerably longer in Ig1 and Ig4, domains that lack any identified Robo1 binding sites. Although these observed patterns are really intriguing they must be interpreted with some caution. Ig and FNIII domains are roughly 80-100 amino acids in length while the peptides are 25 amino acids in length. It means that single peptides cover multiple elements of secondary structure and the overlap can be observed even when the actual interaction determinants are different. Further protein array experiments with different polypeptide libraries or modified polypeptides, including alanine scanning arrays, may help to refine and at least partially verify putative sites of Robo1 oligomerisation.

3.7 Discussion

The main aim of the experiments described in this chapter was to establish a transmembrane signalling mechanism of Robo proteins. Being a type I transmembrane protein the Robo receptor has a single transmembrane α -helix which effectively blocks transfer of conformational changes between extracellular and intracellular parts of the protein, making signal transduction within one molecule impossible. For that reason the type I receptors usually act as homo- or heterooligomers, where multiple molecules react to ligand binding in a coordinated fashion. Not surprisingly, therefore, existing experimental data clearly show that the Robo extracellular domain is capable of oligomerisation *in vitro*

(see section 1.4.1). Such ability is quite common among IgCAM receptors, the protein superfamily that the Robos belong to. These proteins usually employ changes in oligomerisation state as a mechanism to transmit signal across the membrane (see section 1.4.1), thus Slit–Robo signalling may well involve a change in oligomeric status of Robo, both ligand-induced association and dissociation being possible.

Mouse Robo1 was selected as an experimental model for this task. The protein was cloned and two different types of Robo1 constructs were created - full-length and lacking the C-terminal cytoplasmic tail. The constructs were successfully expressed in HEK 293T cells where they, as expected, were transported to the cell surface. Co-immunoprecipitation experiments confirmed that heterologously expressed Robo1 interacts with Slit2 present in cell medium suggesting that the extracellular part of the construct is natively folded and biologically active. The truncated Robo1 construct is signalling deficient by definition, however, the full-length Robo1 construct should harbour signalling activity identical to the wild type protein. Nevertheless, signalling activity of the full-length construct was not detected by any of three different assays employed. As discussed above, Robo signalling is strongly context dependent and an apparent lack of it might be simply caused by the failure to define correct assay conditions. On the other hand, currently it is impossible to discard the possibility that the intracellular part of the full-length construct become deficient after insertion of a fluorescent protein. Although a peculiar distribution of the full-length Robo1 protein may indicate that the cytoplasmic tail interacts with intracellular proteins and thus retains at least partial functionality. Moreover, one can argue that even if the cytoplasmic tail is deficient it would not affect overall transmembrane signalling mechanism of the Robo receptor. Published data and experiments described in this chapter clearly demonstrate that the extracellular Robo domain is capable of oligomerisation both in solution and as a membrane tethered form. It seems that interactions between the extracellular domains are sufficient for Robo1 oligomerisation, and since Slit has access only to the extracellular part, one can argue that the extracellular domain is the main element in the transmembrane signalling mechanism. The C-terminal Robo1 domain would have a more prominent role in the transmembrane signalling mechanism if it had had a “repulsive” activity and was acting as a lever to the homophilic extracellular domain. However, limited available data shows that the cytoplasmic Robo domain most likely oligomerises as well (Simpson et al, 2000b). It is reasonable, therefore, to suggest that the Robo1 constructs having the absent or potentially deficient cytoplasmic tail most likely would follow the transmembrane signalling mechanism of the wild type Robo1 anyway.

In order to test the hypothesis that the Robo receptors transmit signal across the membrane by changing their oligomeric state and establish directionality of ligand induced changes, three different techniques were used to determine the Robo1 oligomeric state in live cells before or after treatment with Slit2: FRET imaging, TR-FRET and co-immunoprecipitation. The co-immunoprecipitation experiments failed to reveal strong Robo1-Robo1 interactions, most likely because of relatively harsh conditions necessary for cell lysis and receptor solubilisation. The fact that under milder conditions (TBS buffer instead of RIPA) the soluble Robo1 ectodomain was able to bind peptides in a protein array experiment largely confirms this assumption. Energy transfer techniques employing live cells, meanwhile, showed strong Robo1 oligomerisation thus supporting the original hypothesis and pointed towards ligand induced dissociation as the Robo1 transmembrane signalling mechanism. Cell treatment with Slit2, however, failed to produce any observable changes in FRET signal both in FRET imaging and TR-FRET experiments.

Experiments described in section 4.2.2 show that HEK 293T cells express native mRNA for Slit1, Slit2, Slit3, Robo1 and Robo2 genes, so one could argue that constitutive oligomerisation of Robo1 constructs is induced by endogenous Slit2. A cell line without endogenous Slit-Robo expression would be a preferable experimental vehicle, however, as the same experiments demonstrate, virtually all transformed cell lines do express some of the Slit or Robo family members (see Figure 4.2). Since cell lines free of endogenous Slit-Robo proteins were not available, the best experimental strategy was to choose one which is widely used and easy to work with i.e. HEK 293T cells. Moreover, even though HEK 293T have high levels of Robo1 mRNA, Western blot experiments show that in comparison to the expression of the recombinant construct, protein levels of endogenous Robo1 are negligible (Figure 4.5B). Correspondingly, many studies successfully used experimental models based on HEK 293T cells heterogeneously expressing Robo1 constructs and treated with Slit2 treatment (Park et al, 2003; Wong et al, 2001; Yang & Bashaw, 2006) indicating that endogenous levels of Slit-Robo are low and do not affect behaviour of an experimental system based on heterologous expression.

One could suggest two additional possible explanations for constitutive Robo1 oligomerisation and the lack of Slit2 effects upon it, either Slit2 or Robo1 proteins are deficient and unable to signal properly or Robo1 transmembrane signalling is not dependant on changes in oligomeric state. Experiments clearly demonstrate that Slit2 is biologically active and able to bind the Robo1 constructs. Also, as discussed above, even though the Robo1 downstream signalling was not detected and the Robo1 intracellular part

potentially could be partially deficient, the employed constructs should follow the transmembrane signalling mechanism of wild type protein. Hence one can argue that changes in oligomeric state were not observed not because of deficiency of the used constructs used, but because the Robo1 proteins do not rely on them to transmit signal across the membrane.

What alternative transmembrane signalling mechanism could Robo1 employ? Coleman and colleagues suggested that proteolytical shedding of the extracellular Robo domain is necessary for receptor activation in *Drosophila* (Coleman et al, 2010). The authors failed to demonstrate a direct connection between Slit binding and Robo cleavage, however, they collected a substantial amount of circumstantial evidence. Based on it, it is possible to envision a mechanism in which Robo oligomerisation restricts the C-terminal tail and in this way prevents downstream signalling. Slit binding may induce conformational changes within the extracellular domain which lead to its cleavage by proteases. The released C-terminal domain would then dissociate into monomers and recruit downstream signalling molecules. In this situation the TR-FRET experiments described in this chapter would most likely fail to register any changes in distance between fluorophores, as the SNAP-tagged extracellular domains presumably would be released into cell media without major conformational changes. On the other hand, FRET imaging experiments should be able to detect dissociation of the C-terminal domain as it employs fluorophores fused to it. However, an additional technical issue exists. In order to measure FRET, the Robo1 constructs were overexpressed above their physiological levels, potentially saturating the proteolytical capacity of Robo1 proteases. In this situation only a small fraction of cellular Robo1 might actually be cleaved. If cleavage is important in the transmembrane signalling mechanism, as proposed by Coleman, it would severely limit the number of actual signalling events making them virtually undetectable in the general background of abundant resting state receptor. Such a mechanism would explain the lack of Slit2 effects both in TR-FRET and FRET imaging experiments. On the other hand, Seki and colleagues demonstrated that in mammalian cells, both extracellular and intracellular Robo1 domains are cleaved in a consecutive and mutually-dependent manner without an apparent involvement of Slit (although the presence of the endogenous Slit cannot be fully dismissed). Upon release the C-terminal Robo1 domain was quickly destroyed by the proteosomes as it became detectable in cell lysates only when proteosomal inhibitors were added (Seki et al, 2010). These observations are more compatible with the idea that the proteolysis is more related to receptor desensitisation or recycling than transmembrane

signalling. In this situation proteolysis most likely would not interfere with FRET measurements. Either way at this point proteolytical cleavage remains a viable mechanism and merits further investigation.

The potential anchoring of full-length Robo1 to intracellular structures also indicates that the Robo1 transmembrane signalling might be more complex than was initially assumed. Conceptually it is possible to imagine a transmembrane signalling mechanism where the Robo1 oligomer detaches from the intracellular complex upon ligand binding, dissociates into monomers and recruits downstream signalling molecules. However, experimental data presented in this chapter does not support it. On the other hand, an alternative mechanism, where constitutively anchored Robo1 receptors act as part of a bigger protein complex, is equally likely. One could imagine a mechanism where Robo1 oligomer directly transmits ligand-induced conformational changes to permanently associated protein complexes within the cell. The observed, apparently constant, association between Robo and Mena proteins supports this idea (Bashaw et al, 2000), nevertheless, it remains highly speculative and further work is necessary to test it.

A considerable amount of effort was spent trying to identify intracellular structures that Robo1 associates with. Co-immunoprecipitation of full-length Robo1 followed by mass spectrometry analysis of precipitate failed to reveal any specific interacting proteins. Technical issues might be suspected, since even known Robo1 binding proteins were not detected. As discussed in section 1.4.2, many studies suggest positive interactions and indirect association between Robo and cadherin - β -catenin complexes. Therefore, one can speculate that the observed membrane patches represent adherens junctions or other cadherin related cell-cell adhesion substructures. On the other hand, the ability of Robo to take part in cell polarity and form membrane domains during heart lumen formation in *Drosophila* was attributed to antagonistic and mutually exclusive interactions between Robo and E-cadherin (Medioni et al, 2008, Santiago-Martinez et al, 2000). Thus the propensity of Robo to form membrane domains might reflect more than simple association with cadherins.

Experiments described in this chapter also illustrate the organisation of the extracellular domain. Published data indicates that the Robo1 extracellular domain most likely exists as oligomer in solution (see section 1.4.1). In agreement with this, some of the peptides based on the primary Robo1 sequence were able to bind the soluble Robo1 ectodomain, revealing potential Robo1-Robo1 interaction sites. These peptide array results indicate multiple and

redundant interaction sites spread over multiple domains (Figure 3.25D). However, it must be mentioned that the peptide array theoretically could detect the intramolecular protein-protein contacts responsible for overall folding of the extracellular Robo1 domain. Thus not all hits necessarily represent genuine oligomerisation sites.

Interestingly, some of the identified sequences mapped to the same structural element of Ig2, Ig3 and Ig5 domains. This conserved motif consists of a flexible, surface exposed loop surrounded by two β -sheets (Figure 3.26). Following the agreed notation for the I-set Ig domains (a subtype of Ig domains all Robo Ig domains belong to) it corresponds to C and D β -sheets and loop between them (Harpaz and Chothia, 1994). Currently it is impossible to infer potential roles of this C-D motif directly. Available structures of separate Robo domains carry very little information about an overall folding mechanism for the extracellular part of Robo1. In an attempt to circumvent this limitation, known structures of oligomeric proteins consisting of I-set Ig domains were examined with the hope that they might reveal a common pattern of oligomerisation interfaces or recurring functions of the C-D motif. The first three Ig domains from the NCAM molecule form an extended structure which dimerises by contacts from the first two Ig domains (Figure 3.27A). In this structure, several amino acids from the C β -sheet take part in the dimerisation interface, however, contacts from other structural elements are more substantial. While the CD-loop and D β -sheet do not contribute to the dimerisation interface in this particular structure, close proximity of these elements to their counterparts on an opposite subunit is intriguing (Figure 3.27A). Crystal packing imposes its own constraints on a protein complex and in some cases the protein in solution might have a slightly different conformation than the observed crystal structure, bringing the CD-loop and D β -sheet from Ig1 and Ig2 into a contact. PTPR σ (protein tyrosine phosphatase receptor) shows a different arrangement of the extracellular domain (Figure 3.27B). In this structure Ig1 and Ig2 are tightly packed against each other with some amino acids from the Ig2 C β -sheet taking part in interdomain contacts, although interactions from other structural elements were more substantial. Additionally, some amino acids from the CD-loop in Ig3 were taking part in the dimerisation interface between Ig2 and Ig3 (Figure 3.27B). Although no strict conclusions can be drawn from these observations, they are encouraging as the C-D motif seems to take part in the oligomerisation and overall folding of the extracellular domains of the I-set Ig proteins.

Robo1 presents a fascinating case where oligomerisation, anchoring with subcellular structures and proteolysis intertwine creating a challenging conundrum for anyone wishing

to elucidate its transmembrane signalling mechanism. It is possible that each of those processes represent a different Robo signalling mode. Robo signalling might have separate targets and mechanisms depending on its membrane localisation or proteolytical cleavage. Data supporting this idea have emerged recently. It appears that the cleaved C-terminal Robo1 domain in mammals is transported to the nucleus (Seki et al, 2010). Although the actual significance of this process is yet to be discovered it echoes the mechanism of Notch signalling where binding of ligand induces proteolytic cleavage and release of the intracellular domain, which enters the cell nucleus to modify gene expression (Oswald et al, 2001).

Multiple biochemical, genetic and biophysical studies will be necessary in order to unravel this biological complexity of Robo1 signalling. On a molecular level it would be extremely useful to reconstitute the stoichiometry and shape of the Robo1 oligomer. An X-ray structure of the whole extracellular Robo1 domain is unlikely, therefore biophysical tools like ultracentrifugation or small-angle X-ray scattering spectroscopy could be used to determine the overall shape of the complex. This model then could be “filled” with known or modelled structures of individual Ig and FnIII domains. Information about potential Robo1-Robo1 contacts gained from the protein array experiments may facilitate such modelling as well. All this would help us to gain a glimpse of the first steps of the transmembrane signalling mechanism, i.e. how and what changes Slit2 binding initiates within the extracellular Robo1 domain. In parallel, biochemical studies must address the oligomeric state of the C-terminal Robo1 domain, its interacting partners and the precise role of proteolytic cleavage. This stepwise accumulation of information about Robo structure and function will eventually lead to elucidation of its transmembrane signalling mechanism.

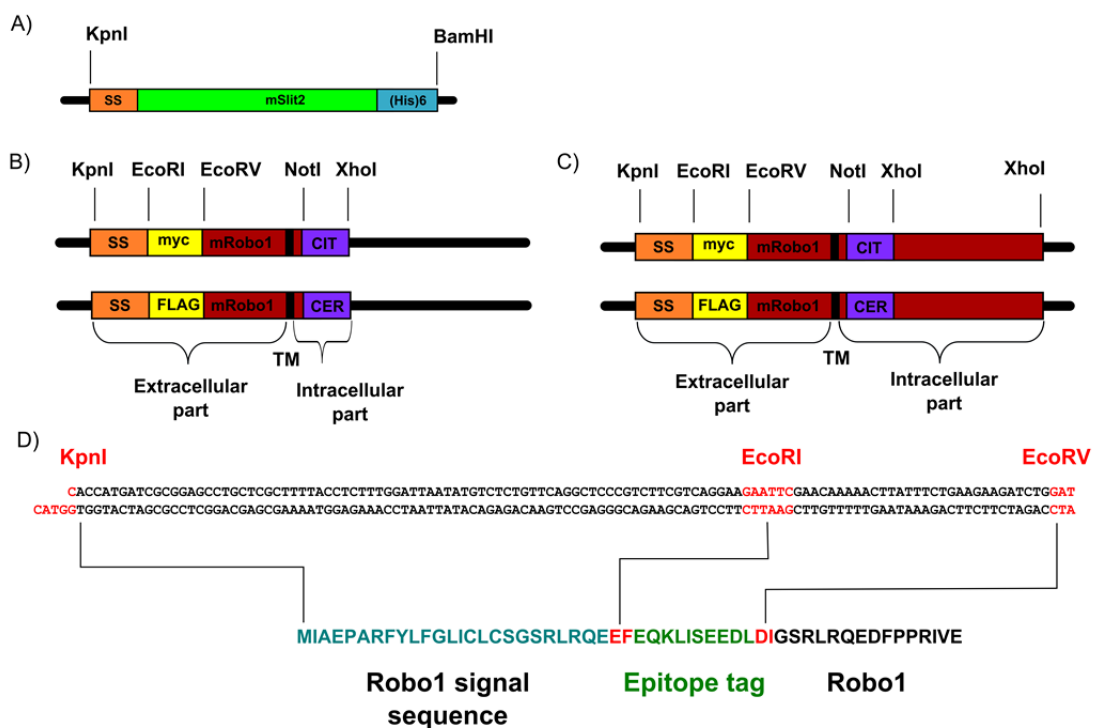


Figure 3.1 Slit2 and Robo1 constructs

Schematic illustrations of Slit2 (A), truncated (B) and full-length Robo1 constructs (C). Transmembrane (TM), extracellular and intracellular parts of the Robo1 constructs are marked respectively. Robo1 constructs were created using a custom designed polylinker region (D).

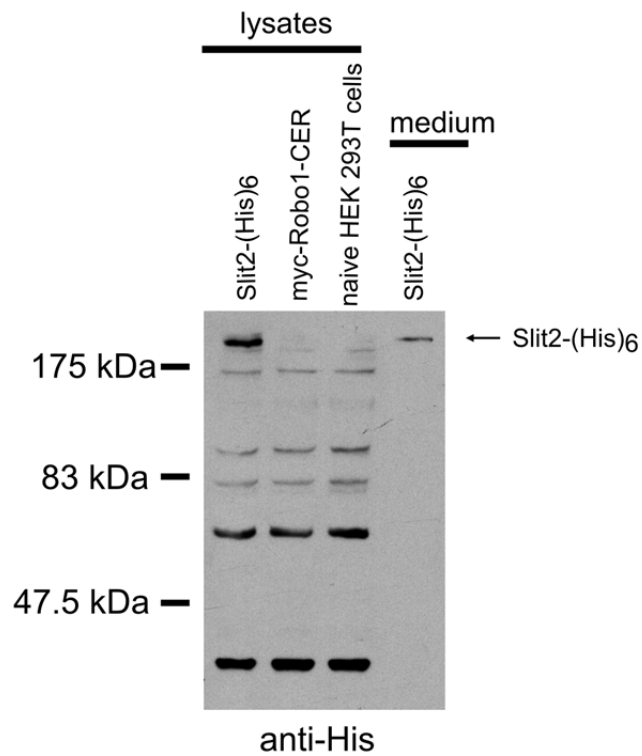


Figure 3.2 Slit2-(His)₆ expression and secretion

HEK 293T cells were transiently transfected with a pcDNA3-Slit2-(His)₆ plasmid or an unrelated DNA construct as a negative control. Samples of cell lysates and medium were resolved by SDS-PAGE and immunoblotted to detect the His tag. The blot is representative of two independent experiments.

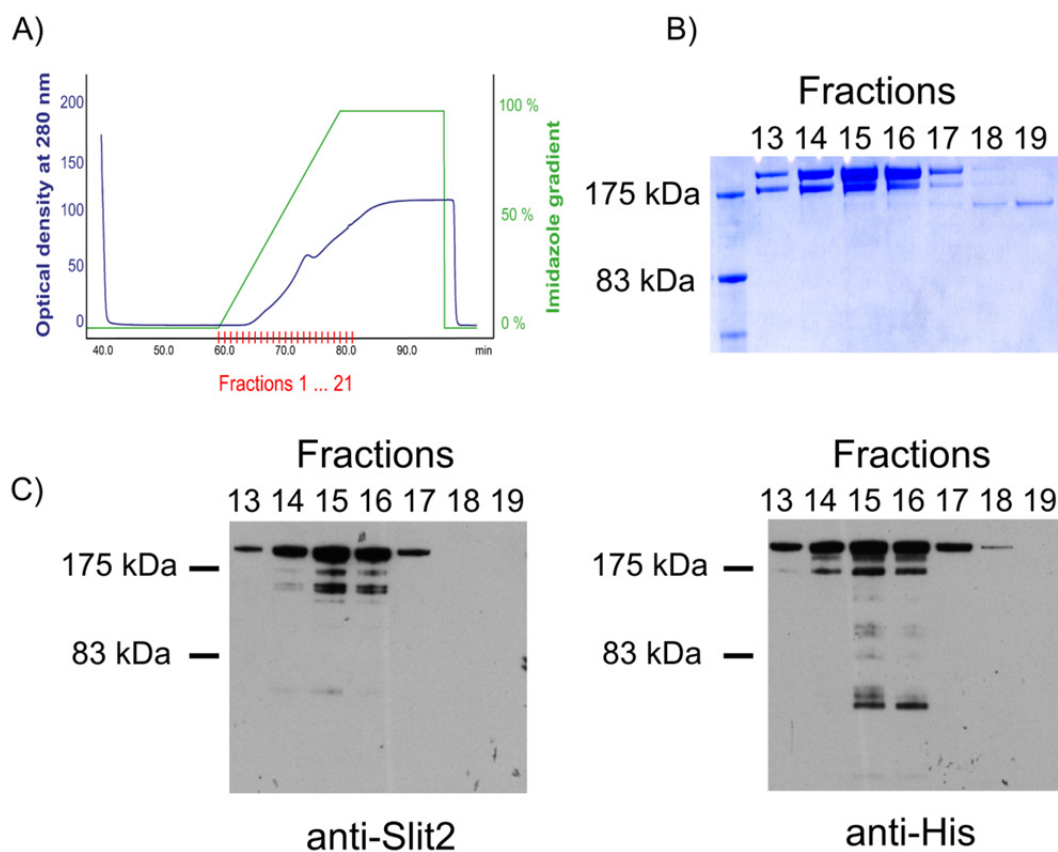


Figure 3.3 Slit2-(His)₆ purification

Slit2-(His)₆ was purified using Ni²⁺ chelating chromatography (A), fractions selected based on UV absorption were additionally analysed using SDS-PAGE (B) and immunoblotting with anti-Slit2 and anti-His antibodies (C).

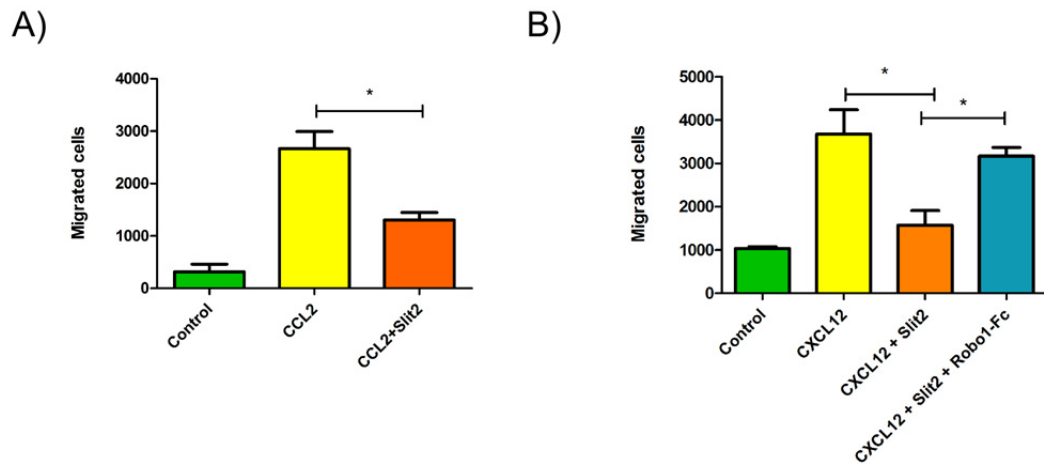


Figure 3.4 Biological activity of Slit2

The biological activity of in house (A) and commercially purchased Slit2 (B) was assessed using transwell leukocyte migration assays. (A) Naive or Slit2-(His)₆ treated (90 ng/ml, 15 min) THP-1 cells were placed into the upper part of a Boyden chamber and allowed to migrate towards 100 ng/ml CCL2 for 3 hours. Migrated cells in the lower chamber were counted using flow cytometry. (B) Naive or Slit2 (R&D Systems) (100 ng/ml, 15 min) treated human PBMCs were placed into the upper part of a Boyden chamber and allowed to migrate towards 10 ng/ml CXCL12 for 3 hours. Alternatively cells were treated with Slit2 pre-incubated with Robo1-Fc chimera (1:4). Results are represented as a mean±SEM, n=3. * p<0.05 as determined by one way ANOVA with Tukey's post test.

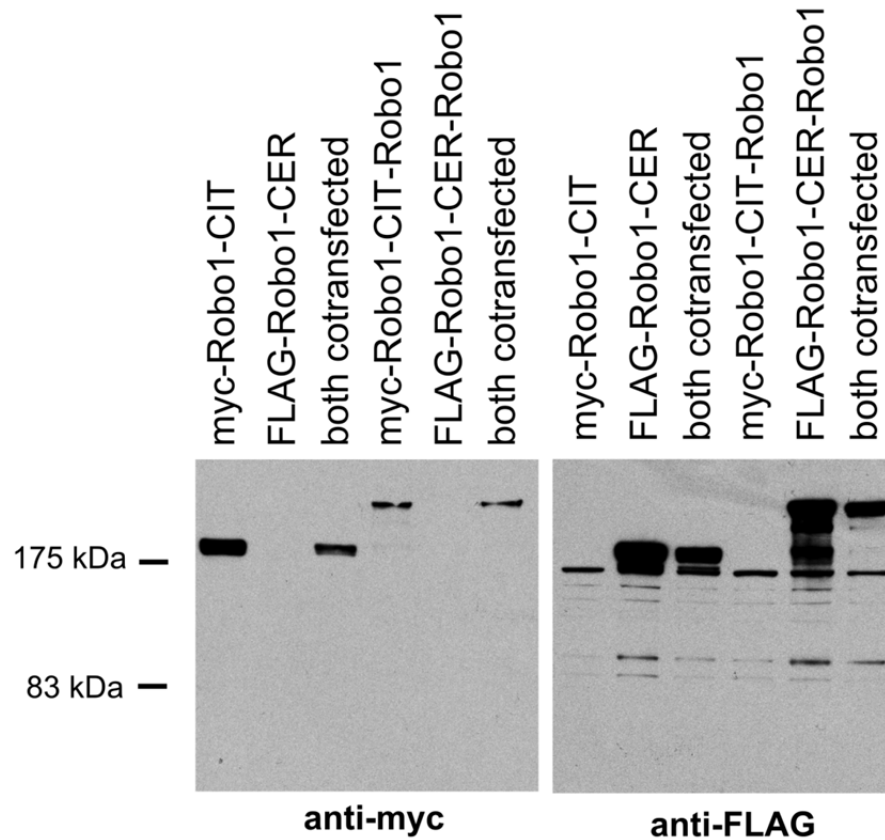


Figure 3.5 Expression of Robo1 constructs

HEK 293T cells were transiently transfected with each of the Robo1 constructs (myc-Robo1-CIT, FLAG-Robo1-CER, myc-Robo1-CIT-Robo1, FLAG-Robo1-CER-Robo1) separately or co-transfected with both truncated or both full-length constructs. Cells were lysed, samples of lysates were resolved by SDS-PAGE and then immunoblotted with anti-myc and anti-FLAG antibodies. Blots are representative of three independent experiments.

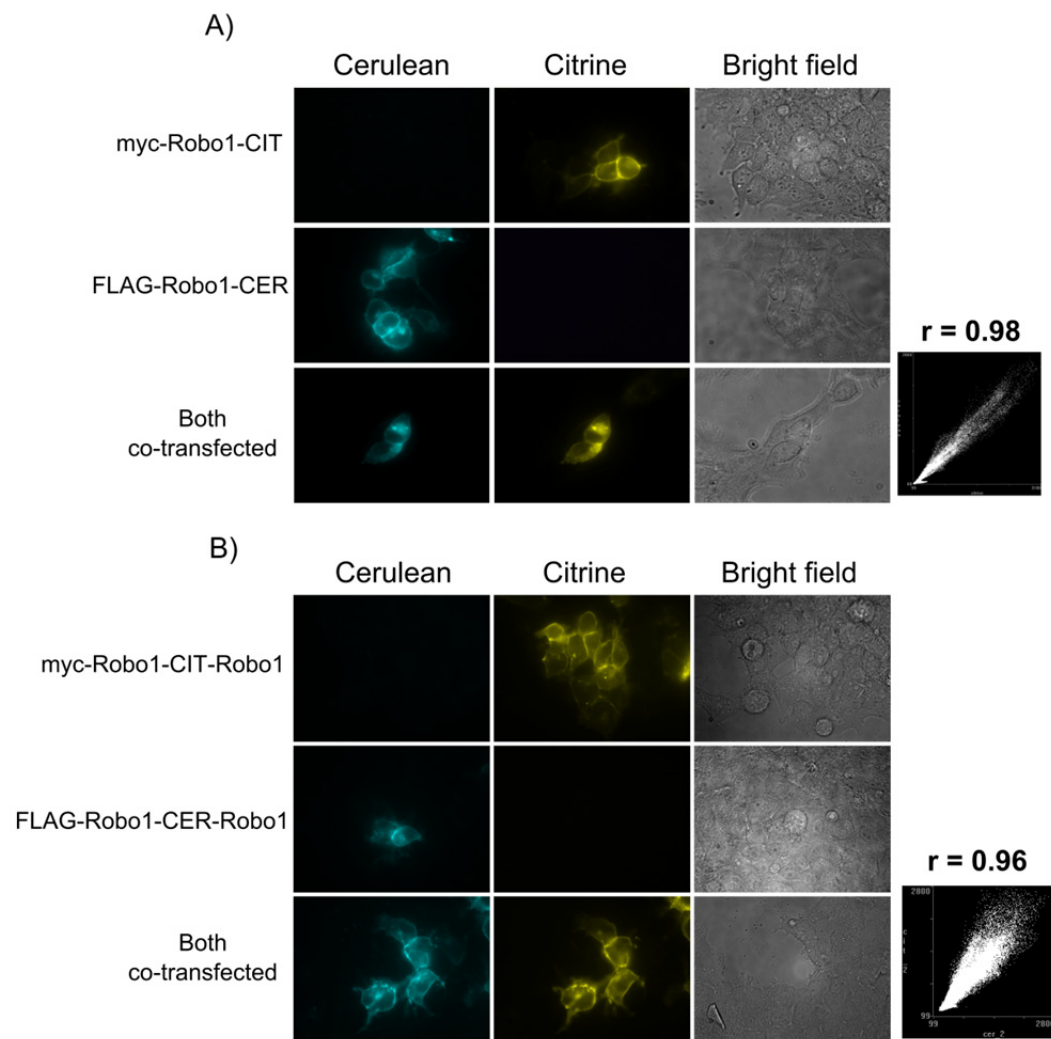


Figure 3.6 Cellular distribution of Robo1 constructs in transiently transfected HEK 293T cells

HEK 293T cells were transiently transfected with the indicated Robo1 constructs and then visualised for Citrine and Cerulean fluorescence with an inverted epifluorescence microscope. Scatter plots show co-localisation between differently tagged Robo1 constructs, r is Pearson's correlation coefficient.

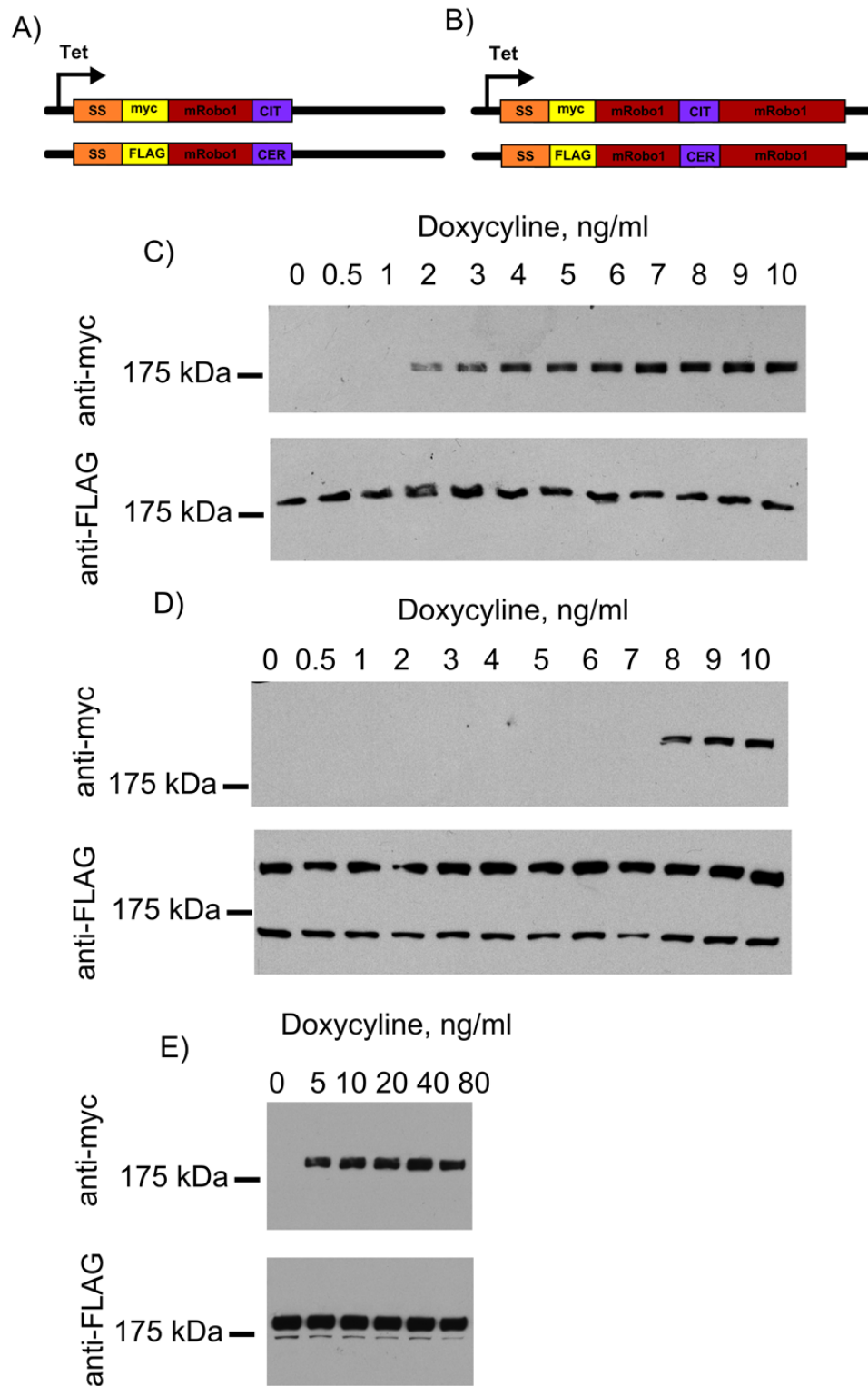


Figure 3.7 Characterisation of double stable cell lines expressing Robo1 constructs

Double stable HEK 293 Flp-In T-REX cell lines (A and B) constitutively expressing truncated FLAG-Robo1-CER (C and E) or full-length FLAG-Robo1-CER-Robo1 (D) proteins were incubated with increasing concentrations of doxycycline for 24 hours to induce myc-Robo1-CIT (C and E) or myc-Robo1-CIT-Robo1 co-expression respectively (D). Cells were lysed and expression of the constructs was assessed using Western blotting. Images C and D are representative of two independent experiments, image E represents a single independent experiment.

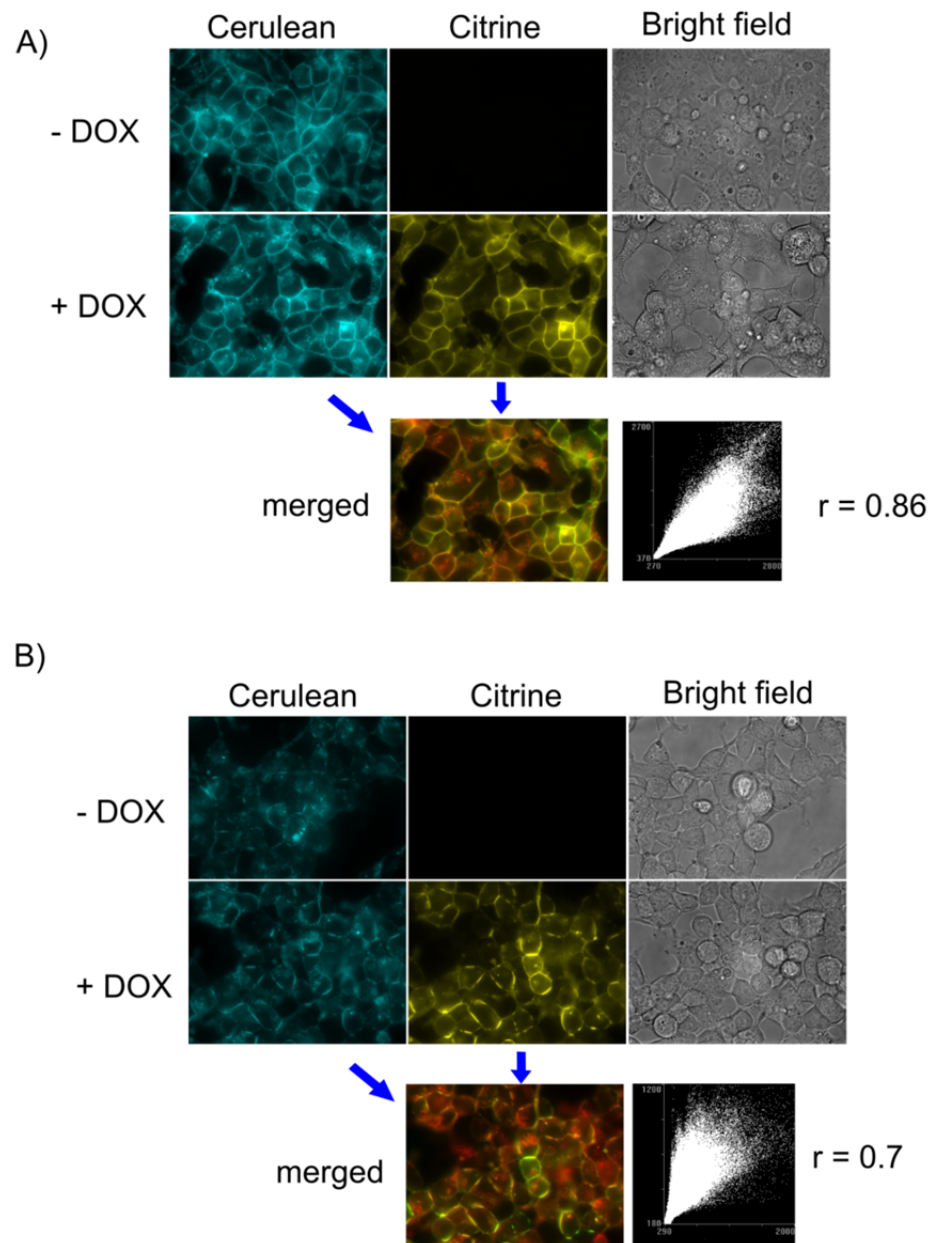


Figure 3.8 Cellular distribution of Robo1 constructs in HEK 293 Flp-In T-REX cells

HEK 293 Flp-In T-REX cell lines constitutively expressing truncated FLAG-Robo1-CER (A) or full-length FLAG-Robo1-CER-Robo1 (B) constructs were incubated with 10 ng/ml of doxycycline to induce co-expression of myc-Robo1-CIT and myc-Robo1-CIT-Robo1 respectively. Construct co-localisation was analysed by merging relevant images pseudo-coloured in red (FLAG-Robo1-CER and FLAG-Robo1-CER-Robo1) and green (myc-Robo1-CIT and myc-Robo1-CIT-Robo1). Scatter plots show co-localisation between differently tagged Robo1 constructs, r is Pearson's correlation coefficient.

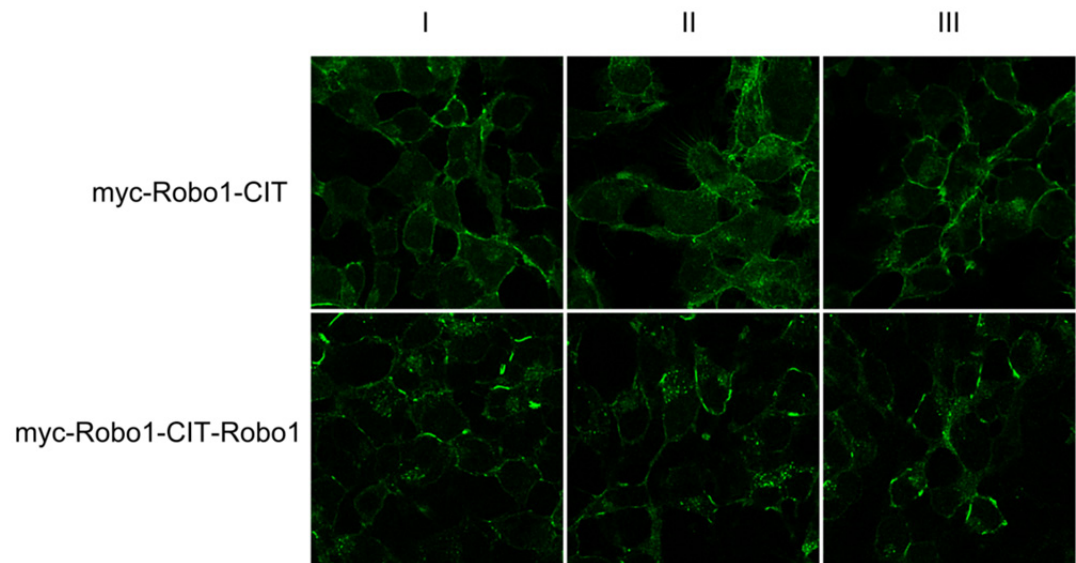


Figure 3.9 Differential membrane distribution of truncated and full-length Robo1 constructs

HEK 293 Flp-In T-REX cells were incubated with 10 ng/ml of doxycycline for 24 hours to induce expression of myc-Robo1-CIT or myc-Robo1-CIT-Robo1 construct. Cells then were fixed and fluorescence of Citrine examined using a confocal microscope. Three different view fields are presented for each construct.

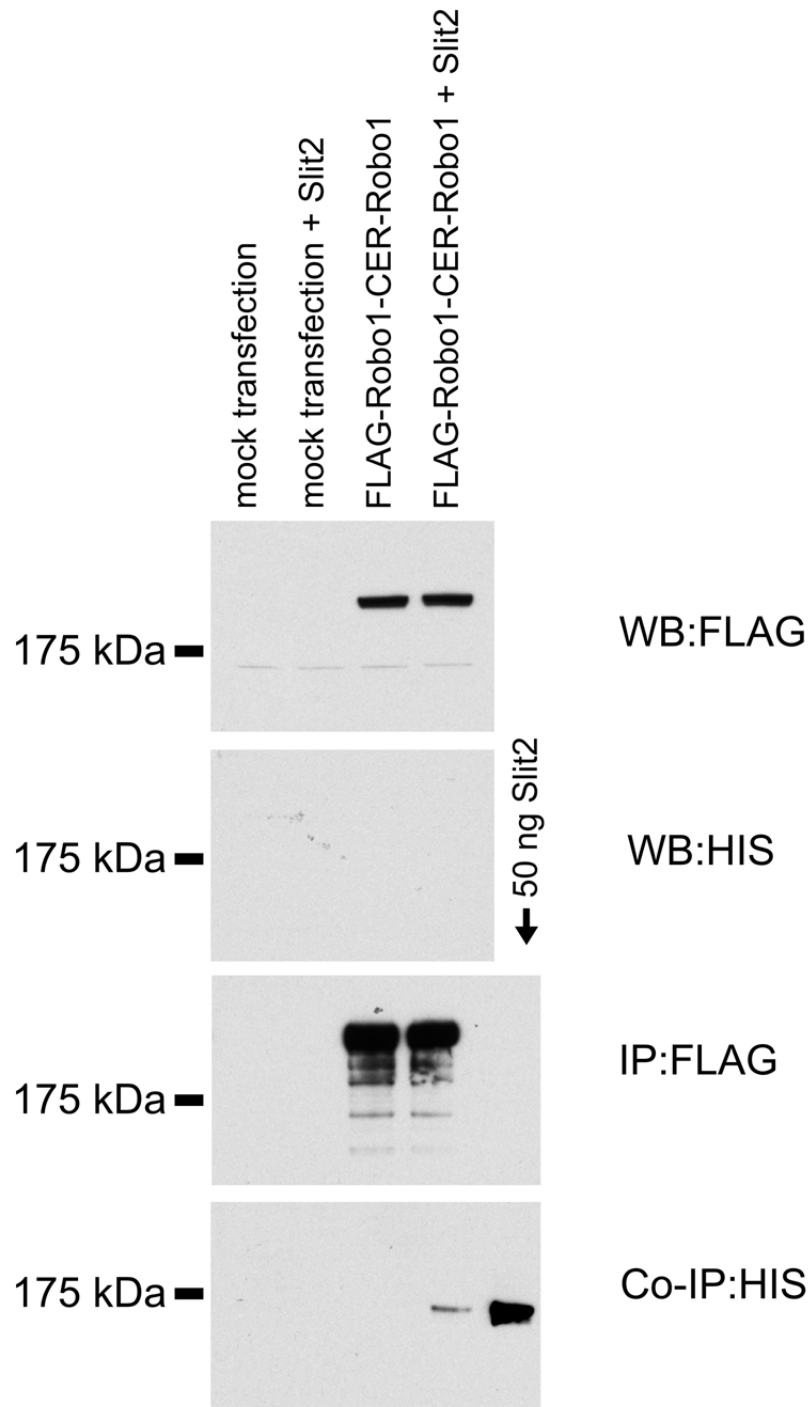


Figure 3.10 Slit2-Robo1 interactions

HEK 293T cells were transfected with mock DNA or the FLAG-Robo1-CER-Robo1 construct. 24 hours after transfection Slit2 (R&D systems) was added to the cell medium to a final concentration of 100 ng/ml. An equal volume of PBS was used as a negative control. Cells were incubated with Slit2 for 15 minutes, washed with ice cold PBS and lysed with RIPA buffer. The Robo1 construct was immunoprecipitated using anti-FLAG antibody-coated agarose beads. Slit2 co-precipitation was detected using an anti-His antibody, since commercial Slit2 from R&D contains this tag. A sample containing 50 ng of Slit2 (R&D systems) was loaded as a positive control for Slit2 detection. Blots are representative of two independent experiments.

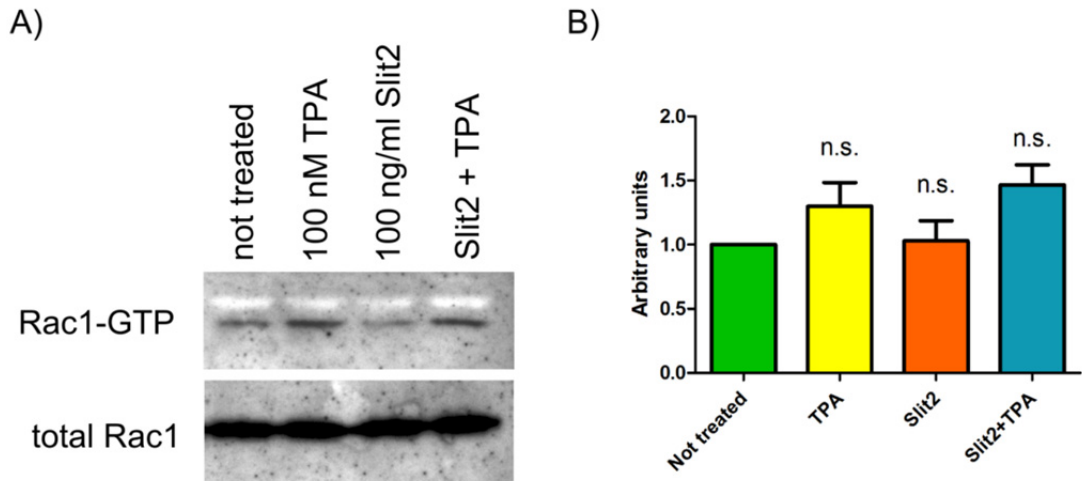


Figure 3.11 Modulation of Rac1 activity

HEK 293 Flp-In T-REX cells were treated with 10 ng/ml of doxycycline for 24 hours to induce expression of myc-Robo1-CIT-Robo1. Cells then were treated with 100 nM of TPA or 100 ng/ml of Slit2 (R&D systems) for 5 minutes. Alternatively, cells were initially treated with Slit2 for 5 minutes and then TPA for an additional 5 minutes. Rac1 activity was measured by precipitating active, GTP-bound Rac1 from cell lysates with PAK protein-coated beads and immunoblotting samples with anti-Rac1 antibody (A). The blot is representative of three independent experiments. The optical density of bands on the blot was measured using ImageQuantTL (GE Healthcare) software, normalised to the non treated sample and expressed as a mean of three independent experiments \pm SEM (n.s.—statistically not significant as determined by one way ANOVA with Bonferroni's post test).

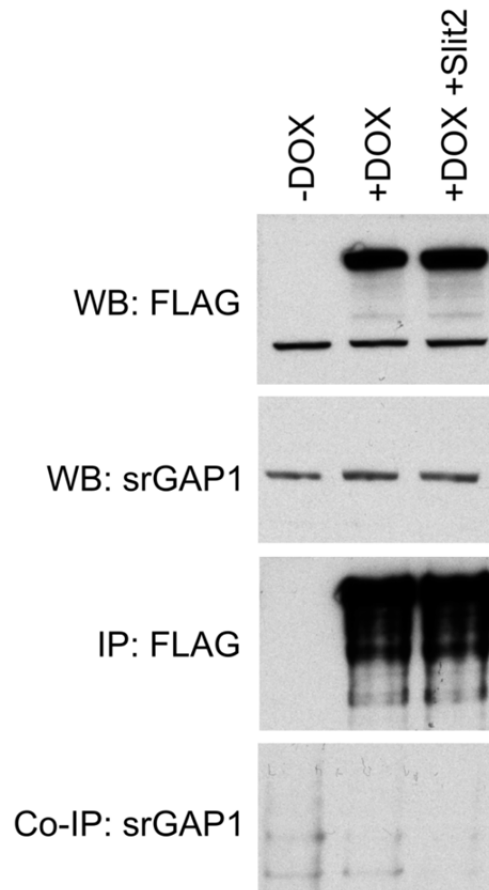


Figure 3.12 Lack of detectable Robo1-srGAP1 interactions

HEK 293 Flp-In T-REX cells constitutively expressing the FLAG-Robo1-CER-Robo1 construct (induced with 10 ng/ml of doxycycline for 24 hours) were treated with 100 ng/ml of Slit2 (R&D) for 15 minutes. Cells were lysed and the Robo1 construct precipitated using anti-FLAG antibody conjugated beads. Co-precipitation of srGAP1 was probed with an anti-srGAP1 antibody. Non-induced and induced but not treated with Slit2 cells were used as negative controls. Blots are representative of two independent experiments.

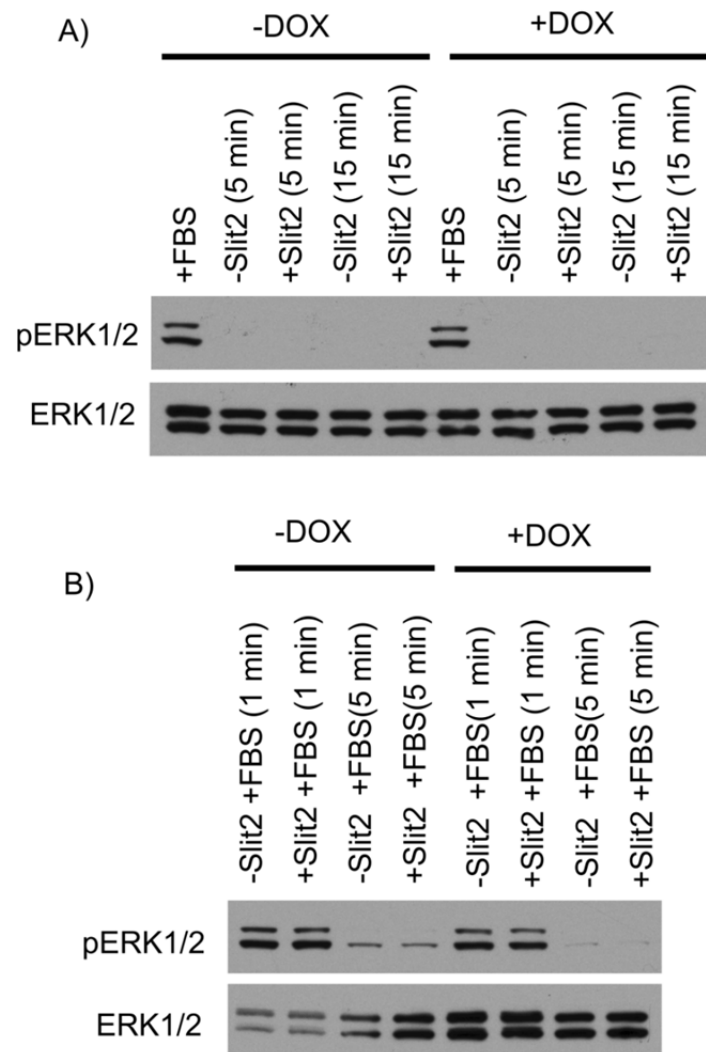


Figure 3.13 Slit2-Robo1 interactions fail to modulate ERK 1/2 activity

HEK 293 Flp-In T-REX cells constitutively expressing the myc-Robo1-CIT-Robo1 construct were used to assess Slit2 ability to activate (A) or inhibit (B) ERK1/2 kinase. Expression of the myc-Robo1-CIT-Robo1 construct was induced by incubating cells with 50 ng/ml of doxycycline for 24 hours. Non-induced cells were used as a negative control. To assess ERK1/2 activation cells were treated with Slit2 (R&D systems) or an equal volume of PBS for 5 and 15 minutes respectively (A). To assess potential Slit2-Robo1 inhibitory effects on ERK1/2 activation cells were pre-treated with 100 ng/ml of Slit2 for 15 minutes and then treated with 10% FBS for 1 or 5 minutes respectively (B). After treatment cells were lysed and the extent of ERK1/2 phosphorylation determined using immunoblotting with antibodies specific for phosphorylated and total ERK1/2. Blots are representative of two independent experiments.

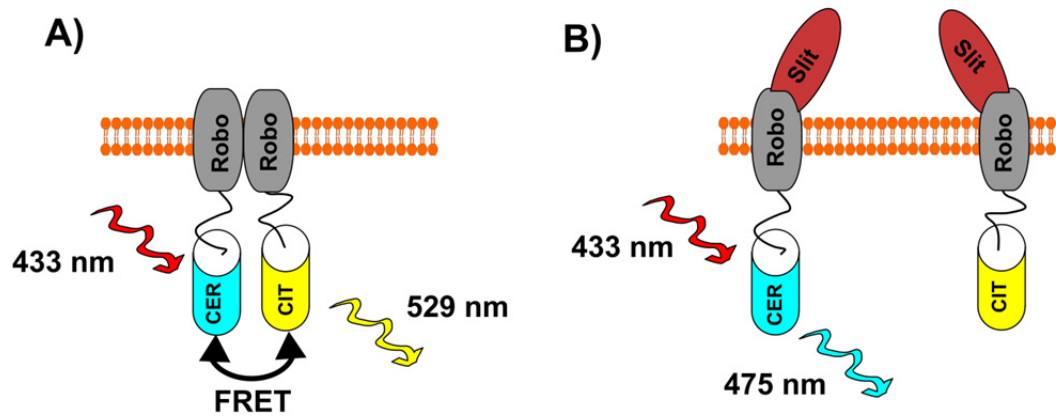


Figure 3.14 The molecular basis of FRET imaging experiments

Schematic illustration of a FRET imaging experiment. If Robo1 in the resting state exists as a dimer, receptor association would bring fluorescent proteins into close proximity allowing energy transfer between the fluorophores (A). If Slit2 causes the Robo1 dimer to dissociate, that would increase average distances between the receptors and their incorporated fluorescent protein thus reducing FRET signal (B). The same principles are valid for an opposite mechanism, i.e. ligand induced association, only here one initially would observe a low FRET signal which would be increased by the addition of the ligand.

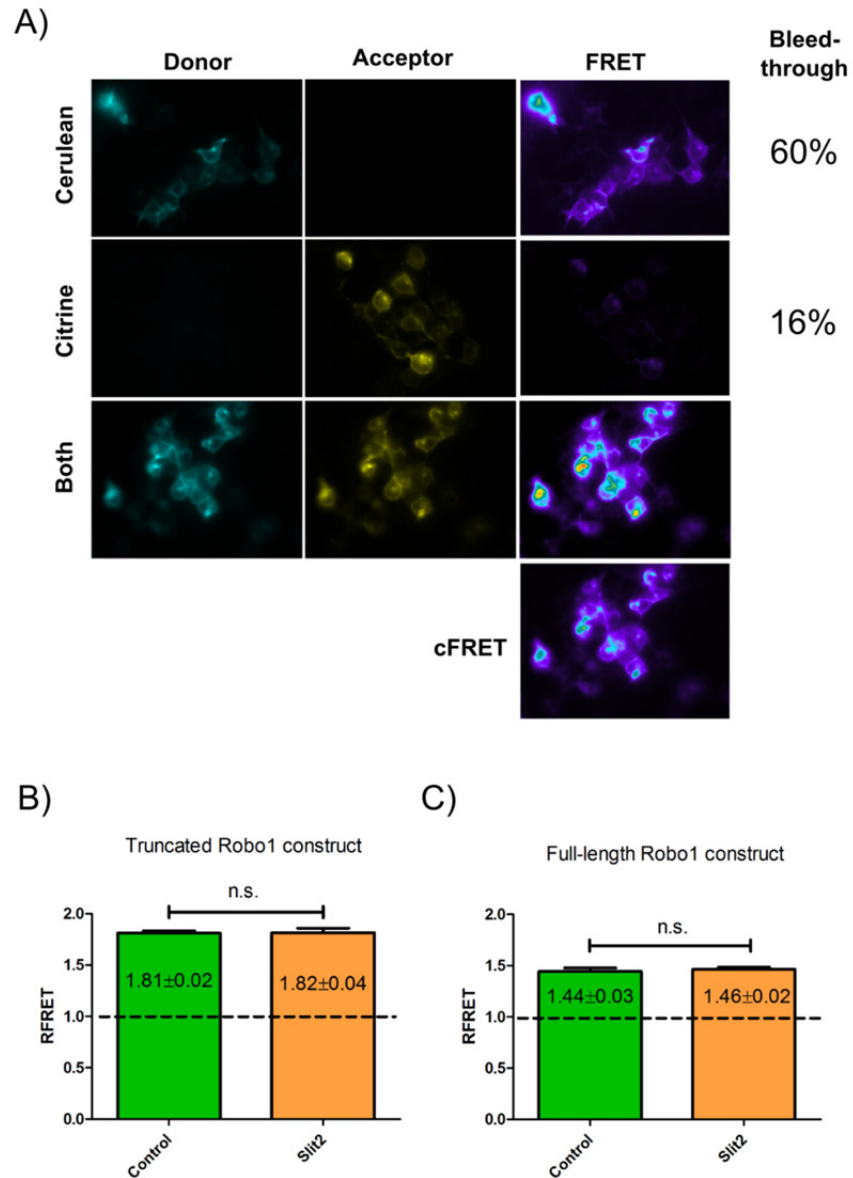


Figure 3.15 FRET analysis of Robo1 oligomerisation in transiently transfected HEK 293T cells

Live HEK 293T cells transiently expressing truncated or full-length Robo1 constructs were visualised and the FRET signal quantified as described in section 2.10. Figure A shows a typical data set for FRET quantification. In order to assess Slit2 effects on FRET signal, prior to visualisation cells were incubated with 90 ng/ml of Slit2 (in house) for 30 minutes. RFRET index for truncated (B) and full-length (C) Robo1 constructs is expressed as a mean of six independent experiments \pm SEM (n.s. – statistically not significant as determined by t-test). One independent experiment represents the mean obtained from averaging RFRET index values of hundreds of ROI in eight different fields of view containing the same batch of transfected cells. The entire dataset was collected over the course of several days.

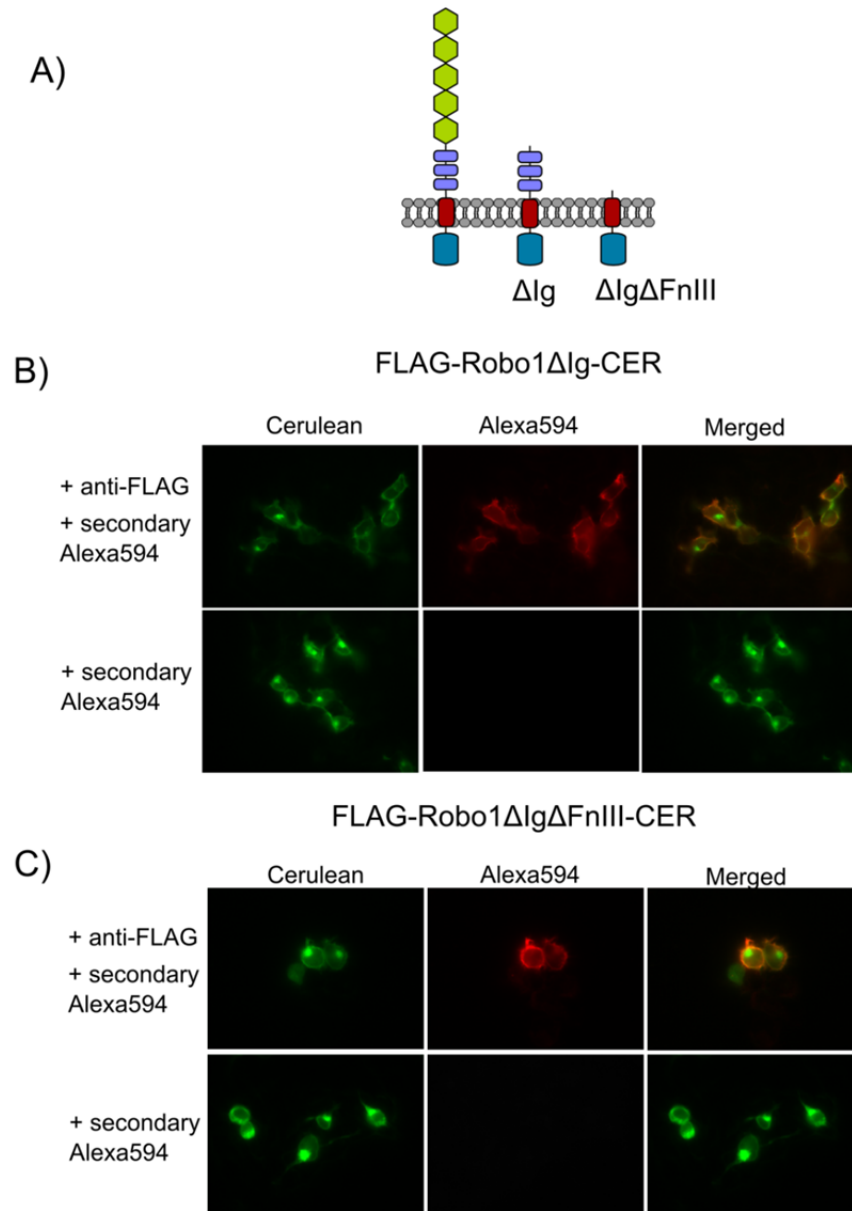


Figure 3.16 Generation of potentially oligomerisation-deficient Robo1 constructs

To attempt to abolish Robo1 oligomerisation, the extracellular part of the receptor was truncated removing Ig domains or Ig and FnIII domains together (A). In order to verify expression and cell surface delivery of newly created constructs, nonpermeabilized HEK 293T cells transiently expressing each of those proteins were fixed and stained with primary anti-FLAG and secondary Alexa594 conjugated antibodies (B and C). Samples without primary antibody served as a negative control. Cells were imaged with inverted an epifluorescence microscope for Cerulean and Alexa594 fluorescence.

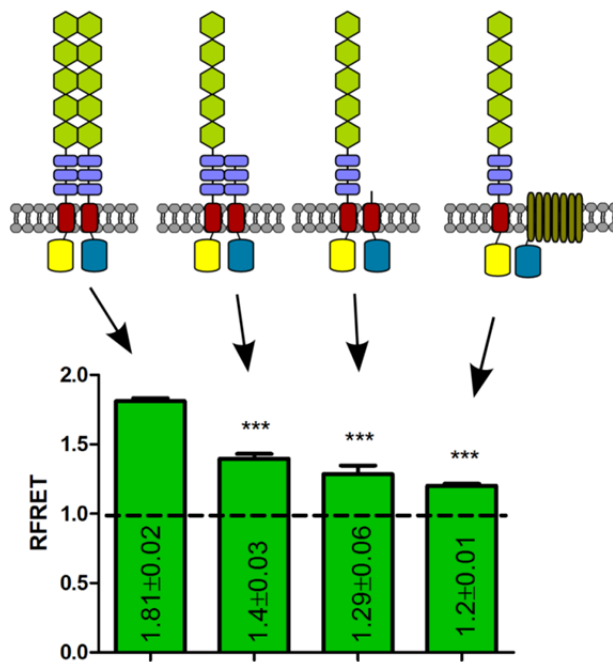


Figure 3.17 FRET analysis of potentially oligomerisation-deficient Robo1 constructs

Live HEK 293T cells transiently co-expressing myc-Robo1-CIT and FLAG-Robo1-CER, FLAG-Robo1 Δ Ig-CER, FLAG-Robo1 Δ Ig Δ FnIII-CER or Robo1 unrelated human muscarinic acetylcholine receptor M3 tagged with Cerulean were visualised and the FRET signal quantified as described in section 2.10. The RFRET index is expressed as a mean of six independent experiments \pm SEM (***) $p < 0.0001$, for differences in the FRET means between an intact protein and N-terminally truncated constructs as determined by one way ANOVA with Dunnett's post test). One independent experiment represents the mean obtained from averaging RFRET index values of hundreds of ROI in eight different fields of view containing the same batch of transfected cells. The entire dataset was collected over the course of several days. FRET index values for myc-Robo1-CIT and FLAG-Robo1-CER pair are taken from Figure 3.15.

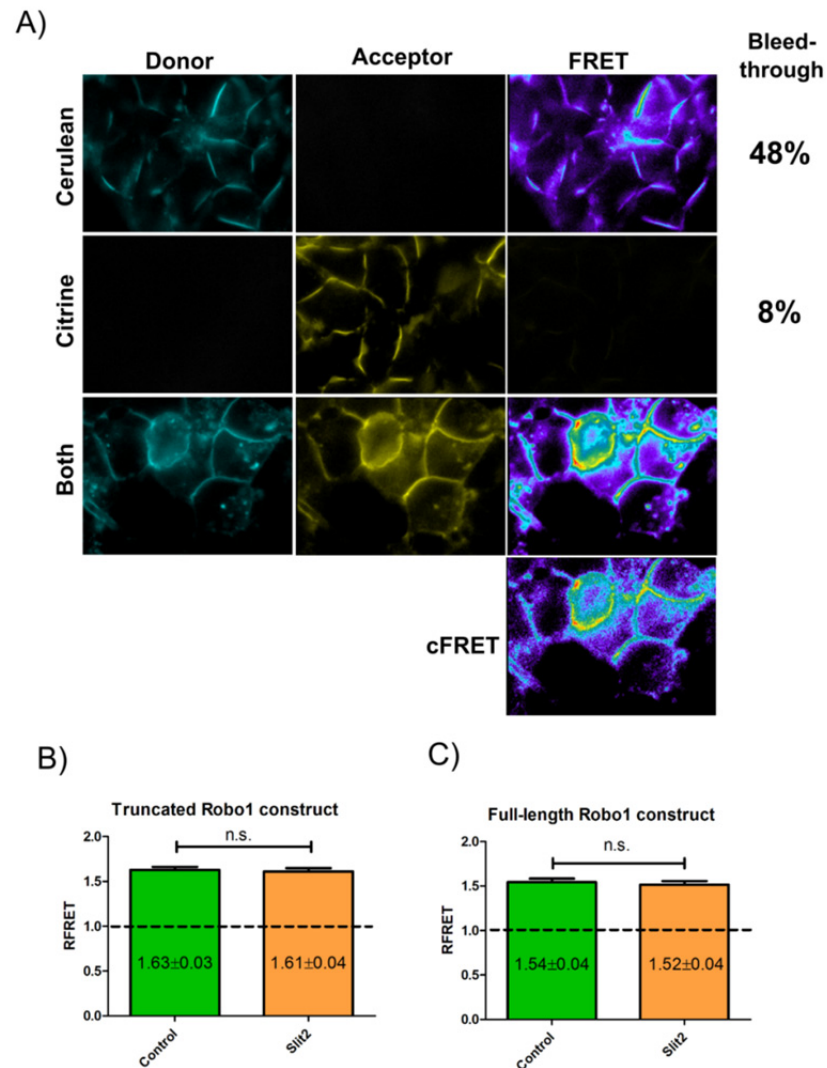


Figure 3.18 FRET analysis of Robo1 oligomerisation in HEK 293 Flp-In T-REX cells

Stable expression of truncated or full-length Robo1 constructs was induced by incubating HEK 293 Flp-In T-REX cells with 50 ng/ml of doxycycline for 24 hours. Donor and acceptor fluorescence was visualised and FRET quantified as described in section 2.10. Figure A shows a typical data set for FRET quantification. In order to assess Slit2 effects on FRET signal, prior to visualisation cells were incubated with 100 ng/ml of Slit2 (R&D systems) for 30 minutes. The RFRET index for truncated (B) and full-length (C) Robo1 constructs is expressed as a mean of six independent experiments \pm SEM (n.s. –statistically not significant as determined with t-test). One independent experiment represents the mean obtained from averaging RFRET index values of hundreds of ROI in eight different fields of view containing the same batch of induced cells. The entire dataset was collected over the course of several days.

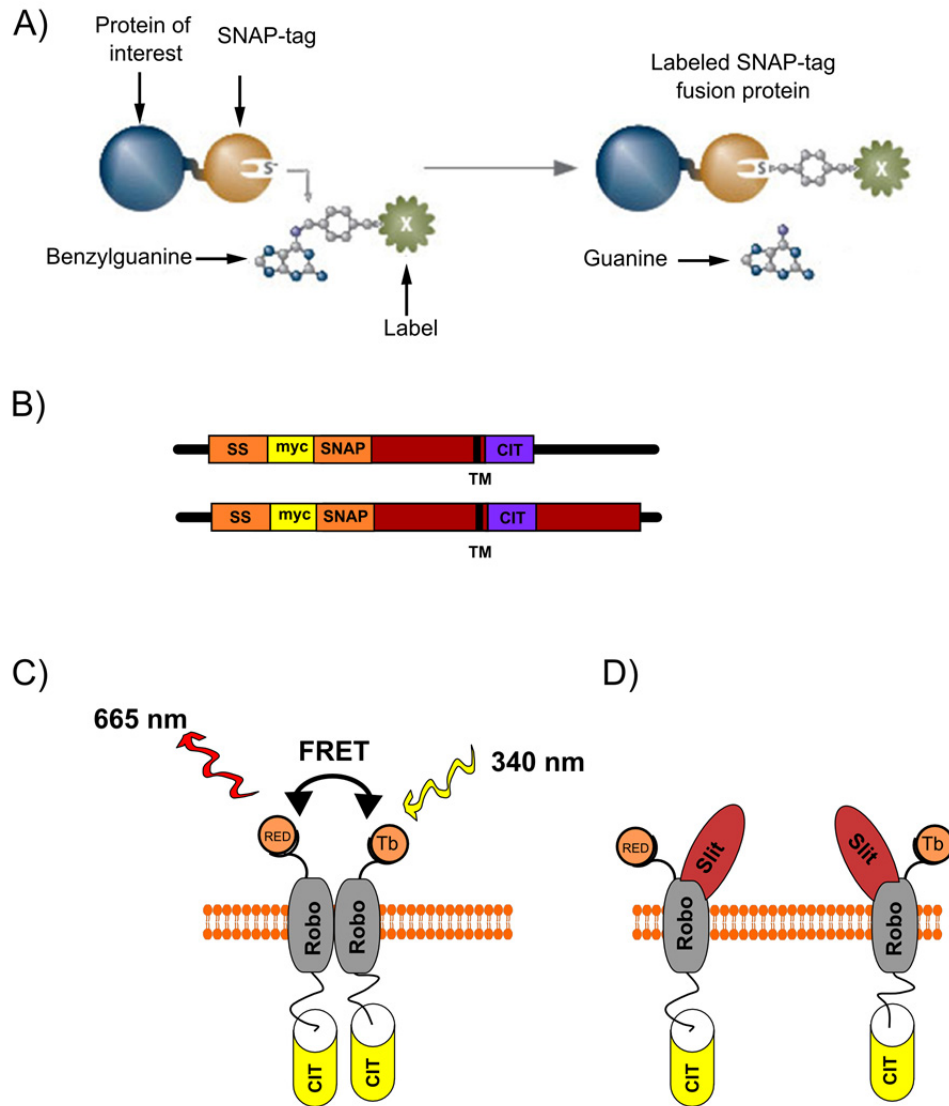


Figure 3.19 Basis of a TR-FRET experiment

Fluorescent labels necessary for a TR-FRET experiment were added to Robo1 constructs using a SNAP labelling system (A, an image reprinted from www.neb.com (2012) with permission from New England Biolabs, <http://tinyurl.com/7oj2o97>). In order to make the existing Robo1 construct compatible with it, a SNAP tag was inserted between an epitope tag and a Robo1 sequence for both truncated and full-length Robo1 constructs. TM stands for transmembrane region (B). Putative Robo1 oligomerisation would bring the fluorescent labels into close proximity yielding a high FRET signal (C). If the addition of Slit2 causes Robo1 oligomer dissociation, a decrease in the FRET signal would be observed (D).

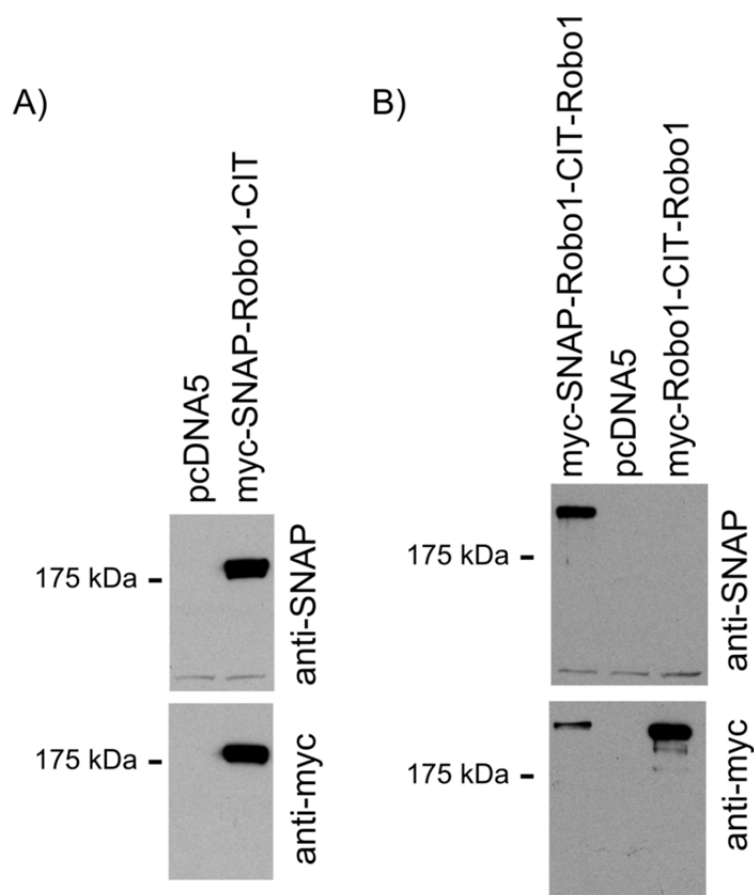


Figure 3.20 Expression of SNAP-tagged Robo1 constructs

HEK 293T cells were transiently transfected with truncated (A) or full-length (B) SNAP-tagged Robo1 constructs or appropriate controls. Cells were lysed, samples of lysates were resolved by SDS-PAGE and then immunoblotted with anti-SNAP and anti-myc antibodies. Blots are representative of two independent experiments.

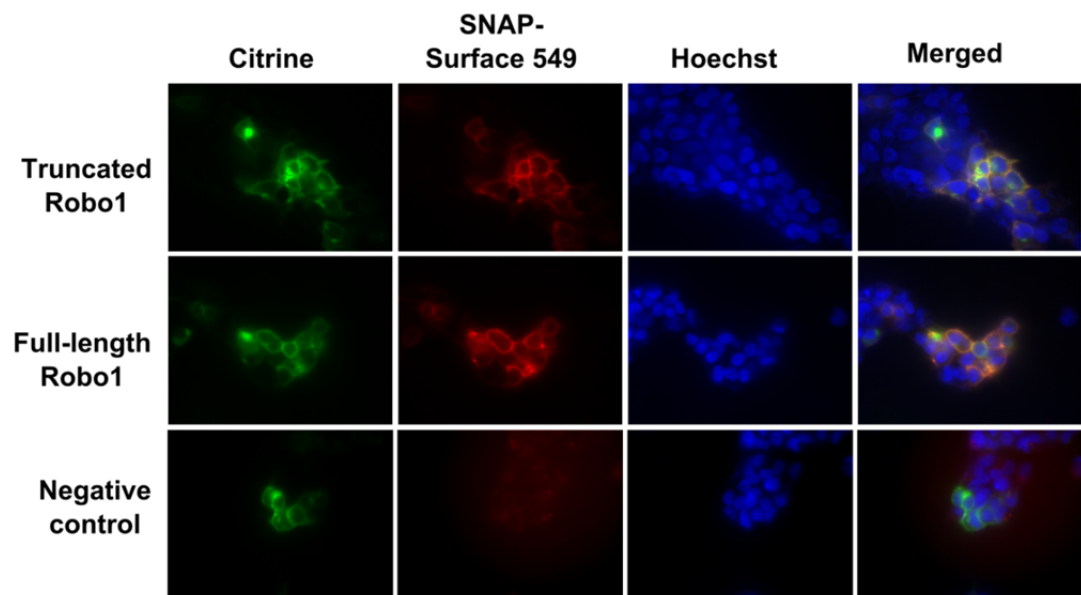


Figure 3.21 SNAP tagged Robo1 construct validation

HEK 293T cells were transiently transfected with truncated (myc-SNAP-Robo1-CIT), full-length (myc-SNAP-Robo1-CIT-Robo1) or SNAP tag lacking (myc-Robo1-CIT, negative control) Robo1 constructs. Nonpermeabilized cells were fixed and stained with Hoechst and SNAP-Surface 549, a cell impermeant, fluorescent SNAP substrate. Fixed cells were imaged with an inverted epifluorescence microscope.

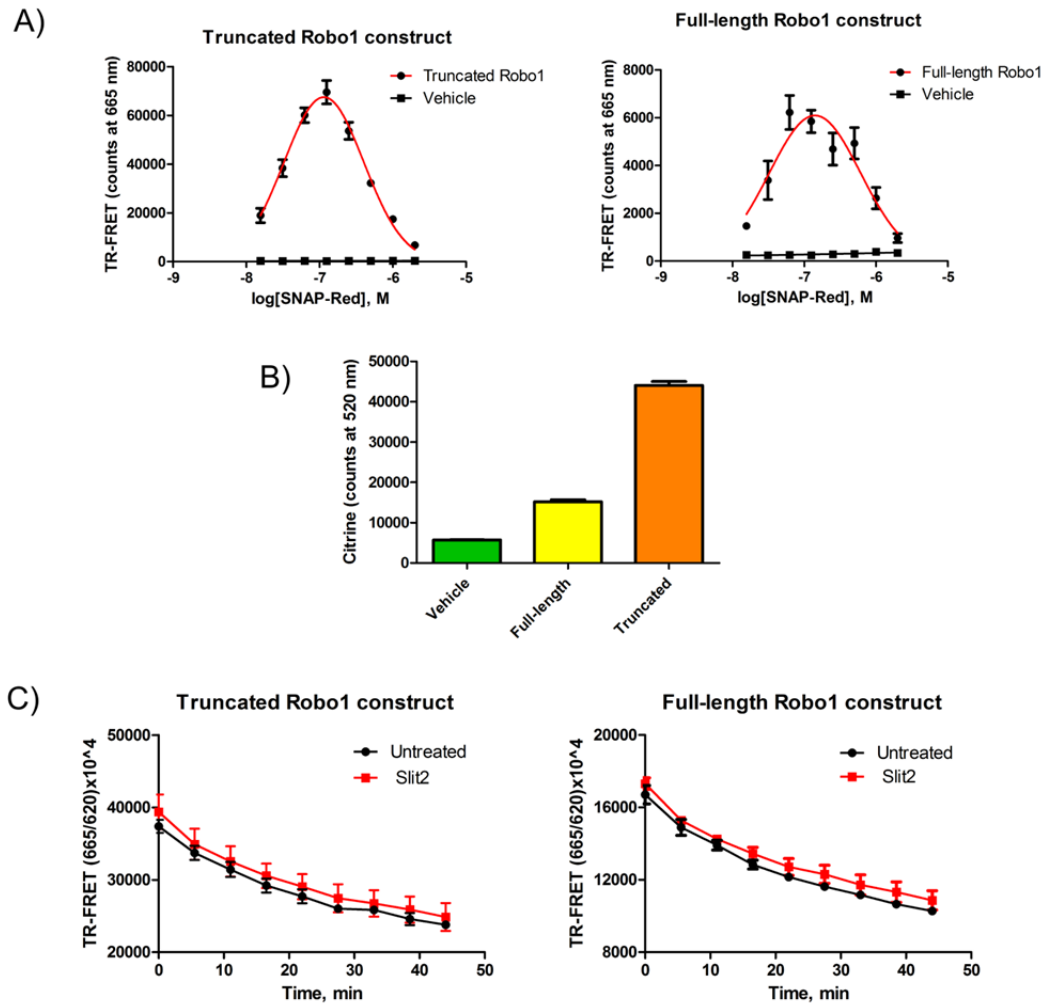


Figure 3.22 TR-FRET measurements

HEK 293T cells were transiently transfected with truncated (myc-SNAP-Robo1-CIT) or full-length (myc-SNAP-Robo1-CIT-Robo1) constructs. Alternatively, mock DNA was used for transfection as a vehicle control. The cells were labelled with a mixture of donor and acceptor SNAP substrate conjugates. The concentration of donor was kept constant at 50 nM, while the concentration of an acceptor was varied between 15 nM and 2 μ M. The raw TR-FRET signal was measured at 665 nm following excitation at 340 nm and expressed as a function of acceptor concentration (A). In order to evaluate expression levels of the Robo1 construct Citrine fluorescence was measured at 520 nm following excitation at 485 nm (B). HEK 293T cells were transiently transfected with truncated (myc-SNAP-Robo1-CIT) or full-length (myc-SNAP-Robo1-CIT-Robo1) Robo1 constructs and labelled with donor and acceptor SNAP substrate conjugates (50 nM Lumi4-Tb, 115 nM RED). 100 ng/ml of Slit2 (R&D systems) or an equal volume of PBS was added to the cells and TR-FRET signal, assessed as the 665/620 nm ratio, was measured over a time course of 45 minutes. Signal values are expressed as a mean of two independent experiments \pm SEM. No statistically significant differences were observed between Slit2 treated and non-treated samples as determined by two-way ANOVA (C).

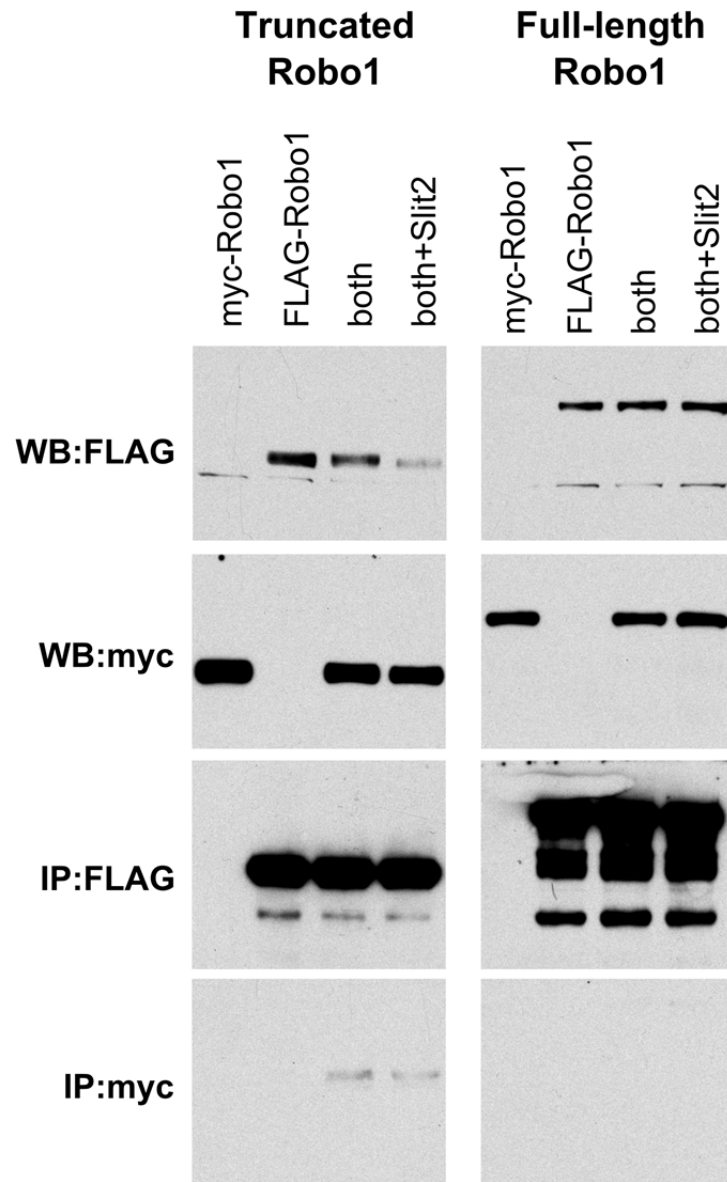


Figure 3.23 Co-immunoprecipitation of differently tagged Robo1 constructs

HEK293T cells were transiently co-transfected with differently tagged truncated or full-length constructs (myc-Robo1-CIT and FLAG-Robo1-CER or myc-Robo1-CIT-Robo1 and FLAG-Robo1-CER-Robo1), maintained for 24 hours and treated with 100 ng/ml of Slit2 (R&D systems) for 30 minutes or PBS as a negative control. The treated cells were lysed and the FLAG-tagged Robo1 constructs were immunoprecipitated from the lysate using anti-FLAG antibody conjugated beads. Co-precipitation of the myc tagged Robo1 constructs was probed using an anti-myc antibody.

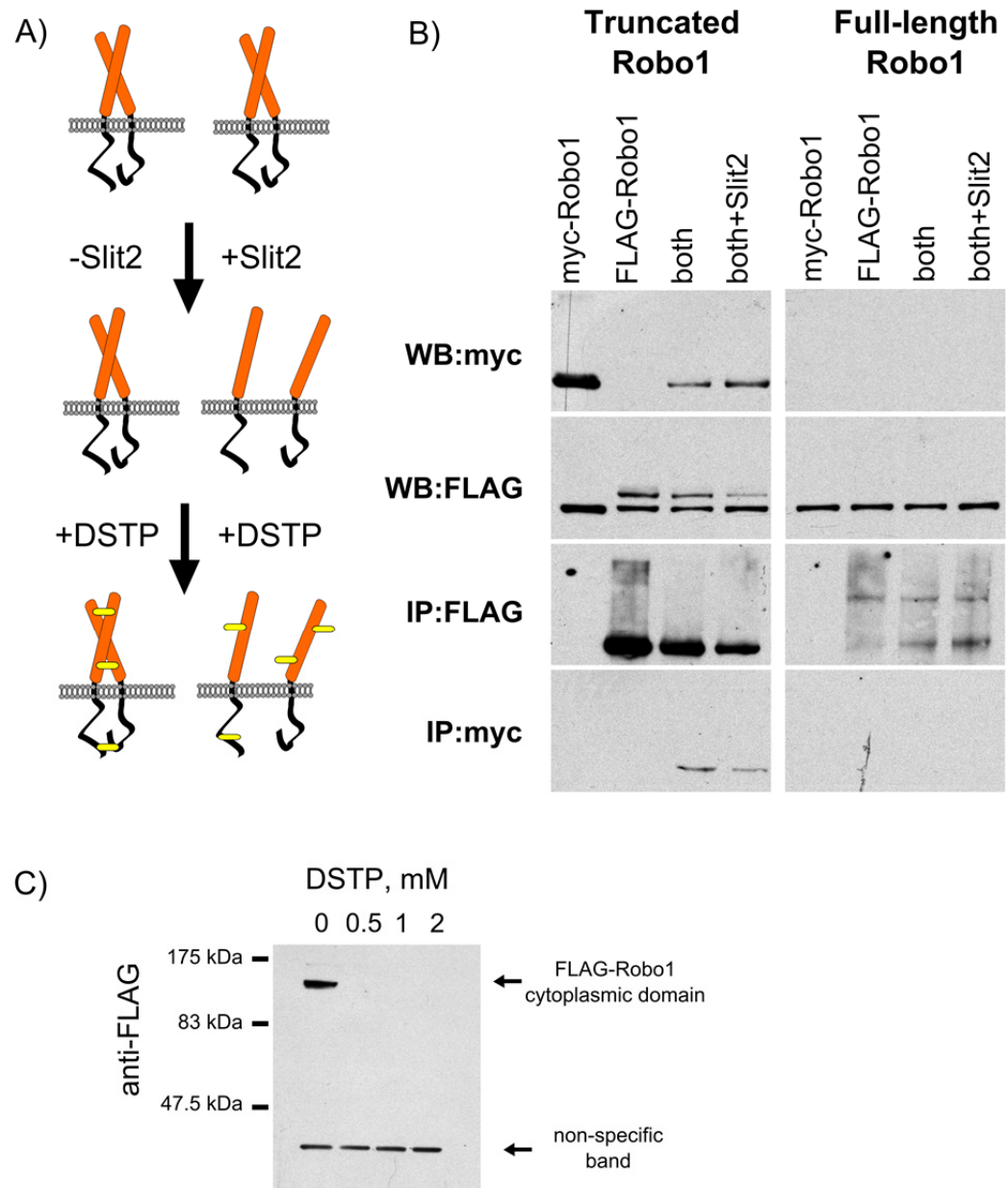


Figure 3.24 Crosslinking and co-immunoprecipitation of differently tagged Robo1 constructs

A schematic illustration of the crosslinking based assessment of the Robo1 oligomeric state (A). HEK293T cells were transiently co-transfected with differently tagged truncated or full-length constructs (myc-Robo1-CIT and FLAG-Robo1-CER or myc-Robo1-CIT-Robo1 and FLAG-Robo1-CER-Robo1), incubated for 24 hours and treated with 100 ng/ml of Slit2 (R&D systems) or PBS as a negative control. The cells were then crosslinked with DTSP reagent, lysed and the FLAG-tagged Robo1 constructs were immunoprecipitated from the lysate using anti-FLAG antibody conjugated beads. Co-precipitation of the myc-tagged Robo1 constructs was probed using an anti-myc antibody. The blot is representative of three independent experiments. (B). In order to assess crosslinking effects on a Robo1 cytoplasmic tail HEK 293T cells were transiently transfected with a construct representing a mouse Robo1 cytoplasmic domain N-terminally tagged with a FLAG tag, crosslinked with different concentrations of DTSP reagent, lysed and analysed with Western blot (C).

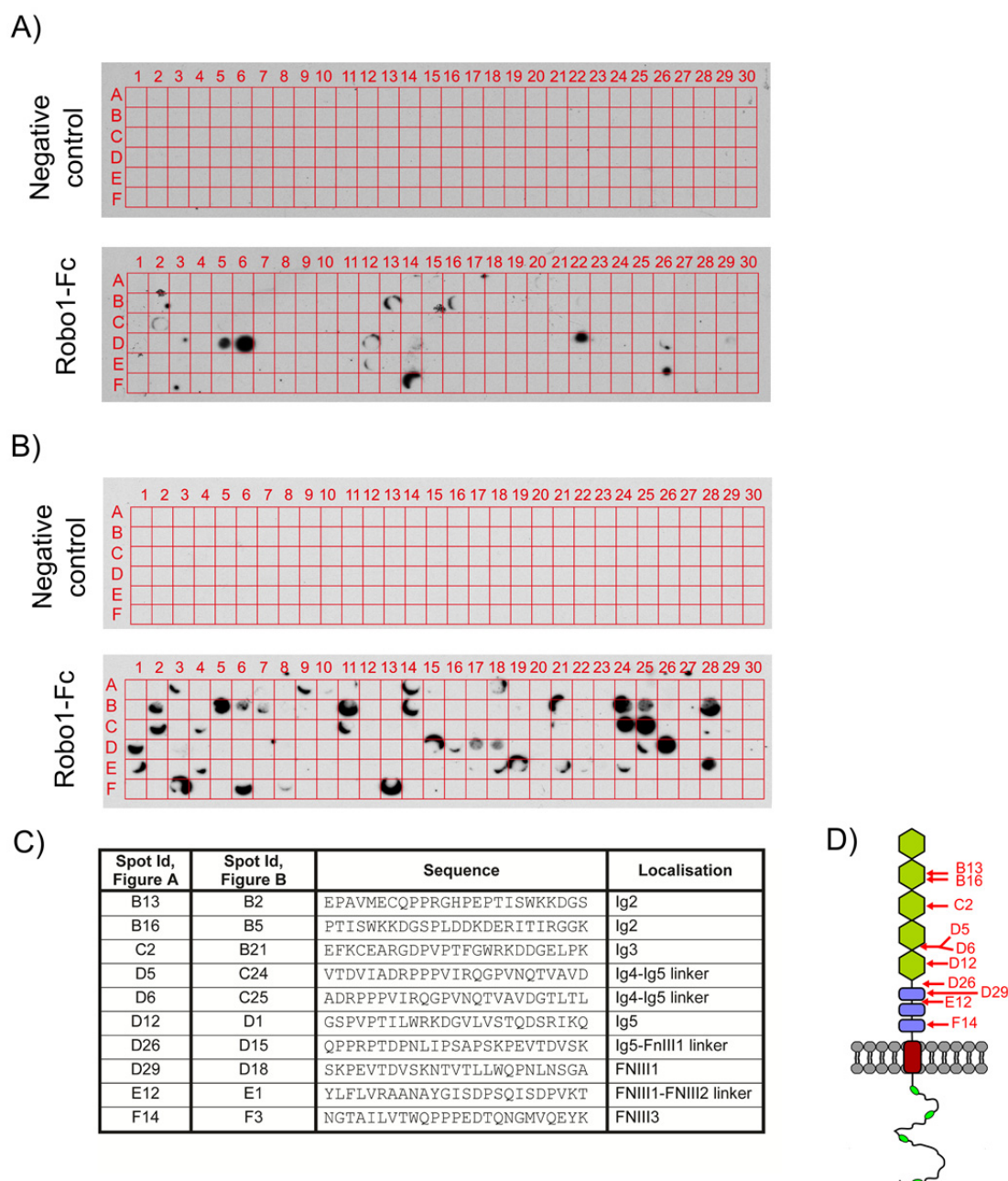


Figure 3.25 Mapping the sites of Robo1 oligomerisation

Peptide arrays were used to screen the complete sequence of the rat Robo1 extracellular domain for sites of association with the soluble rat Robo1 extracellular domain (Robo1-Fc). Two separately produced membranes with identical peptide spots were used in this experiment (A and B). In both cases the same membrane was used both for negative control (anti-Fc antibody only) and Robo1 overlay (Robo1-Fc incubation followed by blotting with anti-Fc antibody). Peptides identified in both experiments are listed in table, where numbers represent spot coordinates on the grid (C). Identified putative Robo1-Robo1 interaction sites (spot ids are listed according to Figure A) are also schematically mapped on to the Robo1 structure (D).

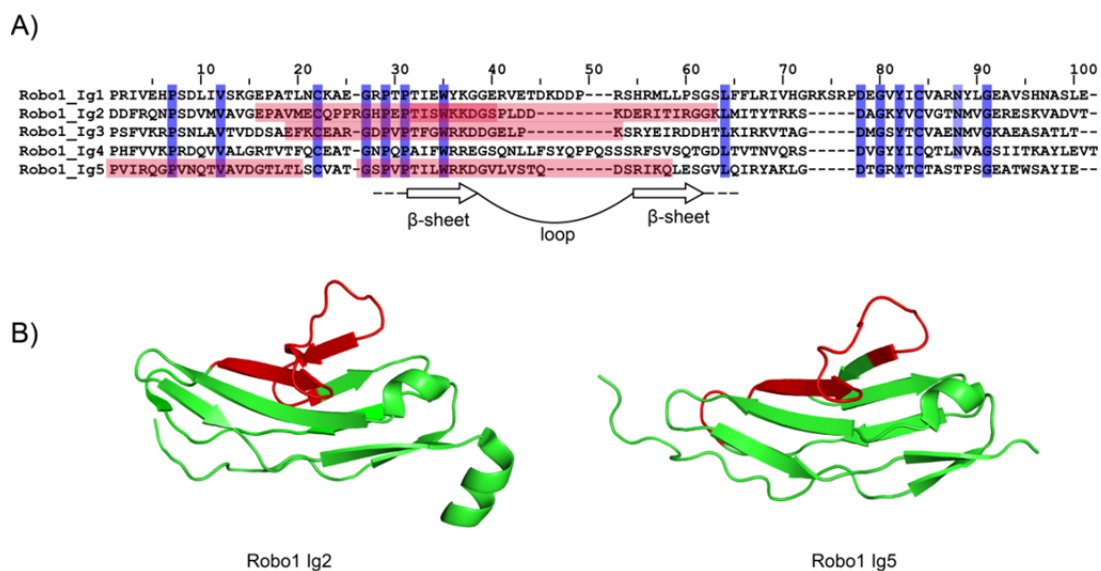


Figure 3.26 Structural conservation of putative Robo1 oligomerisation sites

Putative Robo1 oligomerisation sites were mapped (colour coded pink) on to the sequence alignment of rat Robo1 Ig domains (A) and Robo1 Ig2 [pdb id: 2V9Q] and Ig5 [pdb id: 2EO9] structures (B) revealing a possible common structural element of surface exposed loops surrounded by two β -sheets.

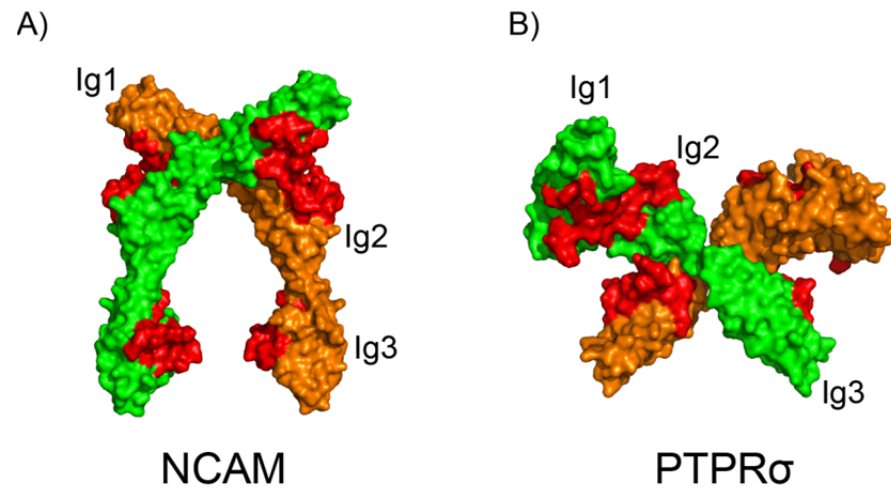


Figure 3.27 Dimerisation interfaces of I-set Ig proteins

Putative Robo1 dimerisation sites were mapped (coloured in red) on to Robo1 related proteins with known dimer structures: NCAM [pDB id: 1QZ1] (A) and PTPRσ [pDB id: 2YD9] (B).

4 Study of Slit-Robo role in the immune system

4.1 Introduction

Substantial evidence indicates that the Slit-Robo signalling axis is utilised by the immune system. Published data show Robo1 expression in various populations of white blood cells. Correspondingly, Slit2 is able to inhibit chemotactic leukocyte movement both *in vitro* and *in vivo* (see section 1.5.8). Moreover, treatment with Slit2 reduces immune responses in various inflammation models. The opposite is true as well, as studies show that inflammatory responses usually coincide with changing expression levels of Slit proteins (Guan et al, 2003; Kanellis et al, 2004; Ye et al, 2010). In summary, Slit and Robo proteins are expressed by various immune system cells and related tissues, they affect progress of inflammation and, conversely inflammation regulates their expression levels. All this indicates that the Slit-Robo signalling axis is coupled to the immune system, however the precise role of these proteins within it remains unknown. Elucidation of Slit-Robo role within the immune system is of fundamental biological importance. Functional interplay between the nervous and immune systems is now well established as additional evidence accumulates and expands in scope (Steinman, 2004; Sternberg, 2006). Many common themes, patterns and organisational principles can be found among these two systems on different levels ranging from organs to molecules (Kioussis & Pachnis, 2009). In fact, all major neuronal guidance molecule families (Slit-Robo, Netrin-DCC, Semaphorin-Plexin, Eph-Ephrin) interact with the immune system in one or other way (Kumanogoh & Kikutani, 2010; Ly et al, 2005; Pasquale, 2008). Thus research into Slit-Robo role within the immune system could potentially advance our understanding of connections between the immune and nervous systems. Besides, possible practical applications are no less important. Broad inhibitory effects of Slit on leukocyte migration might be of value in fighting uncontrolled or chronic inflammation. All together this makes the role of the Slit-Robo signalling axis in the immune system a compelling research object.

Although published data clearly show links between the Slit-Robo signalling axis and the immune system, currently available information is not sufficient to suggest initial hypotheses. One of the possible ways to establish a working hypothesis is a systematic and thorough expression profiling of Slit-Robo protein expression in various mouse tissues. Identification of Slit or Robo expressing leukocyte populations would be especially useful. Different leukocyte subtypes perform different functions and knowing which of them are expressing Slit or Robo proteins may help suggest Slit-Robo functions as well. Moreover,

as mentioned above, various studies indicate that expression levels of Slit proteins are dynamic and regulated in accordance with immune responses. Bioinformatic analysis of transcription factor binding sites (TFBS) could help to elucidate mechanisms underlying this regulation and, by extension, connections between the Slit-Robo signalling axis and the immune system.

4.2 Slit-Robo expression profiling

4.2.1 Slit-Robo expression in mouse organs and tissues

Initially, a broad Slit-Robo expression profile was determined in mouse organs and tissues. Two female C57BL/6 mice were sacrificed and samples of various tissues and organs were collected. Tissues then were flash frozen with liquid nitrogen and ground to a fine powder using a mortar and pestle. Total RNA was extracted and cDNA synthesised as described in sections 2.2.1 and 2.22. In parallel, as a control for genomic DNA contamination, identical cDNA synthesis reactions were performed without reverse transcriptase. Finally, Slit-Robo paralogue or GAPDH (Glyceraldehyde 3-phosphate dehydrogenase, housekeeping gene, positive control) specific primers were used in routine PCR assays. Representative gels for Robo2 and GAPDH are shown in Figure 4.1A and 4.1B and all results are summarised in Figure 4.1C. In agreement with published data, these experiments showed that Slit-Robo mRNA is expressed in a wide range of different tissues and organs. The only exceptions are Slit1 and Robo3, expression of which is confined to the brain and the brain and the kidney respectively. Brain was found to express all family members, which is in keeping with known expression data. Leukocyte rich lymph nodes and spleen have similar expression patterns - strong expression of Robo1, Robo2, Robo4, Slit3 and traces of Slit2. Interestingly, no Slit or Robo expression was detected in bone marrow (BM). This was a surprising result and subsequent publications have shown that BM stromal cells do express Slit2 while hematopoietic stem cells express Robo4 (Shibata et al, 2008; Smith-Berdan et al, 2011). This contradiction most likely is caused by different sensitivity of the experiments in question. Shibata and colleagues failed to notice Slit2 expression in whole BM samples as well and it became detectable only after BM stromal cells were purified and the RT-PCR cycle number was increased to 40 (Shibata et al, 2008). This example illustrates the innate limitation of qualitative RT-PCR with whole organs and tissues. Often, especially when the signal is low, it is not clear which cells express the transcript of interest, as low signal can be explained by low expression in all cells, a small fraction of transcript-rich cells mixed with non-expressers or anything in between. General profiling at the organ level provides a useful general picture, but since observed expression patterns for

Slit-Robo proteins are really broad, more specific tools and approaches are necessary to further “zoom in” on Slit-Robo functions within the immune system.

4.2.2 Slit-Robo expression in cell lines

In addition to mouse tissues, Slit-Robo mRNA expression was assessed in different immortalised cell lines. This experiment had several purposes. The first goal was to reveal any correlation between Slit-Robo expression patterns and cell type which could indicate Slit-Robo role within the immune system. Second, Slit or Robo expressing immortalised cell lines could be employed as a standard for further experiments, for example flow cytometry assays with *ex vivo* hematopoietic cells.

Cells were lysed and total RNA extracted as described in section 2.2.1. cDNA was synthesised and used as a template for PCR with Slit or Robo orthologue-specific primers. Expression of the housekeeping gene GAPDH was used as a positive control, while samples lacking reverse transcriptase served as a negative control for genomic DNA contamination. All results are summarised in Figure 4.2. In general, highly variable expression profiles of Slit and Robo proteins can be observed. It seems that cells of myeloid origin (monocytes, macrophages, megakaryocytes, mast cells) tend to express Robo1 more uniformly than other populations, but apart from that, expression profiles do not follow easily identifiable cell type-related patterns. Interestingly, many cells express both Slit and Robo proteins raising the possibility of autocrine regulation. Another interesting observation relates to Slit1 expression. Mouse tissue profiling described above, and published data, show that Slit1 expression is usually limited to neuronal tissues only. However several hematopoietic cell lines (HUT-78, Jurkat, THP-1) showed strong Slit1 expression at least at the mRNA level (Figure 4.2). It has been reported previously that expression of Slit-Robo proteins can be both silenced and activated during tumour development (see section 1.5.7) so care must be taken when interpreting expression data from oncogenically transformed cell lines, as they not necessarily represent native cells they originated from. Nevertheless, these experiments revealed widespread and highly variable expression of Slit and Robo mRNA in immortalised cell lines.

4.2.3 Slit-Robo expression in *ex vivo* leukocytes

While information about Slit-Robo expression in immortalised cell lines is useful, the most important question to address is Slit-Robo expression in live tissues at the cellular level. Flow cytometry is a standard tool to analyse protein expression in hematopoietic cells and since experimental data and published information show that these cells tend to express

Robo1, it was employed to phenotypically characterise Robo1 expressing leukocyte populations.

Initially, THP-1 cells which express endogenous Robo1 (Figure 4.2) were used as a standard to verify the assay. Cells were labelled with biotinylated anti-Robo1 antibody (R&D Systems), stained with avidin-APC (allophycocyanin) conjugate and analysed using flow cytometry as described in section 2.2.33. This experiment revealed a signal which was definite but weak in comparison to isotype antibody control (Figure 4.3A). These results indicate that either the levels of endogenous Robo1 protein in THP-1 cells are extremely low or that the antibody used is not specific enough. In order to address this issue the assay was repeated using HEK 293 Flp-In T-REX cells able to express a myc-Robo1-CIT construct. Expression of the construct was induced by incubating cells with 50 ng/ml of doxycycline overnight. Cells were then labelled with anti-Robo1 antibody as described above. In parallel, non induced cells were used as a negative control. Fluorescence of the Citrine fluorescence protein present in the Robo1 construct was readily detectable upon incubation with doxycycline, independently demonstrating expression of this protein (Figure 4.3B). In agreement, the anti-Robo1 antibody was able to detect strong and ubiquitous expression of Robo1 (Figure 4.3C). These data show that the flow cytometry assay is functional and the observed weak Robo1 signal in THP-1 cells is most likely caused by low expression levels of the receptor. Consequently, it was used to assess Robo1 expression in hematopoietic cells. Human peripheral blood mononuclear cells (PBMC) were labelled with the anti-Robo1 antibody as described above and analysed using flow cytometry, however, no differences between isotype control and anti-Robo1 antibody were observed (Figure 4.3D). It seems that protein levels of endogenous Robo1 on the surface of human PBMC are extremely low or it is not expressed at all.

An alternative anti-Robo1 antibody from Developmental Studies Hybridoma Bank (DSHB, University of Iowa, Iowa City, USA) was examined in an attempt to optimise detection of endogenous Robo1 by flow cytometry. Hybridomas producing this antibody were acquired from DSHB and cells were grown as described in section 2.2.30. Initially, attempts were made to purify the anti-Robo1 antibody from hybridoma supernatant in order to conjugate it with fluorescent dye. Because this particular antibody is of an IgM isotype, standard antibody purification techniques based on protein G binding could not be applied and a HiTrap IgM Purification HP Column (GE Healthcare) was used instead according to manufacturer's instructions (Figure 4.4A). Collected fractions were analysed by SDS-PAGE revealing protein mixtures without any apparent enrichment of Ig chains (Figure

4.4B). Fractions were combined and the eluate was further tested using Western blot. Cell lines natively expressing Robo1 or HEK 293T cells transiently transfected with myc-Robo1-CIT or FLAG-Robo1-CER constructs were lysed, samples were resolved by SDS-PAGE and immunoblotted with purified anti-Robo1 antibody (DSHB), anti-Robo1 antibody (DSHB) hybridoma supernatant, Robo1 antibody from R&D Systems or anti-myc and anti-FLAG antibodies (Figure 4.5). Expression of what appears to be full-length Robo1 was detected in THP-1 cell lysates by supernatant but not by purified Robo1 antibody (DSHB) (Figure 4.5A). Surprisingly, an identical band was also detected in Jurkat cell lysates which, according to RT-PCR experiments, contain no detectable Robo1 mRNA (Figure 4.5A). Moreover, expression of the myc-Robo1-CIT or FLAG-Robo1-CER constructs was not detected with DSHB antibody even though it was readily visualised with anti-myc, anti-FLAG or anti-Robo1 antibody from R&D Systems (Figure 4.5B). The epitope detected by the DSHB antibody maps to the first FNIII domain and is not affected by known splicing or other modifications. Given this uncertainty about the specificity of the DSHB antibody it was not used for further studies.

Overall, attempts to employ flow cytometry and determine the phenotype of Robo1 expressing hematopoietic cells failed because of lack of suitable anti-Robo1 antibodies. Low levels of endogenous expression might also be a contributing factor as the example with THP-1 cells demonstrates.

4.3 Transcription factor binding site analysis

Various studies indicate that expression levels of Slit and Robo proteins are dynamic and can be regulated in response to external stimuli (Guan et al, 2003; Kanellis et al, 2004; Ye et al, 2010). Therefore it can be reasoned that bioinformatic analysis of transcription factor binding sites (TFBS) in putative Slit-Robo promoter regions might help to elucidate mechanisms underlying this regulation and, by extension, connections between the Slit-Robo signalling axis and other cellular circuits. In other words, knowing the transcription factors involved in Slit-Robo regulation, one may be able to suggest testable hypotheses about the role of Slit-Robo within the immune system.

Identification of regulatory TFBS is not a trivial task. Simple DNA sequence matching with known transcription factor binding sites is not a productive strategy. TFBS usually are ambiguous and loosely defined and a straightforward search for known binding sequences would reveal hundreds of putative sites even in randomly generated DNA. Moreover, promoters vary greatly in terms of their overall structure and defining features and even the current abundance of genomic data have failed to provide meaningful generalisations.

Currently suggested classification, which even by the authors is considered “work in progress”, defines three broad classes of metazoan promoters (Lenhard et al, 2012). Type I “sharp” promoters are easier to analyse since regulatory TFBS tend to cluster in groups relatively close to core promoter elements (like the TATA box) and transcription start sites. Meanwhile, type II and III “broad” promoters span relatively long sequences, lack identifiable core elements and contain multiple transcription start sites which further burdens their analysis (Lenhard et al, 2012). Because of all this variability false-positive errors plague *in silico* promoter analysis and additional methods are needed to remove them. A method called phylogenetic footprinting is usually employed for this purpose (Qiu, 2003). It is based on the principle that functionally important sequences tend to be conserved among multiple species and putative TFBS shared by several different species are more likely to be biologically relevant.

Table 4.1 Transcription factors potentially involved in regulation of Slit-Robo expression

Transcription factor	Biological relevance
EGR1 (early growth response gene 1)	Monocyte/macrophage lineage commitment control
LEF-1/TCF	Wnt signalling axis, cell invasion, matrix protease expression.
Myc/Max/Mad network	Cell proliferation, growth and apoptosis
KLFS (Kruppel like zinc fingers)	Various aspects of development
ETS1 (E26 transformation specific sequence)	Differentiation of haematopoietic cells, invasive cell behavior, hypoxia
NFAT (Nuclear factor of activated T cells)	Developmental cell-cell interactions, cytokine production in T cells, neuronal growth
PAX5	Cell differentiation, nerve system development
STAT	Various aspects of growth, survival and differentiation in cell
IKR	Ikaros zinc finger family, potential regulator of lymphocyte differentiation
MYT1 Myelin transcription factor 1	Differentiation of neurons
NF-κB	Cell survival, immune response, neuronal plasticity

Slit-Robo promoter analysis was started by identifying 5000 bp of upstream sequence for Slit1, Slit2, Slit3, Robo1 and Robo2 orthologues from different mammals in NCBI Entrez Genome database (<http://www.ncbi.nlm.nih.gov/sites/genome>). Robo1 and Robo2 proteins exist as two isoforms which employ different signal peptides. It appears that they arise from alternative transcription sites which are separated by hundreds of kilobases of genomic DNA and therefore most likely are controlled by different promoters (Nural et al, 2007). The shorter isoform (Robo1B/Dutty or Robo2B) is expressed more widely and

strongly than the longer version (Robo1A and Robo2A) (Clark et al, 2002; Yue et al, 2006), thus its upstream sequence was used for promoter analysis. Slit and Robo upstream sequences from different mammalian species were collected and systematically inspected for core promoter elements and CpG islands using MatInspector (Cartharius et al, 2005) and CpG Island Searcher (Takai & Jones, 2003) respectively. This analysis revealed that putative promoters of all examined genes lack identifiable core promoter sequences but clearly contain relatively large CpG islands extending into the coding region (Figure 4.6). According to the nomenclature suggested by Lenhard and colleagues, the Slit-Robo thus are regulated by "broad" Type III promoters which usually have multiple transcription start sites and are associated with developmentally regulated genes (Lenhard et al, 2012).

Identification of CpG islands strongly indicates the presence of biologically relevant TFBS therefore the same upstream sequences of Slit1, Slit2, Slit3, Robo1 and Robo2 orthologues from different species were aligned and analyzed for TFBS using DiaAlign software (fragment of DiaAlign output is exemplified in Figure 4.7) (Cartharius et al, 2005). Only transcription factor binding sites conserved across multiple species were considered for further analysis. Nevertheless, even then, dozens of putative transcription factors potentially involved in regulation were identified for each gene. Some of the more prominent hits are listed in Table 4.1. As one might expect, a lot of the identified transcription factors are related to development. Others have a variety of different functions depending on cellular or tissue context. This reduced the potential usefulness of the promoter analysis since functional pleiotropy meant that no specific connection between Slit-Robo and other particular signalling circuits could be made. The exception was the transcription factor Foxn1 whose binding site was identified in both Slit2 and Slit3 promoters (Figure 4.8). More interestingly, in both cases the distance between putative Foxn1 DNA binding site and the open reading frame of the gene was similar. Positions of transcription start sites, mapped by genome-wide cap analysis of gene expression (CAGE) also indicate biological relevance of Foxn1 site as several transcription start sites (TSS) are located downstream of putative Foxn1 binding site in human and mouse genomes (Figure 4.8). Interestingly, human and mouse Slit2 genes potentially contain an alternative promoter approximately 1500 bp upstream of the Foxn1 site, as a cluster of TFBS identified by DiaAlign overlaps with TSS identified by CAGE (Figure 4.8). This particular TSS seems to be used preferentially in many mouse tissues, as numerous expressed sequence tags (EST, sequenced short random fragments of cDNA), confirm the existence of a Slit2 transcript with a long 5' untranslated region. Nevertheless, the Slit2 upstream

region containing the Foxn1 binding site also includes TSS identified by CAGE both in mouse and human and therefore constitutes a valid putative promoter. All together these CpG, TFBS and TSS patterns strongly indicate biological relevance of Foxn1 binding site and hence all further studies were focused on it.

This spatial conservation serves as additional evidence of biological relevance and hence all further studies were focused on this bioinformatics hit. The transcription factor Foxn1 is a well established master regulator of thymus development. Disruption of this gene leads to a non-functional thymus and severe immunodeficiency since the thymus is crucial for development of T cells and adaptive immunity (Nehls et al, 1994). Given the well established ability of Slit-Robo to regulate cell movement in general, and leukocyte chemotaxis in particular, it is tempting to speculate that these proteins also act as “traffic” regulators in thymus.

4.4 Slit function in thymus

The thymus is a primary lymphoid organ that is found in almost all vertebrates and is responsible for differentiation and development of T lymphocytes. Hematopoietic precursor cells, whose precise lineage is still debatable, migrate into thymus from bone marrow (Desanti et al, 2011; Luc et al, 2012). Then these maturing hematopoietic cells, also called thymocytes, move between different thymic compartments depending on the stage of their development. The thymic cortical region harbours thymocytes during their early stages of development. Cells here undergo T cell receptor (TCR) rearrangement and positive selection which ensures their functionality. They then move into the medullary region of the organ where negative selection takes place and cells not able to “ignore” innate antigens of the organism are destroyed. Finally, mature and functionally competent T cells migrate from the thymus into the periphery where they take part in many different aspects of the adaptive immune response (Love & Bhandoola, 2011).

Thymocyte development completely depends on the interactions with thymic epithelial cells (TEC). Based on their localisation and expressed markers TECs can be subdivided into two populations - cortical (cTEC) and medullary (mTEC). Neither cTEC nor mTEC are homogenous populations and additional subdivisions were suggested by various authors (Gray et al, 2006; Hamazaki et al, 2007). TECs interact with thymocytes both directly, and via secreted molecules, and are indispensable for T cell development within the thymus (Love & Bhandoola, 2011). This dependency is very obvious in some naturally occurring mutations. One classical example is so called the "nude phenotype" which appears both in humans and mice and is characterised by lack of hair, athymia and severe

immunodeficiency (Flanagan, 1966; Frank et al, 1999). It is caused by the mutation in the transcription factor Foxn1 which belongs to the forkhead box transcription factor family (Kaestner et al, 2000). Foxn1 is a master controller of TEC development. Its expression is switched on 11.5 days post coitum (E11.5) in mice enforcing differentiation of the endodermic anlage into thymic epithelium (Rodewald, 2008). Factors controlling Foxn1 expression are currently unknown, so this transcription factor is the earliest known marker of TEC. Lack of Foxn1 becomes apparent as early as E13; TEC progenitors fail to proliferate and differentiate into medullary and cortical compartments and hematopoietic cells are virtually absent in the formed rudimentary thymus (Rodewald, 2008). Studies also demonstrated that Foxn1 retains its functional importance after the birth, as postnatal disruption of Foxn1 leads to histological and functional degeneration of the thymus (Chen et al, 2009; Cheng et al, 2010).

On a molecular level Foxn1 appears to be a transcriptional activator which switches on a set of TEC-related genes, although its targets remain somewhat obscure despite more than a decade of research. Only one gene, FGF2 (fibroblast growth factor), using chromatin immunoprecipitation was directly shown to be regulated by Foxn1 (Weiner et al, 2007). Others, like the Notch ligand DLL4, the chemokine CCL25, the transcription factor Pax-1 or the PD-1 ligand PD-L1 are indicated by circumstantial evidence (Bleul & Boehm, 2001; Liu et al, 2006; Nowell et al, 2011). Identification of positionally conserved Foxn1 binding sites within the putative Slit2 and Slit3 promoters raises the possibility that the Slit-Robo signalling axis is involved in thymic function. The absence of a putative Foxn1 binding site in the upstream Slit1 sequence agrees well with the fact that Slit2 and Slit3 are expressed widely around the body, while Slit1 is generally restricted to the nervous system. In fact, relatively high Slit3 expression in human thymus was reported previously (Dickinson et al, 2004). Similarly, Robo1 expression was reported in thymus as well (Wu et al, 2001). In both cases whole thymus was used for expression analysis and it is impossible to know which cells express the proteins in question. Given the fact that hematopoietic cells mainly express Robo1 it is reasonable to assume that Robo1 is present on thymocytes, while Slit2 is expressed by thymic stromal cells. Foxn1 is known to regulate expression of the CCL25 chemokine in TECs, which is a guidance cue for CCR9-expressing leukocyte migration into the thymus. Using this as a parallel one can speculate that Slits also contribute to the regulation of Robo1 expressing cell movement in the thymus. This hypothesis primarily rests on the prediction that Slit2 and Slit3 are regulated by Foxn1 thus verifying this prediction experimentally was the first step in testing the overall hypothesis.

4.4.1 Slit2 and Slit3 expression in TECs

The Foxn1 knockout mouse is a standard, and readily available, animal model, which could be used to assess Foxn1 effects on Slit2 and Slit3 expression. Unfortunately it is not useful in this particular situation because the thymus in these animals is reduced to a rudiment and therefore comparison of thymic Slit expression between wild type and Foxn1 knockout mice is not practical (Dooley et al, 2005). Instead, Slit2 and Slit3 expression levels were measured in TEC cells isolated from embryonic thymus at different developmental stages. If Slit2 or Slit3 are regulated by Foxn1, and have functions in thymic development, their expression levels should vary accordingly.

Timed pregnant C57BL/6 mice were sacrificed and embryos representing developmental stages E12-E14 (the day when the vaginal plug was detected was considered as E0) were harvested. Embryonic thymi were dissected, pooled and disaggregated into single cell suspensions (Figure 4.9). Cells were stained with antibodies specific for CD45 and EpCAM and the CD45⁻ EpCAM⁺ population purified from the cell mixture using cell sorting by Dr A. White. CD45 is a general leukocyte marker while EpCAM denotes cells of epithelial origin and TECs therefore have a CD45⁻ EpCAM⁺ phenotype. Purified cells were lysed and RNA was extracted as described in section 2.2.1. cDNA was synthesized using total RNA as a template and the copy number of Slit2 and Slit3 mRNA was quantified using QPCR based on SYBR Green chemistry (Figure 4.10).

Due to the laborious nature of the experiment and scarcity of samples only two independent biological replicates (different mothers) were acquired for Slit2 and only one for Slit3. However, Slit2 replicate experiments were performed in different laboratories and each time two different housekeeping genes (GAPDH and TATA binding protein) were used for normalisation with the same outcome. Moreover, QPCR threshold cycle values were reasonably high (Ct 20-25) and no non-specific products were detected using melting curves. Overall data show a clear downregulation of Slit2 and Slit3 mRNA starting at embryonic stage E13 (Figure 4.10). Foxn1 generally is a transcriptional activator so the observed reduction in expression levels is not necessarily related to Foxn1 and might be caused by other regulatory factors. While this experiment failed to prove a causal link between Foxn1 and Slit2 or Slit3 expression, it does not contradict it either, as Slit induction by Foxn1 might happen before E12. Nevertheless, altered Slit2 and Slit3 mRNA levels in TECs show that expression of these proteins is actively regulated during thymic development and suggests that products of these genes may have a role in thymic ontogeny or function.

4.4.2 Analysis of Slit2 knockout mice

The most straightforward way to identify Slit function in the thymus is to determine what effects Slit2 or Slit3 deletion has on the thymus and the immune system in knockout mice. Both Slit2 and Slit3 knockout mice have been reported in the literature. Homozygous Slit2 deletion is perinatally lethal and therefore no effects of this mutation on the immune system have been reported (Plump et al, 2002). Meanwhile, mice lacking functional Slit3, in fact, were created by two independent groups with both reporting closely similar phenotypes. Homozygous Slit3 knockout animals survive into adulthood although they have lower weight, shorter life span and generally are less viable because of an abnormal diaphragm (Liu et al, 2003; Yuan et al, 2003). Major malfunctions of the immune system most likely would have been detected and reported if present, however the authors mention none. Moreover, a figure in one of the original publications describing Slit3 knockout mice shows the open chest cavity, where an apparently normal thymus can be identified (Liu et al, 2003). It is reasonable to assume, therefore, that T cell development in these animals is not severely compromised.

Redundancy between Slit2 and Slit3 genes is possible, as sequence differences between these proteins are relatively small (see section 1.2). If Slit2 and Slit3 can complement each other in thymic development or function, a single knockout would fail to reveal the effects of gene deficiency. Adult double knockout animals (Slit2^{+/-}, Slit3^{-/-}) have been reported in the literature and would have been the most useful model for the studies described here (Jaworski et al, 2010). Unfortunately these mice were not available. It is possible to create a double knockout animal strain by crossing Slit2 and Slit3 deficient mouse strains, but again Slit3 knockout animal were not available and only Slit2 knockout animals were accessible for this study. This therefore leaves the potential issue of Slit2 and Slit3 redundancy unaddressed. However, Slit2 knockout effects are marked and much more obvious than those of Slit3 deletion. While it does not prove absence of redundancy in thymus specifically, it shows that at the general level Slit2 and Slit3 are not completely redundant and that Slit2 knockout mice alone potentially can be useful in providing information about Slit functions.

The perinatal lethality of homozygous Slit2 deletion would not allow assessment of adult animal immune function, but does not interfere with analysis of possible knockout effect on thymic development. One additional problem related to knockout lethality is that it complicates animal breeding. Animal stocks must be kept and bred as heterozygotes (Slit2^{+/-}) which, according to Mendelian laws, results in genotypically mixed litters (in

this particular case final Mendelian ratios will be skewed by early death of homozygous knockout animals). This means that upon dissection every single embryo must be genotyped separately before further analysis of embryonic thymic structure and composition. On the other hand, both wild type and knockout embryos are acquired under almost identical conditions, allowing effective comparison of thymic cellular composition. A scheme illustrating the overall experiment is depicted in Figure 4.11.

Heterozygous (*Slit2*^{+/-}) animals were mated and female mice were inspected for vaginal plugs each morning. The day when the vaginal plug was detected was considered as E0. Pregnant mice were sacrificed and E15 embryos were removed from the adult animal and decapitated. Embryonic thymus, and separate tissue samples for genotyping, were then taken from each individual embryo. Genomic DNA was extracted using Qiagen DNeasy Blood and Tissue kit according to manufacturer's instructions and used as a template in a PCR reaction for genotyping as described in section 2.2.5. Representative genotyping results are shown in Figure 4.12. During the course of the studies described here 88 embryos were genotyped with following results: 28 wt, 37 heterozygous and 23 homozygous *Slit2* knockout animals. Similarly, 56 adult animals were genotyped in total: 19 wt, 37 heterozygous and 0 homozygous. Observed ratios between different genotypes follow the expected Mendelian distribution and confirm previous reports that *Slit2* knockout is perinatally lethal.

In parallel to genotyping, each individual embryonic thymus was disaggregated into a single cell suspension and analysed for cellular composition using flow cytometry. Two different antibody panels were used for this analysis, one to assess composition of thymocytes, the other - composition of TECs.

T cell development and populations present in thymus are relatively well defined. The thymocyte population representing the earliest developmental stage is called double negative (DN) and has the immunotype $CD45^{+} CD4^{-} CD8^{-}$. Following β -selection, which ensures a functional T cell receptor (TCR), thymocytes express CD4 and CD8 leading to the so-called double positive (DP; $CD45^{+} CD4^{+} CD8^{+}$) stage. These cells then undergo positive and negative selection and differentiate into single positive cells (SP; $CD45^{+} CD4^{-} CD8^{+}$ or $CD45^{+} CD4^{+} CD8^{-}$) which represent the last stage of T cell development within the thymus before emigration. By no means all thymocyte populations were listed here as many others can be identified (Love & Bhandoola, 2011). DN, DP and SP cells, however, represent major milestones in T cell development and thus an immunotyping panel

containing antibodies specific to CD45, CD4 and CD8 is sufficient to assess general thymocyte composition and to detect major changes induced by Slit2 knockout if they are present.

Initially, the selected antibody panel was verified using thymocytes from adult mice. Adult C57BL/6 female mice were sacrificed, thymus dissected and thymocytes collected as described in section 2.2.32. Cells were stained with antibodies specific for CD45, CD4 and CD8 markers and analysed using flow cytometry. Dead cells were excluded from further analysis using the viability dye Viaprobe (BD). As expected, four different cell populations were detected (DN, DP and both SPs) confirming the validity of the antibody panel (Figure 4.13A). In contrast to the adult thymocytes, the majority of thymocytes in stage E15 embryos had a “double negative” phenotype. The observed additional “CD4 high” population most likely represents the first stages of “double negative” T cells differentiating into “double positive” (Figure 4.13B). Each population was quantified as a fraction of the parent population to normalize differences between samples caused by uneven tissue disaggregation. Eleven embryos were analyzed this way (2 wt, 5 heterozygote and 4 homozygote Slit2 knockout), but no genotype-related differences in cell populations were observed (Figure 4.13C and D).

Identical analysis was carried out on thymic epithelial cells using antibodies specific for EpCAM, Ly51 and MHC II markers. Dead cells were excluded using Viaprobe dye, TECs were selected by gating on the CD45⁻ EpCAM⁺ population and then analyzed for MHC II and Ly51 expression (Figure 4.14A). cTEC, unlike mTEC, express Ly51 so they can be discriminated based on this marker. Some of the published studies describe several additional subpopulations for TEC cells based on MHC II expression (Chen et al, 2009), so this marker was included into the panel as well. Fifteen E15 embryos were analyzed this way (3 wt, 8 heterozygote and 4 homozygote Slit2 knockouts). The quantity of CD45⁻ EpCAM⁺ cells was not genotype dependant (Figure 4.14B) and on average constituted 3% of total live cells, which closely matches numbers reported elsewhere (Gray et al, 2006). Comparison of the results also failed to reveal any genotype-related differences in MHC II or Ly51 expression demonstrating that mTEC and cTEC composition most likely was not affected by Slit2 knockout (Figure 4.14B).

In summary, analysis of embryonic thymus composition by flow cytometry failed to reveal any effects of Slit2 deletion in leukocyte or TEC compartments. This means that either Slit2 has no role in thymus development or that Slit3 functionally compensates its deletion.

Slit2 knockout mice were created by disrupting the Slit2 gene with insertion of a DNA cassette containing a coding sequence of the Tau-GFP fusion protein (GFP fused to a microtubule binding protein Tau) (Plump et al, 2002). Expression of this construct falls under control of native Slit2 promoter and therefore cells of the knockout animal which normally express Slit2 are marked with GFP fluorescence. This reporter system was employed in order to establish thymic cell populations expressing Slit2 protein and to complement previous PCR-based expression studies. Moreover, it served as an additional verification of animal phenotypes.

Individual embryonic thymi were dissected at stage E15 and disaggregated into single cell suspensions. Cells then were stained with fluorescent dye conjugated antibodies specific for EpCAM, CD45 or Ly51 markers and analysed using flow cytometry. Expression of the Tau-GFP construct was monitored directly by GFP fluorescence. An apparent GFP⁺ cell population was observed in some, but not all, samples (Figure 4.15A and B).

Correspondingly, when these results were matched with genotyping data, a strong correlation was revealed between genotype and abundance of GFP fluorescent cells, confirming their identity (Figure 4.15C). In order to establish their phenotype the GFP⁺ population was gated and analysed for expression of EpCAM, CD45 and Ly51 markers (Figure 4.15D and E). Unexpectedly it turned out that GFP is mainly expressed by CD45⁻ EpCAM⁻ Ly51⁺ cells that are neither thymocytes (lack of CD45 marker) nor TECs (lack of EpCAM marker). This is a surprising finding and at first glance contradicts previous results which indicated TECs as a source of Slit2 expression in thymus. However, GFP fluorescence is somewhat difficult to detect using FACS because the GFP emission spectrum overlap with the autofluorescence of cells causing a poor signal-to-noise ratio. Relatively high GFP expression is necessary for a cell to be unambiguously detected as GFP⁺ in flow cytometry. Transcription of Tau-GFP is controlled by the native Slit2 promoter and expression levels of the construct in different cells are proportional to those of Slit2. So it is not unexpected that some native cell populations might have considerably higher GFP fluorescence than others. The appearance of CD45⁻ EpCAM⁻ Ly51⁺ cells as the only GFP⁺ population may therefore simply mean that these cells have much higher Tau-GFP (and potentially Slit2) expression levels than TECs.

This experiment shows that TECs are not the only source of Slit2 in the thymus. In fact, it seems that CD45⁻ EpCAM⁻ Ly51⁺ cells, whose population size equals that of TECs, express it at higher levels than TECs. Cells with an identical CD45⁻ EpCAM⁻ Ly51⁺ phenotype were described in the literature as pericyte-type mesenchymal cells which

surround blood vessels (Muller et al, 2008). While conjunction of three markers alone does not completely prove that the observed GFP⁺ population is pericytes in nature, matching of the phenotype and the size of the populations is highly suggestive.

Slit2 expressed by pericytes potentially might have different physiological functions than Slit2 expressed by TECs as size and affinity for heparin sulphate most likely restricts Slit2 diffusion localising its activity close to the source.

4.5 Discussion

The main purpose of the experiments described in this chapter was to establish the functions of the Slit-Robo signalling axis in the immune system. Plenty of evidence exists that connects these proteins to the immune system: they are expressed by immune cells, they affect immune responses, and vice versa, immune responses affect their expression levels. Available published data were not sufficient to suggest a testable hypothesis explaining these connections, so initially all efforts were directed towards establishing a working hypothesis.

Analysis of Slit and Robo expression profiles in mouse tissues, and immortalised cell lines, failed to reveal any identifiable function related expression patterns. Slit and Robo proteins, with the exception of Slit1 and Robo3, are widely expressed across the whole animal body and in the majority of tested *in vitro* cell lines. Quite often immortalised cell lines express both Slit and Robo proteins together indicating possible autocrine regulation through the Slit-Robo signalling axis. However, these findings need to be treated with caution as cancerous transformation, which these cells underwent, might affect Slit-Robo transcription. Unfortunately, the most promising experimental approach, Robo1 receptor expression analysis by flow cytometry, was not successful either. Low endogenous Robo1 expression levels, and lack of suitable antibodies, made Robo1 detection in hematopoietic cells technically impractical. Overall, the attempt to generate an initial hypothesis about Slit-Robo function in the immune system via expression profiling was not successful.

An alternative bioinformatics approach was taken and Slit-Robo promoters were analysed with the aim of identifying regulatory mechanisms controlling expression of these proteins as this information might reveal functional connections between the Slit-Robo axis and other systems including the immune system. Initial analysis showed that Slit-Robo promoters lack “classical” core elements but contain other hallmark promoter feature – CpG islands. This means that Slit and Robo promoters belong to Type III promoters according to the classification suggested by Lenhard (Lenhard et al, 2012). These results

closely match known information about Slit-Robo as Type III promoters are usually found in developmentally regulated genes, expression of which is precisely coordinated across different cells and tissues.

Further analysis revealed scores of potential transcription factor binding sites, even though results were "filtered" using phylogenetic footprinting and only binding sites conserved across multiple species were considered. As can be expected, many of the identified transcription factors were related to development, neuron growth and differentiation. Some others, like EGR1, ETS1 and IKR, have roles related to the immune system. However, their functions are very general and thus it was impossible to draw specific conclusions about a potential Slit-Robo role. The exception was the transcription factor Foxn1, binding sites for which were detected both in the Slit2 and Slit3 upstream sequence in approximately the same position. Foxn1 has relatively specific and narrow functions within the immune system and because of that further studies were focused on this particular transcription factor.

Foxn1 generally is a transcriptional activator which controls differentiation of thymic epithelial cells so the presence of its binding sites in the Slit2 and Slit3 promoters suggested that TECs may express Slit proteins. This prediction was tested by measuring Slit2 and Slit3 expression levels in the developing embryonic thymus at different stages. The experiment revealed that TECs do express Slit2 and Slit3 mRNA which is downregulated four-fold starting at E13. It is difficult to suggest a straightforward explanation for these data. The observed downregulation of Slit proteins is not necessarily related to Foxn1. Foxn1 primarily is a transcription activator, although it might act as a repressor under certain circumstances (Bazzi et al, 2009). The possibility exists that Foxn1 switches on early Slit2 and/or Slit3 expression, while downregulation at E13 is triggered by other transcription factors. Interestingly, reduced expression levels roughly coincide with the first entry of thymocyte precursors into the thymus (Hollander et al, 2006). It was observed that, during first wave of immigration, leukocytes initially accumulate in thymic periphery and only later move into the thymus itself (Itoi et al, 2001). It is possible that Slit2 and Slit3, expressed by TECs, contribute to initial immigration restriction which is later removed by downregulation of these proteins. Reduction of Slit expression might also be part of the TEC differentiation programme and protein expression is switched off because it is no longer required for cell function. In general, these data confirm Slit2 and Slit3 expression by TECs and show active regulation of their expression during different

developmental stages, suggesting a functional relevance of Slit2 and Slit3 in thymic development.

In order to elucidate the role for Slit2 in thymic development the cellular composition of the embryonic thymus in wild type and Slit2 knockout mice was compared, but no differences were observed. It seems that deletion of Slit2 alone is not sufficient to affect the thymus, so either Slit2 has no function in thymic development or the remaining functional Slit3 gene compensates for it. Unfortunately, Slit3 knockout mice were not available and issues of Slit2-Slit3 redundancy remain unaddressed.

On the other hand, analysis of Slit2 knockout thymus revealed that TECs are not the main population expressing Slit2. The GFP reporter system present in Slit2 knockout animals showed the highest GFP signal in cells with CD45⁻ EpCAM⁻ Ly51⁺ phenotype which are neither thymocytes nor TECs. An identical CD45⁻ EpCAM⁻ Ly51⁺ population is reported in the literature and corresponds to mesenchymal cells (Muller et al, 2008). These pericyte-type cells, also called NC-Mes, cover the entire thymic vasculature and separate TECs and blood vessel-forming endothelial cells (Foster et al, 2008; Muller et al, 2008). NC-Mes have a completely different developmental programme from that of TECs. They originate from Neural Crest, migrate into the thymus during development and are not dependent on Foxn1. Physiological functions of NC-Mes remain somewhat obscure. In other parts of the body pericytes support blood vessels and regulate their permeability. For example, pericytes are a crucial component of the blood-brain barrier. Like brain, thymus also appears to be highly selective for entering and leaving cells and some authors even suggest the existence of a blood-thymus barrier (Kato, 1997; Raviola & Karnovsky, 1972). It is tempting, therefore, to speculate that NC-Mes are part of the "gate keeping" system in thymus. Indeed, recently it was demonstrated that egress of mature leukocytes from thymus is regulated by NC-Mes cells via sphingosine-1-phosphate signalling (Zachariah & Cyster, 2010). It was also shown that NC-Mes regulate cTEC homeostasis via retinoic acid (Sitnik et al, 2012). So it looks like these pericyte-like mesenchymal cells have important and diverse roles in thymus which we are only beginning to uncover.

What functions Slit2 might fulfil within TECs or NC-Mes remains an open question. Given evidence that pericytes control thymocyte emigration from thymus one might speculate that Slit2 contributes to the regulation of migration. On the other hand, it is worth noting that pericytes and smooth muscle cells, from other organs and tissues, also express Slit2 or Slit3 proteins (Marlow et al, 2010), so it is possible that they play a general role in

maintenance or functions of vasculature which is not thymus specific. Even less can be said about Slit2 or Slit3 role in TECs. Two different aspects of possible Foxn1 and Slit2-Slit3 functions in thymus needs to be recognised here - thymic development and adult functions. The possibility exists that Slit2-Slit3 functions in thymus are purely developmental. These proteins might be involved in intensive TEC precursor migration which predates formation of an anatomically distinct thymus (E10-E11), later expression simply being a remnant of this developmental history (Hollander et al, 2006). The observed Slit2 and Slit3 downregulation at E13 supports this idea. Later development and function of embryonic thymus are also considerably different from that of the fully developed organ. For example, the first waves of leukocytes enter the developing thymus before functional blood vessels are formed, while the mature organ is seeded via blood vessels located at the cortico-medullary junction (Lind et al, 2001; Rodewald, 2008). The phenotype of thymocyte progenitors seeding thymus during development and in adult organism also might be different (Luc et al, 2012). So even if Slit2-Slit3 expressed by TECs are related to leukocyte traffic regulation these functions might be restricted to embryonic stages.

The biggest issue for future research in this area is possible redundancy between Slit2 and Slit3 and ideally embryonic thymus composition needs to be reassessed using double Slit2-Slit3 knockout. This animal model is compatible with embryonic studies thus flow cytometry and immunohistochemistry could be employed to evaluate mutation effects on thymic development and early function. On the other hand, perinatal lethality of Slit2-/- Slit3-/- animals prevents studies of the adult animal and additional “tricks” might be necessary in order to address possible Slit roles in them. Marlow and colleagues, for example, successfully used a transplantation technique where embryonic Slit2-/- Slit3-/- mammary gland tissues were transplanted into Slit+/+ animals, allowing their analysis in the background of an fully developed animal (Marlow et al, 2010). Similarly, a technique which allows transplantation of fetal thymus under the kidney capsule of an adult animal might be also of great use (Jenkinson et al, 2007). An alternative approach is to generate conditional Slit2 knockout animals, however this animal model has not been reported in the literature so far. Overall, Slit-Robo biology perfectly exemplifies that incredible level of integration and connectivity inherent to biological systems, making its studies technically and methodologically demanding. Nevertheless, it is a worthy challenge as it addresses the deepest principles of development and functions of multicellular organisms.

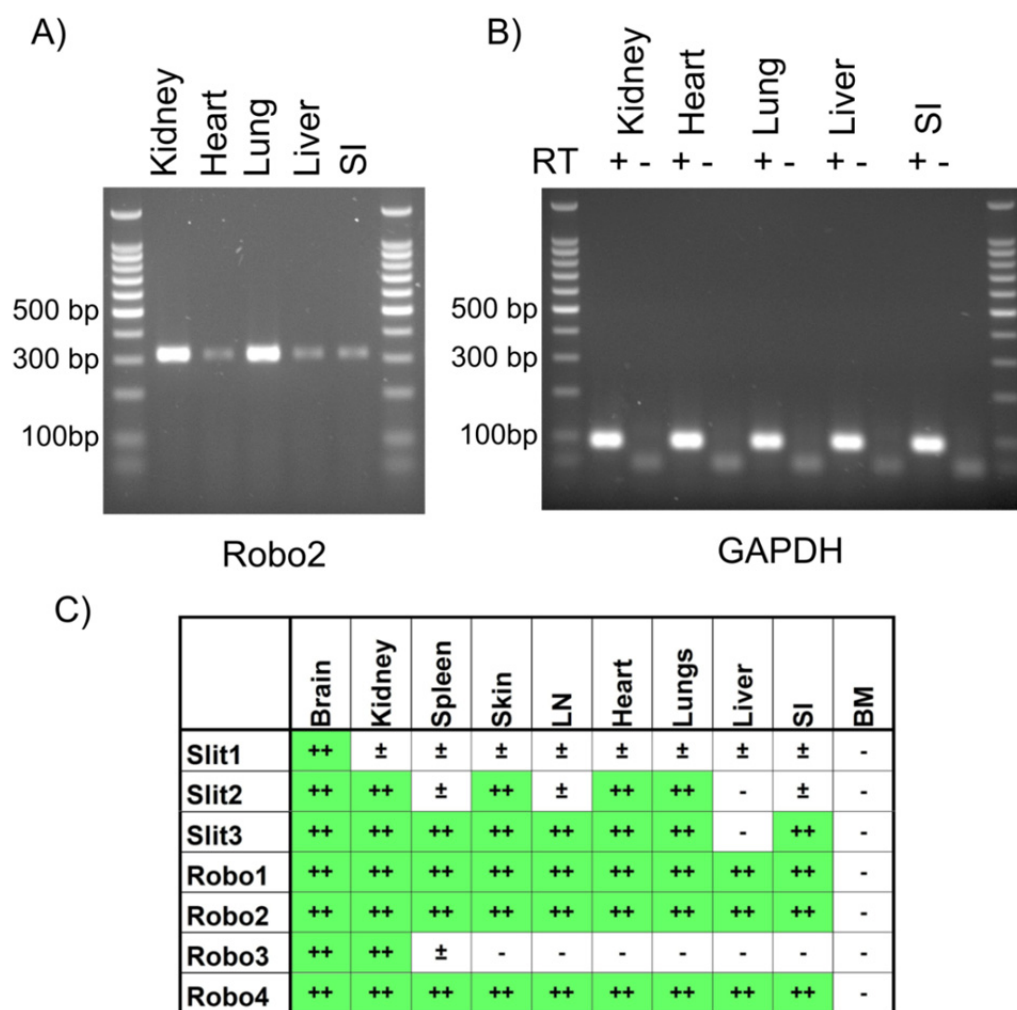

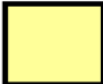


Figure 4.1 Slit-Robo expression in mouse organs and tissues

Expression of Slit and Robo orthologues in mouse tissues was assessed using RT-PCR. Representative gels show PCR with cDNA from various tissues with primers for Robo2 (A) and GAPDH (B) genes. GAPDH detection was used as a positive control (RT+) or control for genomic DNA contamination (RT-). General expression profile was determined from two female C57BL/6 female mice (C). LN - lymph nodes, SI - small intestine, BM - bone marrow. ++ - detected, ± - traces detected, - -not detected.

	Slit1	Slit2	Slit3	Robo1	Robo2	Robo3	Robo4
HEK293 (Neuron like)	Strong expression	Strong expression	Strong expression	Strong expression	Strong expression	Not detected	Not detected
Raji (B-cell like)	Traces	Not detected	Not detected	Not detected	Not detected	Not detected	Not detected
CA46 (B-cell like)	Traces	Not detected	Not detected	Not detected	Not detected	Not detected	Not detected
ACVA-1 (B-cell like)	Traces	Strong expression	Not detected	Strong expression	Not detected	Not detected	Traces
HUT 78 (T-cell like)	Strong expression	Not detected	Not detected	Traces	Not detected	Not detected	Not detected
JURKAT (T-cell like)	Strong expression	Traces	Not detected	Not detected	Not detected	Traces	Not detected
K562 (Myeloid line)	Not detected	Strong expression	Not detected	Not detected	Traces	Not detected	Not detected
THP-1 (Monocytes)	Strong expression	Traces	Not detected	Strong expression	Not detected	Not detected	Not detected
MEG-01 (Megakaryocyte)	Not detected	Not detected	Not detected	Strong expression	Strong expression	Not detected	Not detected
HMC-1 (Mast cells like)	Traces	Not detected	Not detected	Strong expression	Not detected	Not detected	Not detected
3T3 (Fibroblast)	Not detected	Strong expression	Traces	Not detected	Traces	Traces	Not detected
B16(Melanoma)	Not detected	Strong expression	Not detected	Strong expression	Traces	Traces	Not detected
BeWo (Trophoblast)	Not detected	Strong expression	Not detected	Strong expression	Not detected	Not detected	Not detected

 Strong expression

 Traces


 Not detected

Figure 4.2 Slit-Robo expression in cell lines

Assessment of Slit and Robo expression in various cell lines by RT-PCR. All cell lines are of human origin except 3T3 and B16 which originate from mice.

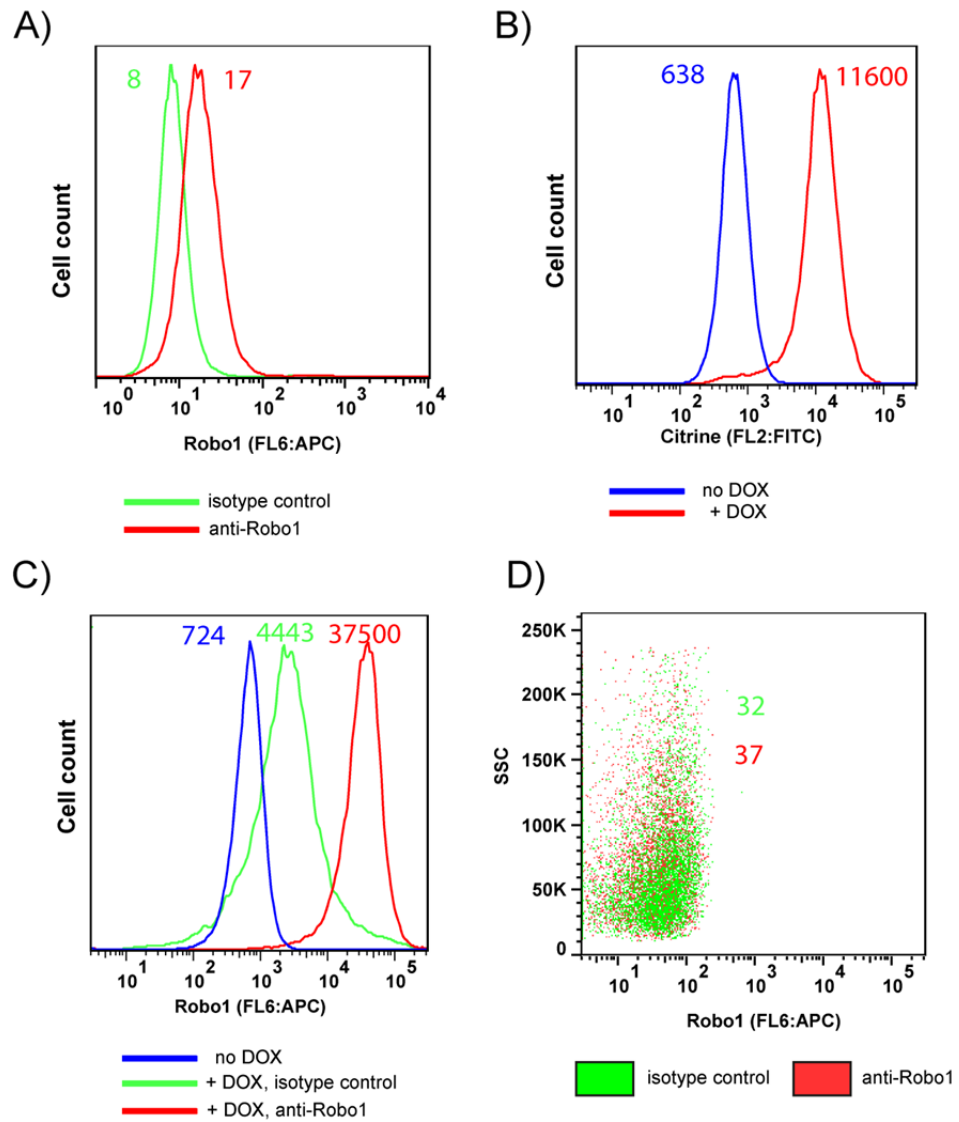


Figure 4.3 Robo1 expression assessment by flow cytometry

THP-1 cells were labelled with biotin conjugated anti-Robo1 antibody (R&D Systems) or biotin conjugated isotype control, stained with avidin-APC conjugate and analysed using flow cytometry (A). Alternatively, expression of myc-Robo1-CIT construct was induced in HEK 293 Flp-In cells by incubating them with 50 ng/ml of doxycycline overnight and myc-Robo1-CIT expression was assessed either directly measuring Citrine fluorescence (B) or labelling cells with biotin conjugated anti-Robo1 antibody and avidin-APC conjugate. Doxycycline induced HEK 293 Flp-In cells labelled with isotype control or non-induced and unstained cells served as negative controls (C). Human PBMC were labelled with biotin conjugated anti-Robo1 antibody or biotin conjugated isotype control, stained with avidin-APC conjugate and analysed using flow cytometry (D). Number indicates median fluorescence intensity of populations. Images B and C are single independent experiments, images A and D are representative of two independent experiments.

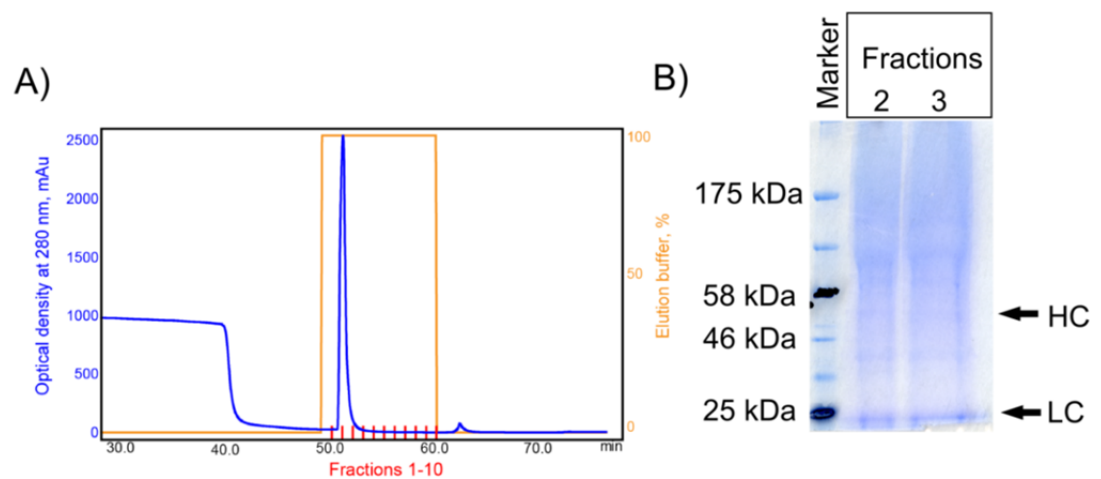


Figure 4.4 Purification of Robo1 (DSHB) antibody

HiTrap IgM Purification HP Column (GE Healthcare) was used to purify Robo1 antibody from hybridoma supernatant (A). Fractions 2 and 3 were selected based on UV adsorbtion and analyzed using SDS-PAGE (B). HC and LC marks expected positions of heavy and light chain of purified antibody.

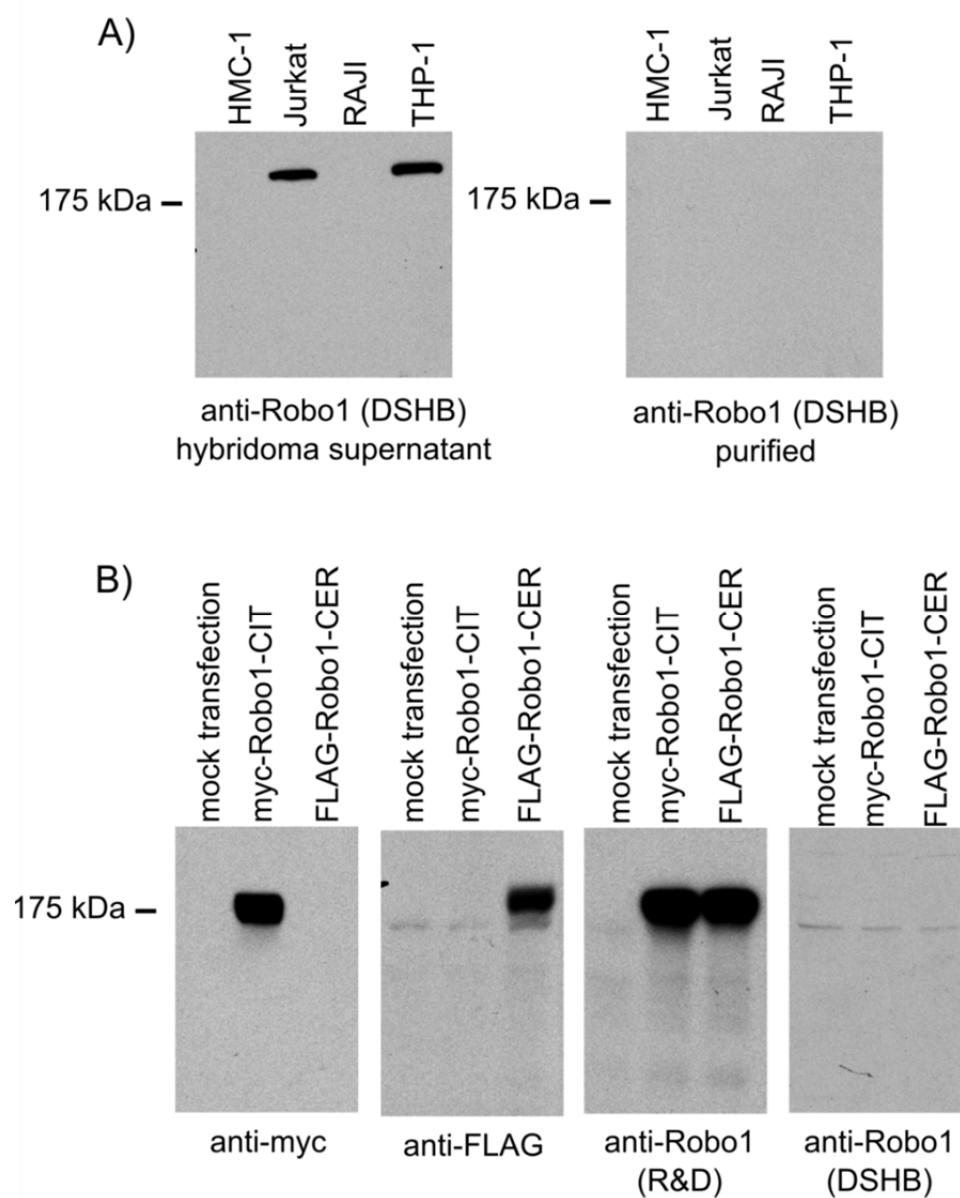


Figure 4.5 Verification of Robo1 (DSHB) antibody function

Anti-Robo1 antibody from Developmental Studies Hybridoma Bank was tested by immunoblotting lysates of hematopoietic cells (A) or HEK 293 Flp-In T-REX cells expressing myc-Robo1-CIT or FLAG-Robo1-CER constructs (B).

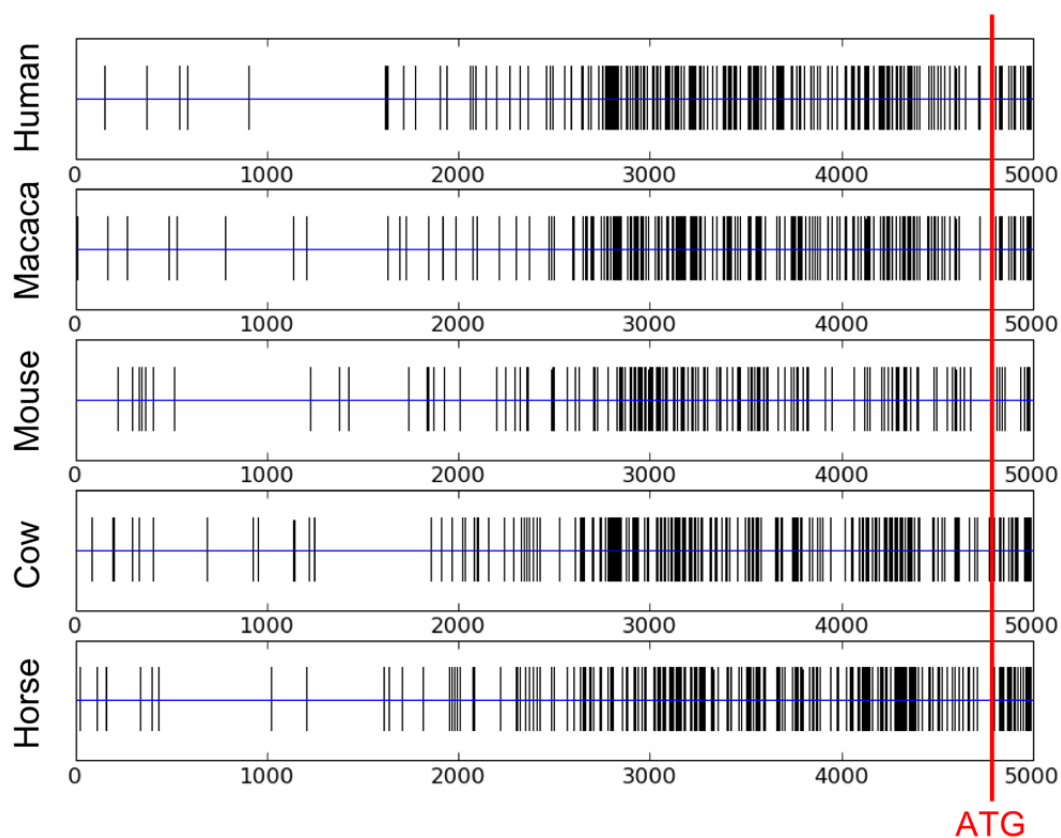


Figure 4.6 CpG islands in the putative *Slit2* promoter

Upstream DNA sequences of *Slit2* orthologues from different species were analyzed for CpG content. Each vertical tick corresponds to a CpG dinucleotide. ATG marks start of the open reading frame.

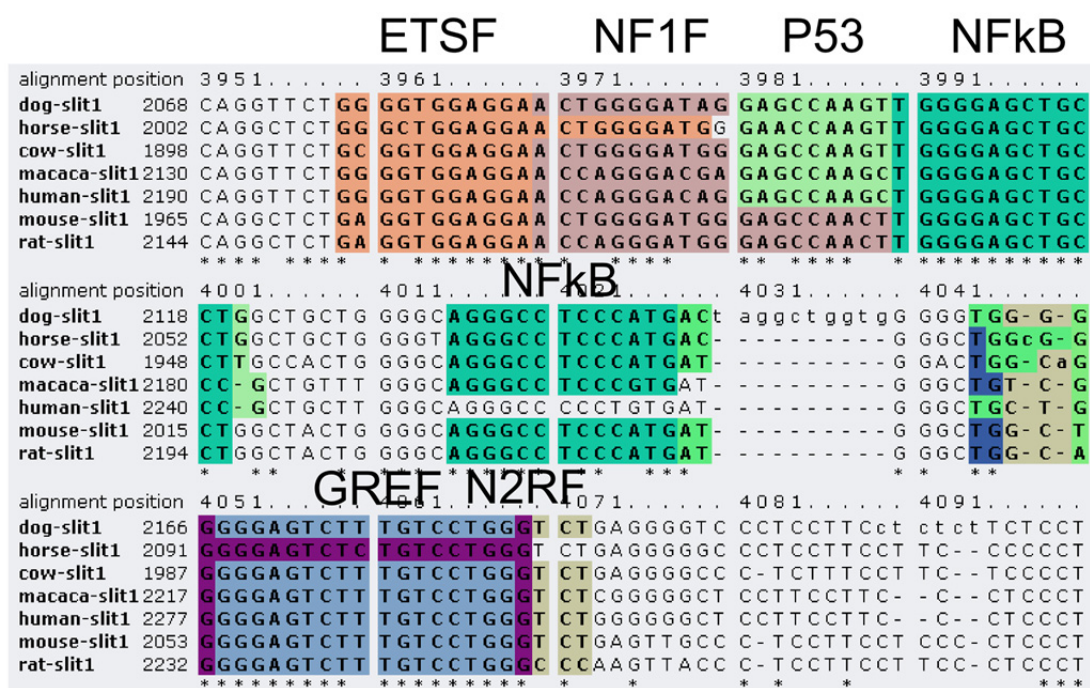


Figure 4.7 Phylogenetic footprinting

Fragment of upstream sequence alignment for Slit1 gene exemplifying output of DiaAlign software. Different colours mark identified conserved transcription factor binding sites.

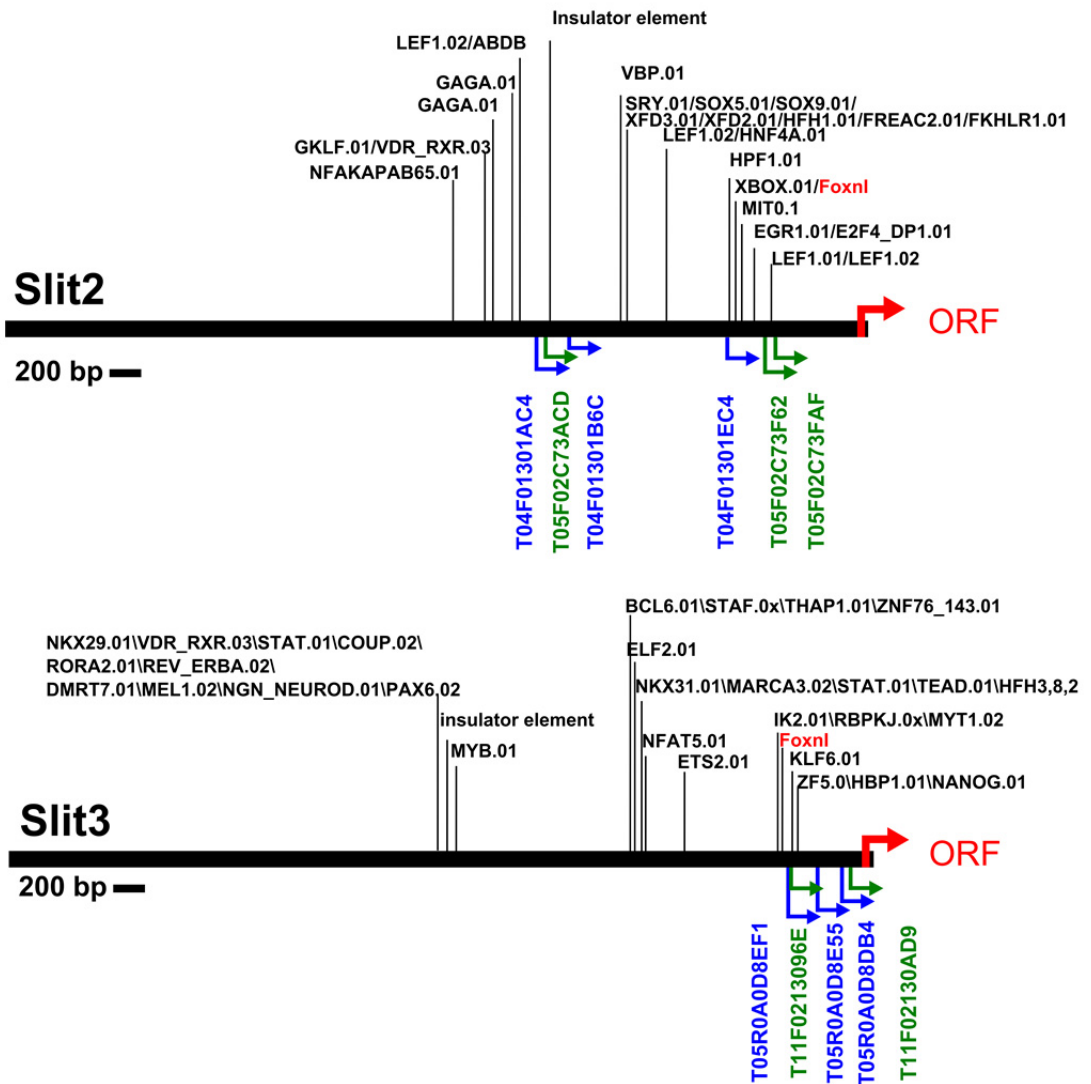


Figure 4.8 Putative Foxn1 binding site

Putative conserved transcription factor binding sites in upstream sequences of *Slit2* and *Slit3* mammalian genes. Foxn1 is marked in red. Transcription start sites listed in a CAGE database are marked with green (mouse) and blue (human) arrows. A number next to the arrow is a tag cluster identifier within the CAGE database.

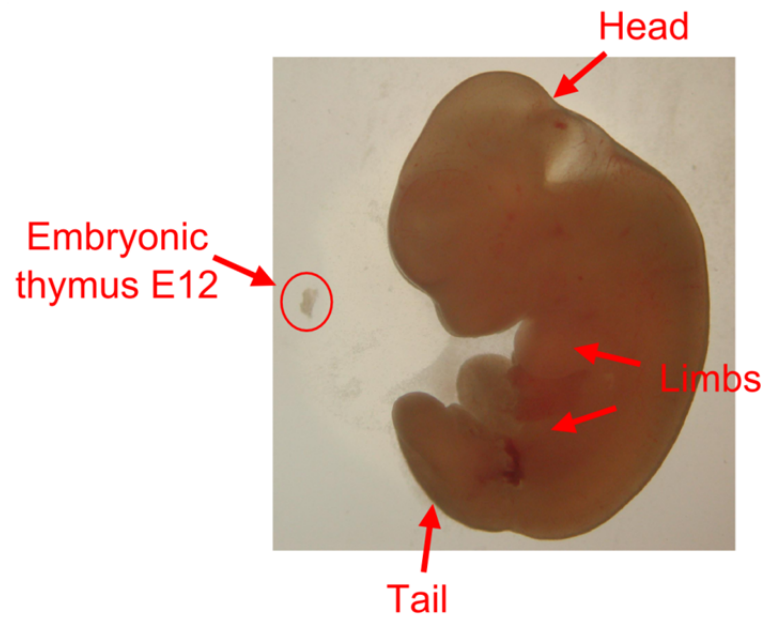


Figure 4.9 Dissection of embryonic thymus

E12 mouse embryo with dissected thymus. Image contributed by Dr. A. White.

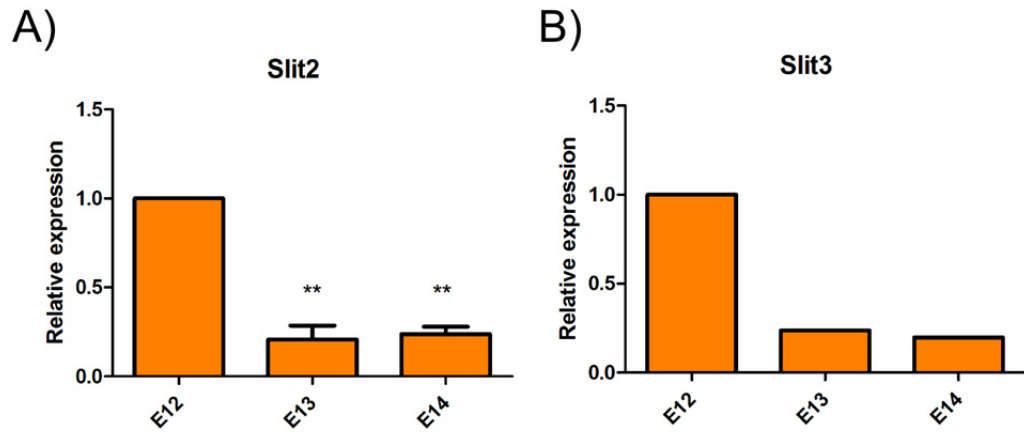


Figure 4.10 Slit2 and Slit3 expression in TECs during thymic development

Relative expression levels of Slit2 (A) and Slit3 (B) in TECs isolated from embryonic thymus at different developmental stages. For Slit2, results are represented as mean \pm SEM, n=2. Slit3 data were acquired from single independent experiment. ** p<0.01 as determined by one way ANOVA with Tukey's post test. Cell isolation was performed by Dr. A. White

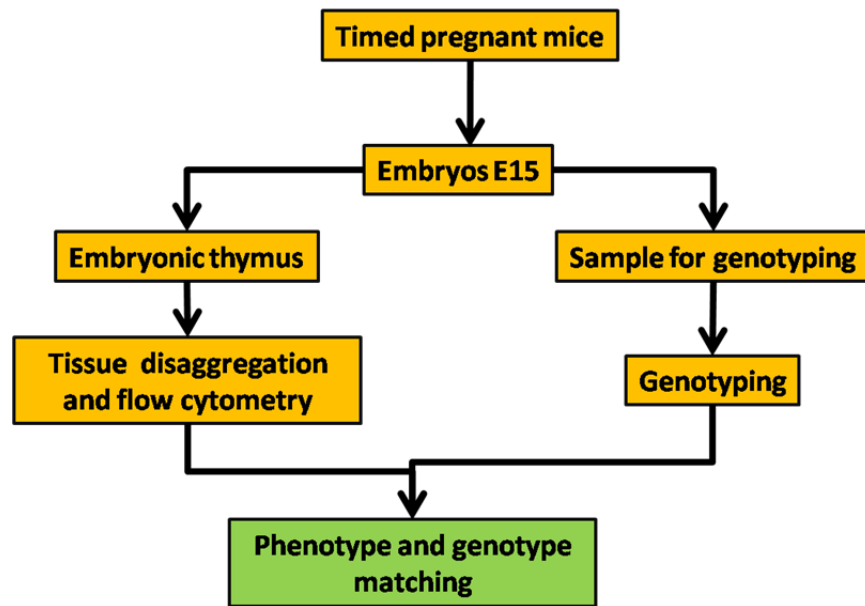


Figure 4.11 Embryonic thymus analysis in Slit2 knockout mice

Diagram illustrating the workflow of embryonic thymus analysis in Slit2 knockout mice. Stage E15 embryos were dissected and decapitated. Embryonic thymus and separate tissue sample for genotyping were taken from each individual embryo. The embryonic thymi were individually disaggregated into a single cell suspension and analysed for cellular composition using flow cytometry. In parallel, each embryo was genotyped using PCR. Finally, flow cytometry and genotyping data were combined and analysed together

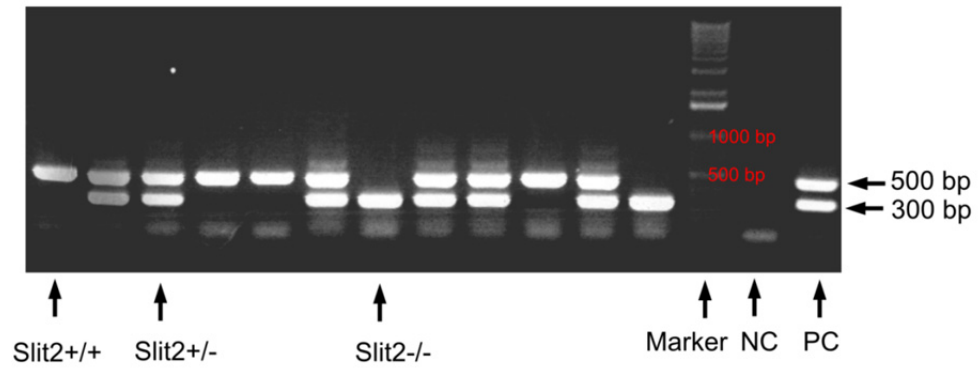


Figure 4.12 Genotyping of Slit2 knockout mouse embryos

Representative results of Slit2 knockout mouse genotyping. Each line represents genotype of different embryo. NC and PC stands for negative control (no template) and positive control (sample of an adult animal tissues) respectively.

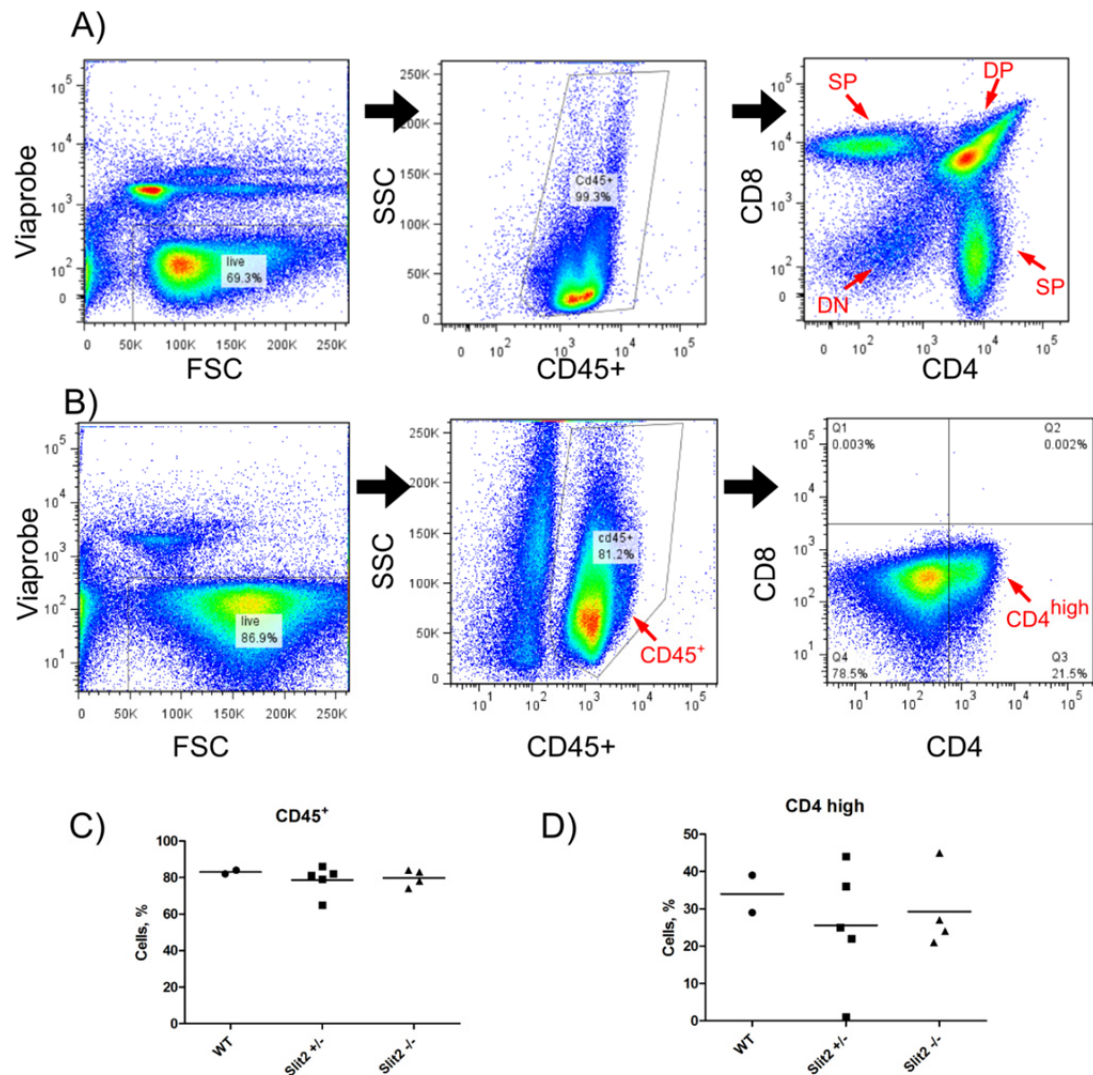


Figure 4.13 Comparison of thymocyte composition in wild type and Slit2 knockout embryos

Thymocytes from adult animal (A) or disaggregated embryonic (E15) thymi (B) were analyzed using flow cytometry. Live cells were selected based on viability dye exclusion, CD45 positive cells were gated and analyzed for CD8 and CD4 expression. CD45 and CD4 positive populations were quantified as a fraction of the parent population and compared according to genotype (C and D). Each dot represents the value for an individual embryo. No statistically significant differences were detected by one way ANOVA. SP stands for single positive, DP – double positive, DN – double negative.

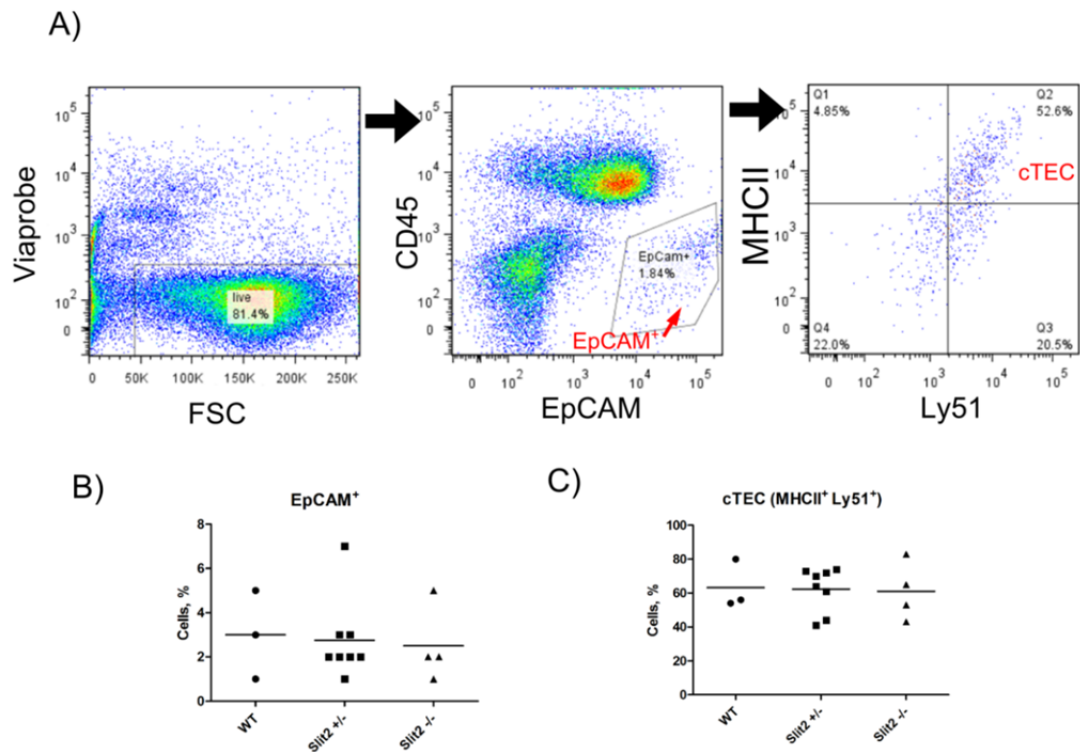


Figure 4.14 Comparison of TEC composition in wild type and Slit2 knockout embryos

TEC composition in embryonic (E15) thymi was analysed using flow cytometry. Live cells were selected based on viability dye exclusion, EpCAM positive cells were gated and analyzed for Ly51 and MHC II expression (A). EpCAM⁺ and Ly51⁺MHC II⁺ population were quantified as a fraction of the parent population and compared according to genotype (B and C). Each dot represents the value for an individual embryo. No statistically significant differences were detected by one way ANOVA.

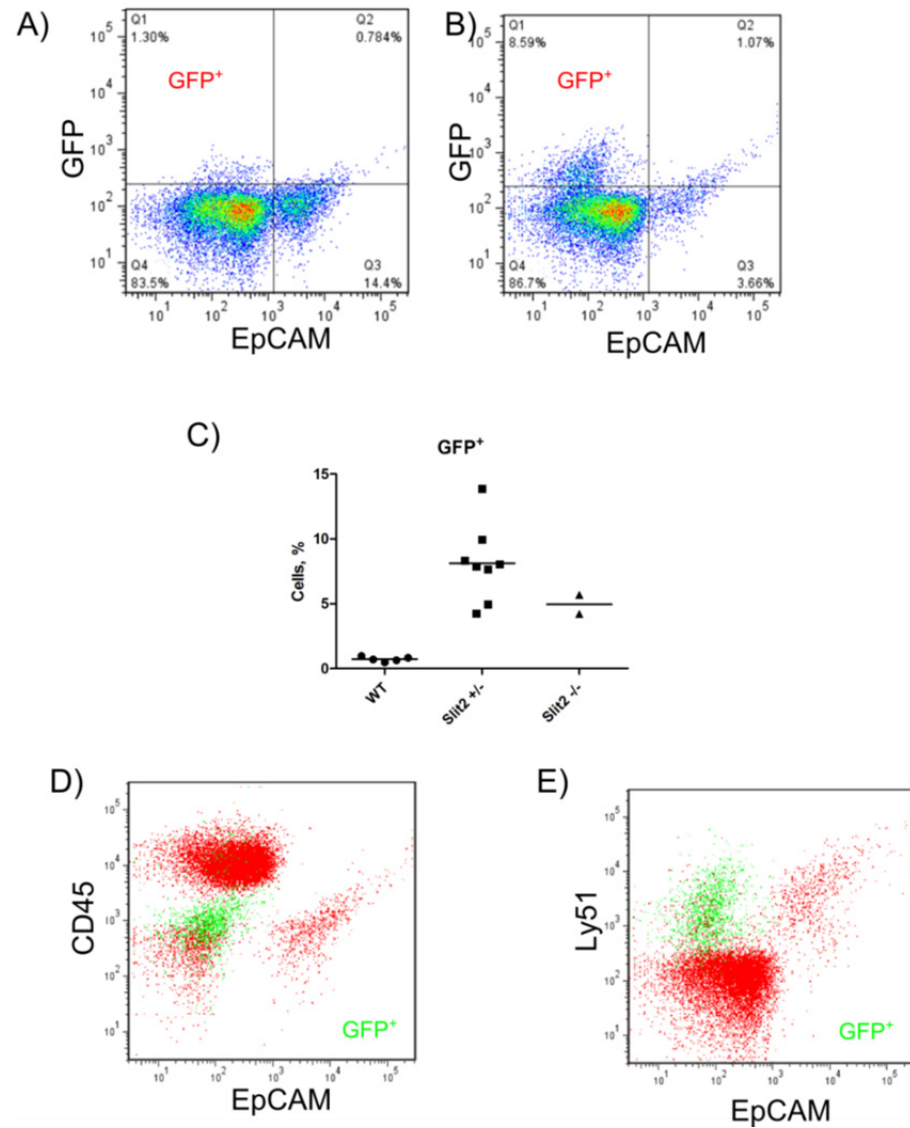


Figure 4.15 Identification of GFP⁺ cell population in embryonic thymus

Size of the putative GFP⁺ population of embryonic thymus cells varied greatly between individual E15 embryos (A and B). This variation had strong correlation with genotype of embryo ($p=0.004$ as determined by one way ANOVA) confirming that it is caused by endogenous expression of GFP in knockout animals (C). Further analysis of marker expression showed that GFP⁺ cells have a CD45⁻ EpCAM⁺Ly51⁺ phenotype (D and E).

5 Final discussions

The aim of this study was to investigate two different aspects of the Slit-Robo signalling axis – its transmembrane signalling mechanism and its functional role in the immune system. These two topics have little in common in terms of standard classification and subdivision of life sciences, however, arbitrary boundaries created by the need to organise knowledge should not limit understanding of a subject. It is especially true for Slit-Robo proteins which are perfect showcases of complex, hierarchical and seamlessly integrated organisation of biological systems. And as it happens, genuine connections between Robo transmembrane signalling mechanism and physiological functions, including that of the immune system, can be envisaged.

Type I receptors containing a single transmembrane helix are incapable of transmitting signal across the membrane within one receptor molecule and therefore they need to recruit the help of other proteins. Consequently, many type I receptors associate into homo or heterooligomers, formation or dissociation of which can be controlled by ligand as a way to transfer signal across the membrane. Compelling pilot evidence had indicated that Robo receptors use a similar mechanism, however experiments described in Chapter 3 strongly contradicts this model. No Slit2 induced changes in Robo1 oligomeric state were observed using FRET imaging or TR-FRET assays even though these experiments clearly show that Robo1 exists as an oligomer *in vivo*. So how does Robo1 transmit signals across the membrane? As discussed in section 3.7, conceptually it is possible to envision several alternative mechanisms. Robo1 might form stable protein complexes which react to Slit2 binding by changes in conformation but not in oligomerisation. Alternately, or even in cooperation with conformational changes, Slit2 binding might induce Robo proteolysis which sheds the C-terminal cytoplasmic tail releasing its signalling capabilities. An even better understanding of transmembrane Robo1 signalling might be gained if one considers it in the context of biological function. The best described, and probably evolutionary most conserved, Slit-Robo role is axon guidance during development. Axon wiring is led by the so called growth cone – a specialised sprout at the tip of the axon which pushes forward using adhesion (Vitriol & Zheng, 2012). Published data show that at least in *Drosophila* Robo receptors are actively and specifically delivered to the growth cones and largely remain in that neuronal compartment (Kidd et al, 1998). Many other receptors responsible for neuronal guidance are present here as well and as the growth cone squeezes through the tissues it simultaneously encounters many different guidance cues which sometimes might

bear opposite directives. Therefore growth cones have a remarkable signal integration capability where final response is determined by amalgamation of many different instructions (Vitriol & Zheng, 2012). Coincidentally, the Slit-Robo signalling axis shows a strong dependence on cellular context not only in neurons but in other cells as well (see section 1.6). Other aspect of growth cone worth noticing is its reliance on adhesion, short range guidance cues and juxtacrine regulation (Lowery & Van Vactor, 2009). At least two major signalling axes are responsible for axon guidance, Eph kinases/ephrin and Semaphorin/Plexin, are juxtacrine in nature i.e. ligands are tethered to the membrane of another cell and physical contact between two cells is necessary for ligand-receptor interactions. Slits are secreted proteins but their size and affinity for heparan sulphate most likely severely restricts their diffusion and Robo receptors encounter most of the Slit molecules embedded into extracellular matrix or adsorbed on the cellular surfaces. In other words Slits might be considered as solid phase ligands acting as haptotactic guidance cues. Moreover, Robo4 recently was shown to serve as a ligand for the UNC5B receptor and while the authors failed to detect Robo4 downstream signalling in response to UNC5B binding, it does not completely exclude the possibility that this signalling axis is bidirectional and Robo4 can be activated by UNC5B receptor under different cellular context (Koch et al, 2011). Taking all these circumstances into account it is reasonable to argue that the Slit-Robo signalling axis is largely juxtacrine in its nature as well. This arrangement might have important implications for transmembrane signalling as it is no longer a matter of two interacting molecules, but that of two interacting surfaces tethered together by ligand-receptor interactions with mechanical tension and shear forces coming in to the play. This theoretical consideration is supported by recent data showing that signalling of EphA2 kinase is affected by mechanical force (Salaita et al, 2010). Interestingly, EphA2 forms clusters consisting of hundreds of molecules, and mechanical force seems to affect their composition and cytoskeleton-based transport which in turn modulates actual effects of downstream signalling (Salaita et al, 2010). This mechanism reminds us of that of T cell receptor activation, another juxtacrine signalling system where TCR is activated by interactions with antigen peptide presented *in trans* by MHC complex on antigen-presenting cells triggering formation of complex macromolecular assemblies, the size and organisation of which controls downstream signalling (van der Merwe & Dushek, 2011). Most interestingly, an increasing number of studies indicate that biomechanical force may trigger and modulate TCR activation (Allard et al, 2012; Husson et al, 2011; Li et al, 2010). Yet another group of receptors interacting with "solid state" ligands are integrins whose ability to form clusters and their sensitivity to biomechanical

force are now well established (Arnaout et al, 2005). So, an interesting pattern emerges from this analysis as it appears that many juxtacrine systems share numerous common properties – receptor cluster formation, sensitivity to mechanical force and close functional cooperation with the cytoskeleton. So called "cis inhibition" potentially is another emerging trait of juxtacrine signalling. It describes the situation when ligand presented *in cis* (on the same cell surface) inhibits effects of the same ligand presented *in trans* (on the surface of the other cell). This peculiar phenomenon was observed for the Notch/DSL, Eph/ephrin and Semaphorin/Plexin juxtacrine signalling axes (Yaron & Sprinzak, 2012). Given all these coincidences it is tempting to speculate that juxtacrine signalling systems might share a common transmembrane signalling mechanism based on interplay between the cell-cell mechanical interactions, receptor clustering and cytoskeleton. Obviously, this idea is highly speculative and much more work needs to be done before it gains any credibility. Nevertheless, in its light many "eccentricities" of Slit-Robo signalling system become somewhat less puzzling. Contradictive and highly variable effects of recombinant Slit in *in vitro* models might be related to the fact that Slit instead of being a "solid state ligand" is presented as a soluble molecule. Cis inhibition is another possible explanation for highly variable *in vitro* assays, as recombinant Slit is likely to adsorb on the surface of assayed cells which theoretically might lead to inhibition of signal *in trans*. Similarly, a long lasting debate about existence of Slit2-Robo4 signalling, where functional assays show signals being transmitted by Slit2-Robo4 axis, but evidence of direct interactions are vague and elusive, might also benefit from mechanistical considerations outlined above.

Interestingly, adhesive and juxtacrine Slit2-Robo4 properties appear to be utilised by hematopoietic stem cells in bone marrow. Smith-Berdan and colleagues observed that Robo4 knockout caused increased efflux of hematopoietic stem cells into the circulation. Surprisingly, neither Robo4 deletion, nor treatment with soluble Slit2 caused observable changes in cell proliferation or *in vitro* migration capabilities of hematopoietic cells, so authors argue that Slit2 expressed by bone marrow stromal cells acts as an adhesive cue for Robo4 expressing hematopoietic cells (Smith-Berdan et al, 2011). Studies described in Chapter 4 indicate that Slit2 and Slit3 are expressed by TECs and that Foxn1 likely contributes to the regulation of these genes. Both bone marrow and thymus stroma have similar roles – formation of niches for hematopoietic cells. It is tempting to speculate therefore that Slit-Robo thymic niches are also defined by Slit2-Robo4 interactions. On the other hand Robo4 is downregulated after hematopoietic stem cells leave the bone marrow (Smith-Berdan et al, 2011). Moreover, TECs are not the only source of Slit2 in thymus as

it is also expressed by pericytes surrounding the vasculature, so these similarities might be only superficial. Nevertheless, these data echo previous conclusions, that Slit-Robo is primarily a juxtacrine signalling axis and one needs to think about two interacting cells or cell - ECM interactions when considering Slit-Robo functions within the immune system.

References

- Alieva NO, Konzen KA, Field SF, Meleshkevitch EA, Hunt ME, Beltran-Ramirez V, Miller DJ, Wiedenmann J, Salih A, Matz MV (2008) Diversity and evolution of coral fluorescent proteins. *PLoS One* **3**: e2680
- Allard JF, Dushek O, Coombs D, van der Merwe PA (2012) Mechanical modulation of receptor-ligand interactions at cell-cell interfaces. *Biophys J* **102**: 1265-1273
- Andrews W, Barber M, Hernandez-Miranda LR, Xian J, Rakic S, Sundaresan V, Rabbitts TH, Pannell R, Rabbitts P, Thompson H, Erskine L, Murakami F, Parnavelas JG (2008) The role of Slit-Robo signaling in the generation, migration and morphological differentiation of cortical interneurons. *Dev Biol* **313**: 648-658
- Andrews W, Liapi A, Plachez C, Camurri L, Zhang J, Mori S, Murakami F, Parnavelas JG, Sundaresan V, Richards LJ (2006) Robo1 regulates the development of major axon tracts and interneuron migration in the forebrain. *Development* **133**: 2243-2252
- Andrews WD, Barber M, Parnavelas JG (2007) Slit-Robo interactions during cortical development. *J Anat* **211**: 188-198
- Anselmo MA, Dalvin S, Prodhan P, Komatsuzaki K, Aidlen JT, Schnitzer JJ, Wu JY, Kinane TB (2003) Slit and robo: expression patterns in lung development. *Gene Expr Patterns* **3**: 13-19
- Arnaout MA, Mahalingam B, Xiong JP (2005) Integrin structure, allostery, and bidirectional signaling. *Annu Rev Cell Dev Biol* **21**: 381-410
- Ba-Charvet KTN, Brose K, Ma L, Wang KH, Marillat V, Sotelo C, Tessier-Lavigne M, Chédotal A (2001) Diversity and specificity of actions of Slit2 proteolytic fragments in axon guidance. *J Neurosci* **21**: 4281-4289
- Banerjee S, Blauth K, Peters K, Rogers SL, Fanning AS, Bhat MA (2010) Drosophila neurexin IV interacts with Roundabout and is required for repulsive midline axon guidance. *J Neurosci* **30**: 5653-5667
- Banfi S, Borsani G, Rossi E, Bernard L, Guffanti A, Rubboli F, Marchitelli A, Giglio S, Coluccia E, Zollo M, Zuffardi O, Ballabio A (1996) Identification and mapping of human cDNAs homologous to Drosophila mutant genes through EST database searching. *Nat Genet* **13**: 167-174
- Bashaw GJ, Goodman CS (1999) Chimeric axon guidance receptors: the cytoplasmic domains of slit and netrin receptors specify attraction versus repulsion. *Cell* **97**: 917-926
- Bashaw GJ, Kidd T, Murray D, Pawson T, Goodman CS (2000) Repulsive axon guidance: Abelson and Enabled play opposing roles downstream of the roundabout receptor. *Cell* **101**: 703-715
- Bauer K, Dowejko A, Bosserhoff A-K, Reichert TE, Bauer R (2011) Slit-2 facilitates interaction of P-cadherin with Robo-3 and inhibits cell migration in an oral squamous cell carcinoma cell line. *Carcinogenesis* **32**: 935-943

- Baumgartner S, Littleton JT, Broadie K, Bhat MA, Harbecke R, Lengyel JA, Chiquet-Ehrismann R, Prokop A, Bellen HJ (1996) A *Drosophila* neurexin is required for septate junction and blood-nerve barrier formation and function. *Cell* **87**: 1059-1068
- Bazin H, Trinquet E, Mathis G (2002) Time resolved amplification of cryptate emission: a versatile technology to trace biomolecular interactions. *J Biotechnol* **82**: 233-250
- Bazzi H, Demehri S, Potter CS, Barber AG, Awgulewitsch A, Kopan R, Christiano AM (2009) Desmoglein 4 is regulated by transcription factors implicated in hair shaft differentiation. *Differentiation* **78**: 292-300
- Bear JE, Gertler FB (2009) Ena/VASP: towards resolving a pointed controversy at the barbed end. *J Cell Sci* **122**: 1947-1953
- Bedell VM, Yeo S-Y, Park KW, Chung J, Seth P, Shivalingappa V, Zhao J, Obara T, Sukhatme VP, Drummond IA, Li DY, Ramchandran R (2005) roundabout4 is essential for angiogenesis in vivo. *Proc Natl Acad Sci U S A* **102**: 6373-6378
- Berney C, Danuser G (2003) FRET or no FRET: a quantitative comparison. *Biophys J* **84**: 3992-4010
- Berthouze M, Venkataramanan V, Li Y, Shenoy SK (2009) The deubiquitinases USP33 and USP20 coordinate beta2 adrenergic receptor recycling and resensitization. *EMBO J* **28**: 1684-1696
- Bleul CC, Boehm T (2001) Laser capture microdissection-based expression profiling identifies PD1-ligand as a target of the nude locus gene product. *Eur J Immunol* **31**: 2497-2503
- Brantley-Sieders DM, Dunaway CM, Rao M, Short S, Hwang Y, Gao Y, Li D, Jiang A, Shyr Y, Wu JY, Chen J (2011) Angiocrine factors modulate tumor proliferation and motility through EphA2 repression of Slit2 tumor suppressor function in endothelium. *Cancer Res* **71**: 976-987
- Brierley DJ, Blanc E, Reddy OV, Vijayraghavan K, Williams DW (2009) Dendritic targeting in the leg neuropil of *Drosophila*: the role of midline signalling molecules in generating a myotopic map. *PLoS Biol* **7**: e1000199
- Brose K, Bland KS, Wang KH, Arnott D, Henzel W, Goodman CS, Tessier-Lavigne M, Kidd T (1999) Slit proteins bind Robo receptors and have an evolutionarily conserved role in repulsive axon guidance. *Cell* **96**: 795-806
- Brou C, Logeat F, Gupta N, Bessia C, LeBail O, Doedens JR, Cumano A, Roux P, Black RA, Israel A (2000) A novel proteolytic cleavage involved in Notch signaling: the role of the disintegrin-metalloprotease TACE. *Mol Cell* **5**: 207-216
- Butler JM, Kobayashi H, Rafii S (2010) Instructive role of the vascular niche in promoting tumour growth and tissue repair by angiocrine factors. *Nat Rev Cancer* **10**: 138-146
- Camurri L, Mambetisaeva E, Davies D, Parnavelas J, Sundaresan V, Andrews W (2005) Evidence for the existence of two Robo3 isoforms with divergent biochemical properties. *Mol Cell Neurosci* **30**: 485-493
- Carlson HJ, Campbell RE (2009) Genetically encoded FRET-based biosensors for multiparameter fluorescence imaging. *Curr Opin Biotechnol* **20**: 19-27

- Cartharius K, Frech K, Grote K, Klocke B, Haltmeier M, Klingenhoff A, Frisch M, Bayerlein M, Werner T (2005) MatInspector and beyond: promoter analysis based on transcription factor binding sites. *Bioinformatics* **21**: 2933-2942
- Chanana B, Steigemann P, Jäckle H, Vorbrüggen G (2009) Reception of Slit requires only the chondroitin-sulphate-modified extracellular domain of Syndecan at the target cell surface. *Proc Natl Acad Sci U S A* **106**: 11984-11988
- Chang CW, Sud D, Mycek MA (2007) Fluorescence lifetime imaging microscopy. *Methods Cell Biol* **81**: 495-524
- Chen B, Blair DG, Plisov S, Vasiliev G, Perantoni AO, Chen Q, Athanasiou M, Wu JY, Oppenheim JJ, Yang D (2004) Cutting edge: bone morphogenetic protein antagonists Dm/Gremlin and Dan interact with Slits and act as negative regulators of monocyte chemotaxis. *J Immunol* **173**: 5914-5917
- Chen H, Puhl HL, 3rd, Koushik SV, Vogel SS, Ikeda SR (2006) Measurement of FRET efficiency and ratio of donor to acceptor concentration in living cells. *Biophys J* **91**: L39-41
- Chen L, Xiao S, Manley NR (2009) Foxn1 is required to maintain the postnatal thymic microenvironment in a dosage-sensitive manner. *Blood* **113**: 567-574
- Chen Z, Gore BB, Long H, Ma L, Tessier-Lavigne M (2008) Alternative splicing of the Robo3 axon guidance receptor governs the midline switch from attraction to repulsion. *Neuron* **58**: 325-332
- Cheng L, Guo J, Sun L, Fu J, Barnes PF, Metzger D, Chambon P, Oshima RG, Amagai T, Su DM (2010) Postnatal tissue-specific disruption of transcription factor FoxN1 triggers acute thymic atrophy. *J Biol Chem* **285**: 5836-5847
- Cho JH, Lépine M, Andrews W, Parnavelas J, Cloutier J-F (2007) Requirement for Slit-1 and Robo-2 in zonal segregation of olfactory sensory neuron axons in the main olfactory bulb. *J Neurosci* **27**: 9094-9104
- Cho JH, Prince JEA, Cloutier J-F (2009) Axon guidance events in the wiring of the mammalian olfactory system. *Mol Neurobiol* **39**: 1-9
- Clark K, Hammond E, Rabbitts P (2002) Temporal and spatial expression of two isoforms of the Dutt1/Robo1 gene in mouse development. *FEBS Lett* **523**: 12-16
- Clegg RM (1995) Fluorescence resonance energy transfer. *Curr Opin Biotechnol* **6**: 103-110
- Coleman HA, Labrador J-P, Chance RK, Bashaw GJ (2010) The Adam family metalloprotease Kuzbanian regulates the cleavage of the roundabout receptor to control axon repulsion at the midline. *Development* **137**: 2417-2426
- Dai CF, Jiang YZ, Li Y, Wang K, Liu PS, Patankar MS, Zheng J (2011) Expression and roles of Slit/Robo in human ovarian cancer. *Histochem Cell Biol* **135**: 475-485
- Dallol A, Forgacs E, Martinez A, Sekido Y, Walker R, Kishida T, Rabbitts P, Maher ER, Minna JD, Latif F (2002) Tumour specific promoter region methylation of the human homologue of the Drosophila Roundabout gene DUTT1 (ROBO1) in human cancers. *Oncogene* **21**: 3020-3028

- Dallol A, Krex D, Hesson L, Eng C, Maher ER, Latif F (2003a) Frequent epigenetic inactivation of the SLIT2 gene in gliomas. *Oncogene* **22**: 4611-4616
- Dallol A, Morton D, Maher ER, Latif F (2003b) SLIT2 axon guidance molecule is frequently inactivated in colorectal cancer and suppresses growth of colorectal carcinoma cells. *Cancer Res* **63**: 1054-1058
- De A, Loening AM, Gambhir SS (2007) An improved bioluminescence resonance energy transfer strategy for imaging intracellular events in single cells and living subjects. *Cancer Res* **67**: 7175-7183
- De A, Ray P, Loening AM, Gambhir SS (2009) BRET3: a red-shifted bioluminescence resonance energy transfer (BRET)-based integrated platform for imaging protein-protein interactions from single live cells and living animals. *FASEB J* **23**: 2702-2709
- de Wit J, Hong W, Luo L, Ghosh A (2011) Role of leucine-rich repeat proteins in the development and function of neural circuits. *Annu Rev Cell Dev Biol* **27**: 697-729
- Desanti GE, Jenkinson WE, Parnell SM, Boudil A, Gautreau-Rolland L, Eksteen B, Ezine S, Lane PJ, Jenkinson EJ, Anderson G (2011) Clonal analysis reveals uniformity in the molecular profile and lineage potential of CCR9(+) and CCR9(-) thymus-settling progenitors. *J Immunol* **186**: 5227-5235
- Dickinson RE, Dallol A, Bieche I, Krex D, Morton D, Maher ER, Latif F (2004) Epigenetic inactivation of SLIT3 and SLIT1 genes in human cancers. *Br J Cancer* **91**: 2071-2078
- Dickinson RE, Hryhorskij L, Tremewan H, Hogg K, Thomson AA, McNeilly AS, Duncan WC (2010) Involvement of the SLIT/ROBO pathway in follicle development in the fetal ovary. *Reproduction* **139**: 395-407
- Dickinson RE, Myers M, Duncan WC (2008) Novel regulated expression of the SLIT/ROBO pathway in the ovary: possible role during luteolysis in women. *Endocrinology* **149**: 5024-5034
- Dooley J, Erickson M, Roelink H, Farr AG (2005) Nude thymic rudiment lacking functional foxn1 resembles respiratory epithelium. *Dev Dyn* **233**: 1605-1612
- Dorsch S, Klotz KN, Engelhardt S, Lohse MJ, Bunemann M (2009) Analysis of receptor oligomerization by FRAP microscopy. *Nat Methods* **6**: 225-230
- Dunaway CM, Hwang Y, Lindsley CW, Cook RS, Wu JY, Boothby M, Chen J, Brantley-Sieders DM (2011) Cooperative signaling between Slit2 and Ephrin-A1 regulates a balance between angiogenesis and angiostasis. *Mol Cell Biol* **31**: 404-416
- Dunker AK, Silman I, Uversky VN, Sussman JL (2008) Function and structure of inherently disordered proteins. *Curr Opin Struct Biol* **18**: 756-764
- Englund C, Steneberg P, Falileeva L, Xylourgidis N, Samakovlis C (2002) Attractive and repulsive functions of Slit are mediated by different receptors in the Drosophila trachea. *Development* **129**: 4941-4951
- Evans TA, Bashaw GJ (2010) Functional diversity of Robo receptor immunoglobulin domains promotes distinct axon guidance decisions. *Curr Biol* **20**: 567-572

- Fan X, Labrador JP, Hing H, Bashaw GJ (2003) Slit stimulation recruits Dock and Pak to the roundabout receptor and increases Rac activity to regulate axon repulsion at the CNS midline. *Neuron* **40**: 113-127
- Fish JE, Wythe JD, Xiao T, Bruneau BG, Stainier DYR, Srivastava D, Woo S (2011) A Slit/miR-218/Robo regulatory loop is required during heart tube formation in zebrafish. *Development* **138**: 1409-1419
- Flanagan SP (1966) 'Nude', a new hairless gene with pleiotropic effects in the mouse. *Genet Res* **8**: 295-309
- Foster K, Sheridan J, Veiga-Fernandes H, Roderick K, Pachnis V, Adams R, Blackburn C, Kioussis D, Coles M (2008) Contribution of neural crest-derived cells in the embryonic and adult thymus. *J Immunol* **180**: 3183-3189
- Frank J, Pignata C, Panteleyev AA, Prowse DM, Baden H, Weiner L, Gaetaniello L, Ahmad W, Pozzi N, Cserhalmi-Friedman PB, Aita VM, Uyttendaele H, Gordon D, Ott J, Brissette JL, Christiano AM (1999) Exposing the human nude phenotype. *Nature* **398**: 473-474
- Freigang J, Proba K, Leder L, Diederichs K, Sonderegger P, Welte W (2000) The crystal structure of the ligand binding module of axonin-1/TAG-1 suggests a zipper mechanism for neural cell adhesion. *Cell* **101**: 425-433
- Fricke C, Lee JS, Geiger-Rudolph S, Bonhoeffer F, Chien CB (2001) astray, a zebrafish roundabout homolog required for retinal axon guidance. *Science* **292**: 507-510
- Fujisawa K, Wrana JL, Culotti JG (2007) The slit receptor EVA-1 coactivates a SAX-3/Robo mediated guidance signal in *C. elegans*. *Science* **317**: 1934-1938
- Fukuhara N, Howitt JA, Hussain S-A, Hohenester E (2008) Structural and functional analysis of slit and heparin binding to immunoglobulin-like domains 1 and 2 of Drosophila Robo. *J Biol Chem* **283**: 16226-16234
- Gazzerro E, Canalis E (2006) Bone morphogenetic proteins and their antagonists. *Rev Endocr Metab Disord* **7**: 51-65
- Geutskens SB, Hordijk PL, van Hennik PB (2010) The chemorepellent Slit3 promotes monocyte migration. *J Immunol* **185**: 7691-7698
- Ghosh S, Ghosh A, Maiti G, Alam N, Roy A, Roychoudhury S, Panda C (2008) Alterations of ROBO1/DUTT1 and ROBO2 loci in early dysplastic lesions of head and neck: clinical and prognostic implications. *Hum Genet* **125**: 189-198
- Gordon GW, Berry G, Liang XH, Levine B, Herman B (1998) Quantitative fluorescence resonance energy transfer measurements using fluorescence microscopy. *Biophys J* **74**: 2702-2713
- Gray DH, Seach N, Ueno T, Milton MK, Liston A, Lew AM, Goodnow CC, Boyd RL (2006) Developmental kinetics, turnover, and stimulatory capacity of thymic epithelial cells. *Blood* **108**: 3777-3785
- Greenberg JM, Thompson FY, Brooks SK, Shannon JM, Akeson AL (2004) Slit and robo expression in the developing mouse lung. *Dev Dyn* **230**: 350-360

- Grieshammer U, Ma L, Plump AS, Wang F, Tessier-Lavigne M, Martin GR (2004) SLIT2-mediated ROBO2 signaling restricts kidney induction to a single site. *Dev Cell* **6**: 709-717
- Gröne J, Doeblner O, Loddenkemper C, Hotz B, Buhr H-J, Bhargava S (2006) Robo1/Robo4: differential expression of angiogenic markers in colorectal cancer. *Oncol Rep* **15**: 1437-1443
- Guan H, Zu G, Xie Y, Tang H, Johnson M, Xu X, Kevil C, Xiong W-C, Elmetts C, Rao Y, Wu JY, Xu H (2003) Neuronal repellent Slit2 inhibits dendritic cell migration and the development of immune responses. *J Immunol* **171**: 6519-6526
- Hall A (2005) Rho GTPases and the control of cell behaviour. *Biochem Soc Trans* **33**: 891-895
- Halperin-Barlev O, Kalcheim C (2011) Sclerotome-derived Slit1 drives directional migration and differentiation of Robo2-expressing pioneer myoblasts. *Development* **138**: 2935-2945
- Hamazaki Y, Fujita H, Kobayashi T, Choi Y, Scott HS, Matsumoto M, Minato N (2007) Medullary thymic epithelial cells expressing Aire represent a unique lineage derived from cells expressing claudin. *Nat Immunol* **8**: 304-311
- Hammond R, Vivancos V, Naeem A, Chilton J, Mambetisaeva E, Mambetisaeva E, Andrews W, Sundaresan V, Guthrie S (2005) Slit-mediated repulsion is a key regulator of motor axon pathfinding in the hindbrain. *Development* **132**: 4483-4495
- Harlow E, Lane D (1999) *Using antibodies*, New York: Cold Spring Harbor Laboratory Press.
- Harpaz Y, Chothia C (1994) Many of the immunoglobulin superfamily domains in cell adhesion molecules and surface receptors belong to a new structural set which is close to that containing variable domains. *J Mol Biol* **238**: 528-539
- Heasman SJ, Ridley AJ (2008) Mammalian Rho GTPases: new insights into their functions from in vivo studies. *Nat Rev Mol Cell Biol* **9**: 690-701
- Helenius IT, Beitel GJ (2008) The first "Slit" is the deepest: the secret to a hollow heart. *J Cell Biol* **182**: 221-223
- Hernández-Miranda LR, Cariboni A, Faux C, Ruhrberg C, Cho JH, Cloutier J-F, Eickholt BJ, Parnavelas JG, Andrews WD (2011) Robo1 Regulates Semaphorin Signaling to Guide the Migration of Cortical Interneurons through the Ventral Forebrain. *J Neurosci* **31**: 6174-6187
- Hivert B, Liu Z, Chuang C-Y, Doherty P, Sundaresan V (2002) Robo1 and Robo2 are homophilic binding molecules that promote axonal growth. *Mol Cell Neurosci* **21**: 534-545
- Hocking JC, Hehr CL, Bertolesi GE, Wu JY, McFarlane S (2010) Distinct roles for Robo2 in the regulation of axon and dendrite growth by retinal ganglion cells. *Mech Dev* **127**: 36-48
- Hohenester E (2008) Structural insight into Slit-Robo signalling. *Biochem Soc Trans* **36**: 251-256
- Hohenester E, Hussain S, Howitt JA (2006) Interaction of the guidance molecule Slit with cellular receptors. *Biochem Soc Trans* **34**: 418-421

- Hollander G, Gill J, Zuklys S, Iwanami N, Liu C, Takahama Y (2006) Cellular and molecular events during early thymus development. *Immunol Rev* **209**: 28-46
- Holmes GP, Negus K, Burridge L, Raman S, Algar E, Yamada T, Little MH (1998) Distinct but overlapping expression patterns of two vertebrate slit homologs implies functional roles in CNS development and organogenesis. *Mech Dev* **79**: 57-72
- Howitt JA, Clout NJ, Hohenester E (2004) Binding site for Robo receptors revealed by dissection of the leucine-rich repeat region of Slit. *EMBO J* **23**: 4406-4412
- Hu H (1999) Chemorepulsion of neuronal migration by Slit2 in the developing mammalian forebrain. *Neuron* **23**: 703-711
- Hu H (2001) Cell-surface heparan sulfate is involved in the repulsive guidance activities of Slit2 protein. *Nat Neurosci* **4**: 695-701
- Hu H, Li M, Labrador J-P, McEwen J, Lai EC, Goodman CS, Bashaw GJ (2005) Cross GTPase-activating protein (CrossGAP)/Vilse links the Roundabout receptor to Rac to regulate midline repulsion. *Proc Natl Acad Sci U S A* **102**: 4613-4618
- Hubert P, Sawma P, Duneau JP, Khao J, Henin J, Bagnard D, Sturgis J (2010) Single-spanning transmembrane domains in cell growth and cell-cell interactions: More than meets the eye? *Cell Adh Migr* **4**: 313-324
- Huminiecki L, Gorn M, Suchting S, Poulsom R, Bicknell R (2002) Magic roundabout is a new member of the roundabout receptor family that is endothelial specific and expressed at sites of active angiogenesis. *Genomics* **79**: 547-552
- Hussain S-A, Piper M, Fukuhara N, Strohlic L, Cho G, Howitt JA, Ahmed Y, Powell AK, Turnbull JE, Holt CE, Hohenester E (2006) A molecular mechanism for the heparan sulfate dependence of slit-robo signaling. *J Biol Chem* **281**: 39693-39698
- Husson J, Chemin K, Bohineust A, Hivroz C, Henry N (2011) Force generation upon T cell receptor engagement. *PLoS One* **6**: e19680
- Hutson LD, Chien CB (2002) Pathfinding and error correction by retinal axons: the role of astray/robo2. *Neuron* **33**: 205-217
- Isaacs NW (1995) Cystine knots. *Curr Opin Struct Biol* **5**: 391-395
- Ito H, Ichi Funahashi S, Yamauchi N, Shibahara J, Midorikawa Y, Kawai S, Kinoshita Y, Watanabe A, Hippo Y, Ohtomo T, Iwanari H, Nakajima A, Makuuchi M, Fukayama M, Hirata Y, Hamakubo T, Kodama T, Tsuchiya M, Aburatani H (2006) Identification of ROBO1 as a novel hepatocellular carcinoma antigen and a potential therapeutic and diagnostic target. *Clin Cancer Res* **12**: 3257-3264
- Itoh A, Miyabayashi T, Ohno M, Sakano S (1998) Cloning and expressions of three mammalian homologues of Drosophila slit suggest possible roles for Slit in the formation and maintenance of the nervous system. *Brain Res Mol Brain Res* **62**: 175-186
- Itoi M, Kawamoto H, Katsura Y, Amagai T (2001) Two distinct steps of immigration of hematopoietic progenitors into the early thymus anlage. *Int Immunol* **13**: 1203-1211
- Jaworski A, Long H, Tessier-Lavigne M (2010) Collaborative and specialized functions of Robo1 and Robo2 in spinal commissural axon guidance. *J Neurosci* **30**: 9445-9453

- Jenkinson WE, Rossi SW, Parnell SM, Jenkinson EJ, Anderson G (2007) PDGFRalpha-expressing mesenchyme regulates thymus growth and the availability of intrathymic niches. *Blood* **109**: 954-960
- Jhaveri D, Saharan S, Sen A, Rodrigues V (2004) Positioning sensory terminals in the olfactory lobe of *Drosophila* by Robo signaling. *Development* **131**: 1903-1912
- Jia L, Cheng L, Raper J (2005) Slit/Robo signaling is necessary to confine early neural crest cells to the ventral migratory pathway in the trunk. *Dev Biol* **282**: 411-421
- Jin J, You H, Yu B, Deng Y, Tang N, Yao G, Shu H, Yang S, Qin W (2008) Epigenetic inactivation of SLIT2 in human hepatocellular carcinomas. *Biochem Biophys Res Commun* **379**: 86-91
- Johnson KG, Ghose A, Epstein E, Lincecum J, O'Connor MB, Vactor DV (2004) Axonal heparan sulfate proteoglycans regulate the distribution and efficiency of the repellent slit during midline axon guidance. *Curr Biol* **14**: 499-504
- Jones CA, London NR, Chen H, Park KW, Sauvaget D, Stockton RA, Wythe JD, Suh W, Larrieu-Lahargue F, Mukouyama Y-S, Lindblom P, Seth P, Frias A, Nishiya N, Ginsberg MH, Gerhardt H, Zhang K, Li DY (2008) Robo4 stabilizes the vascular network by inhibiting pathologic angiogenesis and endothelial hyperpermeability. *Nat Med* **14**: 448-453
- Jones CA, Nishiya N, London NR, Zhu W, Sorensen LK, Chan AC, Lim CJ, Chen H, Zhang Q, Schultz PG, Hayallah AM, Thomas KR, Famulok M, Zhang K, Ginsberg MH, Li DY (2009) Slit2-Robo4 signalling promotes vascular stability by blocking Arf6 activity. *Nat Cell Biol* **11**: 1325-1331
- Kaestner KH, Knochel W, Martinez DE (2000) Unified nomenclature for the winged helix/forkhead transcription factors. *Genes Dev* **14**: 142-146
- Kaneko N, Marín O, Koike M, Hirota Y, Uchiyama Y, Wu JY, Lu Q, Tessier-Lavigne M, Alvarez-Buylla A, Okano H, Rubenstein JLR, Sawamoto K (2010) New neurons clear the path of astrocytic processes for their rapid migration in the adult brain. *Neuron* **67**: 213-223
- Kanellis J, Garcia GE, Li P, Parra G, Wilson CB, Rao Y, Han S, Smith CW, Johnson RJ, Wu JY, Feng L (2004) Modulation of inflammation by slit protein in vivo in experimental crescentic glomerulonephritis. *Am J Pathol* **165**: 341-352
- Kang JY, Lee JO (2011) Structural biology of the Toll-like receptor family. *Annu Rev Biochem* **80**: 917-941
- Kato S (1997) Thymic microvascular system. *Microsc Res Tech* **38**: 287-299
- Kaur S, Castellone MD, Bedell VM, Konar M, Gutkind JS, Ramchandran R (2006) Robo4 signaling in endothelial cells implies attraction guidance mechanisms. *J Biol Chem* **281**: 11347-11356
- Kaur S, Samant GV, Pramanik K, Loscombe PW, Pendrak ML, Roberts DD, Ramchandran R (2008) Silencing of directional migration in roundabout4 knockdown endothelial cells. *BMC Cell Biol* **9**: 61

- Keleman K, Rajagopalan S, Cleppien D, Teis D, Paiha K, Huber LA, Technau GM, Dickson BJ (2002) Comm sorts robo to control axon guidance at the Drosophila midline. *Cell* **110**: 415-427
- Kidd T, Bland KS, Goodman CS (1999) Slit is the midline repellent for the robo receptor in Drosophila. *Cell* **96**: 785-794
- Kidd T, Brose K, Mitchell KJ, Fetter RD, Tessier-Lavigne M, Goodman CS, Tear G (1998a) Roundabout controls axon crossing of the CNS midline and defines a novel subfamily of evolutionarily conserved guidance receptors. *Cell* **92**: 205-215
- Kidd T, Russell C, Goodman CS, Tear G (1998b) Dosage-sensitive and complementary functions of roundabout and commissureless control axon crossing of the CNS midline. *Neuron* **20**: 25-33
- Kim HK, Zhang H, Li H, Wu T-T, Swisher S, He D, Wu L, Xu J, Elmets CA, Athar M, chun Xu X, Xu H (2008) Slit2 inhibits growth and metastasis of fibrosarcoma and squamous cell carcinoma. *Neoplasia* **10**: 1411-1420
- Kioussis D, Pachnis V (2009) Immune and nervous systems: more than just a superficial similarity? *Immunity* **31**: 705-710
- Koch AW, Mathivet T, Larrivée B, Tong RK, Kowalski J, Pibouin-Fragner L, Bouvrée K, Stawicki S, Nicholes K, Rathore N, Scales SJ, Luis E, del Toro R, Freitas C, Bréant C, Michaud A, Corvol P, Thomas J-L, Wu Y, Peale F, Watts RJ, Tessier-Lavigne M, Bagri A, Eichmann A (2011) Robo4 maintains vessel integrity and inhibits angiogenesis by interacting with UNC5B. *Dev Cell* **20**: 33-46
- Kramer SG, Kidd T, Simpson JH, Goodman CS (2001) Switching repulsion to attraction: changing responses to slit during transition in mesoderm migration. *Science* **292**: 737-740
- Kraut R, Zinn K (2004) Roundabout 2 regulates migration of sensory neurons by signaling in trans. *Curr Biol* **14**: 1319-1329
- Kulahin N, Kristensen O, Rasmussen KK, Olsen L, Rydberg P, Vestergaard B, Kastrup JS, Berezin V, Bock E, Walmod PS, Gajhede M (2011) Structural model and trans-interaction of the entire ectodomain of the olfactory cell adhesion molecule. *Structure* **19**: 203-211
- Kumanogoh A, Kikutani H (2010) Semaphorins and their receptors: novel features of neural guidance molecules. *Proc Jpn Acad Ser B Phys Biol Sci* **86**: 611-620
- Latil A, Chêne L, Cochant-Priollet B, Mangin P, Fournier G, Berthon P, Cussenot O (2003) Quantification of expression of netrins, slits and their receptors in human prostate tumors. *Int J Cancer* **103**: 306-315
- Lenhard B, Sandelin A, Carninci P (2012) Metazoan promoters: emerging characteristics and insights into transcriptional regulation. *Nat Rev Genet* **13**: 233-245
- Li E, Hristova K (2010) Receptor tyrosine kinase transmembrane domains: Function, dimer structure and dimerization energetics. *Cell Adh Migr* **4**: 249-254
- Li HS, Chen JH, Wu W, Fagaly T, Zhou L, Yuan W, Dupuis S, Jiang ZH, Nash W, Gick C, Ornitz DM, Wu JY, Rao Y (1999) Vertebrate slit, a secreted ligand for the transmembrane protein roundabout, is a repellent for olfactory bulb axons. *Cell* **96**: 807-818

- Li YC, Chen BM, Wu PC, Cheng TL, Kao LS, Tao MH, Lieber A, Roffler SR (2010) Cutting Edge: mechanical forces acting on T cells immobilized via the TCR complex can trigger TCR signaling. *J Immunol* **184**: 5959-5963
- Li Z, Na X, Wang D, Schoen SR, Messing EM, Wu G (2002) Ubiquitination of a novel deubiquitinating enzyme requires direct binding to von Hippel-Lindau tumor suppressor protein. *J Biol Chem* **277**: 4656-4662
- Lind EF, Prockop SE, Porritt HE, Petrie HT (2001) Mapping precursor movement through the postnatal thymus reveals specific microenvironments supporting defined stages of early lymphoid development. *J Exp Med* **194**: 127-134
- Liu C, Saito F, Liu Z, Lei Y, Uehara S, Love P, Lipp M, Kondo S, Manley N, Takahama Y (2006a) Coordination between CCR7- and CCR9-mediated chemokine signals in prevascular fetal thymus colonization. *Blood* **108**: 2531-2539
- Liu D, Hou J, Hu X, Wang X, Xiao Y, Mou Y, Leon HD (2006b) Neuronal chemorepellent Slit2 inhibits vascular smooth muscle cell migration by suppressing small GTPase Rac1 activation. *Circ Res* **98**: 480-489
- Liu J, Zhang L, Wang D, Shen H, Jiang M, Mei P, Hayden PS, Sedor JR, Hu H (2003) Congenital diaphragmatic hernia, kidney agenesis and cardiac defects associated with Slit3-deficiency in mice. *Mech Dev* **120**: 1059-1070
- Liu Z, Patel K, Schmidt H, Andrews W, Pini A, Sundaresan V (2004) Extracellular Ig domains 1 and 2 of Robo are important for ligand (Slit) binding. *Mol Cell Neurosci* **26**: 232-240
- Logan CY, Nusse R (2004) The Wnt signaling pathway in development and disease. *Annu Rev Cell Dev Biol* **20**: 781-810
- London NR, Zhu W, Bozza FA, Smith MCP, Greif DM, Sorensen LK, Chen L, Kaminoh Y, Chan AC, Passi SF, Day CW, Barnard DL, Zimmerman GA, Krasnow MA, Li DY (2010) Targeting Robo4-dependent Slit signaling to survive the cytokine storm in sepsis and influenza. *Sci Transl Med* **2**: 23ra19
- Long H, Sabatier C, Ma L, Plump A, Yuan W, Ornitz DM, Tamada A, Murakami F, Goodman CS, Tessier-Lavigne M (2004) Conserved roles for Slit and Robo proteins in midline commissural axon guidance. *Neuron* **42**: 213-223
- Love PE, Bhandoola A (2011) Signal integration and crosstalk during thymocyte migration and emigration. *Nat Rev Immunol* **11**: 469-477
- Lowery LA, Van Vactor D (2009) The trip of the tip: understanding the growth cone machinery. *Nat Rev Mol Cell Biol* **10**: 332-343
- Lu X, Le Noble F, Yuan L, Jiang Q, De Lafarge B, Sugiyama D, Breant C, Claes F, De Smet F, Thomas JL, Autiero M, Carmeliet P, Tessier-Lavigne M, Eichmann A (2004) The netrin receptor UNC5B mediates guidance events controlling morphogenesis of the vascular system. *Nature* **432**: 179-186
- Luc S, Luis TC, Boukarabila H, Macaulay IC, Buza-Vidas N, Bouriez-Jones T, Lutteropp M, Woll PS, Loughran SJ, Mead AJ, Hultquist A, Brown J, Mizukami T, Matsuoka S, Ferry H, Anderson K, Duarte S, Atkinson D, Soneji S, Domanski A, Farley A, Sanjuan-Pla A, Carella C, Patient R, de Bruijn M, Enver T, Nerlov C, Blackburn C, Godin I, Jacobsen

- SE (2012) The earliest thymic T cell progenitors sustain B cell and myeloid lineage potential. *Nat Immunol* **13**: 412-419
- Lundström A, Gallio M, Englund C, Steneberg P, Hemphälä J, Aspenström P, Keleman K, Falileeva L, Dickson BJ, Samakovlis C (2004) Vilse, a conserved Rac/Cdc42 GAP mediating Robo repulsion in tracheal cells and axons. *Genes Dev* **18**: 2161-2171
- Ly NP, Komatsuzaki K, Fraser IP, Tseng AA, Prodhon P, Moore KJ, Kinane TB (2005) Netrin-1 inhibits leukocyte migration in vitro and in vivo. *Proc Natl Acad Sci U S A* **102**: 14729-14734
- Ma S, Liu X, Geng J-G, Guo S-W (2010) Increased SLIT immunoreactivity as a biomarker for recurrence in endometrial carcinoma. *Am J Obstet Gynecol* **202**: 68.e61-68.e11
- Macias H, Moran A, Samara Y, Moreno M, Compton JE, Harburg G, Strickland P, Hinck L (2011) SLIT/ROBO1 signaling suppresses mammary branching morphogenesis by limiting basal cell number. *Dev Cell* **20**: 827-840
- MacMullin A, Jacobs JR (2006) Slit coordinates cardiac morphogenesis in Drosophila. *Dev Biol* **293**: 154-164
- Marlow R, Binnewies M, Sorensen LK, Monica SD, Strickland P, Forsberg EC, Li DY, Hinck L (2010) Vascular Robo4 restricts proangiogenic VEGF signaling in breast. *Proc Natl Acad Sci U S A* **107**: 10520-10525
- Marlow R, Strickland P, Lee JS, Wu X, Pebenito M, Binnewies M, Le EK, Moran A, Macias H, Cardiff RD, Sukumar S, Hinck L (2008) SLITs suppress tumor growth in vivo by silencing Sdf1/Cxcr4 within breast epithelium. *Cancer Res* **68**: 7819-7827
- Maurel D, Kniazeff J, Mathis G, Trinquet E, Pin JP, Ansanay H (2004) Cell surface detection of membrane protein interaction with homogeneous time-resolved fluorescence resonance energy transfer technology. *Anal Biochem* **329**: 253-262
- Mauss A, Tripodi M, Evers JF, Landgraf M (2009) Midline signalling systems direct the formation of a neural map by dendritic targeting in the Drosophila motor system. *PLoS Biol* **7**: e1000200
- Medioni C, Astier M, Zmojdzian M, Jagla K, Sémériva M (2008) Genetic control of cell morphogenesis during Drosophila melanogaster cardiac tube formation. *J Cell Biol* **182**: 249-261
- Medioni C, Bertrand N, Mesbah K, Hudry B, Dupays L, Wolstein O, Washkowitz AJ, Papaioannou VE, Mohun TJ, Harvey RP, Zaffran S (2010) Expression of Slit and Robo genes in the developing mouse heart. *Dev Dyn* **239**: 3303-3311
- Melcher K (2004) New chemical crosslinking methods for the identification of transient protein-protein interactions with multiprotein complexes. *Curr Protein Pept Sci* **5**: 287-296
- Mertsch S, Schmitz N, Jeibmann A, Geng J-G, Paulus W, Senner V (2008) Slit2 involvement in glioma cell migration is mediated by Robo1 receptor. *J Neurooncol* **87**: 1-7
- Mille F, Llambi F, Guix C, Delloye-Bourgeois C, Guenebeaud C, Castro-Obregon S, Bredesen DE, Thibert C, Mehlen P (2009) Interfering with multimerization of netrin-1 receptors triggers tumor cell death. *Cell Death Differ* **16**: 1344-1351

- Milligan G, Smith NJ (2007) Allosteric modulation of heterodimeric G-protein-coupled receptors. *Trends Pharmacol Sci* **28**: 615-620
- Morlot C, Hemrika W, Romijn RA, Gros P, Cusack S, McCarthy AA (2007a) Production of Slit2 LRR domains in mammalian cells for structural studies and the structure of human Slit2 domain 3. *Acta Crystallogr D Biol Crystallogr* **63**: 961-968
- Morlot C, Thielens NM, Ravelli RBG, Hemrika W, Romijn RA, Gros P, Cusack S, McCarthy AA (2007b) Structural insights into the Slit-Robo complex. *Proc Natl Acad Sci U S A* **104**: 14923-14928
- Mulik S, Sharma S, Suryawanshi A, Veiga-Parga T, Reddy PBJ, Rajasagi NK, Rouse BT (2011) Activation of endothelial roundabout receptor 4 reduces the severity of virus-induced keratitis. *J Immunol* **186**: 7195-7204
- Muller A, Homey B, Soto H, Ge N, Catron D, Buchanan ME, McClanahan T, Murphy E, Yuan W, Wagner SN, Barrera JL, Mohar A, Verastegui E, Zlotnik A (2001) Involvement of chemokine receptors in breast cancer metastasis. *Nature* **410**: 50-56
- Muller SM, Stolt CC, Terszowski G, Blum C, Amagai T, Kessaris N, Iannarelli P, Richardson WD, Wegner M, Rodewald HR (2008) Neural crest origin of perivascular mesenchyme in the adult thymus. *J Immunol* **180**: 5344-5351
- Nakayama M, Nakajima D, Nagase T, Nomura N, Seki N, Ohara O (1998) Identification of high-molecular-weight proteins with multiple EGF-like motifs by motif-trap screening. *Genomics* **51**: 27-34
- Narayan G, Goparaju C, Arias-Pulido H, Kaufmann AM, Schneider A, Dürst M, Mansukhani M, Pothuri B, Murty VV (2006) Promoter hypermethylation-mediated inactivation of multiple Slit-Robo pathway genes in cervical cancer progression. *Mol Cancer* **5**: 16
- Nehls M, Pfeifer D, Schorpp M, Hedrich H, Boehm T (1994) New member of the winged-helix protein family disrupted in mouse and rat nude mutations. *Nature* **372**: 103-107
- Nguyen-Ba-Charvet KT, Di Meglio T, Fouquet C, Chedotal A (2008) Robos and slits control the pathfinding and targeting of mouse olfactory sensory axons. *J Neurosci* **28**: 4244-4249
- Nishiya N, Kiosses WB, Han J, Ginsberg MH (2005) An alpha4 integrin-paxillin-Arf-GAP complex restricts Rac activation to the leading edge of migrating cells. *Nat Cell Biol* **7**: 343-352
- Nowell CS, Bredenkamp N, Tetelin S, Jin X, Tischner C, Vaidya H, Sheridan JM, Stenhouse FH, Heussen R, Smith AJ, Blackburn CC (2011) Foxn1 regulates lineage progression in cortical and medullary thymic epithelial cells but is dispensable for medullary sublineage divergence. *PLoS Genet* **7**: e1002348
- Nural HF, Farmer WT, Mastick GS (2007) The Slit receptor Robo1 is predominantly expressed via the Dutt1 alternative promoter in pioneer neurons in the embryonic mouse brain and spinal cord. *Gene Expr Patterns* **7**: 837-845
- Nusslein-Volhard C, Wieschaus E, Kluding H (1984) Mutations affecting the pattern of the larval cuticle in *Drosophila melanogaster*. *Development Genes and Evolution* **193**: 267-282

- Okada Y, Jin E, Nikolova-Krstevski V, Yano K, Liu J, Beeler D, Spokes K, Kitayama M, Funahashi N, Doi T, Janes L, Minami T, Oettgen P, Aird WC (2008) A GABP-binding element in the Robo4 promoter is necessary for endothelial expression in vivo. *Blood* **112**: 2336-2339
- Pandya NM, Dhalla NS, Santani DD (2006) Angiogenesis--a new target for future therapy. *Vascul Pharmacol* **44**: 265-274
- Pappu KS, Morey M, Nern A, Spitzweck B, Dickson BJ, Zipursky SL (2011) Robo-3--mediated repulsive interactions guide R8 axons during Drosophila visual system development. *Proc Natl Acad Sci U S A* **108**: 7571-7576
- Park KW, Morrison CM, Sorensen LK, Jones CA, Rao Y, Chien C-B, Wu JY, Urness LD, Li DY (2003) Robo4 is a vascular-specific receptor that inhibits endothelial migration. *Dev Biol* **261**: 251-267
- Parsons L, Harris KL, Turner K, Whittington PM (2003) Roundabout gene family functions during sensory axon guidance in the drosophila embryo are mediated by both Slit-dependent and Slit-independent mechanisms. *Dev Biol* **264**: 363-375
- Pasquale EB (2008) Eph-Ephrin Bidirectional Signaling in Physiology and Disease. *Cell* **133**: 38-52
- Pasquale EB (2010) Eph receptors and ephrins in cancer: bidirectional signalling and beyond. *Nat Rev Cancer* **10**: 165-180
- Patel K, Nash JA, Itoh A, Liu Z, Sundaresan V, Pini A (2001) Slit proteins are not dominant chemorepellents for olfactory tract and spinal motor axons. *Development* **128**: 5031-5037
- Pertz O (2010) Spatio-temporal Rho GTPase signaling - where are we now? *J Cell Sci* **123**: 1841-1850
- Pfleger KD, Dromey JR, Dalrymple MB, Lim EM, Thomas WG, Eidne KA (2006) Extended bioluminescence resonance energy transfer (eBRET) for monitoring prolonged protein-protein interactions in live cells. *Cell Signal* **18**: 1664-1670
- Piper M, Anderson R, Dwivedy A, Weinl C, van Horck F, Leung KM, Cogill E, Holt C (2006) Signaling mechanisms underlying Slit2-induced collapse of Xenopus retinal growth cones. *Neuron* **49**: 215-228
- Plump AS, Erskine L, Sabatier C, Brose K, Epstein CJ, Goodman CS, Mason CA, Tessier-Lavigne M (2002) Slit1 and Slit2 cooperate to prevent premature midline crossing of retinal axons in the mouse visual system. *Neuron* **33**: 219-232
- Pocock R, Benard CY, Shapiro L, Hobert O (2008) Functional dissection of the C. elegans cell adhesion molecule SAX-7, a homologue of human L1. *Mol Cell Neurosci* **37**: 56-68
- Poliak S, Gollan L, Martinez R, Custer A, Einheber S, Salzer JL, Trimmer JS, Shrager P, Peles E (1999) Caspr2, a new member of the neurexin superfamily, is localized at the juxtaparanodes of myelinated axons and associates with K⁺ channels. *Neuron* **24**: 1037-1047
- Prasad A, Fernandis AZ, Rao Y, Ganju RK (2004) Slit protein-mediated inhibition of CXCR4-induced chemotactic and chemoinvasive signaling pathways in breast cancer cells. *J Biol Chem* **279**: 9115-9124

- Prasad A, Paruchuri V, Preet A, Latif F, Ganju RK (2008) Slit-2 induces a tumor-suppressive effect by regulating beta-catenin in breast cancer cells. *J Biol Chem* **283**: 26624-26633
- Prasad A, Qamri Z, Wu J, Ganju RK (2007) Slit-2/Robo-1 modulates the CXCL12/CXCR4-induced chemotaxis of T cells. *J Leukoc Biol* **82**: 465-476
- Qian L, Liu J, Bodmer R (2005) Slit and Robo control cardiac cell polarity and morphogenesis. *Curr Biol* **15**: 2271-2278
- Qiu P (2003) Recent advances in computational promoter analysis in understanding the transcriptional regulatory network. *Biochem Biophys Res Commun* **309**: 495-501
- Rajagopalan S, Nicolas E, Vivancos V, Berger J, Dickson BJ (2000a) Crossing the midline: roles and regulation of Robo receptors. *Neuron* **28**: 767-777
- Rajagopalan S, Vivancos V, Nicolas E, Dickson BJ (2000b) Selecting a longitudinal pathway: Robo receptors specify the lateral position of axons in the Drosophila CNS. *Cell* **103**: 1033-1045
- Raviola E, Karnovsky MJ (1972) Evidence for a blood-thymus barrier using electron-opaque tracers. *J Exp Med* **136**: 466-498
- Reeber SL, Sakai N, Nakada Y, Dumas J, Dobrenis K, Johnson JE, Kaprielian Z (2008) Manipulating Robo expression in vivo perturbs commissural axon pathfinding in the chick spinal cord. *J Neurosci* **28**: 8698-8708
- Rhee J, Buchan T, Zukerberg L, Lilien J, Balsamo J (2007) Cables links Robo-bound Abl kinase to N-cadherin-bound beta-catenin to mediate Slit-induced modulation of adhesion and transcription. *Nat Cell Biol* **9**: 883-892
- Rhee J, Mahfooz NS, Arregui C, Lilien J, Balsamo J, VanBerkum MFA (2002) Activation of the repulsive receptor Roundabout inhibits N-cadherin-mediated cell adhesion. *Nat Cell Biol* **4**: 798-805
- Risau W (1997) Mechanisms of angiogenesis. *Nature* **386**: 671-674
- Rizzo MA, Springer GH, Granada B, Piston DW (2004) An improved cyan fluorescent protein variant useful for FRET. *Nat Biotechnol* **22**: 445-449
- Rodewald HR (2008) Thymus organogenesis. *Annu Rev Immunol* **26**: 355-388
- Ronca F, Andersen JS, Paech V, Margolis RU (2001) Characterization of Slit protein interactions with glypican-1. *J Biol Chem* **276**: 29141-29147
- Rothberg JM, Artavanis-Tsakonas S (1992) Modularity of the slit protein. Characterization of a conserved carboxy-terminal sequence in secreted proteins and a motif implicated in extracellular protein interactions. *J Mol Biol* **227**: 367-370
- Rothberg JM, Hartley DA, Walther Z, Artavanis-Tsakonas S (1988) slit: an EGF-homologous locus of D. melanogaster involved in the development of the embryonic central nervous system. *Cell* **55**: 1047-1059
- Rothberg JM, Jacobs JR, Goodman CS, Artavanis-Tsakonas S (1990) slit: an extracellular protein necessary for development of midline glia and commissural axon pathways contains both EGF and LRR domains. *Genes Dev* **4**: 2169-2187

- Round JE, Sun H (2011) The adaptor protein Nck2 mediates Slit1-induced changes in cortical neuron morphology. *Mol Cell Neurosci* **47**: 265-273
- Sabatier C, Plump AS, Ma L, Brose K, Tamada A, Murakami F, Lee EY-HP, Tessier-Lavigne M (2004) The divergent Robo family protein rig-1/Robo3 is a negative regulator of slit responsiveness required for midline crossing by commissural axons. *Cell* **117**: 157-169
- Salaita K, Nair PM, Petit RS, Neve RM, Das D, Gray JW, Groves JT (2010) Restriction of receptor movement alters cellular response: physical force sensing by EphA2. *Science* **327**: 1380-1385
- Santiago-Martínez E, Soplop NH, Kramer SG (2006) Lateral positioning at the dorsal midline: Slit and Roundabout receptors guide Drosophila heart cell migration. *Proc Natl Acad Sci U S A* **103**: 12441-12446
- Santiago-Martínez E, Soplop NH, Patel R, Kramer SG (2008) Repulsion by Slit and Roundabout prevents Shotgun/E-cadherin-mediated cell adhesion during Drosophila heart tube lumen formation. *J Cell Biol* **182**: 241-248
- Schmid BC, Rezniczek GA, Fabjani G, Yoneda T, Leodolter S, Zeillinger R (2007) The neuronal guidance cue Slit2 induces targeted migration and may play a role in brain metastasis of breast cancer cells. *Breast Cancer Res Treat* **106**: 333-342
- Schulz JG, Ceulemans H, Caussinus E, Baietti MF, Affolter M, Hassan BA, David G (2011) Drosophila syndecan regulates tracheal cell migration by stabilizing Robo levels. *EMBO Reports* **12**: 1039 - 1046
- Seeger M, Tear G, Ferres-Marco D, Goodman CS (1993) Mutations affecting growth cone guidance in Drosophila: genes necessary for guidance toward or away from the midline. *Neuron* **10**: 409-426
- Seiradake E, von Philipsborn AC, Henry M, Fritz M, Lortat-Jacob H, Jamin M, Hemrika W, Bastmeyer M, Cusack S, McCarthy AA (2009) Structure and functional relevance of the Slit2 homodimerization domain. *EMBO Reports* **10**: 736 - 741
- Seki M, Watanabe A, Enomoto S, Kawamura T, Ito H, Kodama T, Hamakubo T, Aburatani H (2010) Human ROBO1 is cleaved by metalloproteinases and gamma-secretase and migrates to the nucleus in cancer cells. *FEBS Lett* **584**: 2909-2915
- Selvin PR (1995) Fluorescence resonance energy transfer. *Methods Enzymol* **246**: 300-334
- Seth P, Lin Y, ichi Hanai J, Shivalingappa V, Duyao MP, Sukhatme VP (2005) Magic roundabout, a tumor endothelial marker: expression and signaling. *Biochem Biophys Res Commun* **332**: 533-541
- Shaw G, Morse S, Ararat M, Graham FL (2002) Preferential transformation of human neuronal cells by human adenoviruses and the origin of HEK 293 cells. *FASEB J* **16**: 869-871
- Sheldon H, Andre M, Legg JA, Heal P, Herbert JM, Sainson R, Sharma AS, Kitajewski JK, Heath VL, Bicknell R (2009) Active involvement of Robo1 and Robo4 in filopodia formation and endothelial cell motility mediated via WASP and other actin nucleation-promoting factors. *FASEB J* **23**: 513-522

- Shiau CE, Bronner-Fraser M (2009) N-cadherin acts in concert with Slit1-Robo2 signaling in regulating aggregation of placode-derived cranial sensory neurons. *Development* **136**: 4155-4164
- Shibata F, Goto-Koshino Y, Morikawa Y, Komori T, Ito M, Fukuchi Y, Houchins JP, Tsang M, Li DY, Kitamura T, Nakajima H (2008) Robo4 is Expressed on Hematopoietic Stem Cells and Potentially Involved in the Niche-Mediated Regulation of the Side Population Phenotype. *Stem Cells* **27**: 183-190
- Simpson JH, Bland KS, Fetter RD, Goodman CS (2000a) Short-range and long-range guidance by Slit and its Robo receptors: a combinatorial code of Robo receptors controls lateral position. *Cell* **103**: 1019-1032
- Simpson JH, Kidd T, Bland KS, Goodman CS (2000b) Short-range and long-range guidance by slit and its Robo receptors. Robo and Robo2 play distinct roles in midline guidance. *Neuron* **28**: 753-766
- Sitnik KM, Kotarsky K, White AJ, Jenkinson WE, Anderson G, Agace WW (2012) Mesenchymal cells regulate retinoic Acid receptor-dependent cortical thymic epithelial cell homeostasis. *J Immunol* **188**: 4801-4809
- Small EM, Sutherland L, Rajagopalan K, Wang S, Olson EN (2010) MicroRNA-218 Regulates Vascular Patterning by Modulation of Slit-Robo Signaling. *Circulation Research* **107**: 1336-1344
- Smith-Berdan S, Nguyen A, Hassanein D, Zimmer M, Ugarte F, Ciriza J, Li D, García-Ojeda ME, Hinck L, Forsberg EC (2011) Robo4 cooperates with CXCR4 to specify hematopoietic stem cell localization to bone marrow niches. *Cell Stem Cell* **8**: 72-83
- Soroka V, Kasper C, Poulsen FM (2010) Structural biology of NCAM. *Adv Exp Med Biol* **663**: 3-22
- Spitzweck B, Brankatschk M, Dickson BJ (2010) Distinct protein domains and expression patterns confer divergent axon guidance functions for Drosophila Robo receptors. *Cell* **140**: 409-420
- Steigemann P, Molitor A, Fellert S, Jäckle H, Vorbrüggen G (2004) Heparan sulfate proteoglycan syndecan promotes axonal and myotube guidance by slit/robo signaling. *Curr Biol* **14**: 225-230
- Stein E, Tessier-Lavigne M (2001) Hierarchical organization of guidance receptors: silencing of netrin attraction by slit through a Robo/DCC receptor complex. *Science* **291**: 1928-1938
- Stein E, Zou Y, Poo M, Tessier-Lavigne M (2001) Binding of DCC by netrin-1 to mediate axon guidance independent of adenosine A2B receptor activation. *Science* **291**: 1976-1982
- Steinman L (2004) Elaborate interactions between the immune and nervous systems. *Nat Immunol* **5**: 575-581
- Stella MC, Trusolino L, Comoglio PM (2009) The Slit/Robo system suppresses hepatocyte growth factor-dependent invasion and morphogenesis. *Mol Biol Cell* **20**: 642-657
- Sternberg EM (2006) Neural regulation of innate immunity: a coordinated nonspecific host response to pathogens. *Nat Rev Immunol* **6**: 318-328

- Strickland P, Shin GC, Plump A, Tessier-Lavigne M, Hinck L (2006) Slit2 and netrin 1 act synergistically as adhesive cues to generate tubular bi-layers during ductal morphogenesis. *Development* **133**: 823-832
- Suchting S, Heal P, Tahtis K, Stewart LM, Bicknell R (2005) Soluble Robo4 receptor inhibits in vivo angiogenesis and endothelial cell migration. *FASEB J* **19**: 121-123
- Sundaresan V, Roberts I, Bateman A, Bankier A, Sheppard M, Hobbs C, Xiong J, Minna J, Latif F, Lerman M, Rabbitts P (1998) The DUTT1 gene, a novel NCAM family member is expressed in developing murine neural tissues and has an unusually broad pattern of expression. *Mol Cell Neurosci* **11**: 29-35
- Takai D, Jones PA (2003) The CpG island searcher: a new WWW resource. *In Silico Biol* **3**: 235-240
- Tanno T, Fujiwara A, Sakaguchi K, Tanaka K, Takenaka S, Tsuyama S (2007) Slit3 regulates cell motility through Rac/Cdc42 activation in lipopolysaccharide-stimulated macrophages. *FEBS Lett* **581**: 1022-1026
- Tanno T, Takenaka S, Tsuyama S (2004) Expression and function of Slit1alpha, a novel alternative splicing product for slit1. *J Biochem* **136**: 575-581
- Tayler TD, Robichaux MB, Garrity PA (2004) Compartmentalization of visual centers in the Drosophila brain requires Slit and Robo proteins. *Development* **131**: 5935-5945
- Tie J, Pan Y, Zhao L, Wu K, Liu J, Sun S, Guo X, Wang B, Gang Y, Zhang Y, Li Q, Qiao T, Zhao Q, Nie Y, Fan D (2010) MiR-218 inhibits invasion and metastasis of gastric cancer by targeting the Robo1 receptor. *PLoS Genet* **6**: e1000879
- Tole S, Mukovozov IM, Huang Y-W, Magalhaes MAO, Yan M, Crow MR, Liu GY, Sun CX, Durocher Y, Glogauer M, Robinson LA (2009) The axonal repellent, Slit2, inhibits directional migration of circulating neutrophils. *J Leukoc Biol* **86**: 1403-1415
- Traka M, Goutebroze L, Denisenko N, Bessa M, Nifli A, Havaki S, Iwakura Y, Fukamauchi F, Watanabe K, Soliven B, Girault JA, Karagogeos D (2003) Association of TAG-1 with Caspr2 is essential for the molecular organization of juxtaparanodal regions of myelinated fibers. *J Cell Biol* **162**: 1161-1172
- Tseng R-C, Lee S-H, Hsu H-S, Chen B-H, Tsai W-C, Tzao C, Wang Y-C (2010) SLIT2 attenuation during lung cancer progression deregulates beta-catenin and E-cadherin and associates with poor prognosis. *Cancer Res* **70**: 543-551
- van der Merwe PA, Dushek O (2011) Mechanisms for T cell receptor triggering. *Nat Rev Immunol* **11**: 47-55
- Vargesson N, Luria V, Messina I, Erskine L, Laufer E (2001) Expression patterns of Slit and Robo family members during vertebrate limb development. *Mech Dev* **106**: 175-180
- Vidi PA, Ejendal KF, Przybyla JA, Watts VJ (2011) Fluorescent protein complementation assays: new tools to study G protein-coupled receptor oligomerization and GPCR-mediated signaling. *Mol Cell Endocrinol* **331**: 185-193
- Vitriol EA, Zheng JQ (2012) Growth cone travel in space and time: the cellular ensemble of cytoskeleton, adhesion, and membrane. *Neuron* **73**: 1068-1081

- Vivanco I, Sawyers CL (2002) The phosphatidylinositol 3-Kinase AKT pathway in human cancer. *Nat Rev Cancer* **2**: 489-501
- Vogel SS, Thaler C, Koushik SV (2006) Fanciful FRET. *Sci STKE* **2006**: re2
- Wang B, Xiao Y, Ding BB, Zhang N, bin Yuan X, Gui L, Qian KX, Duan S, Chen Z, Rao Y, Geng JG (2003) Induction of tumor angiogenesis by Slit-Robo signaling and inhibition of cancer growth by blocking Robo activity. *Cancer Cell* **4**: 19-29
- Wang KH, Brose K, Arnott D, Kidd T, Goodman CS, Henzel W, Tessier-Lavigne M (1999) Biochemical purification of a mammalian slit protein as a positive regulator of sensory axon elongation and branching. *Cell* **96**: 771-784
- Wang L-J, Zhao Y, Han B, Ma Y-G, Zhang J, Yang D-M, Mao J-W, Tang F-T, Li W-D, Yang Y, Wang R, Geng J-G (2008) Targeting Slit-Roundabout signaling inhibits tumor angiogenesis in chemical-induced squamous cell carcinogenesis. *Cancer Sci* **99**: 510-517
- Weiner L, Han R, Scicchitano BM, Li J, Hasegawa K, Grossi M, Lee D, Brissette JL (2007) Dedicated epithelial recipient cells determine pigmentation patterns. *Cell* **130**: 932-942
- Werbowski-Ogilvie TE, Sadr MS, Jabado N, Angers-Loustau A, Agar NYR, Wu J, Bjerkvig R, Antel JP, Faury D, Rao Y, Maestro RFD (2006) Inhibition of medulloblastoma cell invasion by Slit. *Oncogene* **25**: 5103-5112
- Weyers JJ, Milutinovich AB, Takeda Y, Jemc JC, Doren MV (2011) A genetic screen for mutations affecting gonad formation in *Drosophila* reveals a role for the slit/robo pathway. *Dev Biol* **353**: 217-228
- Whitford KL, Marillat V, Stein E, Goodman CS, Tessier-Lavigne M, Chédotal A, Ghosh A (2002) Regulation of cortical dendrite development by Slit-Robo interactions. *Neuron* **33**: 47-61
- Wilson BD, Ii M, Park KW, Suli A, Sorensen LK, Larrieu-Lahargue F, Urness LD, Suh W, Asai J, Kock GA, Thorne T, Silver M, Thomas KR, Chien CB, Losordo DW, Li DY (2006) Netrins promote developmental and therapeutic angiogenesis. *Science* **313**: 640-644
- Wong K, Ren XR, Huang YZ, Xie Y, Liu G, Saito H, Tang H, Wen L, Brady-Kalnay SM, Mei L, Wu JY, Xiong WC, Rao Y (2001) Signal transduction in neuronal migration: roles of GTPase activating proteins and the small GTPase Cdc42 in the Slit-Robo pathway. *Cell* **107**: 209-221
- Wu JY, Feng L, Park HT, Havlioglu N, Wen L, Tang H, Bacon KB, Zh J, Xc Z, Rao Y (2001) The neuronal repellent Slit inhibits leukocyte chemotaxis induced by chemotactic factors. *Nature* **410**: 948-952
- Wu P, Brand L (1994) Resonance energy transfer: methods and applications. *Anal Biochem* **218**: 1-13
- Xia Z, Liu Y (2001) Reliable and global measurement of fluorescence resonance energy transfer using fluorescence microscopes. *Biophys J* **81**: 2395-2402
- Xian J, Clark KJ, Fordham R, Pannell R, Rabbitts TH, Rabbitts PH (2001a) Inadequate lung development and bronchial hyperplasia in mice with a targeted deletion in the *Dutt1/Robo1* gene. *Proc Natl Acad Sci U S A* **98**: 15062-15066

- Xian J, Clark KJ, Fordham R, Pannell R, Rabbitts TH, Rabbitts PH (2001b) Inadequate lung development and bronchial hyperplasia in mice with a targeted deletion in the *Dutt1/Robo1* gene. *Proc Natl Acad Sci U S A* **98**: 15062-15066
- Xu TR, Ward RJ, Pediani JD, Milligan G (2011) The orexin OX(1) receptor exists predominantly as a homodimer in the basal state: potential regulation of receptor organization by both agonist and antagonist ligands. *Biochem J* **439**: 171-183
- Xu Y, Piston DW, Johnson CH (1999) A bioluminescence resonance energy transfer (BRET) system: application to interacting circadian clock proteins. *Proc Natl Acad Sci U S A* **96**: 151-156
- Yang L, Bashaw GJ (2006) Son of sevenless directly links the Robo receptor to rac activation to control axon repulsion at the midline. *Neuron* **52**: 595-607
- Yaron A, Sprinzak D (2012) The cis side of juxtacrine signaling: a new role in the development of the nervous system. *Trends Neurosci* **35**: 230-239
- Yazdani U, Terman JR (2006) The semaphorins. *Genome Biol* **7**: 211
- Ye B-Q, Geng ZH, Ma L, Geng J-G (2010) Slit2 regulates attractive eosinophil and repulsive neutrophil chemotaxis through differential srGAP1 expression during lung inflammation. *J Immunol* **185**: 6294-6305
- Yiin J-J, Hu B, Jarzynka MJ, Feng H, Liu K-W, Wu JY, Ma H-I, Cheng S-Y (2009) Slit2 inhibits glioma cell invasion in the brain by suppression of Cdc42 activity. *Neuro Oncol* **11**: 779-789
- Yoshikawa M, Mukai Y, Okada Y, Yoshioka Y, Tsunoda S-I, Tsutsumi Y, Okada N, Aird WC, Doi T, Nakagawa S (2008) Ligand-independent assembly of purified soluble magic roundabout (Robo4), a tumor-specific endothelial marker. *Protein Expr Purif* **61**: 78-82
- Yu TW, Hao JC, Lim W, Tessier-Lavigne M, Bargmann CI (2002) Shared receptors in axon guidance: SAX-3/Robo signals via UNC-34/Enabled and a Netrin-independent UNC-40/DCC function. *Nat Neurosci* **5**: 1147-1154
- Yuan W, Rao Y, Babiuk RP, Greer JJ, Wu JY, Ornitz DM (2003) A genetic model for a central (septum transversum) congenital diaphragmatic hernia in mice lacking Slit3. *Proc Natl Acad Sci U S A* **100**: 5217-5222
- Yuan W, Zhou L, Chen JH, Wu JY, Rao Y, Ornitz DM (1999) The mouse SLIT family: secreted ligands for ROBO expressed in patterns that suggest a role in morphogenesis and axon guidance. *Dev Biol* **212**: 290-306
- Yuasa-Kawada J, Kinoshita-Kawada M, Rao Y, Wu JY (2009a) Deubiquitinating enzyme USP33/VDU1 is required for Slit signaling in inhibiting breast cancer cell migration. *Proc Natl Acad Sci U S A* **106**: 14530-14535
- Yuasa-Kawada J, Kinoshita-Kawada M, Wu G, Rao Y, Wu JY (2009b) Midline crossing and Slit responsiveness of commissural axons require USP33. *Nat Neurosci* **12**: 1087-1089
- Yue Y, Grossmann B, Galetzka D, Zechner U, Haaf T (2006) Isolation and differential expression of two isoforms of the ROBO2/Robo2 axon guidance receptor gene in humans and mice. *Genomics* **88**: 772-778

- Zachariah MA, Cyster JG (2010) Neural crest-derived pericytes promote egress of mature thymocytes at the corticomedullary junction. *Science* **328**: 1129-1135
- Zhang B, Dietrich UM, Geng J-G, Bicknell R, Esko JD, Wang L (2009) Repulsive axon guidance molecule Slit3 is a novel angiogenic factor. *Blood* **114**: 4300-4309